Quantitative Characterization of Polymeric Engine Oil Additives in Solution by Fluorescence

by

Solmaz Pirouz

A thesis
presented to the University of Waterloo
in fulfillment of the
thesis requirement for the degree of
Doctor of Philosophy
in
Chemistry

Waterloo, Ontario, Canada, 2015

Author's Declaration

I hereby declare that I am the sole author of this thesis. This is a true copy of the thesis, including any required final revisions, as accepted by my examiners.

I understand that my thesis may be made electronically available to the public.

Abstract

The solution behavior of several polymeric oil additives has been characterized by using fluorescence. First, the chemical composition of the polyisobutylene-based dispersants was determined by using the inherent fluorescence of the succinimide moiety of the polyisobutylene succinimide (PIBSI) dispersants and its efficient quenching by secondary amines. A series of PIBSI dispersants were synthesized by reacting one molar equivalent (meq) of polyisobutylene succinic anhydride (PIBSA) with two meqs of hexamethylenediamine, diethylenetriamine, triethylenetetramine, tetraethylenepentamine, and pentaethylenehexamine to yield the corresponding *bis*-PIBSI (*b*-PIBSI) dispersants. Intermolecular association of the dispersants in the solid state or in solution prevented the determination of the chemical composition of the *b*-PIBSI dispersants with traditional methods such as ^{1}H NMR and FTIR. Therefore, two procedures were developed to estimate the amine content of the *b*-PIBSI dispersants based on gel permeation chromatography (GPC) and fluorescence quenching. The fluorescence study showed a decrease in the fluorescence of the succinimide groups with increasing number of secondary amines present in the polyamine linker. A similar method was then applied to determine the level of modification of the *b*-PIBSI dispersants after they were reacted with ethylene carbonate (EC) to generate modified *b*-PIBSI dispersants (M*b*-PIBSI). The fact that the succinimide fluorescence of the M*b*-PIBSI dispersants was quenched much more efficiently by secondary amines than by the urethane groups that resulted from the EC modification of the amines was employed to quantify the level of EC modification of the M*b*-PIBSI dispersants. Moreover fluorescence was used to determine and compare the binding isotherms of a series of *b*-PIBSI and M*b*-PIBSI dispersants as they adsorbed onto the surface of carbon black particles.

Second, the molar fraction of intermolecular associations (f_{inter}) between ethylene-propylene (EP) copolymers was quantitatively determined by using pyrene excimer formation. In these experiments, a series of EP copolymers was maleated to yield EP-MA and then fluorescently labeled with 1-pyrenemethylamine and 2-(2-naphthyl)ethylamine to yield Py-EP and Np-EP, respectively. Fluorescence resonance energy transfer (FRET) experiments between Np-EP and Py-EP provided qualitative evidence of the existence of intermolecular association. A quantitative measure of f_{inter} was obtained by measuring the fluorescence intensity ratio of excimer-to-monomer (I_E/I_M) of the Py-EP solutions. The results showed that f_{inter} remained constant for amorphous Py-EP samples and increased for semicrystalline Py-EP samples upon decreasing the temperature as would have been expected from their chemical composition. This method was then applied to quantitatively measure f_{inter} between EP copolymers in solution in the presence of wax typically found in engine oils. The solution behaviour of four Py-EP copolymers in the presence of wax was characterized. The results showed that the interaction of wax with ethylene sequences in the EP copolymers increased macromolecular associations in solution as reflected by an increase in f_{inter}. In the case of the semicrystalline samples at lower temperatures, however, the formation of microcrystals induced strong polymer-polymer interactions that resulted in the formation of microcrystals and the dissociation of the wax from the polymers.

Together the results presented in this thesis suggest that fluorescence provides reliable information on the chemical composition and behaviour of polymeric oil additives, an information that was otherwise difficult to extract from traditional characterization methods.

Acknowledgements

I would like to express my most sincere gratitude to my supervisor, Prof. Jean Duhamel for his patience, support, guidance, and encouragement during my Ph.D. studies. I am grateful for his mentorship and assistance that made my Ph.D. experience memorable. I was also privileged to have the support of Profs. Mario Gauthier, Juewen Liu, and Costas Tzoganakis as my Ph.D. committee members. I would also like to thank Prof. Michael J. Serpe for agreeing to be the external examiner for my Ph.D. defense.

I wish to gratefully acknowledge financial support from Afton Chemical Corporation, Imperial Oil, and the Natural Sciences and Engineering Research Council of Canada (NSERC). I would also like to thank Dr. Sheng Jiang and Bob Duggal for all their constructive input and collaboration towards my thesis.

I am also very thankful to my friends and colleagues whom I have had the opportunity to meet during my graduate studies at the University of Waterloo. I would like to thank all the current and former lab members of the Duhamel and Gauthier groups who have always helped me to carry out my research. In particular, I would like to thank Yulin Wang, Lu Li, Bingqing Yang, Jamie Yip, and Mike Fowler.

Foremost, I would like to express my sincere gratefulness to my family. Thank you my dearest parents and grandparents for your everlasting love and confidence in me. You have always supported and encouraged me to pursue my dreams and you made it possible for me to make it this far. My thanks are also due to my brother, Sepehr, whom I feel blessed to have on my side. I am particularly grateful to my best friend and soulmate, my husband Kasra. We found each other in this small city far from home and have been together in this journey and

since then you have been a true and great supporter during my good and bad times. Thank you for being there when I need you the most. You are the best thing that ever happened to me.

Dedication

To my beloved Family.

Table of Contents

List of Figures

List of Tables

List of Schemes

List of Abbreviations

ΔH	change in enthalpy
η	viscosity
λ_{em}	emission wavelength
λ_{ex}	excitation wavelength
λ_{Py}	pyrene content
τ_E	fluorescence lifetime of pyrene excimer
τ_M	fluorescence lifetime of excited pyrene monomer
ϕ_E	fluorescence quantum yield of the pyrene excimer
ϕ_M	fluorescence quantum yield of the pyrene monomer
b-MSI-DETA	*bis*-Methyl succinimide diethyltriamine
b-PIBSI	*bis*- polyisobutylene succinimide
BUA	butylamine
C	concentration
C NMR	carbon nuclear magnetic resonance
CMC	critical micelle concentration
D	poorly-stacked long-lived pyrene dimers
DEA	diethylamine
DETA	diethylenetriamine
D_h	hydrodynamic diameter
DSC	differential scanning calorimetry
*E*0	well-stacked pyrene dimers
EC	ethylene carbonate
EEC	end-to-end cyclization
EL	improperly stacked pyrene dimers
EP	ethylene propylene
$f(t)$	rate constant of structureless object that can morph into different conformations with a time-dependent
FA	fluorescence anisotropy
f_{agg}	molar fraction of aggregated pyrenes in solution
FBM	fluorescence blob model
f_{diff}	molar fraction of pyrenes forming excimer via diffusion in solution
FDQ	fluorescence dynamic quenching
f_{free}	molar fraction of isolated pyrenes in solution
f_{inter}	the molar fraction of intermolecular interactions
FLPs	fluorescently labeled polymers

FRET	fluorescence resonance energy transfer
FTIR	Fourier transform infrared spectroscopy
GPC	gel permeation chromatography
H NMR	proton nuclear magnetic resonance
HMDA	hexamethylenediamine
I_1/I_3	ratio of the first to the third peak intensities of the excited pyrene monomer
I_E/I_M	ratio of the excimer to monomer fluorescenc intensities
k_1	diffusion-controlled rate constant of pyrene excimer formation
k_{-1}	dissociation rate constant of pyrene excimer
k_{11}	pyrene excimer formed by intramolecular diffusion
k_{12}	pyrene excimer formed by intermolecular diffusion
k_2	pyrene excimer formed by hydrophobic interaction
k_{blob}	rate constant for excimer formation between one excited and one ground state pyrene inside a same *blob*
k_{cy}	cyclization rate constant
k_{cy}	dissociation rate constant of excimer formed by end-to-end cyclization of a pyrene end-labeled polymer
k_e[M0]	rate constant of pyrene exchange between *blobs* times the concentration of *blobs* that contain zero ground state pyrene
k_e[M1]	rate constant of pyrene exchange between *blobs* times the concentration of *blobs* that contain one ground state pyrene
k_{ex}[*blob*]	rate constant of pyrene exchange between *blobs* times the *blob* concentration
k_{rad}	radiative rate constant
L	chain length
LP	large particle
LS	light scattering
M*b*-PIBSI	modified *bis*-polyisobutylene succinimide
meq	molar equivalents
MFA	model free analysis
M_n	number-average molecular weight
m-PIBSI	*mono*-polyisobutylene succinimide
N_{agg}	average number of hydrophobic pendants per aggregate
N_{IB}	number of isobutylene monomers
N-MSI	*N*-methylsuccinimide
Np-ESI	2-(2-Naphthyl)ethyl Succinimide
N_{SI}	number of succinimide moieties

P_A	peak-to-valley ratio of the pyrene absorption
PDI	polydispersity index
PEHA	pentaethylenehexamine
PIBSA	polyisobutylene succinic anhydride
PPDs	pour point depressants
PS	polystyrene
PTI	Photon Technology International
*P*y	pyrene
Py_{agg}	aggregated pyrenes
Py_{diff}	pyrenes forming excimer via diffusion
Py-EP	pyrene labeled EP-copolymer
Py_{free}	isolated pyrenes
Py-MSI	1-pyrenemethylsuccinimide
$PyNH_2$	1-pyrenemethylamine
Q	quencher
r_{EE}	end-to-end distance
R_o	Förster radius
S/N	signal to noise ratio
SA	succinic anhydride
SDS	sodium dodecyl sulfate
SI	succinimide
SM	semicrystalline
SPC	single photon counting
SS	steady-state
TCB	1,2,4-trichlorobenzen
TEA	triethylamine
TEPA	tetraethylenepentamine
TETA	triethylenetetramine
Tetralin	tetrahydronaphthalene
THF	tetrahydrofuran
UFP	ultrafine particle
UV-Vis	ultraviolet-visible spectroscopy
V_{coil}	volume of a polymer coil
V_h	hydrodynamic volume
VII	viscosity index improver

Chapter 1

Literature Review

This thesis describes how fluorescence can be applied to characterize fluorescently labeled polymers employed as engine oil additives. The first part of this chapter provides an introduction on oil additives focusing mostly on oil dispersants, pour point depressants (PPDs), and viscosity index improvers (VIIs) as well as a brief description of some of the experimental techniques used to characterize their properties. The second part of this chapter presents the fundamentals of fluorescence, some of the interesting features of the fluorescence spectra of pyrene-labeled macromolecules, a description of the different models used in the analysis of the fluorescence decays acquired with pyrene-labeled polymers, and the application of these concepts to study the behavior of fluorescently labeled macromolecules used as oil additives. The final section presents the thesis objectives and outlines the organization of this thesis.

1.1 Oil Additives

The main purpose of an engine oil is to create a lubricating layer between the moving parts of engines. Since a base oil alone cannot meet all requirements of an engine oil, performance-enhancing additives are purposely added to the oil formulation to improve engine efficiency and durability.[1,2] These additives include dispersants, detergents, viscosity index improvers (VIIs), pour point depressants (PPDs), antiwear agents, and antioxidants.[1] Oil additives vary in quantity depending on the specific requirements of an engine oil. The composition of a typical engine oil is shown in Table 1.1.

Table 1.1. Concentration of the main additives used in engine oil formulations (Salino and Volpi, 1978).[1]

Material	Weight (%)	Material	Weight (%)
Base Oil	71.5-96.2	Antioxidant/Wear	0.1-2.0
Metallic Detergent	2-10	Viscosity Index Improver	0.1-3.0
Ashless Dispersant	1-9	Pour Point Depressant	0.1-1.5

Dispersants represent the most important family of chemical additives found in engine oils and they have been used since the 1950s.[3-5] They work by dispersing oil-insoluble combustion by-products such as soot and sludge generated during the normal operation of the engine. Without dispersants, soot and sludge formation causes wear and filter plugging. Like dispersants, detergents have been used since the 1940's by the engine oil industry.[4] Detergents are polar organometallic oil soluble bases which can cling on-to the surface of particles. They are composed of an oil-soluble tail, called the substrate, and a negatively charged head group associated with a metal counterion. They serve two principal functions. First, they lift any deposits off the different surfaces of the engine due to their strong affinity toward these deposits while their oil-soluble tail maintains them in solution. Secondly, detergents neutralize any acids formed during oil combustion by chemically reacting with the acids in order to form harmless neutralized chemicals, thus reducing corrosion.[6]

Besides the deposits left on engine surfaces and the acids generated in the oil, another major chemical that is detrimental to the performance of oil is wax. The problem with any lubricating oil containing wax is that the wax crystallizes at very low temperatures, thus preventing the oil from flowing. Adding PPDs to the oil improves the low temperature properties of the oil by disrupting or preventing the formation of the waxy crystalline

network.[7,8] VIIs are another type of oil additives which are incorporated into the oil to reduce the inherent drop in viscosity that is observed with increasing temperature.[1] Without VIIs, the oil would be too thin at high temperatures to properly coat the engine parts, which would result in a loss of lubrication. At low temperatures, the oil would be too viscous to flow, thus failing to provide the protective lubrication necessary for the frictionless motion of the engine parts. In summary, VIIs are designed to counteract the reduction in oil viscosity observed at high engine temperatures without excessively increasing the viscosity of the oil at lower temperatures.

The presence of chemicals that deposit onto the engine surfaces or generate acids is usually the result of oxidation of the oil hydrocarbons from exposure to oxygen at high temperatures. Adding antioxidants has been shown to decrease the oxidation rate and prevent soot/sludge formation.[1] Finally, a last family of important oil additives consists of antiwear agents which form a protective coating on the metal surfaces of the engine parts and can have an antioxidant effect on the oil as well.[1] Organosulfur and organophosphorus compounds, such as organic polysulfides, phosphates, dithiophosphates, and dithiocarbamates are the most commonly used antiwear agents.[1,6] Among the long list of oil additives presented so far, PPDs, VIIs, and oil dispersants are the only additives that are polymeric in nature and they are discussed in more detail hereafter.

1.1.1 Pour Point Depressants (PPDs)

Two major problems are encountered with lubricating oils at very low temperatures. First, below a certain temperature, the engine oil can no longer flow freely. This temperature is known as the pour point. Secondly, any lubricating oils containing a small amount of wax forms crystalline networks at very low temperatures, which prevents the oil flow.[8,9] Even though most

of the wax is removed during base oil refining, a small amount of wax is required to remain in the oil to achieve the desired oil viscosity. These waxes are composed of asphaltenes which vary in molecular weight and chemical composition. Asphaltenes have a heterogeneous molecular structure with a distribution of aromatic nuclei. They readily aggregate to form colloidal particles, a process that increases the oil viscosity and the probability for wax crystallization.[10] In most cases, an engine generates sufficient shear to disrupt the wax network and allow the oil to flow. However, wax aggregation decreases the engine durability and lifetime, and is an important problem for cold start-up. PPDs are oil additives that ensure the free flow of oil and prevent the formation of waxy crystalline networks at low temperatures.[7-9] Adding small amounts of PPDs can lower the pour point temperature by up to 30 ^{o}C. The addition of PPDs does not prohibit crystallization but simply redirects the crystal growth patterns in a manner that results in the formation of smaller wax crystals.[11] For example, alkyl-substituted aromatic PPDs adsorb onto wax crystals to inhibit their growth while PPDs having a comb structure are designed to co-crystallize with wax crystals.[7] PPDs enable a smoother car start-up, decrease engine wear, and increase engine life.

There are a number of factors that must be considered when selecting a polymer to be used as a PPD. The primary requirement is that the polymer must be soluble in an engine oil over a wide range of temperatures that covers normal engine operation. Since the polymer solubility and its interactions with the oil and other oil additives are affected by temperature, the added polymer must remain compatible with the other species in the oil over the desired temperature range. The selected polymers also need to withstand the violent mechanical shear they are subjected to in the engine.[11,12] For example, high molecular weight polymers are more effective as PPDs but they are also less soluble. Furthermore, the shear generated by an engine

will cleave high molecular weight polymers resulting in the formation of lower molecular weight molecules. This means that when formulating a given PPD for a particular application, selection of a polymer having an appropriate molecular weight is necessary to ensure that the oil remains stable, even after going through numerous extreme temperature cycles.[8]

Different PPDs may be necessary for a same application as product specifications change over time. A list of the best known PPDs include: ethylene-based polyolefins with alkyl side chains,[7] vinyl-acetate copolymers,[11] poly(alkylphenol formaldehyde sulphonate)s,[13] hexa-triethanolamine oleate esters,[10] poly(alkyl methacrylate)s,[8] and copolymers of olefins and maleic anhydride that were post-modified with alcohols or alkyl amines to yield ester, amide, or succinimide functionalities.[14] Viscosity measurements, cross-polarized light microscopy, and differential scanning calorimetery (DSC) can be used to investigate the efficiency of PPDs.[10,11,12]

1.1.2 Oil Dispersants

Dispersants are designed to improve engine performance, decrease fuel consumption, and decrease pollution emission. The dispersants are used to disperse the oil-insoluble combustion by-products that circulate back into the engine oil and ensure that the oil flows freely. Sludge and soot are two of the most obvious by-products. Engine soot or ultrafine particles (UFPs) contain mostly carbon, and may contain hydrogen, oxygen, and traces of nitrogen, sulfur, and metals.[15] These particles, which are typically formed by the incomplete oxidation of fuel during ignition, are smaller than 100 nm in diameter and used to be released into the air with the exhaust gases.[16] Since releasing UFPs from engines into the air causes air pollution, governmental regulations were issued that aimed to reduce UFP emission.[17] To this end, car manufacturers circulate the exhaust gas back into the oil, a procedure that results in higher

concentrations of UFPs in the oil. In turn, increased UFP concentrations lead to UFP aggregation and increase in the viscosity of the oil. UFP aggregation is induced by the polar groups that are generated on their surface during engine operation. In apolar oil, UFPs aggregate into large particles (LPs, d_{LP} = ~1 μm) to minimize their surface exposure to the oil. LPs can cause sludge formation resulting in oil blockage and engine failure. Therefore, dispersants are added to the engine oil to prevent UFP aggregation and in turn sludge formation.[4]

Dispersants are typically composed of a polar head group and an oil-soluble apolar tail. Metallic and ashless dispersants are two types of commonly used oil additives.[4] The polar core of the dispersant is expected to adsorb onto the surface of the UFPs whereas the apolar tail stabilizes the particles in the oil. Dispersants can reduce UFPs aggregation via a steric or electrostatic mechanisms. Metal-containing dispersants have a good dispersancy capacity but the presence of metals can lead to the production of insoluble solids during engine operation. These solid precipitates actually add to the sludge problem. The other type of dispersant is referred to as ashless dispersants. Unlike metallic dispersants, ashless dispersants do not leave any ashes or deposits in the engine. The most common types of ashless dispersants are Mannich type, succinate ester, and succinimide dispersants (Figure 1.1).[4]

A)

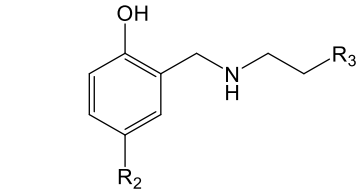

B)

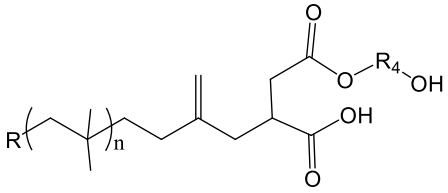

C)

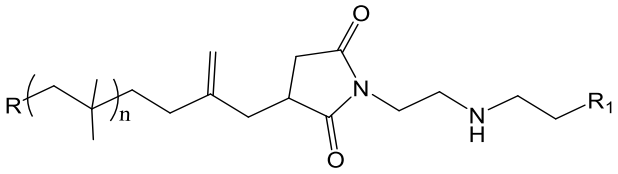

Figure 1.1. Chemical structure of A) Mannich type, B) succinate ester, and C) succinimide dispersants.

Mannich type dispersants (Figure 1.1A) are synthesized in the presence of alkylphenol, formaldehyde, and a polyamine.[4] The second group of ashless dispersants known as succinic esters are produced by the reaction of polyisobutylene terminated at one end with a succinic anhydride moiety (PIBSA) with alcohol (Figure 1.1B). The last and most common group of dispersants are the succinimide dispersants (Figure 1.1C). They were initially developed by Le Suer and Stuart in 1966.[18] The preparation of a polyisobutylene succinimide dispersant (PIBSI) begins by using cationic polymerization to generate a short PIB terminated by a double bond[19] followed by an Alder-ene reaction between the terminal double bond and maleic anhydride at high temperature to yield PIBSA. PIBSA can further react with a polyamine in a 1:1 or 1:2 polyamine:PIBSA ratio to produce *mono*-PIBSI (*m*-PIBSI) and *bis*-PIBSI (*b*-PIBSI) dispersants, respectively.[20,21,22]

In the case of PIBSI dispersants, increasing the number of secondary amines in the polyamine core results in stronger binding onto UFPs, but decreases the compatibility of PIBSI dispersants with other oil additives and engine parts. For example, engine seals play an important role in engine design because they prevent oil leakage. Fluoroelastomers are commonly used as engine seals, due to their good thermal stability and oxidation resistance. However, these materials are sensitive to the basicity of the oil due to dehydrofluorination.[4] The amines used to prepare the PIBSI dispersants make the oil more basic and consequently increase the probability of engine seal degradation. The basicity of the oil can be reduced through post-modification of the PIBSI-dispersants with ethylene carbonate or boric acid.[23,24] This discussion illustrates how the incorporation of oil dispersants into an engine oil formulation requires that numerous factors be carefully considered to allow optimal engine cleanliness while providing acceptable seal compatibility.

1.1.3 Viscosity Index Improvers

VIIs have been added to motor oils since the 1940s to reduce the decrease in viscosity experienced by a liquid subject to an increase in temperature. VIIs are polymers with high molecular weight, typically in the 50,000 to 500,000 $g.mol^{-1}$ range.[1,25] Without VIIs, the oil would be too thin at high temperature to properly coat the moving parts of the engine which would no longer be lubricated. At low temperatures, the oil would be too viscous to flow, which would prevent the motion of the engine parts. VIIs are designed to counteract the reduction in oil viscosity observed at high engine temperatures without excessively increasing the viscosity of the oil at lower temperatures. VIIs play an important role in increasing the oil performance by improving engine parts cleanliness and seal durability and better controlling deposits formation on engine surfaces and viscosity increase due to soot formation.

Semicrystalline polyolefins have been shown to be efficient VIIs. Crystalline sequences within a VII crystallize at low temperature and form dense crystalline microdomains resulting in polymer coils having small hydrodynamic volumes (V_h). Increasing the temperature melts the crystalline microdomains, allows the polymers to swell, and results in a higher V_h for the polymer coils. Since the viscosity of the solution depends on the volume fraction of the solution that is occupied by the polymer coils, expansion of the polymer coils leads to a viscosity increase as shown in Figure 1.2. Therefore, the decrease in engine oil viscosity with increasing temperature is moderated by the expansion of the polymer coil following the melting of the crystalline microdomains. The main consequence of these counteracting phenomena is that, the addition of a VII to an oil ensures that the engine oil viscosity does not change significantly as a function of temperature during the operation of the engine. Synthetic polymers, such as alkyl methacrylate copolymers, olefin copolymers, and hydrogenated styrene-diene copolymers have been used as VIIs.[1,2,26]

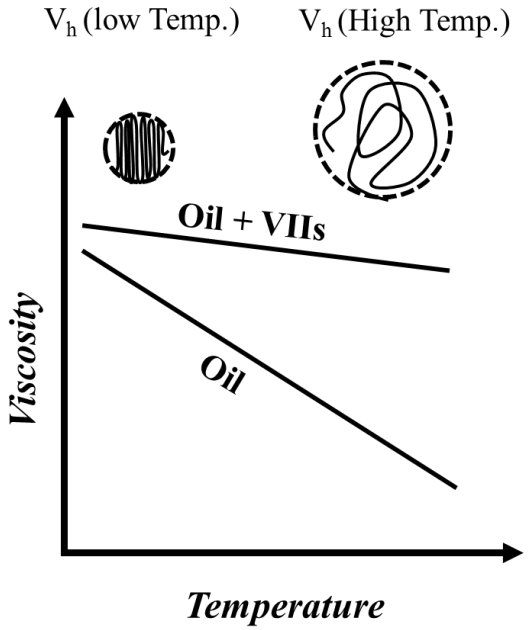

Figure 1.2. Expected change in oil viscosity in the absence and presence of VIIs.

1.2 Characterization of oil additives

The oil industry has been using different polymers as engine oil additives to make their oils perform consistently all year round under low and high temperature conditions. However, when these polymers are exposed to the extreme chemical and physical stresses encountered in an engine, chain cleavage can occur, causing partial or total loss of their functions. The durability of these polymeric additives depends on internal parameters such as the chemical structure and molar ratio of the co-monomers used to prepare a polyolefin, as well as on external factors such as engine type and operation temperature, to name but a few.

For example, the thickening experienced by a solution of VII or PPD increases with the molecular weight of the polymer. However higher molecular weight polymers are more sensitive to shear thinning and chain cleavage. Both effects result in a loss of lubrication at high temperature which causes higher friction and consequently greater damage to the engine, a not so desirable outcome. Consequently the optimal chain length for a polyolefin used as a VII or PPD requires balancing the detrimental effect of chain scission and shear thinning with the desirable effect of increased viscosity.

Depending on the application, the oil additives may need to be evaluated for their ability to provide dispersancy and oxidation stability, maintain a relatively constant oil viscosity at low and high temperatures, minimize chain cleavage under high shear and in the presence of other oil additives, and form lubricating films having a proper thickness. Over the years, several techniques have been applied to assess the effectiveness of these synthetic polymers as oil additives. These techniques include viscosity, cross-polarized light microscopy, light scattering (LS), carbon nuclear magnetic resonance (^{13}C NMR), Fourier transform infrared spectroscopy (FTIR), gel permeation chromatography (GPC), differential scanning calorimetry (DSC), and

fluorescence measurements.[1] Among all these characterization techniques, only fluorescence can be used to characterize the oil additives at the molecular level over a broad range of concentrations and temperatures. The fluorescence-based techniques employed to study macromolecules in solution are now described.

1.2.1 Fluorescence Study on Solutions of Fluorescently Labeled Polymers (FLPs)

Many of the techniques introduced so far have been used to characterize polymer chains in solution and the solid-state at the macroscopic and microscopic levels. Capillary viscometry, DSC, X-ray scattering, NMR, and atomic force microscopic (AFM) have been applied to the study of polyolefins.[27-29] Beside all these techniques, fluorescence can be used to characterize polymer chains at the molecular level both at high and low polymer concentrations.[30] Of particular interest, the highly sensitive fluorescence signal allows experiments to be performed on solution concentrations that are typically about 2 orders of magnitude lower than those needed by any other technique.[31]

Fluorescence is a photophysical phenomenon whereby the absorption of electromagnetic radiation by a chromophore is followed by the emission of light at longer wavelengths.[32] An energy diagram of this phenomenon is shown in Figure 1.3. For fluorescence to occur, a molecule must absorb a photon and be promoted from its ground state to an excited vibrational state of a higher electronic state. Then the excited molecule rapidly relaxes via internal conversion to the lowest vibrational level of the first electronic excited state S_1 as shown by the dashed arrow. At this stage two electronic transitions are possible. The first, also referred to as fluorescence, occurs when an excited electron emits without changing its spin. The second transition not shown in Figure 1.3 is observed when the excited electron changes its spin to occupy a lower energy level called a triplet state. Relaxation of the electron from the

triplet state to the ground state is accompanied by the emission of a photon in a process that is referred to as phosphorescence. Whether through fluorescence or phosphorescence, the emitted photon has a lower energy than the absorbed photon. Although the lifetime of the excited state is very short, it is long enough to allow the acquisition of a time-resolved fluorescence or phosphorescence decay. Some of the different fluorescence phenomena that are applied to study polymers include excimer formation,[31] fluorescence resonance energy transfer (FRET),[31] fluorescence anisotropy (FA),[33] and fluorescence dynamic quenching (FDQ).[34-36] Fluorescence excimer formation is discussed in more detail hereafter.

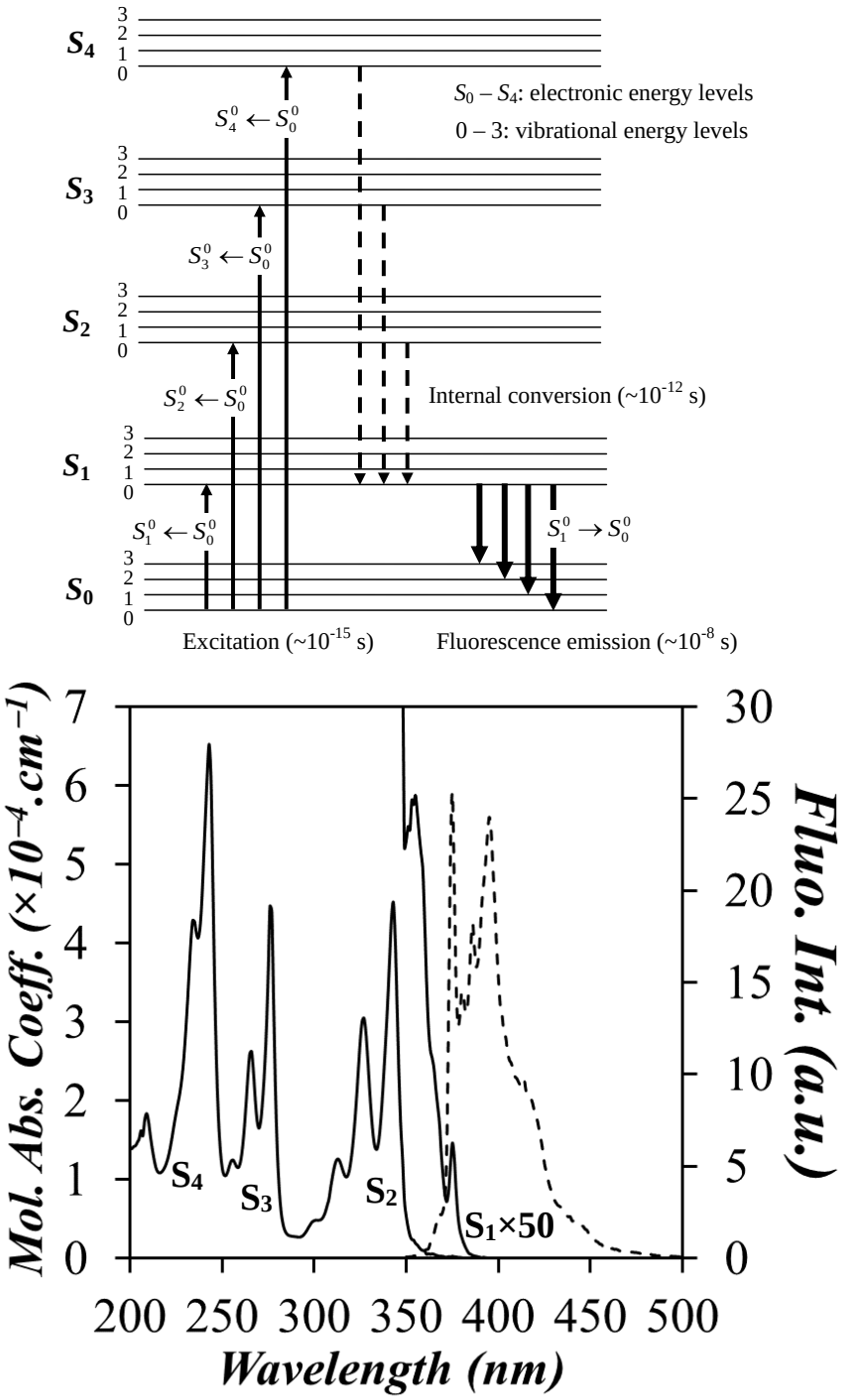

Figure 1.3. Jablonsky diagram (top) and corresponding transitions (bottom) found in the absorption (—) and fluorescence emission (- - -) spectra of 1-pyrenemethylsuccinimide (Py-MSI) in THF. ([Py-MSI] = 3.6×10^{-5} and λ_{ex} = 343 nm for the emission spectrum)

Most polymers do not fluoresce and they need to be fluorescently labeled. The fluorescent label is covalently attached wherever reactive groups can be found on the macromolecule, typically at the chain ends or randomly along the backbone. Pyrene, naphthalene, and succinimide are some of the fluorophores that have been used to study fluorescently labeled polyolefins but the bulk of the studies so far has been conducted with the dye pyrene. Consequently, the properties of pyrene are described in more details in this section.

1.2.1.1 Pyrene Labeled Polymers

In many ways, pyrene can be viewed as an ideal chromophore. It has a long-lived excited state that provides a wide temporal window to probe the internal dynamics of macromolecules in solution, a large molar absorbance coefficient and fluorescence quantum yield that enable its detection at extremely low concentration, and a fluorescence spectrum that is sensitive to its microenvironment.[37-39] Furthermore an excited pyrene can also form an excimer upon encounter with a ground state pyrene. The photophysical processes that lead to the fluorescence of pyrene are well described by the Jablonsky diagram shown in Figure 1.3. Its implications for the absorption and fluorescence spectra of the dye are illustrated with 1-pyrenemethylsuccinimide (Py-MSI) in tetrahydrofuran (THF). The absorption spectrum of Py-MSI is composed of several strong absorbance bands at 243, 276, and 343 nm and a much weaker band at 375 nm. These transitions represent the excitation of pyrene from the ground state S_0^0 to the lowest vibrational energy level of the higher electronic energy levels S_4^0, S_3^0, S_2^0, and S_1^0, respectively. The $S_0^0 \rightarrow S_1^0$ band is very weak since this transition is symmetry forbidden in the case of pyrene.[40]

In order to select a suitable wavelength to excite pyrene, one needs to consider the range of wavelengths where pyrene has a large molar absorption coefficient to allow its efficient excitation while avoiding the shorter wavelengths where many solvents and impurities might

absorb. Based on the absorption spectrum shown in Figure 1.3, pyrene is usually excited at wavelengths between 334 and 345 nm depending on the pyrene derivative and the solvent being used. The excited pyrene can then either fluoresce with its natural lifetime as a monomer (τ_M) between 370 and 425 nm, or diffusionally encounter a ground state pyrene with a rate constant k_1 to form an excimer species which fluoresces between 425 and 600 nm.[38] Excimer formation can be described by Birks' Scheme as shown in Scheme 1.1 where τ_M and τ_E are the lifetimes of the excited pyrene monomer and excimer, respectively, and k_1 and k_{-1} are the rate constants of excimer formation and dissociation, respectively.

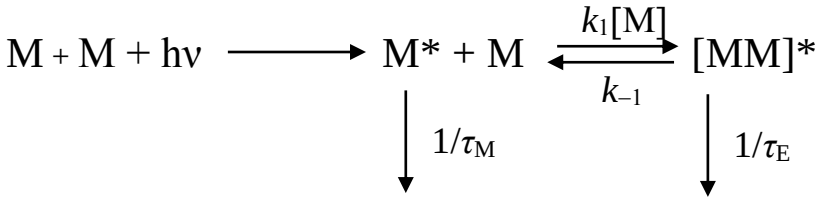

Scheme 1.1. Birks' scheme describing pyrene excimer formation.

Pyrene has been widely used as a fluorescent probe to investigate polymer chain and side chain dynamics and inter- and intramolecular interactions between and within polymers.[30,31,41,42] Inter- and intramolecular polymeric interactions have been characterized by probing the process of excimer formation between pyrene labels covalently attached onto a polymer. Pyrene excimer formation has been found to depend on the chemical structure of the polymeric backbone, the solvent quality toward the polymer, and the solvent viscosity.[30,42-45]

The steady-state fluorescence spectrum of a pyrene labeled EP copolymer (Py-EP) is shown in Figure 1.4. The excited pyrene monomer emission is characterized by several sharp peaks between 360 and 425 nm whereas the pyrene excimer emission features a broad and structureless band in the 440–600 nm wavelength range. Qualitative information on the extent

of excimer formation can be obtained from the ratio of the fluorescence intensity of the excimer (I_E) over that of the monomer (I_M) in the steady-state fluorescence spectrum. In the case of the spectrum shown in Figure 1.4, I_M and I_E are calculated by integrating the fluorescence spectrum over the wavelengths 372–379 nm and 500–530 nm, respectively. The wavelength range chosen to calculate I_E, which is slightly shifted from the excimer maximum at 480 nm, and I_M are selected to minimize any possible interference between the fluorescence spectra of the two fluorescent species.

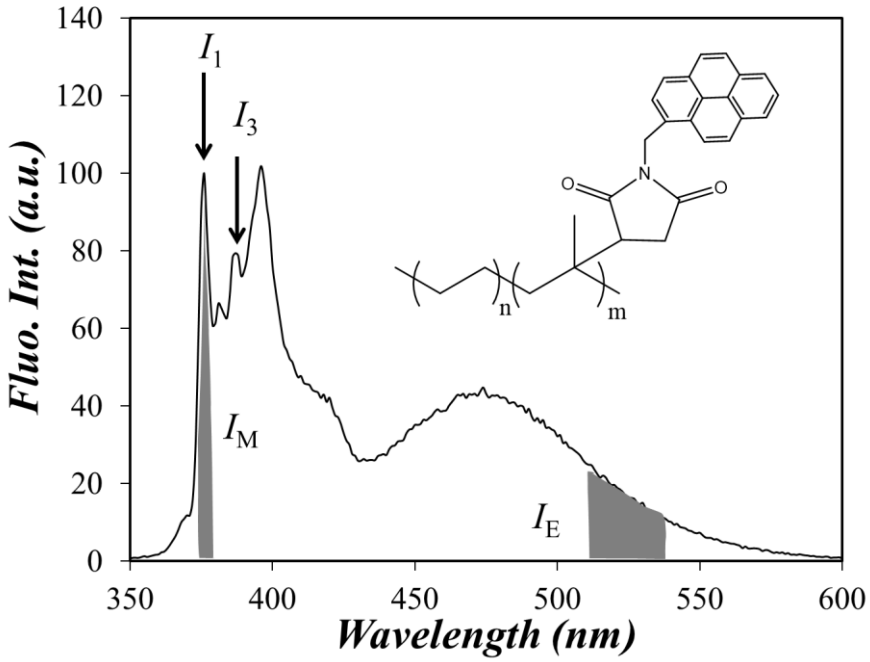

Figure 1.4. Steady-state fluorescence spectrum of a pyrene labeled amorphous EP copolymer in toluene. (λ_{ex} = 344 nm, Conc.: 0.1 g.L^{-1}, λ_{py} = 108 µmol/g of polymer)

Information about the polarity of the medium surrounding pyrene can also be retrieved from the steady-state fluorescence spectrum. This information can be determined by calculating the ratio of the fluorescence intensity of the first (I_1) to the third (I_3) peak. The I_1/I_3 ratio is

larger for pyrene in polar solvents such as water and lower for pyrene in non-polar solvents like hexane.[46]

1.2.2 Modeling the Kinetics of Pyrene Excimer Formation

The first quantitative analysis of the monomer and excimer fluorescence decays of molecular pyrene in organic solvent was successfully conducted in 1963 by Birks.[47] This analysis was then adapted by Winnik in 1980 to describe the kinetics of pyrene excimer formation for a series of pyrene end-labeled monodisperse polystyrenes, and was then expanded to characterize the rate constant of end-to-end cyclization (EEC) for different polymeric backbones.[48,49] Birks' scheme used to characterize the EEC kinetics of pyrene end-labeled monodisperse chains could not be applied to pyrene-labeled macromolecules that formed excimer with multiple rate constants. Therefore developing a new model was essential. In 1999, the Fluorescence Blob Model (FBM) was introduced by Duhamel to deal with the complex kinetics of excimer formation encountered with polymers randomly labeled with pyrene.[36] Although the FBM can handle considerably complex fluorescence decays, it does not apply to polymer samples which are not randomly labeled such as pyrene end-labeled dendrimers. To address this analytical gap, the Model Free Analysis (MFA) was introduced in 2005 to provide quantitative information about the kinetics of excimer formation for any type of fluorescently-labeled macromolecules where the dye and the product of the quenching reaction yield two distinct emissions.[50] Birks' scheme, FBM, and the MFA are briefly described hereafter.

1.2.2.1 Birks' Scheme

Birks' Scheme was first introduced in 1963 to study excimer formation in solutions of molecularly dissolved pyrene and was then adopted in 1980 to describe excimer formation between an excited and a ground state pyrene covalently attached to the ends of a monodisperse

polystyrene.[47] As shown in Scheme 1.2, the excited monomer can either fluoresce with its natural lifetime, τ_M, or it can diffusionally encounter a ground state monomer to form an excimer which fluoresces with its natural lifetime τ_{E0}. In Scheme 1.2, $<k_1>$ and k_{-1} are the rate constants for diffusional formation and dissociation of the excimer, respectively. At low temperatures (T < 35 °C), k_{-1} for pyrene is smaller than the excimer radiative rate constant ($k_E = 1/\tau_{E0}$) due to the strong excimer binding energy that is induced by the four aromatic rings constituting the chromophore.[48]

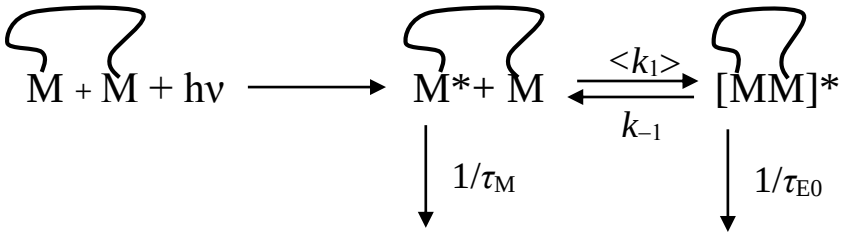

Scheme 1.2. Modified Birks' Scheme applied to pyrene end-labeled polymer chains.

The pseudo-unimolecular rate constant $<k_1>$, which is used to describe the excimer formation that occurs intramolecularly between two monomers attached to the chain ends of the polymer can be expressed by Equation 1.1,

$$<k_1> = k_1 \times [M]_{loc} \qquad (1.1)$$

where $[M]_{loc}$ is the local monomer concentration in the polymer coils and k_1 is the bimolecular rate constant for diffusive encounters. The expression for the time-dependent concentrations of the excited monomer [*M**] and excimer [*E**] derived from Scheme 1.2 are shown in Equations 1.2 and 1.3, respectively.

$$[M^*]_{(t)} = \frac{[Py^*_{diff}]_o}{\sqrt{(X-Y)^2 + 4 < k_1 > k_{-1}}} \left((X - \tau_2^{-1}) \times \exp(-t/\tau_1) - (X - \tau_1^{-1}) \times \exp(-t/\tau_2) \right) + [Py^*_{free}]_0 \exp(-t/\tau_M)$$

(1.2)

$$[E^*]_{(t)} = \frac{k_1 [Py^*]_o}{\sqrt{(X-Y)^2 + 4 < k >_1 k_{-1}}} \left(-\exp(-t/\tau_1) + \exp(-t/\tau_2) \right) \quad (1.3)$$

In the above equations, $[Py^*_{diff}]_o$ and $[Py^*_{free}]_o$ represent the initial concentrations of those pyrenes that form an excimer by diffusion and that never form an excimer, respectively. The parameters X and Y equal $<k_1> + \tau_M^{-1}$ and $k_{-1} + \tau_{E0}^{-1}$, respectively, and the expressions for the decay times τ_1 and τ_2 are given in Equations 1.4 and 1.5, respectively.

$$\tau_1^{-1} = \frac{X + Y + \sqrt{(X-Y)^2 + 4 < k_1 > k_{-1}}}{2} \quad (1.4)$$

$$\tau_2^{-1} = \frac{X + Y - \sqrt{(X-Y)^2 + 4 < k_1 > k_{-1}}}{2} \quad (1.5)$$

Birks' Scheme can only be applied when excimer formation is described by a single rate constant, a condition most likely to be obeyed when the excimer-forming chromophore is covalently attached to the ends of a monodisperse polymer.[34,35,39,48,51] Unfortunately, labeling a macromolecule at two specific positions separated by a constant chain length is a synthetic challenge. Consequently, new approaches needed to be developed in order to probe the novel macromolecular architectures that were enabled over the years by new advances in polymer synthesis.

1.2.2.2 Fluorescence Blob Model (FBM)

T he FBM was first established in 1999 as a means to describe quantitatively the chain dynamics of polymers randomly labeled with a dye capable of forming an excimer.[36] The FBM can be used to describe the kinetics of encounter between an excited dye and its quencher, both randomly attached onto a macromolecule, where quenching occurs on contact and the product of the quenching process does not revert back to the excited dye and quencher. Pyrene excimer formation, with its negligible dissociation rate constant at temperatures lower than 35 ^{o}C, fulfills these conditions. In the case of pyrene excimer formation, the excited dye and quencher would be an excited and a ground state pyrene monomer, respectively. Since the labeling is random, any two dye and quencher along the polymer are separated by different chain lengths so that quenching takes place according to a distribution of rate constants. However since an excited dye can only probe a finite volume within the polymer coil referred to as a *blob*, the *blob* can be used as a unit volume to divide the polymer coil into a cluster of *blobs* among which the randomly attached dyes and quenchers distribute themselves according to a Poisson distribution. Inside a *blob*, two monomer units bearing an excited dye and a quencher diffuse slowly with a rate constant k_{blob} to bring the two labels within a distance where they can rearrange quickly into a conformation conducive of efficient quenching with a large rate constant k_2. An interesting feature about pyrene is that, since pyrene acts as both the dye and quencher, a single labeling step is required to prepare the polymer. In the case of pyrene, the monomer and excimer fluoresce with a lifetime τ_M and τ_{E0}, respectively. Some poorly stacked pyrenes form long-lived excimers that emit with a lifetime τ_{EL}. A description of the different pyrene species encountered along the chain is shown in Scheme 1.3.

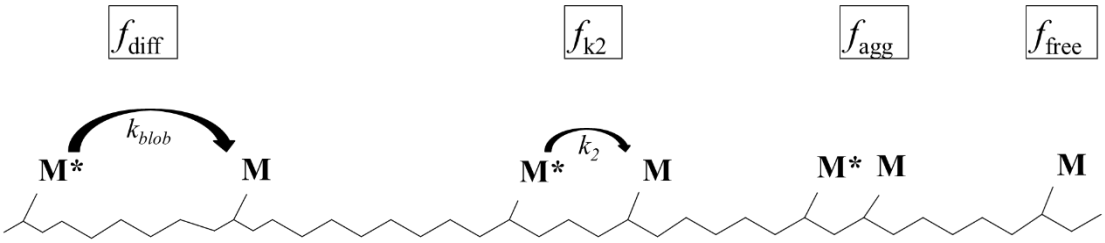

Scheme 1.3. Illustration of the different pyrene species that are generated along the polymer chain.

Scheme 1.3 describes the four distinct fluorescent species that are encountered along a chain randomly labeled with pyrene. The region to the right represents those pyrenes that are isolated and cannot form excimer within the lifetime of the pyrene monomer (τ_M). These isolated pyrenes are referred to as Py_{free}. They behave in the same manner as if they were not attached to the polymer and they represent a molar fraction f_{free} of the total pyrene population. In the region to the left, slow diffusive backbone motions bring an excited and a ground state pyrene monomer in close proximity with a rate constant k_{blob}. These pyrenes undergoing diffusive motions are referred to as Py_{diff} and they represent a molar fraction f_{diff} of the total pyrene population. The pyrenes that are in close proximity and need to rearrange quickly with a rate constant k_2 to form an excimer are referred to as Py_{k2}. They represent a molar fraction f_{k2} of the total pyrene concentration. Finally, pyrenes attached next to each other along the chain have a high probability of forming ground state pyrene aggregates that can be excited directly to form an excimer. These aggregated pyrenes are identified according to whether they are made of pyrenes (*E*0) that are properly stacked and yield an excimer that emits with a lifetime τ_{E0} or pyrenes (*EL*) that are improperly stacked and emit with a long lifetime τ_{EL}. The molar fractions f_{E0} and f_{EL} represent the aggregated pyrene molecules that are present as *E*0 and *EL* species,

respectively. The sum $f_{E0}+f_{EL}$ is taken as the molar fraction f_{agg} representing all aggregated pyrene species (Py_{agg}).

The kinetics of excimer formation between the pyrene species shown in Scheme 1.3 can be described by Scheme 1.4. The different reaction path-ways presented in Scheme 1.3 could be used to derive Equations 1.6 and 1.7 employed in the fit of the monomer and excimer fluorescence decays according to the FBM.

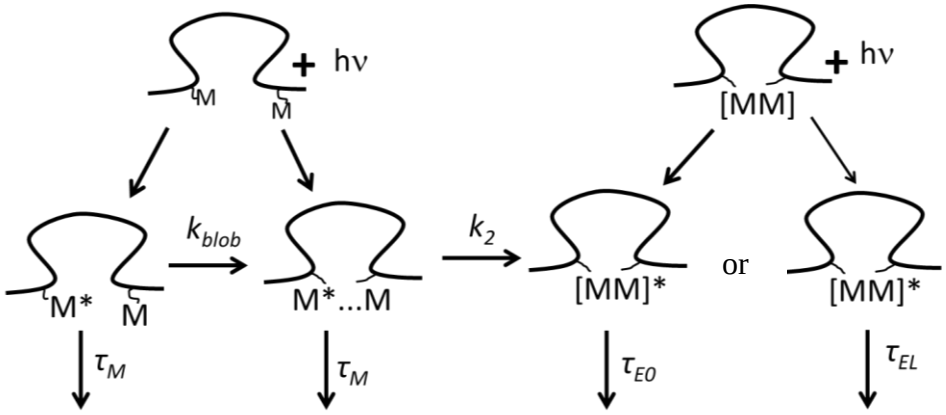

Scheme 1.4. Excimer formation between pyrenes randomly attached onto a polymer.

$$[M^*]_{(t)} = [Py^*_{diff}]_{(t)} + [Py^*_{k2}]_{(t)} = [Py^*_{diff}]_o \exp\left(-\left(A_2 + \frac{1}{\tau_M}\right)t - A_3\left(1-\exp(-A_4 t)\right)\right)$$

$$+\left([Py^*_{k2}]_o + [Py^*_{diff}]_o e^{-A_3} \sum_{i=0}^{\infty} \frac{A_3^i}{i!} \frac{A_2 + iA_4}{A_2 + iA_4 - k_2}\right) \exp\left(-\left(k_2 + \frac{1}{\tau_M}\right)t\right)$$

$$-[Py^*_{diff}]_o e^{-A_3} \sum_{i=0}^{\infty} \frac{A_3^i}{i!} \frac{A_2 + iA_4}{A_2 + iA_4 - k_2} \exp\left(-\left(A_2 + iA_4 + \frac{1}{\tau_M}\right)t\right) \qquad (1.6)$$

$$[E^*]_{(t)} = k_2\left(\left([Py^*_{k2}]_o + [Py^*_{diff}]_o e^{-A_3}\sum_{i=0}^{\infty}\frac{A_3^i}{i!}\frac{A_2+iA_4}{A_2+iA_4-k_2}\right)\times\frac{\exp\left(-\frac{t}{\tau_{E0}}\right)-\exp\left(-\left(k_2+\frac{1}{\tau_M}\right)t\right)}{k_2+\frac{1}{\tau_M}-\frac{1}{\tau_{E0}}}\right.$$

$$\left.+[Py^*_{diff}]_o e^{-A_3}\sum_{i=0}^{\infty}\frac{A_3^i}{i!}\frac{A_2+iA_4}{A_2+iA_4-k_2}\frac{\exp\left(-\left(A_2+iA_4+\frac{1}{\tau_M}\right)t\right)-\exp\left(-\frac{t}{\tau_{E0}}\right)}{A_2+iA_4+\frac{1}{\tau_M}-\frac{1}{\tau_{E0}}}\right)$$

$$+[E0^*]_o\times\exp\left(-\frac{t}{\tau_{E0}}\right) \qquad (1.7)$$

The parameters A_2, A_3, and A_4 used in Equations 1.6 and 1.7 are given in Equation 1.8.

$$A_2 = < n > \frac{k_{blob}k_e[blob]}{k_{blob}+k_e[blob]} \qquad A_3 = < n > \frac{k_{blob}^2}{\left(k_{blob}+k_e[blob]\right)^2}$$

$$A_4 = k_{blob}+k_e[blob] \qquad (1.8)$$

In these equations, $<n>$ is the average number of ground state pyrenes per *blob* and $k_e\times[blob]$ is the product of the exchange rate constant k_e of ground-state pyrenes exchanging between *blobs* and [*blob*] is the local concentration of *blobs* inside the polymer coil.

To date, the FBM has been applied to the characterization of linear chains randomly labeled with pyrene.[30,36] It has been shown to yield the same quantitative information about the internal dynamics of linear chains as the information obtained with the Birks' scheme analysis of short end-labeled monodisperse polymers.[52,53] It is currently the only analytical tool capable

of probing the internal dynamics of long polydisperse chains and it is thus particularly well-suited to characterize VIIs used in the oil-additive industry.

1.2.2.3 Model Free Analysis (MFA)

The MFA was designed to deal with any type of macromolecular architecture including cases where neither Birks' scheme nor the FBM apply to describe excimer formation between pyrene labels covalently attached to a macromolecule.[50] Examples of such cases include dendrimers whose ends are labeled with pyrene, and polymeric bottle brushes whose side chains are terminated by a pyrene label.[39] In these examples the fluorescently-labeled macromolecules are neither randomly labeled with pyrene nor linear monodisperse chains terminated at both ends with a pyrene label. The MFA enables the experimentalist to study macromolecules where the chromophores can be attached at more than two specific positions, and which are not randomly distributed within the macromolecule.[54] According to the framework of the MFA, the macromolecule is viewed as a structureless object that can morph into different conformations with a time-dependent rate constant $f(t)$ as shown in Scheme 1.5.

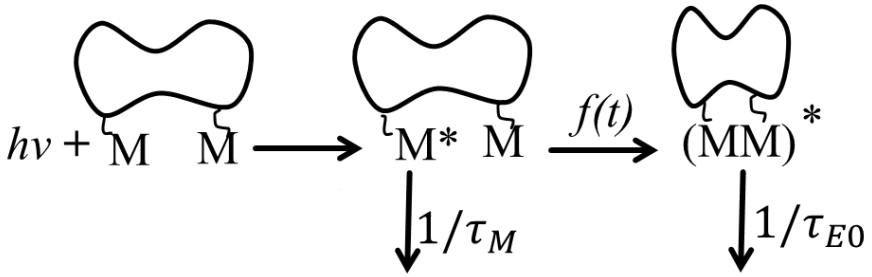

Scheme 1.5. Excimer formation between pyrene groups covalently attached onto a macromolecule according to the MFA.

In the MFA, no assumption is made about the mathematical form of the rate of excimer formation. Instead the monomer decay is fitted with a sum of exponentials as shown in Equation 1.9 and Scheme 1.5 is used to express the excimer concentration as shown in Equation 1.10.

$$[M^*_{diff}]_{(t)} = [Py^*_{diff}]_o \times \sum_{i=1}^{n} a_i \times \exp(-t/\tau_i) + [Py^*_{free}]\exp(-t/\tau_M) \tag{1.9}$$

$$[E0^*]_{(t)} = -[Py^*_{diff}]_o \times \sum_{i=1}^{n} a_i \times \frac{\frac{1}{\tau_i} - \frac{1}{\tau_M}}{\frac{1}{\tau_i} - \frac{1}{\tau_{E0}}} \times \exp(-t/\tau_i) + \left([E0^*]_o + [Py^*_{diff}]_o \times \sum_{i=1}^{n} a_i \times \frac{\frac{1}{\tau_i} - \frac{1}{\tau_M}}{\frac{1}{\tau_i} - \frac{1}{\tau_{E0}}} \right)$$

$$\times \exp(-t/\tau_{E0}) + [EL^*]_o \exp(-t/\tau_{EL}) \tag{1.10}$$

In Equations 1.9 and 1.10, a_i and τ_i represent the amplitude and decay time of the i^{th} exponential, respectively, and n represents the number of exponentials used to fit the monomer decays. The average rate constant of excimer formation, $<k>$, can be determined from the parameters retrieved from the MFA and its expression is given by Equation 1.11,

$$<k> = \frac{1}{<\tau>} - \frac{1}{\tau_M} \tag{1.11}$$

where $<\tau>$ represents the number-average lifetime of the Py^*_{diff} species in solution whose expression is given by Equation 1.12.

$$< \tau >= \frac{\sum_{i=1}^{n} a_i \tau_i}{\sum_{i=1}^{n} a_i} \qquad (1.12)$$

As for the FBM, the quantities $[Py^*_{diff}]_o$, $[Py^*_{free}]_o$, $[E0^*]_o$, and $[EL^*]_o$ can be used to determine the molar fractions f_{diff}, f_{free}, f_{E0}, and f_{EL}, respectively. To this date, the MFA has been applied to the broadest range of macromolecular architectures that has ever been studied with pyrene excimer fluorescence.[55] One interesting feature of the global analysis of monomer and excimer fluorescence decays according to the MFA or FBM is that these analyses can retrieve quantitatively the amount of unreacted pyrene derivatives left after the synthesis of the pyrene labeled macromolecules. Another important feature of the MFA is the ability to calculate the absolute fluorescence intensities I_M and I_E using the parameters retrieved from the MFA of the time-resolved fluorescence decays. The I_E/I_M ratios obtained from the MFA represent absolute quantities and therefore, can be directly compared between different laboratories.

1.2.3 Applications

Inspired by the development spearheaded by the Winnik group in Toronto of applications based on the use of pyrene excimer fluorescence to probe polymer behaviour in solution, Jao then at Texaco led a team of researchers who pyrene-labeled an EP copolymer to monitor its behaviour in solution by using fluorescence.[44] Being familiar with the chemistry employed to prepare the dispersants used in the oil additive industry, they maleated the EP copolymer and reacted the succinic anhydride groups with 1-pyrenebutyrylhydrazine (PBH). In 1992, they reported the first example of fluorescence spectra acquired with a Py-EP in two apolar solvents, namely methylcyclohexane and tetrahydronaphthalene (tetralin).[44] One interesting feature about the

PBH-EP copolymer was that the remaining hydrazine proton could H-bond with carbonyls (see Figure 1.5). The concentration regime where pyrene excimer formation occurred intramolecularly was determined from the sharp breakpoint in a plot of I_E/I_M versus polymer concentration. After correcting for the different viscosities of methylcyclohexane (η = 0.68 mPa.s at 25 ^oC) and tetralin (η = 2.02 mPa.s at 25 ^oC), the product $\eta \times (I_E/I_M)$ was found to be twice larger in tetralin than in methylcyclohexane. Such a result would typically indicate that $[Py]_{loc}$ was much larger in tetraline than in methylcyclohexane, except that the authors also reported a distortion in the fluorescence spectra whereby the monomer emission at 375 nm was substantially reduced in tetralin compared to methylcyclohexane. Thus, the increase in $\eta \times (I_E/I_M)$ might simply have been a consequence of the lower I_M value at 375 nm obtained in tetralin for this Py-EP sample.

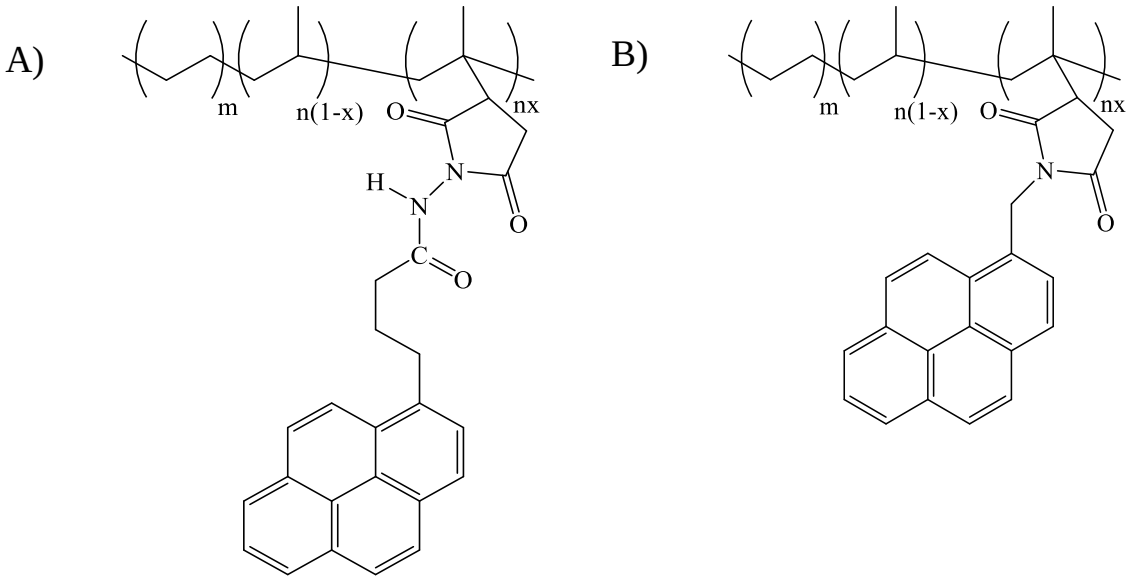

Figure 1.5. Chemical structure of the maleated EP copolymers reacted with A) 1−pyrenebutyrylhydrazine and B) 1-pyrenemethylamine.

Following this early study, research on the behaviour of Py-EPs in solution was taken on by the Winnik and Fendler laboratories in Toronto and Syracuse, respectively. This work led to two important observations. The first and most important result was that the spacers shown in Figure 1.5 and used to covalently attach pyrene to the EP backbone promoted strong interactions in apolar hydrocarbons like hexane or methylcyclohexane. Starting with an amorphous EP copolymer containing 60 mol% ethylene that was maleated and reacted with 1-pyrenemethylamine (PMA) to yield PMA-EP, Nemeth et al. measured the hydrodynamic diameter (D_h) of this Py-EP sample as a function of polymer concentration.[56] In apolar hexane ($\varepsilon = 1.89$), D_h showed a dramatic increase with polymer concentration while the increase was much less pronounced in more polar THF ($\varepsilon = 7.5$). The level of pyrene aggregation obtained by measuring the peak-to-valley ratio or P_A value in the absorption spectra also confirmed that pyrene aggregation was strong for PMA-EP in hexane but practically absent in THF.[57] Similar observations were made by Jao et al. by comparing the excitation and emission fluorescence spectra and the rise time in excimer fluorescence decays of a PBH-EP sample in apolar methylcyclohexane and THF.[58] The excitation spectra of PBH-EP were red-shifted in methylcyclohexane but showed hardly any shift in THF. Changing the excitation wavelength from 340 nm where the pyrene monomers absorb to 350 nm where the pyrene aggregates mostly absorb led to a more than two-fold increase in the I_E/I_M ratio in methylcyclohexane, whereas a similar shift in excitation wavelength changed the I_E/I_M ratio by less than 10% in THF. The excimer decays of the PBH-EP sample showed a pronounced rise time of 5.4 ns and 17.2 ns in methylcyclohexane and in THF, respectively. The short rise time in methylcyclohexane indicated that the pyrene groups leading to excimer formation where much closer to each other

than in THF. All these observations[56,58] supported the claim that apolar aliphatic solvents induced strong pyrene aggregation for both PMA-EP and PBH-EP. The second conclusion of these early studies was that the simple models describing the kinetics of excimer formation between pyrene labels attached at the two ends of a monodisperse chain did not apply to Py-EPs in solution and that quantitative analysis of the monomer and excimer fluorescence decays acquired with the Py-EP samples required a re-think of the models used to fit the fluorescence decays. The inadequacy of these early fitting routines was routed in the fact that the Py-EP copolymers did not have a narrow molecular weight distribution and that their labeling followed the distribution of succinic anhydride pendants generated during the maleation of the EP sample. Since excimer formation between two pyrene labels separated by a given chain length (L) is well-described by a single rate constant $k_{ex}(L)$, the random attachment of pyrene labels onto an EP copolymer resulted in a distribution of chain lengths L_i separating every two pyrenes, and thus a distribution of rate constants $k_{ex}(L_i)$ for excimer formation. Considering that all the models dealing with pyrene excimer formation could take into account no more than two rate constants of excimer formation due to resolution issues in the analysis of multiexponential fluorescence decays, a wide gap needed to be bridged to conduct a quantitative analysis of the fluorescence decays acquired with Py-EPs.[59]

The first attempt to quantitatively analyze the fluorescence decays of a PBH-EP in solution took advantage of the resemblance of the monomer decays with those obtained for molecular pyrene dissolved in sodium dodecyl sulfate (SDS) micelles.[60] Assuming that an excited pyrene can only diffuse within a small sub-volume of the polymer coil referred to as a *blob* while it remains excited, the polymer coil can be viewed as a cluster of *blobs* where the pyrene labels distribute themselves randomly according to a Poisson distribution. The kinetics

of pyrene excimer formation could then be handled in the same manner as for pyrene dissolved in surfactant micelles, and this analysis model was called the Fluorescence Blob Model (FBM). In this first application of the FBM, the exchange of ground state pyrenes between *blobs* was neglected. The fit of the fluorescence decays of PBH-EP in THF and in methylcyclohexane was satisfactory but showed some imperfections in the residuals and autocorrelation function of the residuals. The reason for these imperfections was attributed to the fact that this early version of the FBM did not account for the exchange of pyrenes among *blobs*. This feature was added later on to the analysis programs based on the FBM.[36,39]

The existence of a distribution of rate constants $k_{ex}(L_i)$ for pyrene excimer formation was duly recognized by Nemeth et al., who proposed a mathematical framework based on the use of a binomial function to handle the $k_{ex}(L_i)$ distribution of a Py-EP sample.[61] However while the FBM could be expressed by a relatively simple mathematical equation that could be applied to fit the fluorescence decays, no such expression was derived for the binomial function. Instead, the authors fitted the decays with a sum of three exponentials, and used the contribution to the fluorescence decays of those excited monomers that did not form excimer and emitted with their natural lifetime $\tau_{M,}$ to find the probability that a backbone unit be labeled with pyrene. The recovered probability was reasonable, but the study did not provide much additional information in terms of description of polymer chain dynamics. Furthermore, the absence of a mathematical equation to fit the entire fluorescence decays meant that the validity of the binomial distribution of rate constants for pyrene excimer formation still remained to be demonstrated. To this date, the FBM provides the only mathematical equation that can be used to fit globally the fluorescence decays of the pyrene monomer and excimer of randomly labeled macromolecules.[39]

The first global FBM analysis of the monomer and excimer fluorescence decays acquired with a PBH-EP sample in THF and hexane was attempted in 1999. Despite the addition of exchange of pyrene labels between *blobs*, the fits of the decays were poor in hexane showing strong deviations in the residuals at the early times. These deviations were attributed to the presence of pyrene aggregates where excimer formation occurred on a fast time scale. This observation led to the proposal that excimer formation took place as a sequence of two successive steps. Molecularly separated pyrene labels would diffuse slowly toward each other in the first step controlled by a rate constant k_{blob}, but their encounter would be driven by the polar linker which would lead to the aggregation of the pyrene labels resulting in their efficient excimer formation with a large rate constant k_2 ($k_2 >> k_{blob}$) in a second step. This sequential approach for the process of excimer formation in solutions of PBH-EP proved highly successful resulting in excellent decay fits.[62] In these experiments, k_2 and k_{blob} were found to equal 2.1 (± 0.2) $\times 10^8$ s^{-1} and 2.1 (± 0.4) $\times 10^7$ s^{-1}, respectively. Most importantly, the molar fraction (f_{agg}) of aggregated pyrenes could be determined quantitatively and was found to equal 0.57 (± 0.05) in hexane.

The studies of pyrene excimer formation in Py-EP solutions resulted in two important outcomes for the modeling of pyrene excimer formation. The first was the introduction of the FBM that provided a new means to handle the complex distribution of rate constants for excimer formation in randomly labeled polymers. The second was the realization that excimer formation between pyrene labels attached onto a macromolecule takes place in a sequential manner with a first slow diffusive step controlled by backbone motion that brings the two pyrenes close to each other followed by a rapid rearrangement of the pyrene labels to form an excimer. The validity of these concepts was further confirmed by studying pyrene excimer

formation for oligoisobutylenes terminated at one end with a succininic anhydride unit (PIBSA) and labeled with either PBH or PMA to yield PBH-PIBSA and PMA-PIBSA, respectively.[63] In these experiments, the slow diffusive process taking place in solution to bring the terminal pyrenyl groups into contact could be approximated by a single rate constant, which represented a major simplification as compared to the distribution of rate constants that needed to be handled for solutions of Py-EP copolymers. The molar fraction of aggregated pyrenes was determined quantitatively and is shown in Figure 1.6 as a function of pyrene concentration. The effect that the H-bonding capability of PBH-PIBSA has on its intermolecular association in hexane is clearly illustrated in Figure 1.6 where f_{agg} remains larger than 0.6 over the entire concentration range studied. PMA-PIBSA was found to aggregate also in hexane, but to a much lesser extent than PBH-PIBSA, since its succinimide group could not H-bond. In the case of PMA-EP in hexane, interactions between the pyrene groups are believed to be induced by the polar succinimide groups. In THF, little aggregation took place and the linker connecting pyrene to the EP backbone showed no effect on aggregation. The non-zero f_{agg} value obtained in THF is attributed to the presence of a small fraction of doubly-maleated PIBSA molecules which after pyrene labeling, form excimer intramolecularly even at very low pyrene concentrations.

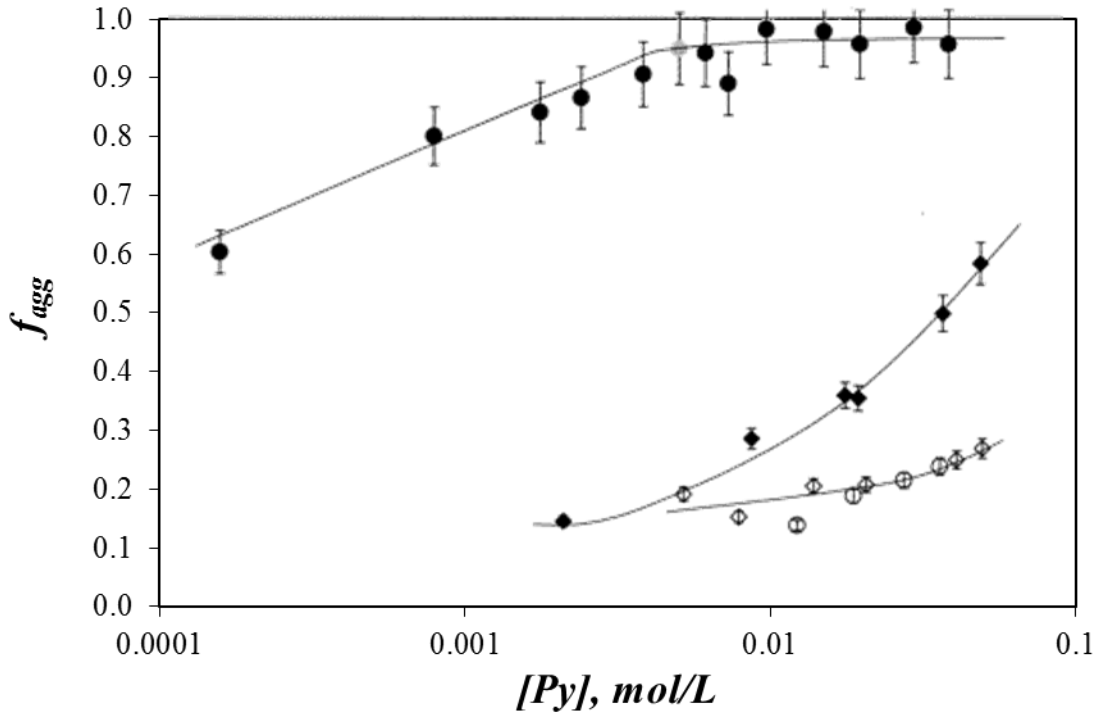

Figure 1.6. Plot of f_{agg} versus pyrene concentration for PBH-PIBSA in hexane (●) and THF (○) and PMA-PIBSA in hexane (♦) and THF (◊).[63]

The ability to recover f_{agg} from the quantitative analysis of fluorescence decays was also applied to characterize the level of succinic anhydride clustering in a maleated EP copolyme.[64] Since clustering of associative pendants along a polymer leads to a stronger associative behaviour of the modified polymer in solution which is accompanied by a stronger rheological response, the level of clustering in modified EP copolymers is an important molecular parameter. In particular, the polymeric dispersants used by the oil additive industry bear pendants that are insoluble in an oil formulation and thus tend to aggregate in a manner that leads to a viscosity increase. Clustering of these pendants along the chain provides another parameter that affects the oil viscosity. To this end, Zhang et al. used two PMA-EP copolymers,

with one copolymer having a more clustered distribution of succinic anhydride pendants than the other.[57] Fluorescence decay analysis for dilute PMA-EP solutions in THF yielded an f_{agg} value that increased from 0.34 ± 0.01 to 0.51 ± 0.00 as the level of clustering increased. The PMA-EP samples with a larger clustering of pyrene labels showed a stronger increase in viscosity with polymer concentration in hexane, thus demonstrating the effect that clustering had on the viscosity of a solution of modified EP copolymers.

The contribution of the carbonyl groups to the polar aggregation of succinimide pendants in hexane was clearly demonstrated by Zhang and Duhamel by reducing the succinimide carbonyls of a PMA-EP sample with $LiAlH_4$ to generate pyrrolidine units.[65] The reduced PMA-EP sample in hexane formed much less excimer, as its P_A value equaled 2.8 as compared to 1.9 before reduction, and the excimer decay showed a risetime which was absent for the sample before reduction. Furthermore, the photophysical parameters retrieved with the reduced PMA-EP sample in hexane were similar to those obtained for the same sample in THF before reduction. These results demonstrated that the succinimide carbonyls contributed substantially to the aggregation of the succinimide pendants in apolar aliphatic solvents such as hexane or methylcyclohexane. While this conclusion was reasonable based on the chemical procedure used to prepare the Py-EP samples, it complicated the study of EP copolymers in solution tremendously since their solution behaviour could be masked by the strong aggregation undergone by the succinimide pendants in aliphatic solvents. Indeed, strong aggregation of the succinimide pendants of a Py-EP sample would induce the efficient formation of pyrene excimer regardless of the behaviour of the EP backbone in solution. In these experiments, pyrene excimer formation would provide information on the association mechanism but not on the EP copolymer.

To remedy this problem, a series of experiments conducted in mixtures of toluene and hexane by Zhang and Duhamel established that the high level of association of a PMA-EP sample in hexane could be decreased to a level similar to that found in THF if apolar hexane (ε = 1.89) was substituted by toluene, another apolar solvent (ε = 2.38).[66] This observation opened the route for using pyrene excimer fluorescence of Py-EP samples to characterize the behaviour of EP copolymers in solution. This conclusion was immediately taken advantage of to investigate whether pyrene excimer fluorescence could be employed to probe the collapse undergone by the polymer coil of a semicrystalline EP copolymer at low temperature.[31] To this end, an amorphous and a semicrystalline EP copolymer having ethylene contents of, respectively, 60 and 80 mol% were maleated and reacted with PMA to yield PMA-EP(60) and PMA-EP(80). EP(80) had an interesting composition with a semicrystalline core flanked by two amorphous stretches. The fluorescence spectra of PMA-EP(60) and PMA-EP(80) were acquired at different temperatures. The I_E/I_M ratios were determined and plotted as a function of temperature in Figure 1.7. The I_E/I_M–vs–T profiles were complex, exhibiting one break point at 25 ^oC for all the samples, and two additional breakpoints at −5 and −20 ^oC for the semicrystalline EP copolymer. The breakpoint observed at 25 ^oC was attributed to the inversion temperature observed in Steven-Ban plots when the excimer begins to dissociate before it has time to emit.[67] At temperatures lower than 25 ^oC, excimer dissociation is negligible and I_E/I_M is directly proportional to the rate constant of excimer formation, which is itself inversely proportional to solvent viscosity. Consequently I_E/I_M increased with increasing temperature for PMA-EP(60) due to the decrease in solvent viscosity associated with an increase in temperature. The lower viscosity favors diffusive encounters between pyrene labels which results in a larger I_E/I_M ratio. The behaviour exhibited by the PMA-EP(60) sample in Figure 1.7 was typical of

any pyrene-labeled polymer in solution. What was unexpected in Figure 1.7 is the plateau region of the I_E/I_M ratio observed for PMA-EP(80) in toluene between –5 and –20 °C. As it turned out, this plateau was due to the intramolecular collapse of the polymer coil induced by microcrystal formation as the solution temperature was lowered from –5 to –20 °C. This reduction in polymer coil size as the temperature was decreased led to an increase in $[Py]_{loc}$ which offsets the viscosity-induced decrease in I_E/I_M. The collapse of the polymer coil was confirmed by conducting intrinsic viscosity measurements as a function of temperature which showed a drop in $[\eta]$ in the same temperature range where I_E/I_M plateaued. Additional FRET experiments demonstrated that the peculiar composition of EP(80) also enabled this polymer to form microcrystals intramolecularly even at polymer concentrations as high as 2 $g.L^{-1}$. The ability of EP(80) to form microcrystals intramolecularly was attributed to its microstructure where the amorphous overhangs would stabilize the microcrystals generated by the semicrystalline core of the polymer in solution.

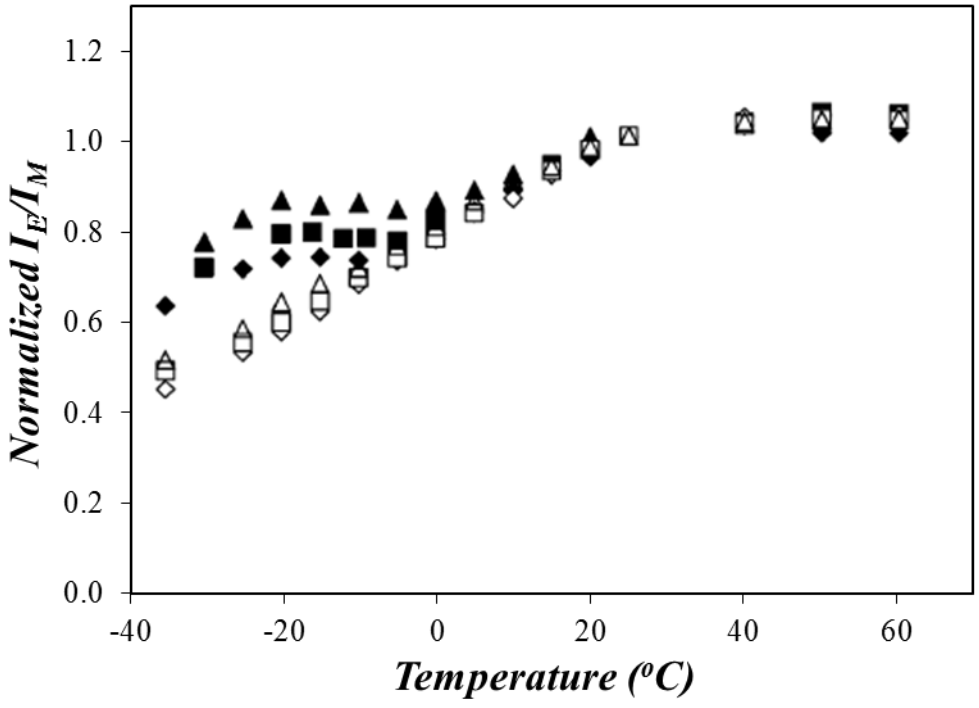

Figure 1.7. Normalized I_E/I_M ratio of Py-EPs plotted as a function of temperature at various concentrations in toluene (triangles, 0.02 g/L; squares, 0.1 g/L; diamonds, 2 g/L). Full and empty symbols are for PMA-EP(80) and PMA-EP(60), respectively.[31]

The I_E/I_M–vs–T profiles shown in Figure 1.7 provided a clear indication of whether a polyolefin would generate microcrystals in solution. However, whereas the special microstructure of the EP(80) sample allowed it to undergo an intramolecular collapse with decreasing temperature, such behaviour was deemed highly unlikely for semicrystalline EP copolymers with ethylene and propylene monomers randomly incorporated into the backbone. For such semicrystalline EP copolymers, the formation of microcrystals at lower solution temperature would indicate a worsening of the solvent quality toward the polymer which would be accompanied by an increase in intermolecular interactions. Since such associations would lead to the formation of polymer aggregates that would affect the viscosity of the solution, Pirouz et al. investigated whether pyrene excimer fluorescence could be applied to measure quantitatively the molar fraction (f_{inter}) of intermolecular interactions taking place in solution.[42]

In their experiments, Pirouz et al. used an amorphous and a semicrystalline EP copolymer containing 60 and 78 mol% of ethylene monomer randomly distributed along the EP(60) and EP(78) backbones. The polymers were maleated and pyrene-labeled with PMA. Plots of I_E/I_M-vs-T were generated between –30 and +25 ^oC for 10 $g.L^{-1}$ PMA-EP solutions in toluene as well as mixtures of 0.01 $g.L^{-1}$ PMA-EP and 10 g/L of the corresponding unlabeled EP copolymer in toluene. These plots are shown in Figure 1.8. The I_E/I_M-vs-T profiles obtained for the 10 $g.L^{-1}$ PMA-EP(60) solution and the mixtures containing 0.01 $g.L^{-1}$ of PMA-EP with an excess of unlabeled EP copolymer showed a linear increase with increasing temperature over

the entire temperature range. As in Figure 1.8 for the amorphous PMA-EP(60) sample, excimer formation was controlled by the solution viscosity that decreased with increasing temperature. By comparison, the 10 g.L^{-1} PMA-EP(78) solution showed a much more complex behaviour as the solution temperature was increased with I_E/I_M increasing first from −30 to −15 °C, decreasing from −15 to 0 °C, and increasing again from 0 to +25 °C. In fact, the anomalous behaviour observed between −15 to 0 °C in Figure 1.8 for PMA-EP(78) in toluene was similar to that found between −20 and −5 °C in Figure 1.7 for PMA-EP(80),[31] another semicrystalline polymer. Intrinsic viscosity measurements as a function of temperature also confirmed that EP(78) underwent a collapse in the same temperature range where the I_E/I_M ratio behaved in an unexpected manner. As for EP(80), this behaviour was attributed to the formation of crystalline microdomains by EP(78) in toluene that would lead to an enhancement of $[Py]_{loc}$ and thus of the I_E/I_M ratio. This feature of the I_E/I_M-vs-T profiles seems to be common for semicrystalline polymers.[31,42]

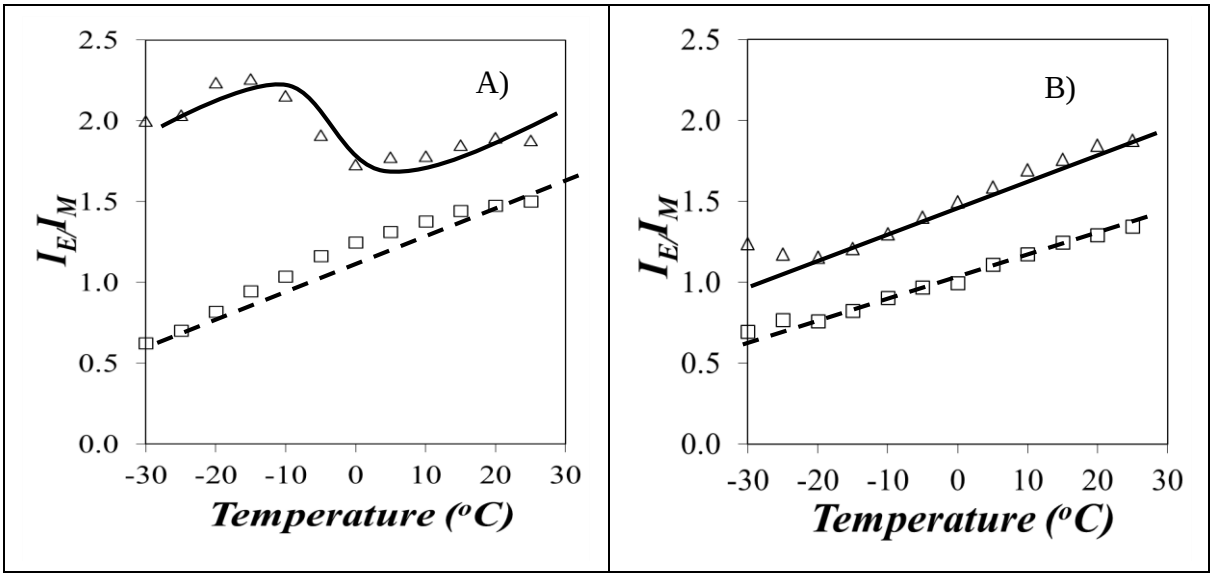

Figure 1.8. I_E/I_M -vs-T. A) (△) PMA-EP(78) (10 g.L^{-1}), (□) mixture of PMA-EP(78) (0.01 g.L^{-1}) and EP(78) (10 g.L^{-1}). B) (△) PMA-EP(60) (10 g.L^{-1}), (□) mixture of PMA-EP(60) (0.01 g.L^{-1}) and EP(60) (10 g.L^{-1}).[42]

The four I_E/I_M-vs-T profiles showed in Figure 1.8 could be analyzed further to determine the molar fraction (f_{inter}) of intermolecular interactions taking place between pyrene pendants, and thus EP copolymers in solution. This was accomplished by taking advantage of the inherent dependency of the I_E/I_M ratio on $[Py]_{loc}$ experienced by an excited pyrene attached to a polymer as shown in Equation 1.13.[68]

$$\left(I_E/I_M\right)(T)=K(T)\times[Py]_{loc} \tag{1.13}$$

In Equation 1.13, $K(T)$ is a function of the fluorescence quantum yields of the pyrene monomer and excimer and the rate constants for excimer formation and dissociation, all kinetic parameters that depend on temperature. But at a set temperature, $K(T)$ is a constant that takes the same value whether the I_E/I_M ratio is acquired with a concentrated or a dilute solution. Taking this fact into account, solutions containing 10 g.L^{-1} PMA-EP and a mixture of 0.01 g.L^{-1} PMA-EP with 10 g.L^{-1} EP yielded the ratios $I_E/I_M\begin{pmatrix}\text{intra \&}\\ \text{inter}\end{pmatrix}$ and $I_E/I_M(intra)$ which were equal to $K(T)\times[Py]_{loc}\begin{pmatrix}intra\,\&\\ inter\end{pmatrix}$ and $K(T)\times[Py]_{loc}(intra)$, respectively. This analysis of the I_E/I_M ratios led to the derivation of Equation 1.14 which was then applied to determine f_{inter}.

$$f_{inter} = \frac{[Py]_{loc}\binom{inter\,\&}{intra} - [Py]_{loc}(intra)}{[Py]_{loc}\binom{inter\,\&}{intra}} = \frac{I_E / I_M\binom{inter\,\&}{intra} - I_E / I_M(intra)}{I_E / I_M\binom{inter\,\&}{intra}} \qquad (1.14)$$

Most interestingly, the complex temperature dependency of $K(T)$ was eliminated from Equation 1.14 where $K(T)$ cancels out. The four I_E/I_M-vs-T profiles shown in Figure 1.8 were processed according to Equation 1.14 to yield plots of f_{inter} as a function of temperature for the two PMA-EP(60) and PMA-EP(78) samples. The f_{inter}-vs-T profiles shown in Figure 1.9 could be readily interpreted. The molar fraction f_{inter} remained constant with temperature for PMA-EP(60) as was expected for this amorphous polymer, but f_{inter} showed two clear-cut temperature regimes for PMA-EP(78). At temperatures lower than –5 °C, f_{inter} equalled 0.62 ± 0.07 but it decreased to 0.23 ± 0.03 for temperatures greater than –5 °C. The decrease in f_{inter} at higher temperature was a consequence of the melting of microcrystals involving several EP(78) chains and it demonstrated that for this EP copolymer, microcrystal formation took place intermolecularly in solution. Most importantly, the ability to use f_{inter} to quantify the level of intermolecular interactions between EP copolymers used as VIIs by the oil additive industry represented a major advance in the characterization of the behaviour of VIIs in solution. It can now be applied to probe the effect that different oil components have on each other in the intricate formulation of engine oils.

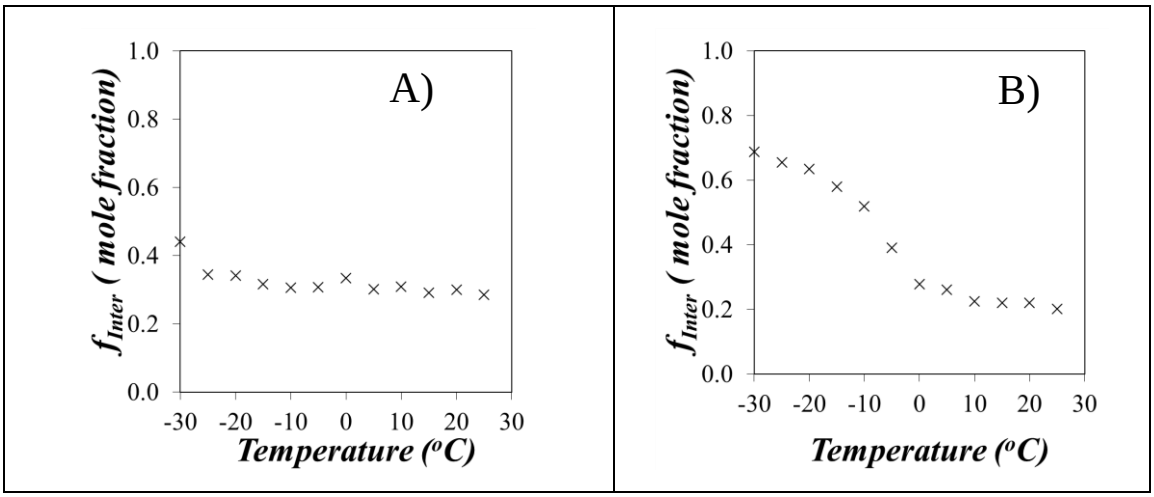

Figure 1.9. Molar fraction f_{inter} of pyrene labeled EP copolymers forming excimer intermolecularly for A) PMA-EP(60) and B) PMA-EP(78) at a concentration of 10 $g.L^{-1}$.[42]

1.2.4 Conclusions

This chapter has highlighted how maleated EP copolymers labeled with pyrene derivatives can be used to probe the behaviour of modified EPs in solution. For instance, the reaction of a maleated EP copolymer with PBH results in a Py-EP copolymer that generates strong intermolecular associations via H-bonding in aliphatic solvents. Consequently, experiments conducted with PBH-EP samples provide information at the molecular level about the associative behaviour of modified EPs typically used as dispersants in the oil additive industry. These associations can be probed qualitatively from the study of the absorption, excitation, and emission spectra of Py-EP solutions or the rise time in the excimer decays. Models have also been proposed that provide information about the associative strength of a given PBH-EP sample in an aliphatic solvent by determining the molar fraction f_{agg} obtained through the quantitative global analysis of the pyrene monomer and excimer fluorescence decays.

On the other hand, the reaction of PMA with a maleated EP yields a Py-EP that does not form H-bonds. However the succinimide moieties used to connect the pyrene label to the EP backbone are polar enough to induce intermolecular associations in apolar aliphatic solvents like hexane or methylcyclohexane. Fortunately these strong polar interactions appear to vanish in apolar toluene. As a result, the study of PMA-EP samples in toluene provides information about the behaviour of EP copolymers in solution. Taking advantage of the direct relationship that exists between the I_E/I_M ratio and $[Py]_{loc}$, information about the level of intermolecular interactions that are being generated between polymers in solution could be quantified from the molar fraction f_{inter}. f_{inter} was shown to increase markedly when the solution temperature reached the point where a semicrystalline EP copolymer would form crystalline microdomains in solution. For amorphous EP copolymers, f_{inter} remained constant as a function of temperature.

The advances for the characterization of polyolefins in solution described in this review demonstrate how pyrene excimer fluorescence can be used effectively to probe a variety of behaviours encountered by Py-EP samples in solution. It provides a powerful analytical means to investigate both quantitatively and qualitatively polymer-polymer interactions in solution and seems to be particularly well-suited to study the solution behaviour of polyolefins used by the oil additive industry.

1.3 Thesis Objectives

The first objective of this thesis was to apply fluorescence to characterize the chemical composition and level of modification of polyisobutylene-based dispersants. The second objective of this thesis was to characterize the intermolecular associations taking place between fluorescently labeled EP copolymers in the presence or absence of engine wax in toluene as a

function of temperature. The experiments that were implemented to achieve these objectives are presented hereafter.

^{1}H NMR, FTIR, and GPC are some of the typical techniques used to determine the chemical composition and the molecular weight distribution of macromolecules in general and PIBSI dispersants in particular. However this thesis presents experimental evidence that the results obtained by these techniques on PIBSI dispersants are unreliable due to the existence of strong intra- and intermolecular interactions between the PIBSI molecules induced by H-bonding between secondary amine protons and succinimide carbonyls. Taking advantage of the inherent fluorescence of the succinimide moiety of PIBSI-dispersants and its efficient quenching by secondary amines, this thesis established a quick and straightforward analytical method based on succinimide fluorescence to characterize the chemical composition of PIBSI dispersants and their level of modification.

The second accomplishment of this thesis was to quantitatively measure the actual level of intermolecular associations between semicrystalline EP copolymers in solution, by using pyrene excimer formation to determine the molar fraction of macromolecules (f_{inter}) involved in intermolecular associations. Calculating f_{inter} with traditional methods such as FRET is mathematically challenging due to the time-dependency of FRET on the spatial distribution of donors and acceptors diffusing in solution. In contrast, f_{inter} can be determined in a simple and straightforward manner by using pyrene-labeled macromolecules. These experiments took advantage of the ability of an excited pyrene to form an excimer on contact and of the proportionality that exists between the fluorescence intensity ratio I_E/I_M and the local pyrene concentration $[Py]_{loc}$, an increase in I_E/I_M reflecting an increase in $[Py]_{loc}$ which would follow from intermolecular associations. The I_E/I_M ratios of pyrene-labeled macromolecules acquired

at high and low polymer concentration can be combined to yield f_{inter} as was shown in Equation 1.14. This procedure is straightforward and provides a powerful means to the experimentalist to probe how the presence of other oil additives affects the level of intermolecular associations for a selected macromolecule (PPD, VII, or dispersant) which has been labeled with pyrene.

Considering the importance of VIIs, PPDs, and dispersants in oil additive formulations, the developments presented in this thesis should prove of high interest to the large community of scientists and engineers interested in the formulation of oil additives.

1.4 Thesis Outline

This thesis is composed of seven chapters. Chapter 1 is a literature review of polymeric additives typically used in engine oils and the application of pyrene fluorescence to retrieve quantitative information about the behaviour of these additives in solution. Chapter 2 evaluates the efficiency of different methods used to characterize the chemical composition of polyisobutylene-based dispersants in apolar solvents. In this chapter, fluorescence experiments were found to be more reliable than FTIR and ^{1}H NMR measurements. In Chapter 3, a new method based on succinimide fluorescence is proposed to evaluate the level of chemical modification applied to PIBSI dispersants. Chapter 4 introduces a procedure to determine quantitatively the level of intermolecular interactions between fluorescently labeled EP copolymers in toluene as a function of temperature. Chapter 5 uses fluorescence to study the effect that the microstructure of six different EP copolymers had on their behaviour in toluene as a function of temperature. In Chapter 6, the effect that the presence of wax has on the level of intermolecular association between EP copolymers was determined by using pyrene excimer fluorescence. Chapter 7 reviews the many conclusions that were reached in this thesis and

provides suggestions for future work. Chapters 2 and 4 have been published as a research article[69] and a patent,[42] respectively.

Chapter 2

Characterization of the Chemical Composition of Polyisobutylene-Based Oil-Soluble Dispersants by Fluorescence

2.1 Overview

A novel methodology based on fluorescence quenching measurements is introduced to determine quantitatively the amine content of polyisobutylene succinimide (PIBSI) dispersants used as engine oil additives. To this end, a series of five PIBSI dispersants were prepared by reacting two molar equivalents (meq) of polyisobutylene succinic anhydride (PIBSA) with one meq of hexamethylenediamine (HMDA), diethylenetriamine, triethylenetetramine, tetraethylenepentamine, and pentaethylenehexamine to yield the corresponding *b*-PIBSI dispersants. After having demonstrated that the presence of hydrogen bonds between the polyamine linker and the succinimide carbonyls of the dispersants prevents the quantitative analysis of the ^{1}H NMR and FTIR spectra of the dispersants to determine their chemical composition, alternative procedures based on gel permeation chromatography (GPC) and fluorescence quenching were implemented to estimate the amine content of the *b*-PIBSI dispersants. Taking advantage of the doubling in size that occurs when two moles of PIBSA are reacted with one mole of HMDA, a combination of GPC and FTIR analysis was employed to follow how the chemical composition and molecular weight distribution of the polymers produced evolved with the reaction of PIBSA and HMDA mixed in different molar ratios. These experiments provided the PIBSA-to-HMDA molar ratio yielding the largest *b*-PIBSI dispersants and this molar ratio was then selected to prepare the four other dispersants. Having prepared five *b*-PIBSI dispersants with a well-defined secondary amine content, the fluorescence of the succinimide groups was found to decrease with increasing number of secondary amines present in the polyamine linker. This result suggests that fluorescence quenching provides a valid method to determine the chemical composition of *b*-PIBSI dispersants which is otherwise difficult to characterize by standard ^{1}H NMR and FTIR spectroscopies.

2.2 Introduction

Dispersants, detergents, viscosity modifiers, and antiwear and antioxidation components are chemicals that are purposely added to engine oils to improve its performance during the operation of gasoline and diesel engines. These additives are designed to improve engine efficiency and durability. Dispersants represent the most important family of chemical additives and they have been used in engine oils since the 1950s.[1-3] They constitute up to 10 wt% of an engine oil formulation and around 50 wt% of the total chemical additives found in the oil.[4] They work by dispersing oil-insoluble combustion by-products such as soot and sludge generated during the normal operation of the engine.

Soot or ultrafine particles (UFPs) are either carbon-rich and/or metallic in nature. Typically, these particles, which result from the incomplete oxidation of fuel during ignition, are smaller than 100 nm in diameter and can be released to the air with the exhaust gases.[5] Since released UFPs are responsible for a number of ailments that can lead to heart and lung failure, governmental regulations have been issued to reduce UFP emission.[6-8] To this end, diesel and gasoline engine manufacturers circulate the exhaust gas back into the oil[9] where UFPs remain trapped before the exhaust gas is released to the air, in turn, resulting in higher concentrations of UFPs in the oil that promote UFPs aggregation.[10] UFPs aggregation is due to the polar groups formed on the surface of UFPs following fuel oxidation. The UFPs aggregate into large particles (LPs) with a diameter on the order of 1 μm to minimize their surface exposure to the oil. The LPs eventually precipitate out of solution generating soot that is detrimental to the good operation of the engine. Dispersants added to the oil prevent the formation of LPs. They adsorb onto the surface of UFPs, stabilizing them by a steric or electrostatic mechanism which reduces the aggregation of UFPs into LPs.[2,11,12]

Polyisobutylene succinimide dispersants (PIBSI) are the most common non-ionic dispersants used in the oil industry. In fact, the ability of polyisobutylene (PIB) to interact with apolar liquids has been employed in several other applications that include the synthesis of PIB-containing crosslinked acrylate networks capable of absorbing crude oil[13] or dispersants that can stabilize pigments[14] or carbon nanotubes.[15] PIBSI were initially developed by Le Suer and Stuart in 1966.[16-19] The preparation of PIBSI begins by generating a polyisobutylene chain terminated at one end with a succinic anhydride group (PIBSA). PIBSA can be prepared by an Alder-ene reaction between the terminal double bond located at the end of polyisobutylene and maleic anhydride at high temperature.[17,20] The reaction of PIBSA with a polyamine in a 1:1 or 1:2 polyamine:PIBSA ratio generates *mono*-PIBSI (*m*-PIBSI) and *bis*-PIBSI (*b*-PIBSI) dispersants, respectively.[21-24] Since increasing the number of secondary amines in the polyamine core of PIBSI dispersants results in stronger binding onto UFPs, using a large number of secondary amines should theoretically lead to better oil performance. In practice however, the secondary amines make the oil more basic which is detrimental to the integrity of the engine seals. The basicity of the oil can be reduced through post-modification of the PIBSI-dispersants with ethylene carbonate or boric acid.[25,26] These considerations underline the importance of knowing the secondary amine content of PIBSI dispersants. As it turns out, this information is not easily obtained, as characterization techniques based on FTIR or ^{1}H NMR spectroscopies[22,27] which are typically used by chemists to determine the chemical composition of unknown compounds are not suitable for this purpose. The experiments described hereafter suggest that interactions between the succinimide groups and the secondary amines is responsible for complicating the analysis of the chemical composition of PIBSI dispersants by FTIR or ^{1}H NMR spectroscopies.

Taking advantage of the inherent fluorescence of the succinimide moiety of PIBSI dispersants and its efficient quenching by secondary amines, this study establishes a quick and straightforward analytical method to characterize the secondary amine content of PIBSI-dispersants based on the fluorescence quenching of the succinimide group. Considering how important the secondary amine content of PIBSI-dispersants is to understand their solution properties, this work is expected to interest scientists aiming to design oil-soluble dispersants with improved properties.

2.3 Experimental

***Chemicals*.** Acetone (HPLC grade, Caledon), hexane (HPLC grade, Caledon), xylene (reagent grade, 98.5%, EMD), tetrahydrofuran (THF, HPLC grade, Caledon), dodecane (anhydrous, 99%, Sigma-Aldrich), and 2-dodecanone (GC grade, 97%, Sigma-Aldrich) were used as received. The chemicals hexamethylenediamine (HMDA, 98%), diethylenetriamine (DETA, 99%), triethylenetetramine (TETA, 97%), tetraethylenepentamine (TEPA, technical grade), pentaethylenehexamine (PEHA, technical grade), octylamine (99%), 1-pyrenemethylamine hydrochloride ($PyNH_2$-HCl, 95%), *N*-methylsuccinimide (*N*-MSI, 99%), butylamine (BUA, 99%), diethylamine (DEA, 99.5%), and triethylamine (TEA, 99.5%) were purchased from Sigma-Aldrich and were employed without further purification. Polyisobutylene succinic anhydride (PIBSA) was supplied by Imperial Oil.

Proton Nuclear Magnetic Resonance (^1H NMR). A Bruker 300 MHz high resolution NMR spectrometer was used to acquire the ^{1}H NMR spectra of the dispersants in deuterated chloroform ($CDCl_3$, 99.8%, Cambridge Isotope Laboratory Inc.). A sample concentration of about 10 mg/mL was used to obtain ^{1}H NMR spectra of the polymer samples with a reasonable signal to noise (S/N) ratio.

***Fourier Transform Infrared* (*FTIR*).** All FTIR spectra were obtained with a Bruker Tensor 27 FTIR spectrometer using NaCl FTIR cells. Deuterated chloroform ($CDCl_3$, 99.8%, Cambridge Isotope Laboratory Inc.) was used as solvent in all the samples preparations. Polymer solutions prepared with $CDCl_3$ were deposited dropwise onto the NaCl FTIR cell. The solvent was evaporated under a stream of nitrogen leaving behind a polymer film. All samples had an absorbance of less than 1 to optimize the S/N ratio.

***Gel Permeation Chromatography* (*GPC*).** A Viscotek GPC max VE 2001 instrument equipped with a Viscotek TDA 305 triple detector array comprised of a refractive index, viscosity, and light scattering detector was used. The samples were passed through a divinylbenzene mixed bed (8.0 mm×300 mm) Polyanalytik column. Tetrahydrofuran (THF) was used as the solvent at a flow rate of 1.0 mL/min. All the samples were filtered using 0.2 μm Millipore polytetrafluoroethylene (PTFE) filters before injection and the sample concentration was less than 10 mg/mL. Due to their low molecular weight (< 6,000 $g.mol^{-1}$), the polyisobutylene samples used in this study did not scatter light strongly enough to yield a reliable light scattering signal and the light scattering detector of the GPC instrument could not be used to determine their absolute molecular weight. Instead the GPC instrument determined the apparent molecular weight of the polyisobutylene samples as it was calibrated with polystyrene standards.

***UV-Visible Spectrophotometer* (UV-Vis).** Absorbances were measured on a Cary 100 UV-Visible spectrophotometer with quartz cells having a 0.1-100 mm path length. Absorbances were measured in the 200–600 nm wavelength range.

Steady-State Fluorescence. A Photon Technology International (PTI) LS-100 steady-state fluorometer equipped with an Ushio UXL-75Xe Xenon arc lamp and a PTI 814 photomultiplier detection system was used to acquire the fluorescence spectra.

Time-Resolved Fluorescence. An IBH time-resolved fluorometer fitted with a 340 nm nano-LED light source was used to acquire the fluorescence decays. Light scattering and background corrections were applied to fit the fluorescence decays. The fluorescence decay curves of the PIBSI-dispersants were fitted by a sum of exponentials as shown in Equation 2.1,

$$i(t) = \sum_{i=1}^{n_{\text{exp}}} a_i \times \exp(-t / \tau_i) \tag{2.1}$$

where n_{exp} represents the number of exponentials used and the parameters a_i and τ_i represent the amplitude and decay time of the i^{th} exponential, respectively. The decay fits were considered to be good if the χ^2 value was smaller than 1.30 and the residuals and the autocorrelation of the residuals were randomly distributed around zero.

Synthesis of the Polyisobutylene Succinimide (PIBSI) Dispersants. The polyisobutylene succinimide (PIBSI) dispersants were synthesized by reacting different amine derivatives with PIBSA using PIBSA-to-polyamine mole ratios of 1:1 or 2:1 in order to generate *mono*-PIBSI (*m*-PIBSI) and *bis*-PIBSI (*b*-PIBSI) dispersants, respectively. Scheme 2.1 describes the reaction between the succinic anhydride of PIBSA and the primary amine of the polyamines to generate the *b*-PIBSI dispersants.[21,23] In the current study, octylamine, diethylenetriamine (DETA), triethylenetetramine (TETA), tetraethylenepentamine (TEPA), pentaethylenehexamine (PEHA), and hexamethylenediamine (HMDA) were used as polyamines and their chemical structures are given in Table 2.1.

All the PIBSI dispersants were synthesized according to Scheme 2.1 using the same molar ratio of succinic anhydride of PIBSA to primary amines of the polyamine. The synthesis of *b*-PIBSI-TEPA is described in more detail as an example. Before conducting the reaction presented in Scheme 2.1, PIBSA supplied by Imperial Oil was precipitated to remove low molecular weight impurities that might be present in the sample. The crude PIBSA sample (10 g) was dissolved in 10 mL of hexane at 50 ^{o}C. Then the warm PIBSA solution was gradually added into 500 mL of cold acetone where it precipitated. The PIBSA suspension was centrifuged at room temperature for 20 minutes. The supernatant was discarded, and the pellet was dried overnight at 60-70 ^{o}C in a vacuum oven.

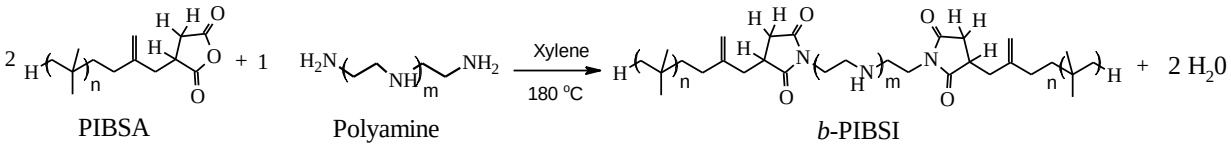

Scheme 2.1. Synthesis of succinimide dispersants.

Since the succinic anhydride of PIBSA is moisture sensitive and can react with water to yield succinic acid which is much less reactive than succinic anhydride, dehydration of the succinic acid was carried out. To this end, PIBSA purified by precipitation from acetone (2 g, 0.66 mmol succinic anhydride equivalent) was dissolved in 20 mL of xylene and placed into a two-neck round-bottom flask equipped with a Dean-Stark apparatus to remove the water generated during the dehydration conducted at 130-140 ^{o}C in refluxing xylene for 10 h under nitrogen atmosphere. Successful dehydration was confirmed by comparison in Figure 2.1 of the FTIR absorption for partially hydrated PIBSA (Trace a) with that of dehydrated PIBSA (Trace

b). The FTIR spectrum of partially hydrated PIBSA shows two absorptions bands at 1705 $cm^{-1}$and 1785 cm^{-1} due to the carbonyl groups of succinic acid and succinic anhydride (SA), respectively. After dehydration, the absorption at 1705 cm^{-1} disappeared, demonstrating that all succinic acid groups were converted back to their SA form.

Table 2.1. Chemical structures of the amine derivatives used to prepare the PIBSI dispersants.

Polyamine	**Chemical Structure**
Octylamine	CH_3-$(CH_2)_7$-NH_2
Diethylenetriamine (DETA)	H_2N-$(CH_2CH_2$-$NH)_2$-H
Triethylenetetramine (TETA)	H_2N-$(CH_2CH_2$-$NH)_3$-H
Tetraethylenepentamine (TEPA)	H_2N-$(CH_2CH_2$-$NH)_4$-H
Pentaethylenehexamine (PEHA)	H_2N-$(CH_2CH_2$-$NH)_5$-H
Hexamethylenediamine (HMDA)	H_2N-$(CH_2)_6$-NH_2

After having left the PIBSA solution refluxing in xylene for 10 h, TEPA (0.063 g, 0.33 mmol) was added to achieve a 1:2 polyamine-to-PIBSA ratio and the reaction was left to proceed at the same temperature under nitrogen for another 10 h. When the reaction was complete, the reaction mixture containing the product was washed three times with 30 mL of 1 M HCl, 1 M NaOH, 0.5 M $NaHCO_3$, and Milli-Q water. The product was then dried overnight

at 70 ^{o}C in a vacuum oven. FTIR spectroscopy was used to confirm the successful synthesis of *b*-PIBSI-TEPA. Comparison of the FTIR spectrum of *b*-PIBSI-TEPA (Trace c in Figure 2.1) with that of PIBSA (Trace b) shows the appearance of a new absorption band at 1705 cm^{-1} in Trace c due to the carbonyl groups of the succinimide ring and the disappearance of the band at 1785 cm^{-1} in Trace b. *b*-PIBSI-DETA, *b*-PIBSI-TETA, *b*-PIBSI-TEPA, *b*-PIBSI-PEHA, *b*-PIBSI-HMDA, and *m*-PIBSI-octylamine all showed similar FTIR spectra (see Figure S2.1 in Supporting Information).

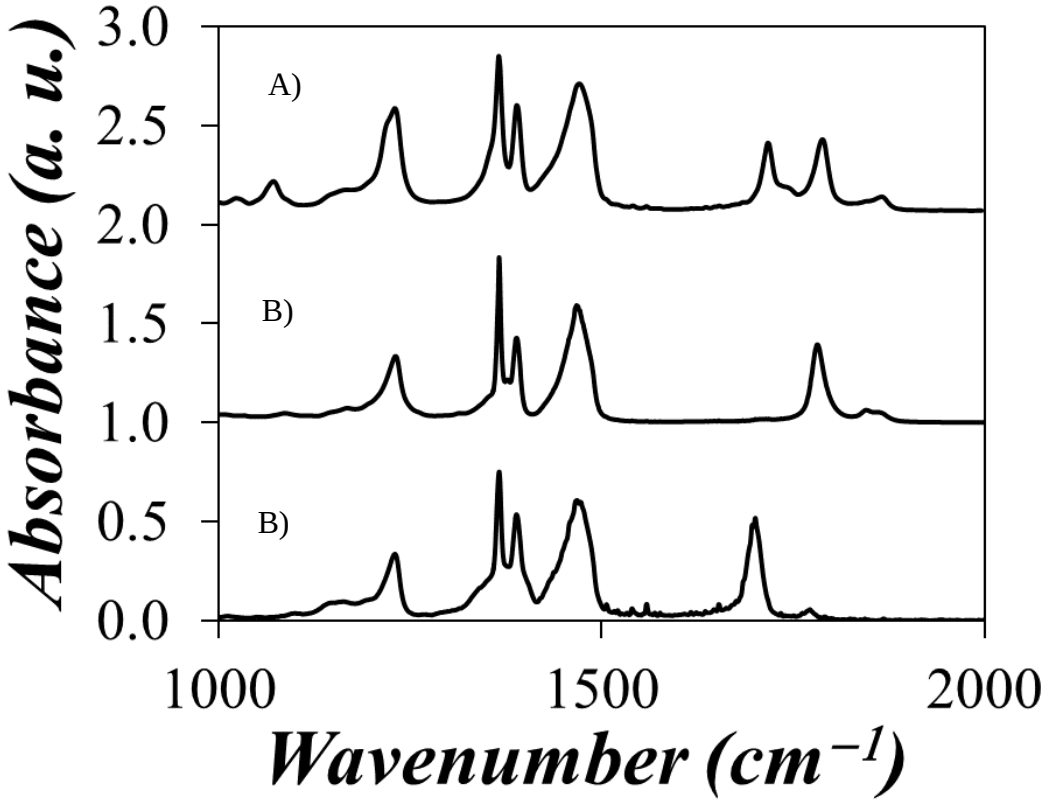

Figure 2.1. FT-IR spectra of A) partially hydrated PIBSA, B) dehydrated PIBSA, and C) *b*-PIBSI-TEPA.

The formation of secondary amides is unlikely during the preparation of the *b*-PIBSI dispersants. If this were the case, an absorption band at 1640 cm^{-1}, which is clearly absent in the FTIR spectrum of *b*-PIBSI-TEPA, would appear as in the synthesis of *m*-PIBSI-TEPA (see Figure S2.2 in Supporting Information). The reaction with a 2:1 molar ratio of TEPA:SA led to the formation of succinamide bonds rather than the desired succinimide ring.

***Synthesis of bis-MethylSuccinimide-DETA* (*b-MSI-DETA*).** *bis*-Methyl succinimide-DETA (*b*-MSI-DETA) was prepared by reacting two molar equivalents of methylsuccinic anhydride (MSA) with one molar equivalent of DETA in refluxing xylene at 130-140 ^{o}C according to Scheme 2.2. A typical reaction proceeded as follows. MSA (0.5 g, 4.4 mmol) and DETA (0.23 g, 2.2 mmol) were dissolved in 10 mL of xylene. The reaction mixture was added in a two neck round bottom flask equipped with a Dean-Stark trap, water condenser, and a nitrogen inlet and outlet to remove the water generated during the reaction conducted at 130-140 ^{o}C for 20 h.

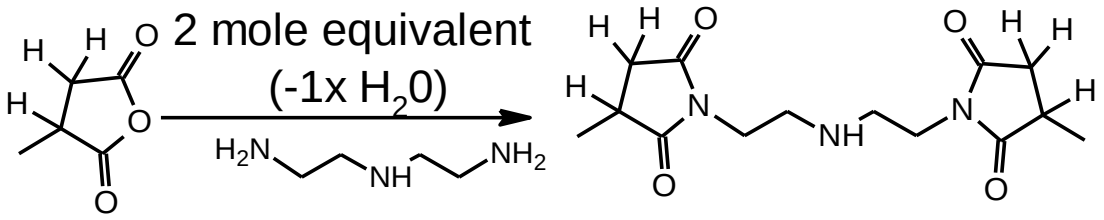

Scheme 2.2. Reaction of MSA and DETA to yield *b*-MSI-DETA.

After the reaction, 50 mL of xylene was added to the 10 mL reaction mixture. The 60 mL solution was washed separately with 10 mL of 0.5 M HCl solution, 10 mL of 0.5 M $NaHCO_3$, and 10 mL of Milli-Q water. Each extraction was repeated three times in order to remove the unreacted DETA. The organic fraction was collected. After the extractions were

completed, the final product was dried in a vacuum oven. Since *b*-MSI-DETA is water-soluble, the yield after the three extractions was low around 10%.

***Synthesis of mono-PIBSI-Pyrenemethylamine* (*m-PIBSI-PyNH*$_2$).** 1-Pyrenemethylamine hydrochloride ($PyNH_2 \cdot HCl$) (0.302 g, 1.11 mmol) was dissolved in water (280 mL) and transferred to a separatory funnel. After addition of three NaOH pellets to the solution, $PyNH_2$ was extracted using hexanes (~100 mL) and deionized water. Finally, the extracted $PyNH_2$ was dried in a vacuum oven at 60 ^oC for 2-3 h.[28]

PIBSA (1 g, 0.33 mmol equivalent of SAH units) was dissolved in dodecane (8 mL) and placed in a two-neck round-bottom flask equipped with a dean-stark apparatus. The solution was heated at 180 °C for 8 h under nitrogen atmosphere to convert the succinic acid in the polymer to its anhydride form, and the dehydration process was monitored by FTIR (see Figure 2.1). After 8 h, an excess of $PyNH_2$ (185 mg, 0.80 mmol) was added and the temperature was kept at 180 °C for another 14 hrs. The final product was then dissolved in hexane and precipitated in acetone 5-6 times to remove all unreacted $PyNH_2$. The precipitated product was dried in a vacuum oven at 80-90 °C overnight.

2.4 Results and Discussion

The succinimide moiety of PIBSI dispersants is known to fluoresce.[29-32] Since secondary and tertiary amines are known quenchers of fluorescence,[33] it was reasoned that the quenching of succinimide by amines might provide a novel, rapid, and straightforward analytical method to characterize the chemical composition of *b*-PIBSI dispersants in terms of the number of secondary amines per gram of dispersant. To this end, a series of *b*-PIBSI dispersants of known chemical composition needed to be synthesized and characterized. The chemical composition of PIBSA was determined by ^1H NMR, FTIR, UV-Vis absorption, and a procedure based on

GPC analysis. Knowledge of the chemical composition of PIBSA enabled the preparation of reaction mixtures that contained the correct molar ratio of succinic anhydride to primary amines that ensured the successful synthesis of a series of *b*-PIBSI dispersants with a well-defined content of secondary amines. Attempts at determining the chemical composition of the *b*-PIBSI dispersants by ^{1}H NMR and FTIR were inconclusive however, certainly due to the unavoidable association of the dispersants in the solid state or in organic solvents that complicated the quantitative analysis of the ^{1}H NMR and FTIR spectra. Steady-state and time-resolved fluorescence measurements appeared to be impervious to these complications yielding a linear increase in quenching efficiency of the fluorescent succinimide units with increasing number of secondary amines. The following describes how these experiments were conducted.

Proton Nuclear Magnetic Resonance (^{1}H NMR). The assignment of the ^{1}H NMR spectrum of PIBSA was done by comparing it to that of methyl succinic anhydride (SA) shown in Figure S2.3 in Supporting Information. As shown in Figure S2.3 protons **1** and **2** of MSA do not have identical chemical shifts since they are diastereotopic. Protons **1** and **2** appear at 2.6 and 3.2 ppm, respectively, due to the rigid ring structure and the presence of the carbonyl groups in the SA cycle. The proton **3** signal overlaps with proton **2**, and it is strongly deshielded by the methyl group of MSA. Protons **4** are represented as a doublet at 1.45 ppm. The single peaks at 1.5 and 7.25 ppm are due to the presence of residual water and chloroform in the sample, respectively.

The ^{1}H NMR spectrum of PIBSA is shown in Figure 2.2. The SA protons of PIBSA are expected to have similar chemical shifts as those of protons **1**, **2**, and **3** in MSA. In the ^{1}H NMR spectrum of PIBSA, the peaks at 2.6 and 3.3 ppm represent the protons in the succinic anhydride ring. The peaks at 1.1 and 1.4 ppm represent, respectively, the methyl and the methylene protons of the PIB backbone obtained in a 3:1 ratio. Finally, the peak at 5.6 ppm may be due to the

presence of vinylidene groups generated during the cationic polymerization of PIB that did not react with maleic anhydride during the Alder-ene reaction. The sharp peak at 7.3 ppm is due to chloroform. The ratio of the integrals of the peaks at 1.4 and 3.3 ppm were used to calculate the average number of IB monomers (N_{IB}) in a PIBSA molecule per SA moiety (N_{SA}). The N_{SA}/N_{IB} ratio was found to equal 1:55 ± 2.

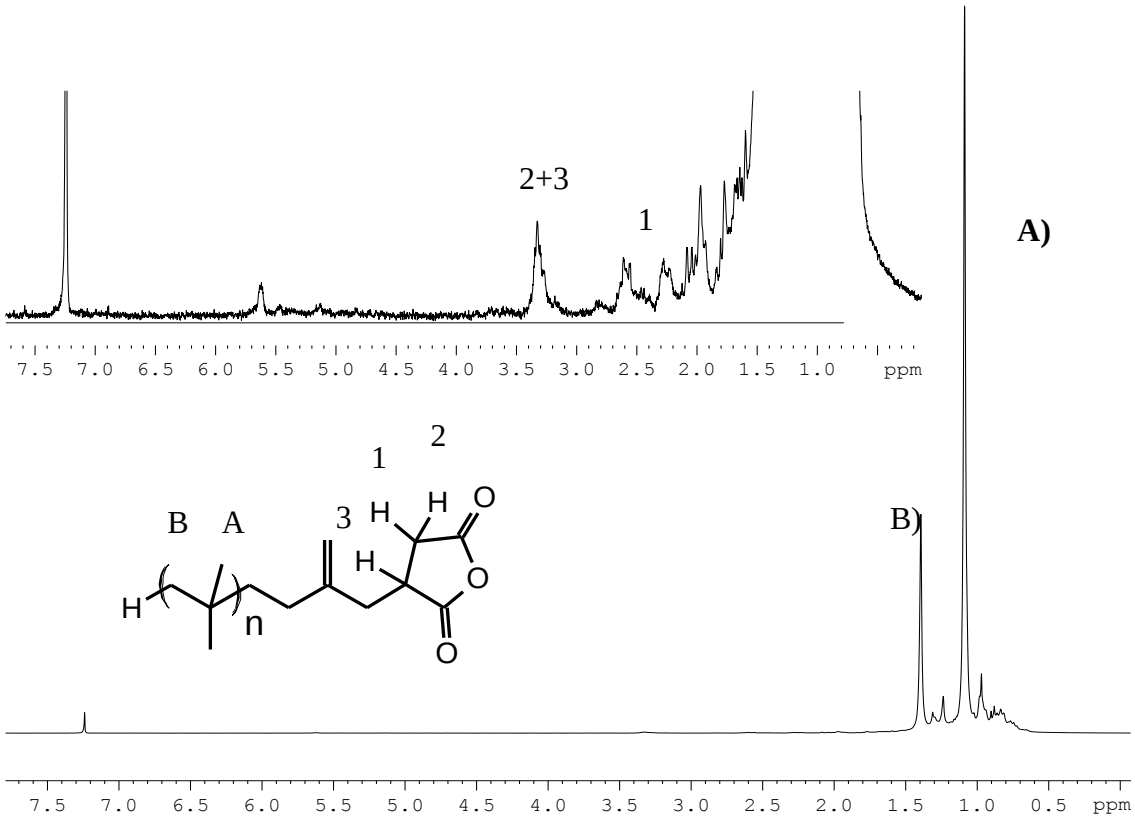

Figure 2.2. ^{1}H NMR spectrum of PIBSA.

The ^{1}H NMR peak assignment for the *b*-PIBSI samples was done as follows. The polar core of the *b*-PIBSI dispersants carried different numbers of secondary amines depending on the polyamine used in the synthesis. Amine protons usually yield broad peaks in the ^{1}H NMR spectrum whose integration cannot be relied upon for quantitative analysis. *bis*-Methyl

succinimide diethyltriamine (*b*-MSI-DETA) was used as a model compound to help with the peak assignment of the ^{1}H NMR spectrum of *b*-PIBSI-DETA.

When MSA was reacted with DETA, the succinic anhydride proton **1** and the overlapping protons **2** and **3** shifted upfield from 3.3 and 2.6 ppm to 2.9 and 2.4 ppm, respectively (Figure 2.3). This shift is due to the substitution of the oxygen in the SA ring by the less electronegative nitrogen atom. Furthermore, new peaks appeared at 3.5 and 2.8 ppm due to the ethylene protons **5** and **6** in the DETA core of *b*-MSI-DETA. Comparison of the ^{1}H NMR spectra of *b*-PIBSI-DETA and *b*-MSI-DETA shows that the peaks at 2.7 and 3.5 ppm are due to the protons **6** and **5** of the ethylene segments of the polyamine linker, whereas the peaks at 2.5 and 3.0 ppm are due to the succinimide ring protons **1** and **2+3** of *b*-PIBSI-DETA. The peaks at 1.4 and 1.1 ppm (not shown in the zoomed-in ^{1}H NMR spectra in Figure 2.3) represent the methylene and methyl protons of the PIB backbone, respectively. The sharp peaks at 2.25 and 2.3 ppm are due to traces of xylene.

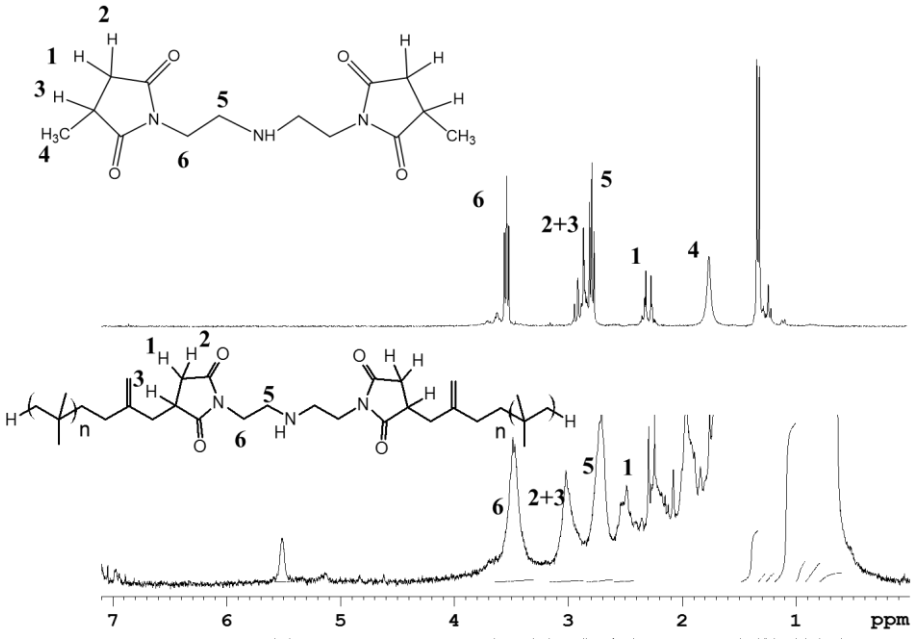

Figure 2.3. ^{1}H NMR spectrum of *b*-MSI-DETA (top) and *b*-PIBSI-DETA (bottom) (300 MHz, $CDCl_3$).

The chemical composition of *b*-PIBSI-DETA was determined in terms of the number of succinimide moieties (N_{SI}) per number of isobutylene monomers (N_{IB}) by taking the ratio of the integrals of the peaks at 3.5 and 1.4 ppm in the ^{1}H NMR spectrum shown in the bottom panel of Figure 2.3. An N_{SI}/N_{IB} ratio of 1:32 ± 1 was obtained, similar to that of all other *b*-PIBSI samples and much smaller than the N_{SA}/N_{IB} ratio of 1:55 ± 2 found for PIBSA. This discrepancy in chemical composition between PIBSA and the *b*-PIBSI dispersant could be due to the purification procedure that might selectively eliminate the PIB-rich fraction of the *b*-PIBSI samples or some unexplained spectroscopic artifact due to H-bonding of the secondary amines in the polar core which might affect the peak intensities in the ^{1}H NMR spectra.

Fourier Transform Infrared (FTIR). FTIR spectroscopy was also used to determine the chemical composition of PIBSA using a calibration curve established by Walch and Gaymans

whose expression is given in Equation 2.2.[25] This calibration curve relates the N_{SA}/N_{IB} ratio of the number of SA groups to isobutylene (IB) units with the ratio of the FTIR absorbance at 1785 cm^{-1} and 1390 cm^{-1}.

$$\frac{N_{SA}}{N_{IB}} = 0.024 \times \frac{abs(1785\ cm^{-1})}{abs(1390\ cm^{-1})} \tag{2.2}$$

The N_{SA}/N_{IB} ratio was found to equal 1:49 ± 1 for PIBSA, implying that the PIBSA sample contained one succinic anhydride unit per 49 isobutylene units. This result agrees with the ratio of 1:55 ± 2 found by ^{1}H NMR. Theoretically, the FTIR spectra can also be used to determine the chemical composition of PIBSI dispersants. A similar calibration curve whose expression is given in Equation 2.3 was established to relate the ratio of the moles of IB units per succinimide (SI) for PIBSI, namely the N_{SI}/N_{IB} ratio, to the ratio of the absorbances at 1705 cm^{-1} and 1390 cm^{-1}. Using Equation 2.3, the N_{SI}/N_{IB} ratios of *b*-PIBSI-DETA and *b*-PIBSI-TEPA were found to equal (1:31 ± 2) and (1:34 ± 2), respectively, which was different from the N_{SA}/N_{IB} ratio obtained for PIBSA found to equal 1:49 ± 1. The N_{SI}/N_{IB} ratio obtained by FTIR was similar to that observed by ^{1}H NMR implying that the longer PIB chains would have been selectively removed from the resulting *b*-PIBSI-TEPA product which was unlikely to have happened during the acid and base washes conducted to purify PIBSI. Consequently another procedure was applied to determine the chemical composition of the PIBSI dispersant.

$$\frac{N_{SI}}{N_{IB}} = 0.035 \times \frac{abs(1705\ cm^{-1})}{abs(1390\ cm^{-1})} \tag{2.3}$$

***Gel Permeation Chromatography* (*GPC*).** The inconsistencies encountered in the characterization of the PIBSI dispersants when using ^{1}H NMR and FTIR spectroscopy complicated the determination of the appropriate amounts of PIBSA and polyamine that had to be placed in the reaction vessel to yield the *b*-PIBSI dispersants. Since the goal of this study was to prepare a series of *b*-PIBSI dispersants whose size should be double that of PIBSA, GPC was employed as a third characterization technique to determine which composition of PIBSA and polyamine reactants in the reaction mixture would yield the *b*-PIBSI product having the largest molecular weight and as little as possible unreacted PIBSA reactant.

The GPC trace obtained for PIBSA is shown in Figure 2.4. PIBSA eluted at an elution volume (V_{el}) of 27 mL. A low molecular weight impurity was found to elute at a V_{el} of 29 mL. The origin of this impurity is unknown. It did not participate in the reaction leading to the synthesis of the *b*-PIBSI dispersants as it was also found in the GPC trace of the purified product. It might represent a small fragment of unreacted PIB. Using a calibration curve based on polystyrene standards, the apparent number-averaged molecular weight M_n for PIBSA was determined to equal 1,200 g/mol. M_n obtained by the direct analysis of the GPC trace was much lower than that of 2,800 g/mol predicted from the N_{SA}/N_{SI} ratio of 1:49 ± 1 and 1:55 ± 2 obtained by FTIR and ^{1}H NMR, respectively, assuming that each PIBSA chain is terminated with a single SAH group. The reason for this discrepancy in M_n value can be traced back to the calibration of the GPC instrument that was conducted with polystyrene (PS) instead of PIB standards, thus yielding apparent M_n values.

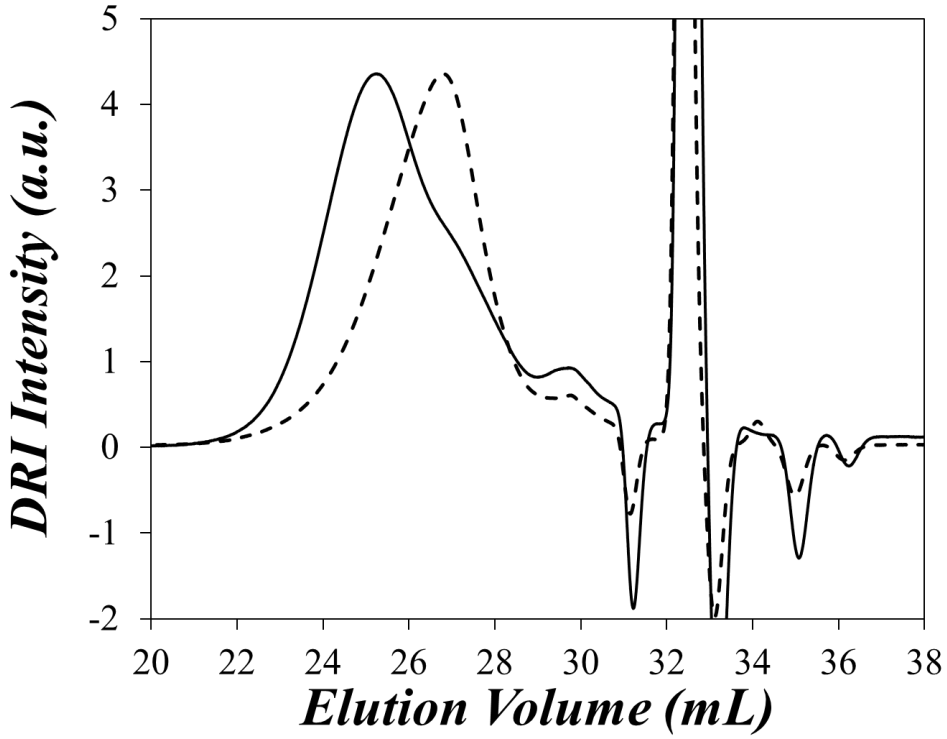

Figure 2.4. GPC traces of (---) PIBSA and (—) *b*-PIBSI-TEPA.

GPC analysis of the product of the reaction between 1 molar equivalent (meq) of a polyamine like TEPA and 2 meq of PIBSA yielded a main peak in Figure 2.4 that was shifted to a lower elution volume compared to PIBSA reflecting the expected increase in molecular weight. Moreover, a shoulder appeared on the right side of the main peak at elution volume of 27 mL. Similar features were observed with all *b*-PIBSI dispersants. The shoulder found at 27 mL in the GPC traces of the dispersant can be due to interactions between the packing material of the GPC column and the secondary amines of the polar core of the *b*-PIBSI dispersant. However, it was also noted that the shoulder eluted at the same position as PIBSA and could also have been unreacted PIBSA resulting from the use of an erroneous N_{SA}/N_{IB} ratio to prepare the reaction mixture with a 2:1 molar ratio of PIBSA to polyamine. This observation led to the

hypothesis that GPC analysis could be used to determine the optimal reaction mixture composition that would minimize the amount of unreacted PIBSA left in the reaction product. Therefore, PIBSA was reacted with different amounts of hexamethylenediamine (HMDA) because full reaction of HMDA with PIBSA eliminates the possibility that secondary amines might adsorb onto the GPC column. The ratio of HMDA to PIBSA, namely the [HMDA]/[PIBSA] ratio expressed in mmol of HMDA per grams of PIBSA, was changed from 0.1 to 0.4.

As the [HMDA]/[PIBSA] ratio decreased from 0.4 to 0.17 mmol/g, the shoulder intensity at V_{el} = 27 mL decreased steadily until it reached a minimum value (Figure 2.5). However, a further decrease in the [HMDA]/[PIBSA] ratio resulted in an increase of the shoulder intensity. The ratio of the shoulder intensity to the intensity of the main peak was calculated and plotted as a function of the [HMDA]/[PIBSA] ratio in Figure 2.6.

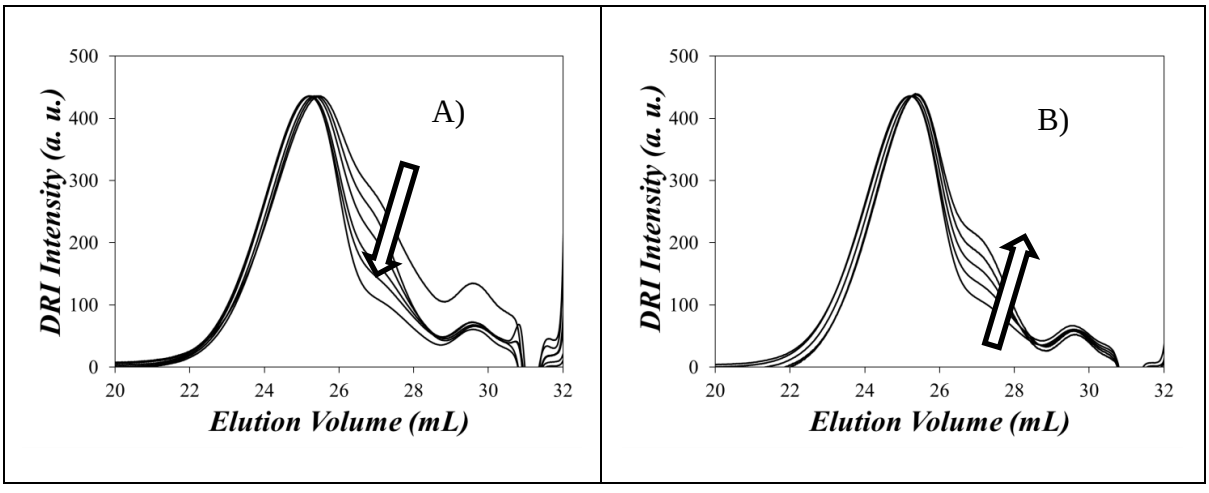

Figure 2.5. GPC traces of *b*-PIBSI-HMDA samples obtained from the reaction of PIBSA and HMDA. A) [HMDA]/[PIBSA] is varied from 0.40 mmol/g (top) to 0.17 mmol/g (bottom) and B) [HMDA]/[PIBSA] is varied from 0.17 mmol/g (bottom) to 0.10 mmol/g (top).

Low [HMDA]/[PIBSA] ratios ensured that all HMDA molecules had reacted with PIBSA so that the reaction mixture contained unreacted PIBSA and *b*-PIBSI-HMDA. As the [HMDA]/[PIBSA] ratio was further increased, less unreacted PIBSA could be found in the reaction mixture and the ratio of the shoulder-to-main peak intensities decreased in Figure 2.6. Although more *b*-PIBSI-HMDA was produced as more HMDA was added, the formation of some *m*-PIBSI-HMDA cannot be ruled out. Consequently, the reaction mixture must have contained some PIBSA, *m*-PIBSI-HMDA, and *b*-PIBSI-HMDA. PIBSA and *m*-PIBSI-HMDA are expected to elute at the same position in the GPC trace, but more PIBSA or *m*-PIBSI-HMDA are expected to be present in the mixture at low or high [HMDA]/[PIBSA] ratios, respectively. The plot of the ratio of the shoulder-to-main peak intensities as a function of the [HMDA]/[PIBSA] ratio indicates that *b*-PIBSI-HMDA is produced in the highest yield when the ratio passes through a minimum for an [HMDA]/[PIBSA] ratio of 0.17 mmol/g. This [HMDA]/[PIBSA] ratio corresponds to a chemical composition for PIBSA described by an N_{SA}/N_{IB} ratio of (1:52). This result agrees with the chemical composition of PIBSA determined by FTIR (1:49 ± 1) and ^{1}H NMR (1:55 ± 2) spectroscopy.

A better understanding of the nature of the functional groups that were present in the reaction mixtures was obtained by acquiring the FTIR spectra of the products recovered from the reaction mixtures at different [HMDA]/[PIBSA] ratios. Figure S2.4 shows the FTIR spectra acquired for the reaction mixtures obtained with [HMDA]/[PIBSA] ratios of 0.1 and 0.4 mmol/g corresponding to positions on the left and the right of the 0.17 mmol/g minimum in Figure 2.6. Overall, many spectral features were retained, but variations in the region of the FTIR spectra corresponding to the carbonyl functional groups were clearly visible. The absorbance band of the carbonyl shifted from 1785 cm^{-1} to 1705 cm^{-1} when the

[HMDA]/[PIBSA] ratio changed from 0.1 to 0.4 mmol/g. This behaviour was monitored in all FTIR spectra and plots of the Abs(1705 cm^{-1})/Abs(1390 cm^{-1}) and Abs(1785 cm^{-1})/Abs(1390 cm^{-1}) ratios are given in Figure 2.6 as a function of the [HMDA]/[PIBSA] ratio. Figure 2.6 demonstrates that an increase in the [HMDA]/[PIBSA] ratio resulted in an increase of the absorbance at 1705 cm^{-1} indicating succinimide formation that was accompanied by a decrease of the absorbance at 1785 cm^{-1} reflecting the disappearance of the SA units. Almost all SA units had disappeared from the reaction mixture when the shoulder-to-main peak intensity ratio reached its minimum value in Figure 2.6 for an [HMDA]/[PIBSA] ratio of 0.17 mmol/g. For [HMDA]/[PIBSA] ratios greater than 0.17 mmol/g, the absorbance at 1785 cm^{-1} was equal to zero indicating that all PIBSA had reacted and that all SA units had been converted to succinimides. Surprisingly, the absorbance at 1705 cm^{-1} continued to increase. Since [HMDA]/[PIBSA] ratios larger than 0.17 mmol/g are expected to generate greater amounts of *m*-PIBSI-HMDA with a free primary amine, the trend shown in Figure 2.6 suggests that interactions due to hydrogen bond formation between the primary amine of *m*-PIBSI-HMDA and the succinimide groups of *m*-PIBSI-HMDA and *b*-PIBSI-HMDA lead to an increase in the absorbance at 1705 cm^{-1}.

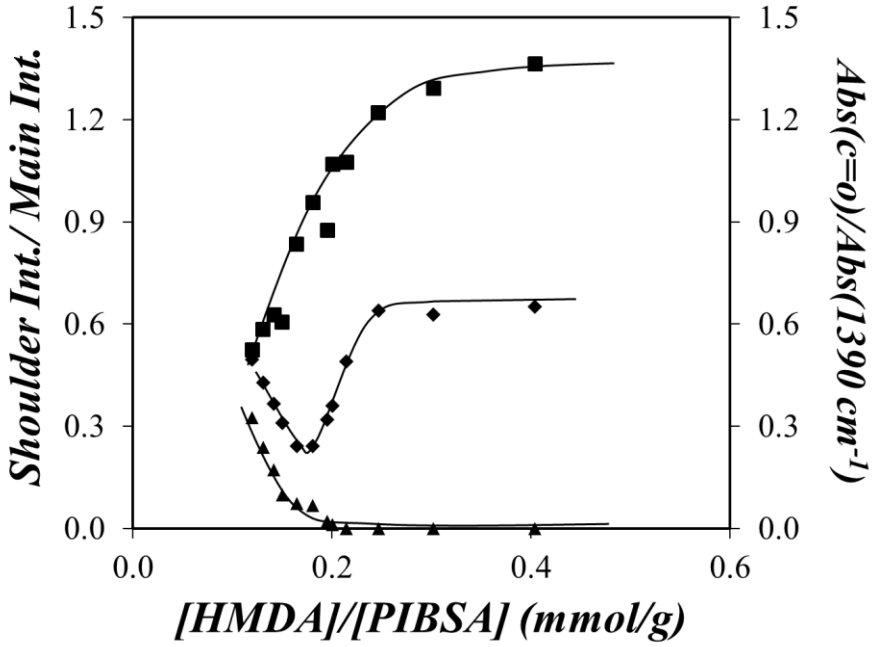

Figure 2.6. Plots of Abs(1705 cm^{-1})/Abs(1390 cm^{-1}) (■), Abs(1785 cm^{-1})/Abs(1390 cm^{-1}) (▲), and shoulder-to-peak intensity ratio of the GPC traces (◆) versus the [HMDA]/[PIBSA] ratio.

In turn, this effect might be responsible for the discrepancy found by FTIR between the chemical composition of PIBSA (N_{SA}/N_{IB} = 1:49 ± 1) and the PIBSI dispersants (N_{SI}/N_{IB} = 1:33). Since hydrogen bonds are absent in the mixtures of methylsuccinimide and PIB used to generate the calibration curve given in Equation 2.3, the absorbance at 1705 cm^{-1} is overestimated in the FTIR spectra obtained for polymer mixtures containing some *m*-PIBSI-HMDA and Equation 2.3 yields a larger SI-content than expected from the known N_{SA}/N_{IB} ratio of PIBSA. In summary, trends obtained in Figure 2.6 clearly demonstrate that the ability of FTIR spectroscopy to provide qualitative information about the chemical composition of PIBSI dispersants is strongly undermined when hydrogen bonds are present in the sample.

The trends shown in Figure 2.6 established that a reaction mixture containing 0.17 mmol of polyamine per gram of PIBSA yields a PIBSI dispersant that would contain a minimum amount of unreacted PIBSA and a maximum amount of *b*-PIBSI dispersant. Consequently, a [polyamine]/[PIBSA] ratio of 0.17 mmol/g was used to prepare all the PIBSI dispersants reported in this study. The summary of the chemical compositions determined by different techniques for all the PIBSI dispersants prepared in this study is given in Table 2.2.

Table 2.2. The summary of the chemical compositions of the PIBSI dispersants as determined by ^{1}H NMR, FTIR, GPC, and UV-Vis.

Dispersants	Chemical Composition	^{1}H NMR	FTIR (Peak Height)	GPC	UV-Vis
PIBSA	N_{SA}/N_{IB}	1:55 ± 2	1:49 ± 1	1:52	-
m-PIBSI-PyNH$_2$	N_{SI}/N_{IB}	1:45	1:44	-	1:55 ± 1
m-PIBSI-Octylamine	N_{SI}/N_{IB}	*	1:39	-	-
b-PIBSI-HMDA	N_{SI}/N_{IB}	1:32 ± 2	1:49 ± 2	-	-
b-PIBSI-DETA	N_{SI}/N_{IB}	1:33 ± 1	1:31 ± 2	-	-
b-PIBSI-TETA	N_{SI}/N_{IB}	1:30 ± 2	1:32 ± 1	-	-
b-PIBSI-TEPA	N_{SI}/N_{IB}	1:32 ± 1	1:34 ± 2	-	-
b-PIBSI-PEHA	N_{SI}/N_{IB}	1:33 ± 1	1:32 ± 1	-	-

* Small shoulder on the peak at 3.4 ppm of the ^{1}H NMR spectrum of *m*-PIBSI-Octylamine made the calculation of the N_{SI}/N_{IB} ratio inaccurate.

UV-Visible spectrophotometer. UV-Vis spectroscopy was also used to further confirm the chemical composition of PIBSA and help substantiate further the proposal that interactions between the PIBSI-dispersants were responsible for the discrepancies found between the

N_{SA}/N_{IB} ratios for PIBSA by FTIR, ^{1}H NMR, and GPC analysis and the N_{SI}/N_{IB} ratio found for all *b*-PIBSI dispersants by FTIR and ^{1}H NMR. To this end, PIBSA was reacted with 1-pyrenemethylamine ($PyNH_2$) to yield *m*-PIBSI-$PyNH_2$. Using the molar absorbance coefficient of 1-pyrenemethylsuccinimide in THF found to equal 44,535 M^{-1} cm^{-1} at 344 nm, the pyrene content and thus the succinimide content of *m*-PIBSI-$PyNH_2$ yielded an N_{SI}/N_{IB} ratio of 1:55 ± 1, in agreement with the N_{SA}/N_{IB} ratio of 1:52 ± 4 found for PIBSA.[29]

The advantage of using a pyrene derivative is that the absorbance of pyrene reflects the existence of pyrene-pyrene interactions.[33] This is achieved by monitoring the ratio of the peak absorbance at 343 nm to that of the adjacent trough in Figure S2.5 to obtain the P_A value. A P_A value of 3.0 or greater suggests that no pyrene-pyrene interactions are present. A lower P_A value indicates that pyrene aggregates exist. The absorption spectrum of a 0.14 g L^{-1} *m*-PIBSI-$PyNH_2$ solution in THF corresponding to a pyrene concentration of 0.04 mmol L^{-1} yielded a P_A value of 3.04, confirming the absence of pyrene aggregates in THF.

Since differences between the N_{SA}/N_{IB} ratio for PIBSA and the N_{SI}/N_{IB} ratio of all PIBSI-dispersants observed by ^{1}H NMR and FTIR spectroscopy were attributed to interactions between the PIBSI dispersants, solutions of *m*-PIBSI-$PyNH_2$ were prepared under conditions that would mimic those encountered when acquiring a ^{1}H NMR and FTIR spectrum. To this end, *m*-PIBSI-$PyNH_2$ was dissolved in deuterated chloroform at a same concentration as that used for ^{1}H NMR (10 mg/mL) and the UV-Vis absorption spectrum was acquired. A P_A value of 2.45 was obtained (Figure 2.7) suggesting the formation of *m*-PIBSI-$PyNH_2$ aggregates in deuterated chloroform. Similarly, a solid paste of *m*-PIBSI-$PyNH_2$ was applied on one of the walls of the UV-Vis cell to generate a polymer film similar to that used for the FTIR

experiments. The P_A value for the film was equal to 1.71, confirming that *m*-PIBSI-$PyNH_2$ aggregates are also generated in the solid state (Figure 2.7).

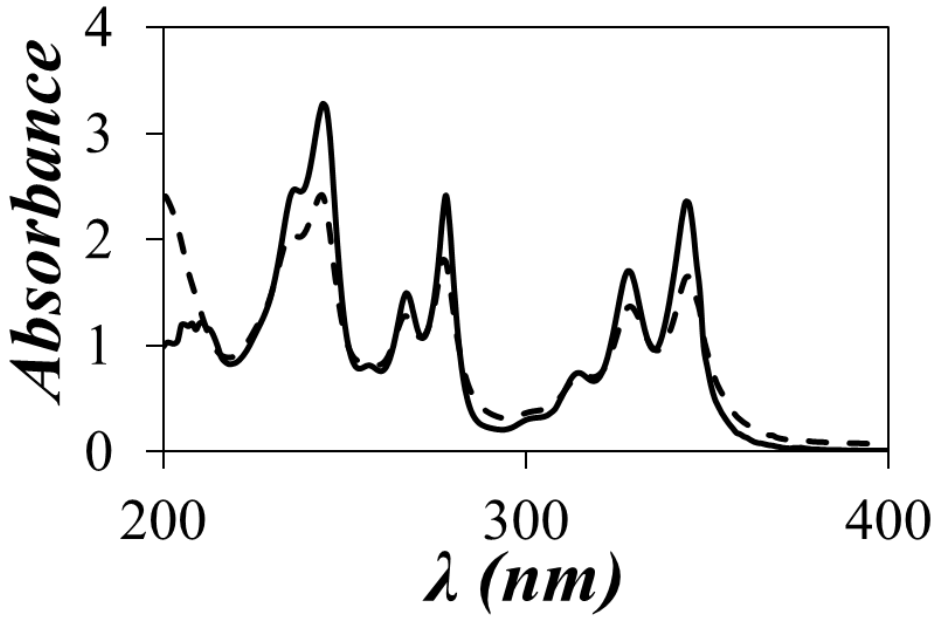

Figure 2.7. UV-Vis absorption spectra for a 0.04 mol L^{-1} solution of *m*-PIBSI-$PyNH_2$ in d-chloroform (—) and *m*-PIBSI- $PyNH_2$ in the solid state (- - -).

It is noteworthy that since *m*-PIBSI-$PyNH_2$ bears no free primary amine, the *m*-PIBSI-$PyNH_2$ aggregates are induced by polar interactions between the succinimide groups in the apolar chloroform and the PIB film. Although π-π interactions must certainly strengthen the association between the pyrene groups once the *m*-PIBSI-$PyNH_2$ aggregates are being formed, pyrene being highly soluble in chloroform does not drive the association. The polar succinimide pendants are responsible for inducing the aggregation. The presence of residual amounts of primary and secondary amines for the PIBSI-dispersants prepared with polyamines other than HMDA increases the strength of these interactions, which lead to distorted signals in the FTIR and ^{1}H NMR spectra.

Since all the techniques used to characterize the chemical composition of PIBSA converged on an N_{SA}/N_{IB} ratio of 1:52 ± 4 for PIBSA, corresponding to a chemical composition of 0.34 mmol of SA units per gram of PIBSA, reaction mixtures containing 0.17 mmol of polyamine per gram of PIBSA were used to conduct the synthesis of all the *b*-PIBSI dispersants prepared in this study. The experiments conducted so far indicated that the characterization of the chemical composition of *b*-PIBSI dispersants by FTIR and ^{1}H NMR spectroscopy was challenging since aggregation of the succinimide moieties promoted by the presence of amines distorted the ^{1}H NMR and FTIR spectra. This conclusion led us to investigate whether another technique would be better suited to determine the chemical composition of *b*-PIBSI dispersants. Since the *b*-PIBSI dispersants contain two fluorescent succinimide moieties and a number of secondary amines that are efficient quenchers of fluorescence, fluorescence quenching experiments were conducted on the *b*-PIBSI dispersants to determine whether the fluorescence signal of the succinimide units would be sensitive to the number of secondary amines in the polyamine core.

Steady-State and Time-Resolved Fluorescence Measurements. The intrinsic fluorescence of PIBSA and some PIBSI dispersants has already been reported.[32] Since secondary and primary amines are known to be efficient fluorescent quenchers,[34] we investigated whether fluorescence experiments would provide information about the chemical composition of the PIBSI dispersants. To determine the best excitation and emission wavelengths to monitor the fluorescence of PIBSA and the *b*-PIBSI dispersants, the fluorescence spectra of these polymers were acquired at excitation wavelengths selected in the 250-420 nm range. The fluorescence spectra of the polymer solutions in THF were broad and structureless. For all samples, the emission shifted to higher wavelengths as the excitation wavelength was increased past 360 nm

(Figure 2.8). This behaviour indicates that PIBSA and the *b*-PIBSI dispersants contain more than one chromophore and that changing the excitation wavelength enables the photoselection of different chromophores. Since the *b*-PIBSI dispersants contained a fluorescent succinimide group, the fluorescence of the *b*-PIBSI dispersants was also compared to that of *N*-methylsuccinimide (*N*-MSI). Excitation of *N*-MSI at different wavelengths resulted in a set of fluorescence spectra centered around the same emission wavelength confirming the excitation of a single chromophore. The position (λ_{max}) and fluorescence intensity (I_{max}) at the fluorescence maximum were recorded and plotted on a same figure as a function of the excitation wavelength (λ_{ex}) as shown in the insert of Figure 2.8. For all *b*–PIBSI dispersants, as λ_{ex} increased, λ_{max} remained constant within experimental error and equal to 423 ± 5 for all samples before increasing rapidly with increasing λ_{ex} for λ_{ex} greater than 360 nm. This behaviour suggests that a main chromophore is photo-selected for λ_{ex} values between 300 and 360 nm, and that other chromophores are being excited at higher λ_{ex}. For all *b*-PIBSI dispersants, the fluorescence intensity at the fluorescence maximum (I_{max}) in the fluorescence spectrum increased steadily with increasing λ_{ex} until it passed through a maximum at λ_{ex} = 360 nm. For λ_{ex} greater than 360 nm, I_{max} decreased continuously with increasing λ_{ex}. The behaviour of I_{max} as a function of λ_{ex} is the result of a number of effects such as changes in the molar absorbance coefficient of the chromophore in this range of λ_{ex} values. Together the trends shown in Figure 2.8 suggest that excitation of the solutions of dispersant in THF yields a maximum fluorescence signal when excited at 360 nm. Consequently, this excitation wavelength was used for all experiments thereafter.

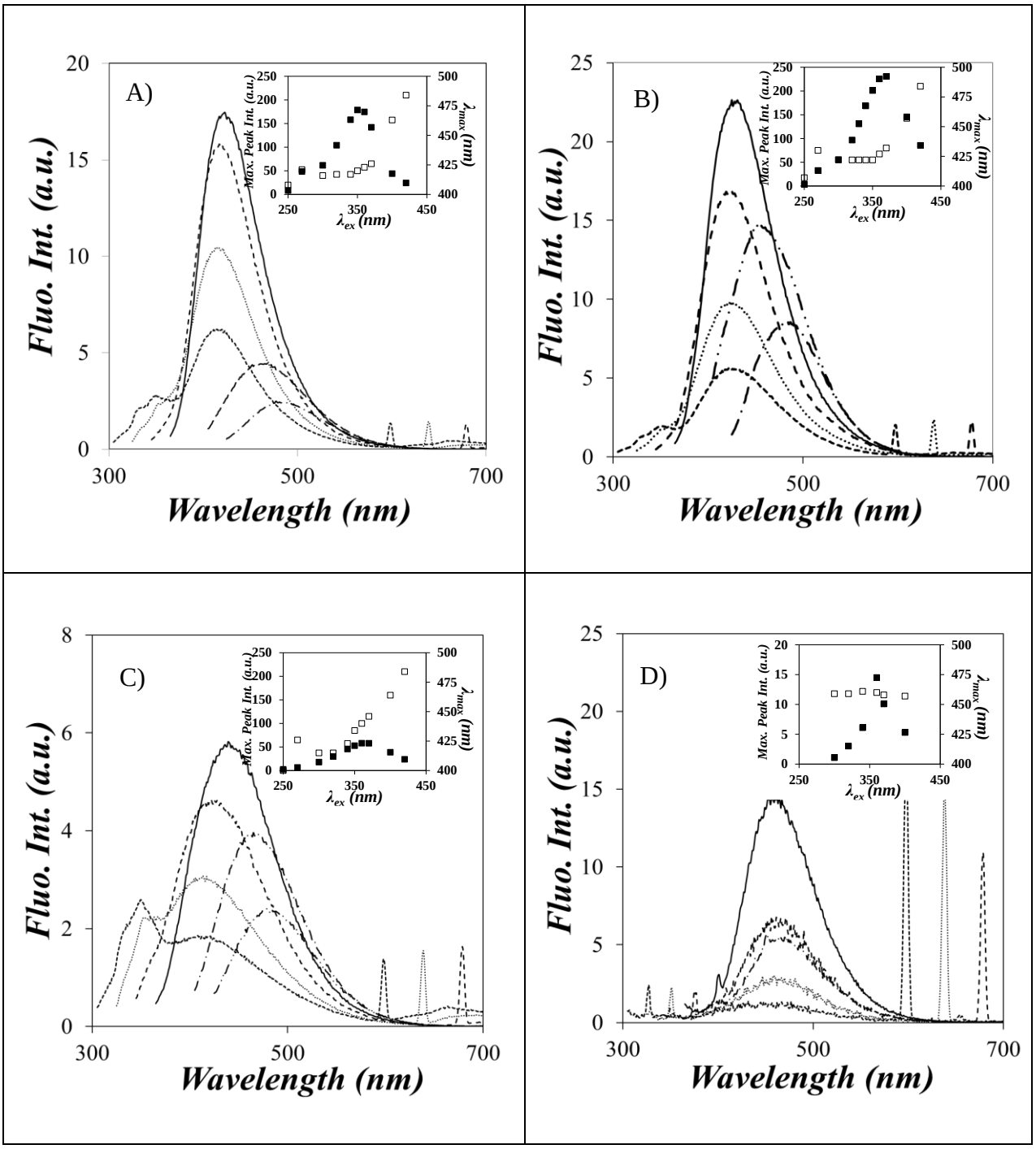

Figure 2.8. Steady-state fluorescence spectra of A) PIBSA (8 g/L), B) *b*-PIBSI-HMDA (8 g/L), C) *b*–PIBSI-PEHA (8 g/L), and D) *N*-methyl succinimide (0.45 mol/L). (----) λ_{ex} = 300 nm, (…) λ_{ex} = 320 nm, (- - -) λ_{ex} = 340 nm, (▬▬) λ_{ex} = 360 nm, (— ‒) λ_{ex} = 400 nm, and (— ‒ ‒) λ_{ex} = 420 nm in THF. Insert: Maximum peak intensity (I_{max}) (■) and maximum peak intensity wavelength (λ_{max}) (□) versus excitation wavelength (λ_{ex}).

Although a maximum in fluorescence intensity was found upon exciting the solutions of PIBSA and all *b*-PIBSI dispersants at λ_{ex} = 360 nm, it was noticeable that the fluorescence of the PIBSA solution was blue shifted and weaker than that of the *b*-PIBSI-HMDA solution. Overlaying the fluorescence spectra of the 8 g/L solutions of *b*-PIBSI-HMDA, *b*-PIBSI-DETA, *b*-PIBSI-TETA, *b*-PIBSI-TEPA, and *b*-PIBSI-PEHA in Figure 2.9 clearly showed that the fluorescence intensity decreased with increasing number of secondary amines in the polyamine linker of the dispersant. Since secondary amines are known to be efficient fluorescence quenchers.[33,34] the trends shown in Figure 2.9 indicate that *b*-PIBSI-HMDA with no secondary amine and *b*-PIBSI-PEHA with four secondary amines yield the highest and lowest fluorescence intensities, respectively. In turn, this photophysical effect might be beneficial to infer the chemical composition of a given *b*-PIBSI dispersant by comparing the decrease of its fluorescence intensity to that of *b*-PIBSI-HMDA. As a result, the photophysical properties of the series of *b*-PIBSI dispersants listed in Table 2.2 was investigated.

The information contained in Figure 2.9 can be summarized by plotting the ratio of the fluorescence intensity of the unquenched emitter (i.e. *b*-PIBSI-HMDA) over that of the quenched emitters (i.e. the other *b*-PIBSI dispersants), namely the I_0/I ratio, as a function of the number of secondary amines found in the polyamine linker. This was done in Figure 2.10. Within experimental error, the I_0/I ratio was found to increase linearly with increasing number of secondary amines.

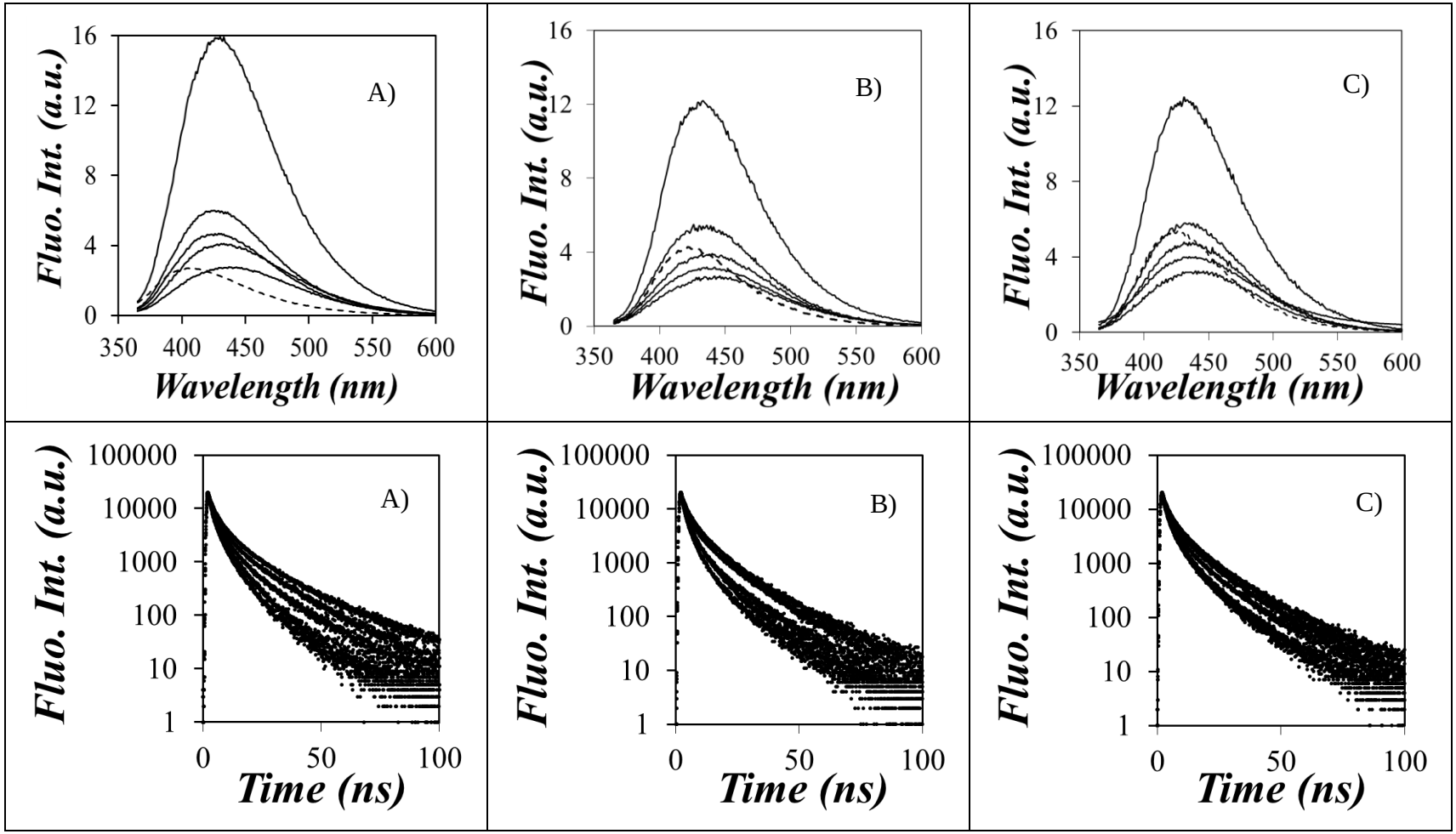

Figure 2.9. Top: Steady-state fluorescence spectra of (- - -) PIBSA and (—) *b*-PIBSI dispersants. Bottom: Time-resolved fluorescence decays. From top to bottom: *b*-PIBSI-HMDA, *b*-PIBSI-DETA, *b*-PIBSI-TETA, *b*-PIBSI-TEPA, and *b*-PIBSI-PEHA in A) dodecane, B) THF, and C) dodecanone. (C_{PIBSI} = 8 g/L, λ_{ex} = 360 nm, and λ_{em} = 428)

More information about the nature of fluorescence quenching, particularly whether it is static, dynamic, or a mixture of both, can be obtained by conducting time-resolved fluorescence measurements. To this end, the fluorescence decays of the *b*-PIBSI dispersants were acquired using excitation and emission wavelengths of 360 and 428 nm, respectively. The corresponding fluorescence decays are shown in Figure 2.9. They were all strongly multiexponential. The decays were fitted with a sum of three-to-four exponentials and the number-average lifetime was determined (Equation 2.4). The pre exponential factors and decay times retrieved from this analysis are provided in SI (Tables S2.1-S2.4). The ratio τ_0/τ, where τ_o and τ are, respectively, the number-average lifetime in the absence and presence of secondary amines in the polyamine linker, was plotted as a function of the number of secondary amines in Figure 2.10. Here again, a linear increase in τ_0/τ, with increasing number of secondary amines was observed. The ratios I_0/I and τ_0/τ did not overlap however indicating that static quenching is taking place.

$$\tau = \sum_{i=1}^{n} a_i \tau_i \Big/ \sum_{i=1}^{n} a_i \tag{2.4}$$

Static quenching occurs when interactions between fluorophore and quencher are present. These associations are likeliest to happen when secondary amines and fluorophores are located in close proximity within the macromolecule, again strongly suggesting that the succinimide moieties of the *b*-PIBSI dispersants are responsible for the fluorescence of the *b*-PIBSI dispersants centered at 423 ± 5 nm when exciting the solution at 360 nm. If one considers the volume V_{core} defined by the two succinimide moieties and the polyamine linker, increasing the number of secondary amine quenchers in the polyamine spacer increases the local concentration of secondary amines in V_{core} and thus, the efficiency of quenching as observed Figure 2.10.

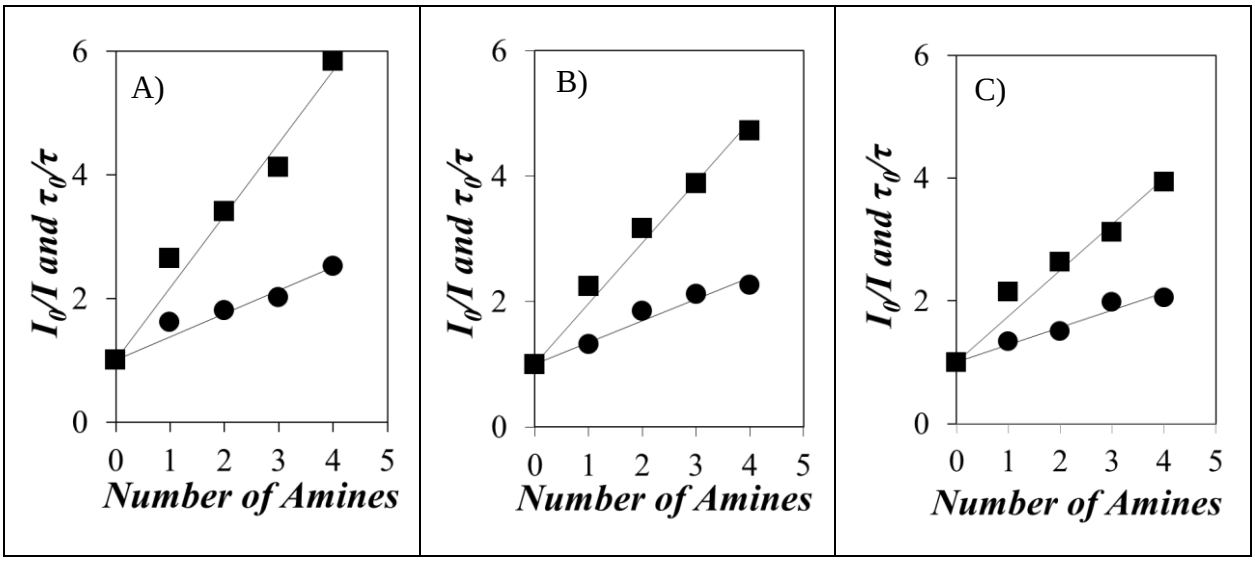

Figure 2.10. Stern-Volmer plot for the quenching of *b*-PIBSI dispersants by secondary amines in A) dodecane, B) THF, and C) dodecanone. ((■) I_0/I and (●) $<\tau>_0/<\tau>$)

The ability of amines at quenching the fluorescence of the succinimide units was confirmed by monitoring the quenching of *N*-MSI by butylamine (BUA), diethylamine (DEA), and triethylamine (TEA) in THF. As shown in Figure S2.6, the fluorescence intensity of *N*-MSI decreased strongly with increasing concentration of BUA, DEA, and TEA. Dynamic fluorescence quenching of *N*-MSI was also apparent in the fluorescence decays of *N*-MSI presented in Figure S2.6 that show a faster decay of *N*-MSI with increasing BUA, DEA, and TEA concentration. With the data collected for *N*-MSI in Figure S2.6, the I_0/I and τ_0/τ ratios were determined and plotted as a function of BUA, DEA, and TEA concentrations in Figure 2.11. The trends obtained for the I_0/I and τ_0/τ ratios in Figure 2.11 are similar to those obtained with the *b*-PIBSI dispersants, the ratios showing a linear increase with increasing BUA, DEA, and TEA concentration. With all three amines, the I_0/I ratio took larger values than the τ_0/τ ratio demonstrating the existence of static quenching. The only difference between the plots shown

in Figures 2.10 and 2.11 is that quenching occurs intramolecularly with the *b*-PIBSI dispersants and intermolecularly with *N*-MSI. The similarity of the trends obtained strongly suggests that the secondary amines in the polyamine linker of the *b*-PIBSI dispersants are quenching the fluorescent succinimide moieties connecting PIB to the polyamine.

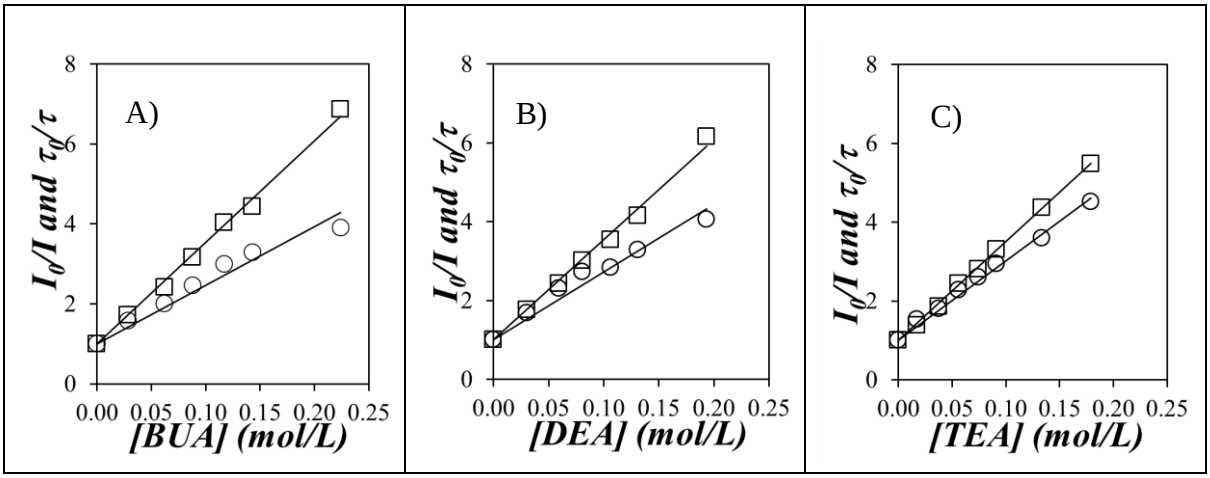

Figure 2.11.Stern-Volmer plot for the quenching of *N*-MSI by A) BUA, B) DEA, and C) TEA in THF. ((□) I_0/I and (○) $<\tau>_0/<\tau>$)

In order to describe the quenching experiments more quantitatively, Scheme 2.3 was introduced. In Scheme 2.3, a chromophore *M* forms a complex *MQ* in the presence of a quencher molecule *Q* with an equilibrium constant K_S. The absorption of a photon by the uncomplexed chromophore *M* present in solution with a molar fraction *f* generates the excited species *M**, which can either fluoresce with a lifetime τ_0 or be quenched by diffusive encounter with *Q* with a rate constant k_Q. A molar fraction 1–*f* of the chromophore *M* is also present in the form of the complex *MQ* in the solution. Excitation of the complex *MQ* results in no fluorescence, as the excited chromophore *M** is quenched instantaneously due to its

complexation with *Q*. Scheme 2.3 yields Equations 2.5 and 2.6 that describe the τ_0/τ and I_0/I ratios, respectively.

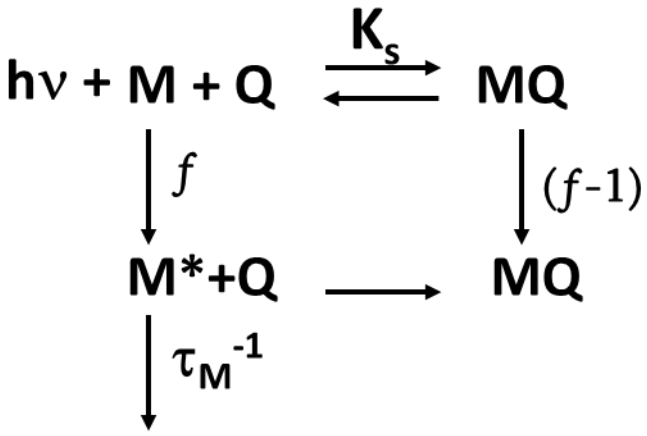

Scheme 2.3. Photophysical processes undergone by chromphore M subject to static and dynamic quenching.[35]

The quencher concentration [*Q*] in Equations 2.5 and 2.6 represents either the local concentration of secondary amines in the volume defined by the polyamine linker of the *b*-PIBSI dispersants, or the concentration of BUA, DEA, and TEA in the *N*-MSI solution. The product $k_Q \times \tau_0$ represents the efficiency of dynamic quenching. It will be referred to as K_D (= $k_Q \times \tau_o$) hereafter. Using this nomenclature, the slope of the plot between the I_0/I ratio and [*Q*] yields the sum K_{app} *(*$= K_S + K_D$), whereas the slope of the plot between the τ_0/τ ratio and [*Q*] yields K_D. Consequently, the constants K_S and K_D could be estimated from the slope of the straight lines shown in Figures 2.10 and 2.11. Their values are listed in Tables 2.3 and 2.4.

$$\frac{\tau_0}{\tau} = 1 + k_Q \tau_0 \times [Q] \qquad (2.5)$$

$$\frac{I_0}{I} = 1 + (K_S + k_Q\tau_0) \times [Q] + K_S k_Q \tau_0 \times [Q]^2 \approx 1 + (K_S + k_Q\tau_0) \times [Q] \quad (2.6)$$

The quenching experiments were conducted in dodecane, dodecanone, and THF for the *b*-PIBSI dispersants. In the case of *b*-PIBSI in THF and dodecane, $K_S/(K_S+K_D)$ is about twice larger than $K_D/(K_S+K_D)$ demonstrating the importance of static quenching in these experiments. The introduction of a carbonyl group by using dodecanone instead of dodecane reduces the ability of the secondary amines to bind to the succinimides. As expected, the $K_S/(K_S+K_D)$ ratio decreased from 0.68 ± 0.01 in dodecane to 0.58 ± 0.02 in dodecanone.

Table 2.3. τ_0, K_D, and K_s values derived from the Stern-Volmer plots for *b*-PIBSI shown in Figure 2.11.

Solvent	τ_0 **(ns)**	K_D	K_S	K_S/K_{app}	K_D/K_{app}
Dodecane	4.8	0.38 (± 0.00)	0.82 (± 0.01)	0.68 (± 0.01)	0.32 (± 0.00)
THF	4.4	0.34 (± 0.01)	0.63 (± 0.01)	0.65 (± 0.01)	0.35 (± 0.01)
Dodecanone	4.5	0.29 (± 0.01)	0.41 (± 0.01)	0.58 (± 0.02)	0.42 (± 0.01)

Due to solubility issues in dodecane and dodecanone, quenching of *N*-MSI by BUA, DEA, and TEA was solely conducted in THF. In the case of BUA and DEA, the $K_S/(K_S+K_D)$ ratio took values of 0.36 ± 0.00 and 0.30 ± 0.00, respectively. The $K_S/(K_S+K_D)$ value was slightly higher for BUA in comparison to DEA probably due to the ability of BUA to H-bond more strongly to *b*-MSI. Interestingly, the $K_S/(K_S+K_D)$ ratio decreased from 0.36 ± 0.00 for

BUA to 0.09 ± 0.00 for TEA which could not H-bond with *N*-MSI, thus confirming the nature of the interactions between the succinimide groups and the secondary and primary amines. Finally, k_Q was found to increase according to the sequence BUA < DEA< TEA.

The results obtained thus far suggest that the fluorescent succinimide moieties constituting the *b*-PIBSI dispersants are quenched efficiently by secondary amines. Hydrogen bonding between the succinimide carbonyls and the secondary amine protons leads to static quenching whose magnitude increases linearly with the number of secondary amines present in the polyamine linker joining two PIB chains.

Table 2.4. Data obtained from Stern-Volmer plot with the *N*-MSI in presence of BUA, DEA, and TEA in THF.

Name	τ_0 (ns)	k_Q ($M^{-1}ns^{-1}$)	K_D (M^{-1})	K_{app} (M^{-1})	K_S/K_{app}	K_D/K_{app}
***N*–MSI+BUA**	10.1	1.60 (± 0.00)	16.00 (± 0.01)	25.14 (± 0.02)	0.36 (± 0.00)	0.64 (± 0.00)
***N*-MSI+DEA**	10.1	1.74 (± 0.02)	17.44 (± 0.02)	25.17 (± 0.01)	0.30 (± 0.00)	0.70 (± 0.00)
***N*-MSI+TEA**	10.1	2.28 (± 0.00)	22.81 (± 0.00)	25.08 (± 0.02)	0.09 (± 0.00)	0.91 (± 0.00)

The linear relationship found to exist between the I_0/I and τ_0/τ ratios and the moles of secondary amines in the polyamine spacer of the *b*-PIBSI dispersants is expected to provide a novel analytical method toward the characterization of the chemical composition of *b*-PIBSI dispersants. Based on the linear Stern-Volmer plot shown in Figure 2.10, the amines content of an unknown *b*-PIBSI dispersant could now be determined by measuring its fluorescence intensity I and average life time τ and comparing them to the corresponding I_0 and τ_0 values

obtained with *b*-PIBSI-HMDA dispersant prepared with the same PIBSA unit used to prepare the unknown *b*-PIBSI dispersant.

2.5 Conclusions

The chemical composition of several PIBSI dispersants prepared with different molar ratios of PIBSA and hexamethylene diamine was characterized quantitatively by using a combination of GPC and FTIR analysis. This study confirmed that the existence of hydrogen bonds between the secondary amines of the polyamine spacer and the succinimide carbonyls of *b*-PIBSI dispersants represents a serious impediment to the characterization of the chemical composition of these dispersants by standard ^{1}H NMR and FTIR spectroscopies. By contrast, the procedure combining GPC and FTIR analysis enabled the determination of appropriate reaction conditions to prepare a series of five *b*-PIBSI dispersants with polyamine linkers having a well-defined number of secondary amines.

Having established that techniques such as ^{1}H NMR and FTIR provide unreliable information about the chemical composition of *b*-PIBSI dispersants, steady-state and time-resolved fluorescence quenching experiments were carried out on the five *b*-PIBSI dispersants prepared with a known number of secondary amines in the polyamine linker to investigate whether the fluorescence emitted by the succinimide groups present in the *b*-PIBSI dispersants would respond to the number of secondary amines of a given *b*-PIBSI dispersant. As the number of secondary amines was increased in the polyamine linker used to prepare the dispersants, the fluorescence intensity I and average lifetime τ of the *b*-PIBSI dispersants were found to decrease. Stern-Volmer plots of the ratios I_0/I and τ_0/τ as a function of the number of secondary amines showed a linear behavior suggesting that fluorescence quenching measurements can provide a reliable measure of the secondary amine content of a given *b*-

PIBSI dispersant. This result should be of high practical interest to scientists involved in the design of dispersants used as oil-additives.

Chapter 3

Chemical Modification of Polyisobutylene Succinimide Dispersants and Characterization of their Associative Properties

3.1 Overview

The secondary amines found in *b*-PIBSI dispersants prepared by attaching two polyisobutylene chains to a polyamine core via two succinimide moieties were reacted with ethylene carbonate (EC). The reaction generated urethane bonds on the polyamine core to yield the modified *b*-PIBSI dispersants (M*b*-PIBSI). Five dispersants were prepared by reacting two molar equivalents (m_{eq}) of polyisobutylene terminated at one end with a succinic anhydride moiety (PIBSA) with one m_{eq} of hexamethylenediamine (HMDA), diethylenetriamine (DETA), triethylenetetramine (TETA), tetraethylenepentamine (TEPA), and pentaethylenehexamine (PEHA) to yield the corresponding *b*-PIBSI dispersants. Characterization of the level of secondary amine modification for the M*b*-PIBSI dispersants with traditional techniques such as FTIR and ^{1}H NMR spectroscopies was greatly complicated by interactions between the carbonyls of the succinimide groups and unreacted secondary amines of the M*b*-PIBSI dispersants. Therefore, an alternative procedure was developed based on fluorescence quenching of the succinimides by secondary amines and urethane groups. The procedure took advantage of the fact that the succinimide fluorescence of the M*b*-PIBSI dispersants was quenched much more efficiently by secondary amines than by the urethane groups that resulted from the EC modification of the amines. While EC modification did not proceed for *b*-PIBSI-DETA and *b*-PIBSI-TETA certainly due to steric hindrance, 60 and 70% of the secondary amines found in the longer polyamine core of *b*-PIBSI-TEPA and *b*-PIBSI-PEHA had reacted with EC as determined by the fluorescence quenching analysis. Furthermore, the ability of the M*b*-PIBSI dispersants to adsorb at the surface of carbon black particles used as mimic of the carbonaceous particles typically found in engine oils was compared to that of their unmodified analogs.

3.2 Introduction

Dispersants have been extensively used as oil additives since the 1950s. They are designed to improve engine oil performance and decrease fuel consumption and pollution emission.[1-3] Their purpose is to decrease soot aggregation, a process that can thicken the oil to the point where it generates sludge that prevents the flow of oil. Soot and sludge are carbon-rich and/or metallic in nature and result from the incomplete oxidation of fuel during ignition. Soot or ultrafine particles (UFPs) are smaller than 100 nm in diameter, but they aggregate over time into large particles (LPs) with a diameter on the order of 1 μm to minimize exposure of their polar surface to the oil.[4,5] The formation of LPs can cause engine failure through wear and oil blockage. Dispersants adsorb onto the surface of UFPs, stabilizing them by a steric or electrostatic mechanism, which reduces the aggregation of UFPs into LPs.[1,5,6]

Metallic and ashless dispersants are two types of commonly used oil additives. Metal-containing dispersants have a good dispersancy capacity but the presence of metals can lead to the production of insoluble solids upon degradation. These solid salts actually add to the sludge problem. The other type of dispersants is referred to as ashless dispersants. Unlike metallic dispersants, ashless dispersants do not leave any ashes or embers in the engine.[1] Polyisobutylene succinimide (PIBSI) dispersants are the most common ashless dispersants used in the oil industry today and were initially developed in 1966.[7-10] They are constituted of a polyamine head and a PIB stabilizing tail. For a given succinimide dispersant, a higher number of secondary amines in the polyamine head results in better adsorption of the dispersant onto the polar surface of UFPs, but the basic polyamine linker of PIBSI dispersants compromises their compatibility with the fluorocarbon elastomers that are used as engine seals and this issue represents a challenging problem to the industry.[3,6,11,12]

A number of approaches have been introduced to reduce the basicity of dispersant amines such as their modification with boric acid or ethylene carbonate.[12-14] Although such capping agents generally improve the compatibility of the dispersants with engine seals and the other compounds of the oil formulation, capping makes the dispersants less efficient. The preparation of modified *bis*-polyisobutylene succinimide dispersants (M*b*-PIBSI) begins by generating the non-modified PIBSI dispersant as follows. Reaction of a polyisobutylene chain terminated at one end with a succinic anhydride group (PIBSA)[9,15,16] with a polyamine terminated at both ends with two primary amines in a 1:2 polyamine:PIBSA ratio generates *bis*-PIBSI (*b*-PIBSI) dispersants.[17-19] The *b*-PIBSI dispersants can be post-modified with reactants such as boric acid or ethylene carbonate to generate M*b*-PIBSI. While these reactions have been reported in the literature for decades, a recent report has established that the characterization of *b*-PIBSI dispersants remains challenging by techniques based on FTIR or ^{1}H NMR spectroscopies due to complications caused by interactions generated between the succinimide groups and secondary amines of *b*-PIBSI dispersants.[20]

Interestingly the same study also found that the inherent fluorescence of the succinimide groups in the *b*-PIBSI dispersants was efficiently quenched by secondary and tertiary amines, and that the quenching efficiency increased linearly with increasing number of secondary amines in the polyamine linker used to prepare the *b*-PIBSI dispersants. Since chemical post-modification of *b*-PIBSI dispersants is a common practice in the oil additive industry, and considering the challenges associated with the characterization of the chemical composition of *b*-PIBSI dispersants with traditional techniques, this report investigates the extent to which fluorescence quenching of the succinimide groups found in *b*-PIBSI dispersants could provide information about the chemical composition of M*b*-PIBSI dispersants. To this end, M*b*-PIBSI

dispersants were prepared by ethylene carbonate post-modification of *b*-PIBSI dispersants and the ability of FTIR, ^{1}H NMR, and fluorescence at providing quantitative information about their chemical composition was assessed.

The chemical composition and structure of the dispersants are known to influence the reduction in sludge formation. The adsorption isotherms analysis can provide information on how effectively different dispersants bind onto the surface of carbon black particles (CBPs) used as mimics of UFPs.[18,21-23] The adsorption isotherms of a series of PIBSI dispersants have been determined in apolar hexane earlier and the results showed an increase in the association strength of the dispersant with increasing number of secondary amines in the polyamine core.[18] The present study compares the adsorption isotherms of *b*-PIBSI and M*b*-PIBSI dispersants onto CBPs by using the inherent fluorescence of the succinimide groups. The results indicate that EC-post-modification of *b*-PIBSI dispersants lowers their ability to bind onto CBPs. It confirms that a trade-off must be reached between the reduction in secondary amine basicity through EC modification of *b*-PIBSI dispersants and their ability to latch onto the surface of UFPs.

3.3 Experimental

***Chemicals*.** Acetone (HPLC grade, Caledon), hexane (HPLC grade, Caledon), xylene (reagent grade, 98.5%, EMD), deuterated chloroform ($CDCl_3$, 99.8%, Cambridge Isotope Laboratory Inc.), tetrahydrofuran (THF, HPLC grade, Caledon), dodecane (anhydrous, 99%, Sigma-Aldrich), ethyl ether (anhydrous, 99% Sigma-Aldrich), ethyl acetate (HPLC, 99.7% Sigma-Aldrich), and 2-dodecanone (GC grade, 97%, Sigma-Aldrich) were used as received. The chemicals hexamethylenediamine (HMDA, 98%), diethylenetriamine (DETA, 99%), triethylenetetramine (TETA, 97%), tetraethylenepentamine (TEPA, technical grade),

pentaethylenehexamine (PEHA, technical grade), dibutylamine (DBA, 99.5%), octylamine (99%), *N*-methyl succinimide (*N*-MSI, 99%), butylamine (BUA, 99%), diethylamine (DEA, 99.5%), triethylamine (TEA, 99.5%), ethylene carbonate (EC, 98%), magnesium sulfate anhydrous (97%), and activated charcoal (100 mesh) were purchased from Sigma-Aldrich and were employed without further purification. Polyisobutylene succinic anhydride (PIBSA) was supplied by Imperial Oil.

***Proton Nuclear Magnetic Resonance* (*^{1}H NMR*).** A Bruker 300 MHz high resolution NMR spectrometer was used to acquire the ^{1}H NMR spectra at a polymer concentration of about 10 mg/mL in $CDCl_3$.

***Fourier Transform Infrared* (*FTIR*).** A Bruker Tensor 27 FTIR spectrometer was used to acquire all FTIR spectra with an absorbance smaller than unity to avoid saturation of the detector. Polymer solutions prepared in $CDCl_3$ were deposited drop-wise onto a NaCl FTIR plate. The solvent was evaporated under a stream of nitrogen leaving behind a thin polymer film.

***UV-Visible Spectrophotometer*.** Absorbance measurements were conducted on a Cary 100 UV-Visible spectrophotometer. Absorption spectra were acquired between 200 and 600 nm with quartz cells having path lengths of 0.1, 1, or 10 mm.

***Steady-State Fluorescence*.** A Photon Technology International (PTI) LS-100 steady-state fluorometer was used to acquire the fluorescence spectra. The instrument was equipped with an Ushio UXL-75Xe Xenon arc lamp and a PTI 814 photomultiplier detection system. The emission spectra were excited at 360 nm and acquired from 365 to 600 nm.

***Time-Resolved Fluorescence*.** All solutions were excited at 360 nm with a 340 nm nano-LED light source fitted onto an IBH time-resolved fluorometer to acquire their fluorescence decays

at 428 nm. Fluorescence decay analysis included light scattering and background corrections. The sum of exponentials shown in Equation 3.1 was applied to fit the fluorescence decays of the *b*-PIBSI dispersants.

$$i(t) = \sum_{i=1}^{n_{exp}} a_i \times \exp(-t/\tau_i) \tag{3.1}$$

In Equation 3.1, n_{exp} represents the number of exponentials used in the decay analysis and the parameters a_i and τ_i represent the amplitude and decay time of the i^{th} exponential, respectively. The decay fits were deemed satisfactory if the χ^2 value was smaller than 1.30 and the residuals and the autocorrelation of the residuals were randomly distributed around zero.

Synthesis of 2-Hydroxyethyl N,N-Dibutyl Carbamate. 2-Hydroxyethyl *N,N*-dibutyl carbamate (HEDBC) was prepared by reacting one molar equivalent of dibutylamine (DBA) with a slight excess of ethylene carbonate (EC) according to Scheme 3.1.

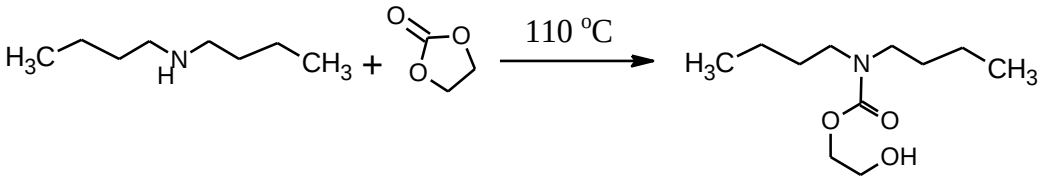

Scheme 3.1. Reaction of dibutylamine (DBA) and ethylene carbonate (EC).

DBA (4.0 g, 31 mmol) and EC (2.8 g, 32 mmol) were added in a two neck round bottom flask capped with a water condenser. The reaction was carried out without solvent under nitrogen at 110 °C for 20 hours. The product mixture was dissolved in 100 mL of diethyl ether, and extracted with 100 mL of HCl (1 M) solution. Unreacted EC partitioned into the aqueous layer whereas the carbamate products stayed in the organic layer. Magnesium sulfate anhydrous

was used to dry the ether fraction and was removed by filtration. Column chromatography with silica gel was performed to isolate the desired product. A 1:1 ratio of hexane and ethyl acetate solution was used as the eluent and the products were separated. Three different compounds were found in the organic layer. The ^{1}H NMR spectra of the desired compound obtained after separation via column chromatography is shown as Supporting Information in Figure S3.1.

Comparison of the spectra of DBA and HEDBC indicates that the peak of the methylene protons **1** of the butyl groups next to the nitrogen shifted from 2.5 to 3.15 ppm. Proton **1** of HEDBC is also broader since the amine proton of DBA is substituted by the more rigid carbamate group in HEDBC. New peaks appeared at 2.8, 3.8, and 4.2 ppm. The triplet at 2.8 ppm represented the alcohol proton while the peaks at 3.8 and 4.2 ppm were assigned to the methylene protons α and β to the alcohol, respectively.

***Synthesis of the Polyisobutylene Succinimide (PIBSI) Dispersants*.** The polyisobutylene succinimide (*b*-PIBSI) dispersants were prepared from the reaction of one molar equivalent (m_{eq}) of different polyamine derivatives with two m_{eq} of PIBSA as described in Scheme 3.2. In the current study, hexamethylenediamine (HMDA), diethylenetriamine (DETA), triethylenetetramine (TETA), tetraethylenepentamine (TEPA), and pentaethylenehexamine (PEHA) were used as polyamines and their chemical structure is given in Table 3.1. All *b*-PIBSI dispersants were synthesized according to Scheme 3.2 based on a procedure that has been described in detail in an earlier publication.[18,20]

Table 3.1. Chemical structures of the amine derivatives used to prepare the *b*-PIBSI dispersants.

Polyamine	**Chemical Structure**
Hexamethylenediamine (HMDA)	H_2N-$(CH_2CH_2)_3$-NH_2
Diethylenetriamine (DETA)	H_2N-$(CH_2CH_2$-$NH)_2$-H
Triethylenetetramine (TETA)	H_2N-$(CH_2CH_2$-$NH)_3$-H
Tetraethylenepentamine (TEPA)	H_2N-$(CH_2CH_2$-$NH)_4$-H
Pentaethylenehexamine (PEHA)	H_2N-$(CH_2CH_2$-$NH)_5$-H

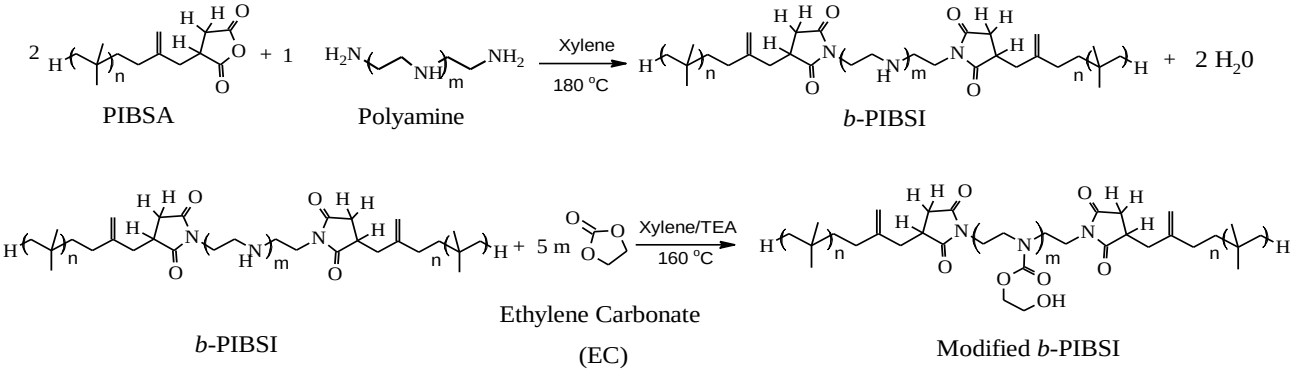

Scheme 3.2. Synthesis and modification of succinimide dispersants.

Successful reaction was confirmed by comparison of the FTIR absorption of de-hydrated PIBSA (Trace A) with that of the *b*-PIBSI dispersant (Trace B) in Figure 3.1. The FTIR spectrum of PIBSA shows an absorption band at 1785 cm^{-1} due to the carbonyl groups of succinic anhydride (SA). After reaction, the absorption at 1785 cm^{-1} disappeared and a new peak appeared at 1705 cm^{-1} in Trace B due to the succinimide carbonyls.

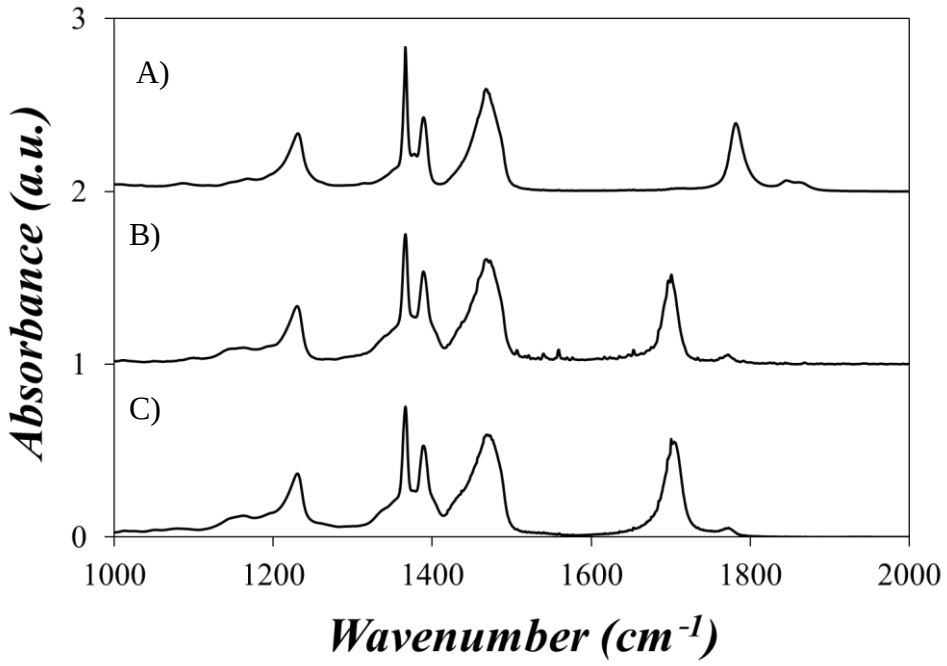

Figure 3.1. FT-IR spectra of A) dehydrated PIBSA, B) *b*-PIBSI-PEHA, and C) M*b*-PIBSI-PEHA.

***Modification of the Polyisobutylene Succinimide (Mb-PIBSI) Dispersants*.** The post-modification of all *b*-PIBSI dispersants was conducted in the same manner and is described in detail for *b*-PIBSI-PEHA. *b*-PIBSI-PEHA (0.50 g, 77 μmol) and EC (0.14 g, 1.54 mmol) were mixed with a 1:5 excess molar ratio of secondary amines-to-EC. The mixture was then dissolved in xylene (1.00 g, 1.14 mL) and TEA (0.50 g, 0.69 mL). The modification reaction was carried out in a sealed reaction vessel since EC tends to evaporate at the temperature used for the modification reaction. Furthermore, the reaction mixture was degassed with nitrogen for 15 minutes before the reaction and after each sampling of the reaction mixture made to monitor the reaction progress. After degassing, the mixture was heated to 160 ^{o}C and kept at this temperature for 24 hrs. Aliquots were withdrawn over time through a rubber septum tightly fastened to the reaction vessel to follow the reaction progress. After completion, the reaction

product was washed with 20 mL of distilled water three times. Finally the product was dried in a vacuum oven at 70 ^{o}C overnight.

***Gel Permeation Chromatography* (*GPC*).** A Viscotek GPC max VE 2001 instrument equipped with a Viscotek TDA 305 triple detector array comprised of a refractive index, viscosity, and light scattering detector was used. The samples were passed through a divinylbenzene mixed bed Polyanalytik column. Tetrahydrofuran (THF) was used as the solvent at a flow rate of 1.0 mL/min. All samples were filtered using 0.2 μm Millipore polytetrafluoroethylene (PTFE) filters before injection and the sample concentration was less than 10 mg/mL. Due to their low molecular weight (< 6,000 g.mol^{-1}), the polyisobutylene samples used in this study did not scatter light strongly enough to yield a reliable light scattering signal and the light scattering detector of the GPC instrument could not be used to determine their absolute molecular weight. Instead the GPC instrument determined the apparent molecular weight of the polyisobutylene samples as it was calibrated with polystyrene standards.

The GPC trace obtained for PIBSA, *b*-PIBSI-PEHA, and M*b*-PIBSI-PEHA are shown in Figure S3.2. PIBSA eluted at an elution volume (V_{el}) of 25 mL. GPC analysis of the product of the reaction between 1 molar equivalent (m_{eq}) of a polyamine like PEHA and 2 m_{eq} of PIBSA yielded a main peak in Figure S3.2 that was shifted to a lower elution volume (V_{el} = 23 mL) as compared to PIBSA, reflecting the expected increase in molecular weight. From the overlaying of the GPC traces obtained for *b*-PIBSI-PEHA (trace B) and M*b*-PIBSI-PEHA (trace C) in Figure S3.2, it could be concluded that modification of the PIBSI dispersants with EC did not affect their molecular weight distribution (MWD).

3.4 Results and Discussion

In this study, fluorescence was used as an analytical method to characterize the level of modification of M*b*-PIBSI dispersants in terms of the number of unreacted secondary amines per gram of dispersant. This characterization method took advantage of the fluorescence of the succinimide moieties found in the M*b*-PIBSI dispersants and the fact that they are being quenched with a different efficiency by secondary amines and urethane groups.[20,24-27] Furthermore, by using the inherent fluorescence of the succinimide groups, the adsorption isotherm of *b*-PIBSI and M*b*-PIBSI dispersants onto carbon black particles (CBPs) were obtained to determine the effect that the chemical composition of the polar core has on the adsorption of the dispersants. The chemical composition and adsorption of the oil soluble dispersants *b*-PIBSI-DETA, *b*-PIBSI-TEPA, *b*-PIBSI-PEHA, M*b*-PIBSI-TEPA, and M*b*-PIBSI-PEHA onto CBPs were studied in dodecane. These experiments are described hereafter.

Proton Nuclear Magnetic Resonance (^{1}H NMR). PIBSA was used as the starting material in the synthesis of M*b*-PIBSI. PIBSA was reacted with DETA, TETA, TEPA, and PEHA to produce a series of *b*-PIBSI dispersants which were post-modified with EC to generate M*b*-PIBSI. The ^{1}H NMR spectra of PIBSA, *b*-PIBSI-TEPA, and M*b*-PIBSI-TEPA are shown in Figure S3.3. In the spectrum of PIBSA presented in Figure S3.3A, the peaks at 2.6 and 3.3 ppm represent the protons in the succinic anhydride ring. After reaction with a polyamine, these peaks shifted to 2.5 and 3.0 ppm in Figure S3.3B, and new peaks appeared at 2.8 and 3.5 ppm representing the ethylene protons in the polar core of the *b*-PIBSI dispersant. In all polymer samples, the peaks at 1.1 and 1.4 ppm (not shown in Figure S3.3) represent, respectively, the methylene and the methyl protons of the PIB backbone obtained in a 1:3 ratio. The peak at 5.5 ppm was found for all polymer samples and might be due to the presence of vinyl groups

generated during the Alder-ene reaction of PIBSA. The sharp peaks at 2.25 and 2.3 ppm in Figure S3.3C are due to traces of xylene. The assignment of the ^{1}H NMR spectrum of M*b*-PIBSI-TEPA (Figure S3.3C) was done by comparing it to that of HEDBC (Figure S3.1). The two peaks at 3.8 and 4.2 ppm found in the ^{1}H NMR spectrum of M*b*-PIBSI-TEPA correspond to the methylene protons in the carbamate side chain, with a same chemical shift as that found in the ^{1}H NMR spectrum of HEDBC in Figure S3.1. In the spectrum of M*b*–PIBSI–TEPA, the peak at 2.8 ppm was reduced and the peak at 3.5 ppm was enlarged as the environment of the methylene protons in the α position to the central carbamate became similar to that of the methylene protons in the α position to the succinimide groups. Based on ^{1}H NMR, modification of *b*-PIBSI-DETA and *b*-PIBSI-TETA was inefficient, showing no peak at 3.8 and 4.2 ppm after reaction with EC as shown in Figures S3.4A and B. The fact that modification was successful with *b*-PIBSI-TEPA and *b*-PIBSI-PEHA (Figures S3.4C and D) which both have a longer, and thus more accessible, polyamine spacer suggests that the absence of reaction observed with *b*-PIBSI dispersants having a shorter linker might be the result of steric hindrance.

In an ideal case, when all secondary amines have reacted, ^{1}H NMR spectroscopy can be used to determine the exact yield of the modified dispersants. But in practice, there remain some unreacted secondary amines in the polyamine linker that might cause aggregation due to H-bonding between the secondary amine protons and the succinimide carbonyls, and lead to distortion by broadening of the ^{1}H NMR peaks due to slower tumbling. Equation 3.2 was applied to calculate the modification yield of *b*-PIBSI dispersants by using the number of urethane moieties (N_{UR}) generated in the polyamine linker per number of isobutylene monomers (N_{IB}).

$$Yield\,\% = \frac{(\frac{N_{UR}}{N_{IB}})_{\mathrm{Re}\,al.}}{(\frac{N_{UR}}{N_{IB}})_{Ideal}} \tag{3.2}$$

According to our previous paper,[20] the ratio of succinimide moiety to N_{IB} in a *b*-PIBSI molecule equals 1:52 for *b*-PIBSI dispersants, but distortion of the ^{1}H NMR spectra due to aggregation of the dispersants resulted in an apparent 1:32 ratio based on integration of the ^{1}H NMR peaks. Thus $(N_{UR}/N_{IB})_{Ideal}$ in Equation 3.2 equals $\frac{m}{2}(N_{SI}/N_{IB})$ where m represents the number of secondary amines in the polymer linker and N_{SI}/N_{IB} equals 1:52 or 1:32 assuming that aggregation of the dispersants does not or does occur, respectively. Assuming no aggregation, reaction yields of 106 ± 2 % and 95 ± 1 % were calculated for M*b*-PIBSI-TEPA and M*b*-PIBSI-PEHA, respectively, suggesting complete modification of the secondary amines of the polyamine linker. On the other hand, reaction yields of 66 ± 2 % and 62 ± 2 % were calculated for M*b*-PIBSI-TEPA and M*b*-PIBSI-PEHA, respectively, assuming aggregation of the dispersant and using the apparent N_{SI}/N_{IB} ratio equalled to 1:32. As it turns out, the fluorescence quenching experiments described later on demonstrate unambiguously that complete modification of the secondary amines did not occur, but that partial modification of the secondary amines took place in a proportion similar to what was determined by ^{1}H NMR assuming aggregation of the modified dispersants.

Fourier Transform Infrared (FTIR). The FTIR spectra were obtained for the *b*-PIBSI and M*b*-PIBSI dispersants. The peak at 1705 cm^{-1} characteristic of the succinimide or carbamate carbonyls was monitored in terms of its band intensity I_{max} (with respect to the signal at 1390 cm^{-1}) and full width at half maximum (FWHM). The results presented in Table 3.2 showed that

b-PIBSI-DETA, *b*-PIBSI-TETA, *b*-PIBSI-TEPA, and *b*-PIBSI-PEHA have a larger I_{max} and FWHM in comparison to *b*-PIBSI-HMDA due to intermolecular aggregation induced by H-bonding between the secondary amines of the spacer and the succinimide carbonyls (Figure 3.1 and Table 3.2).[20] Furthermore, the FTIR results for M*b*-PIBSI-DETA and M*b*-PIBSI-TETA did not show any changes in I_{max} and FWHM within experimental error when compared to their unmodified analogs as expected since ^{1}H NMR analysis indicated that EC modification did not proceed with these two samples. The FTIR results for M*b*-PIBSI-TEPA and M*b*-PIBSI-PEHA indicated that I_{max} and FWHM for the peak at 1705 cm^{-1} became larger after modification (Figure 3.1 and Table 3.2). This analysis confirmed the successful modification of the *b*-PIBSI dispersants prepared with a longer polyamine linker observed by ^{1}H NMR. The increase in I_{max} and FWHM results from the increased number of carbonyl groups found in the polar core of these dispersants after EC modification. The summary of the I_{max} and FWHM values for the *b*-PIBSI dispersants before and after modification are shown in Table 3.2.

Table 3.2. Maximum peak intensity ($\frac{I_{max}(1705\ cm^{-1})}{I_{max}(1390\ cm^{-1})}$) and full width half max (FWHM) values calculated from FTIR spectrum.

Polymer	$\frac{I_{max}(1705\ cm^{-1})}{I_{max}(1390\ cm^{-1})}$	FWHM	Polymer	$\frac{I_{max}(1705\ cm^{-1})}{I_{max}(1390\ cm^{-1})}$	FWHM
b-PIBSI-HMDA	0.35	13			
b-PIBSI-DETA	0.54	14	M*b*-PIBSI-DETA	0.49	15
b-PIBSI-TETA	0.53	16	M*b*-PIBSI-TETA	0.51	16
b-PIBSI-TEPA	0.49	16	M*b*-PIBSI-TEPA	0.64	26
b-PIBSI-PEHA	0.52	20	M*b*-PIBSI-PEHA	0.65	35

Steady-State and Time-Resolved Fluorescence Measurements. Fluorescence was applied to estimate the level of modification of the M*b*-PIBSI dispersants. The intrinsic fluorescence of the succinimide groups has been shown to be efficiently quenched by the secondary amines of the polyamine spacer of *b*-PIBSI dispersants.[20] Since the EC modification of *b*-PIBSI dispersants replaces the secondary amines of the *b*-PIBSI polyamine linker by urethane functions, the ability of a urethane group to quench the fluorescence of succinimide moieties was determined by monitoring the fluorescence of *N*-methyl succinimide (*N*-MSI) as a function of 2-hydroxyethyl *N*,*N*-dibutyl carbamate (HEDBC) concentration in THF. Figure 3.2A for the steady-state fluorescence spectra and Figure 3.2B for the time-resolved fluorescence decays showed that addition of up to 0.3 M HEDBC to the *N*-MSI solution resulted in a smaller than 50% decrease in the fluorescence intensity (I) and number average lifetime $<\tau>$.[20] By comparison, quenching of the fluorescence of *N*-MSI by 0.3 M diethylamine (DEA) would have resulted in a much more pronounced 88% decrease in I and a 78% reduction in $<\tau>$.[20] The pre-exponential factors and decay times retrieved from the multiexponential analysis of the fluorescence decays have been reported in Table S3.1 in Supporting Information (SI). The spectra and decays shown in Figures 3.2A and B were then used to determine the ratios I_0/I and $<\tau>_0/<\tau>$ which were then plotted as a function of HEDBC concentration in Figure 3.2C. I_0 and $<\tau>_0$ represent the fluorescence intensity and number average lifetime of *N*-MSI in the absence of HEDBC. The trends obtained in Figure 3.2C with I_0/I and $<\tau>_0/<\tau>$ yield similar straight lines which suggested that little static quenching occurred contrary to what was observed for the quenching of *N*-MSI by DEA.[20] The similar lines observed for the I_0/I and $<\tau>_0/<\tau>$ trends reflect the absence of static quenching and thus aggregation between MSI and HEDBC. It also indicates that the propensity of the hydroxyl proton of HEDBC to H-bond with the carbonyls

of *N*-MSI is much weaker than the amine proton of DEA. The slope obtained for $<\tau>_0/<\tau>$ in Figure 3.2C can be used to determine the quenching rate constant (k_Q) found to equal 2.5 ± 0.2×10^8 $M^{-1}.s^{-1}$, 7 times smaller than the k_Q value of 17.4 ± 0.2×10^8 $M^{-1}.s^{-1}$ obtained for the quenching of *N*-MSI by DEA indicating that the urethane moiety of HEDBC constitutes a much weaker quencher for *N*-MSI compared to the secondary amine group of DEA. The substantial reduction in quenching observed from DEA to HEDBC should lead to obvious changes in the fluorescence response of the succinimide moieties found in the *b*-PIBSI dispersants after modification of their secondary amines by EC.

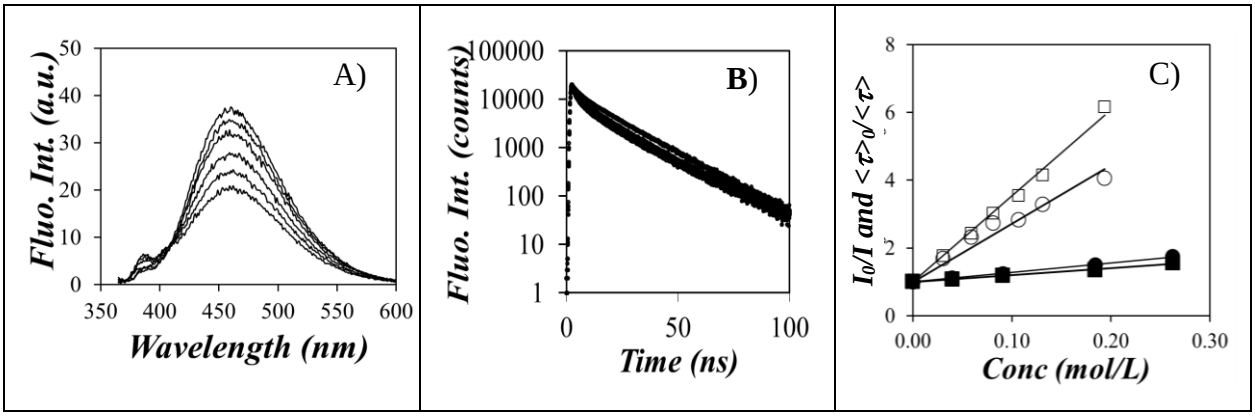

Figure 3.2. A) Steady-state fluorescence spectra and B) fluorescence decay of *N*-MSI quenched with HEDBC in THF. C) Stern-Volmer plot for the quenching of *N*-MSI with HEDBC ((■) I_0/I and (●) $<\tau>_0/<\tau>$) and DEA ((□) I_0/I and (○) $<\tau>_0/<\tau>$) in THF. From top to bottom: The HEDBC concentrations in Figures 3.2A and 3.2B varied from 0 M to 0.3 M. ($C_{N\text{–MSI}}$ = 0.45 mol/L, λ_{ex} = 360 nm, λ_{em} = 428 nm).

This was indeed observed in Figure 3.3A and B where the fluorescence intensity increased after modification of the *b*-PIBSI dispersants with EC. However the increase in fluorescence intensity shown in Figure 3.3A and B was quite minor compared to what would

have been expected based on the reduction in fluorescence quenching observed in Figure 3.2C upon replacing a secondary amine by a urethane group. In fact, the complete modification of the secondary amines in the linker into urethane groups should have resulted in an increase in the fluorescence intensity of M*b*–PIBSI–TEPA and M*b*-PIBSI-PEHA corresponding to 81% and 77% of the fluorescence intensity of *b*-PIBSI-HMDA shown as a reference in Figure 3.3. The fact that this was not observed led to the conclusion that not all secondary amines in *b*-PIBSI-TEPA and *b*-PIBSI-PEHA had been modified upon reaction with EC. This conclusion was further supported by the visual inspection of the fluorescence decays of M*b*–PIBSI-TEPA and M*b*-PIBSI-PEHA, which showed hardly any difference with the dispersants before modification.

The fluorescence spectra and decays shown in Figures 3.3A–D were analyzed to determine the corresponding fluorescence intensity I and number average lifetime $<\tau>$ for M*b*-PIBSI-TEPA and M*b*-PIBSI-PEHA. The pre-exponential factors and decay times retrieved from the decay analysis have been listed in Table S3.2. Using *b*-PIBSI-HMDA as a reference for the I_0 and $<\tau>_0$ values of unquenched succinimide groups in *b*-PIBSI dispersants as done in an earlier publication,[20] the ratios I_0/I and $<\tau>_0/<\tau>$ for the two modified dispersants were plotted in Figure 3.4 as a function of the number of secondary amines in the linker, along the I_0/I and $<\tau>_0/<\tau>$ ratios which were obtained earlier for the unmodified dispersants *b*-PIBSI-DETA, *b*-PIBSI-TETA, *b*-PIBSI-TEPA, and *b*-PIBSI-PEHA.[20] The same trends were obtained in dodecane, THF, and dodecanone. The $<\tau>_0/<\tau>$ ratios showed minor differences for the dispersants before and after modification. The I_0/I ratios showed more substantial changes but took values that were much larger than unity, contrary to what was expected if the EC modification had been complete.

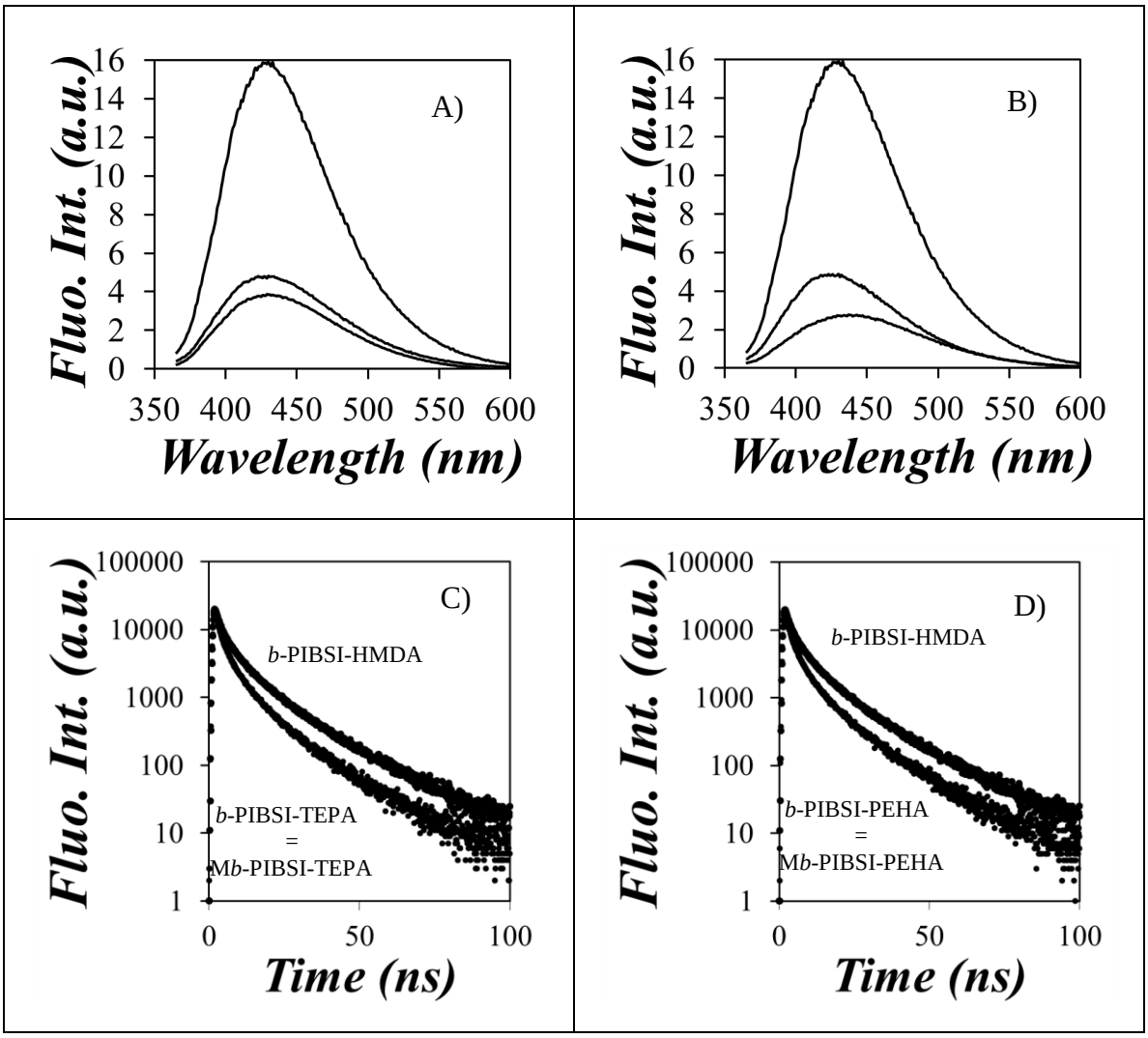

Figure 3.3. Steady-state fluorescence spectra (A and B) and time-resolved fluorescence decays (C and D). From top to bottom A) and C): *b*-PIBSI-HMDA, M*b*-PIBSI-TEPA, and *b*-PIBSI-TEPA dispersants in dodecane and B) and D): *b*-PIBSI-HMDA, M*b*-PIBSI-PEHA, and *b*-PIBSI-PEHA dispersants in dodecane. (λ_{ex} = 360 nm, λ_{em} = 428 nm)

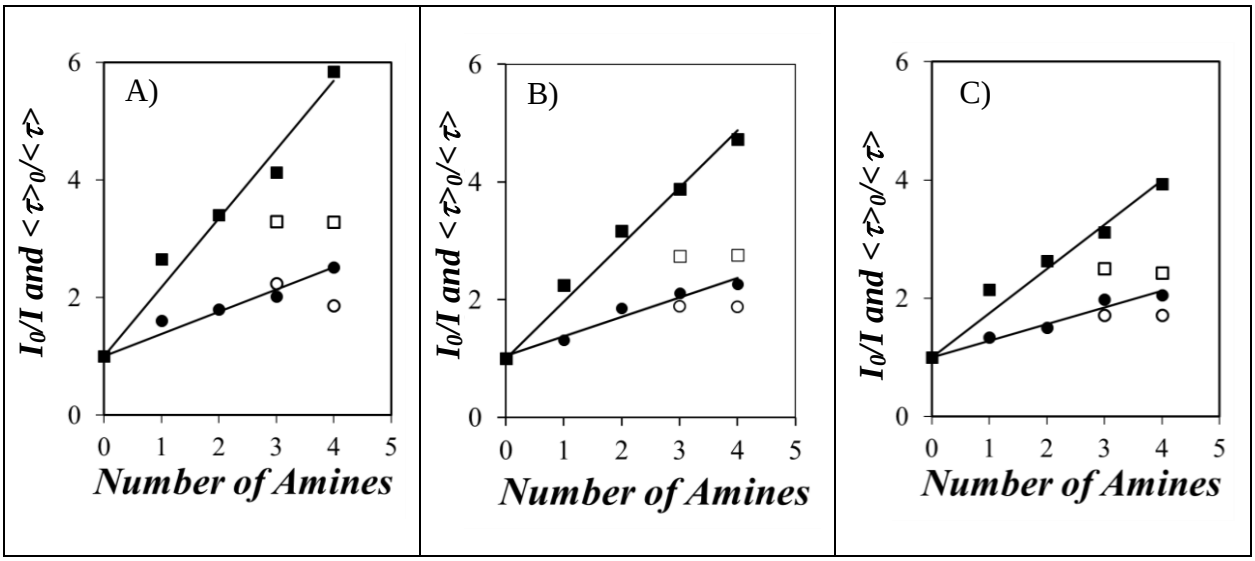

Figure 3.4. (●) I_0/I and (■) $<\tau>_0/<\tau>$ of *b*-PIBSI dispersants and (○) I_0/I and (□) $<\tau>_0/<\tau>$ of M*b*-PIBSI dispersants versus number of secondary amines, in A) dodecane, B) THF, and C) dodecanone.

The poor recovery in fluorescence signal observed after the EC modification of the polyamine linkers was attributed to the incomplete transformation of the secondary amines in the linker into the urethane groups. In turn, the unreacted secondary amines could H-bond effectively with the carbonyls of the succinimide and urethane groups, resulting in a substantial static quenching as observed from the different I_0/I and $<\tau>_0/<\tau>$ ratios. The I_0/I ratio probes both the static and dynamic quenching of the succinimide groups and its expression is provided in Equation 3.3. Because I_0/I responds to both types of quenching, it is much more sensitive than the ratio $<\tau>_0/<\tau>$ that is influenced by dynamic quenching only. Therefore, the I_0/I ratio was selected to probe the effect that EC modification of the PIBSI secondary amines would have on the efficiency of quenching.

$$\frac{I_0}{I} = 1 + (\alpha\, K_{SV}[Q]_0 + (1-\alpha)\, K_{SV}^{M}[Q]_0) \qquad (3.3)$$

In Equation 3.3, I_0 and I represent the fluorescence intensity of *b*-PIBSI-HMDA and that of the modified dispersants, respectively. The constants K_{SV} (= K_S+K_D) and K^M_{SV} are the Stern-Volmer constants resulting from dynamic (K_D) and static quenching (K_S) of the unmodified and modified dispersants, respectively. $[Q]_0$ corresponds to the local concentration of secondary amines in the unmodified *b*-PIBSI dispersant and is equal to m/V_{core} where m and V_{core} are, respectively, the number of secondary amines (m) in the polyamine spacer of the dispersant and the core volume (V_{core}) which is assumed to be the same for our dispersants. The fraction α represents the molar fraction of unreacted secondary amines in the polyamine linker remaining after EC modification. The fraction α after EC modification was retrieved by rearranging Equation 3.3 into Equation 3.4.

$$\frac{I_0}{I} - 1 = \frac{K_{SV}}{V_{core}} m(\alpha + (1-\alpha)\frac{K_{SV}^{M}}{K_{SV}}) = \frac{K_{SV}}{V_{core}} m(\alpha + (1-\alpha)\, K') \qquad (3.4)$$

In Equation 3.4, $\frac{K_{SV}}{V_{core}}$ is the slope of the plot I_0/I versus the number of amines obtained for unmodified dispersants shown in Figure 3.4. $\frac{K_{SV}}{V_{core}}$ was found to equal 0.96 ± 0.01 for the *b*-PIBSI dispersants in THF, but the ratio $\frac{K_{SV}^{M}}{K_{SV}}$ in Equation 3.4 is unknown. Therefore, K' whose expression is given in Equation 3.5 was used to calculate α. K' can be approximated by

taking the ratio of K_{SV}^{HEDBC} for HEDBC to K_{SV}^{DEA} for DEA obtained in THF whose values have been listed in Table 3.3. This derivation takes advantage of the similarity in chemical composition between DEA and the secondary amines in the polyamine linker of the *b*-PIBSI dispersants on the one hand and between HEDBC and the urethane groups on the other hand. Based on the data listed in Table 3.3, the *K*' value was found to equal 0.079 ± 0.001.

$$K' = \frac{K_{SV}^{M}}{K_{SV}} = \frac{K_{SV}^{HEDBC}}{K_{SV}^{DEA}} \tag{3.5}$$

Table 3.3. K_{sv} constants obtained from Stern-Volmer plot resulting from quenching of *N*-MSI by DEA, TEA, and HEDBC in THF.

Name	K_{SV} (M^{-1})
DEA	25.17 ± 0.01
TEA	25.08 ± 0.02
HEDBC	1.98 ± 0.02

Application of this procedure to the I_0/I ratios shown in Figure 3.4 for M*b*-PIBSI-TEPA and M*b*-PIBSI-PEHA yielded an α value in Equation 3.4 of 0.4 and 0.3, respectively, suggesting that 60 ± 1 and 70 ± 1 % of the secondary amines had reacted (Table 3.4). Incidentally, this conclusion agrees remarkably well with the findings by ^{1}H NMR that 66 ± 2 and 62 ± 2 % of all secondary amines in the polyamine linker of, respectively, M*b*-PIBSI-TEPA and M*b*-PIBSI-PEHA had reacted when assuming that dispersant association took place in solution and assuming an apparent N_{SI}/N_{IB} ratio of 1:32. The fact that none of the one and two secondary amines in the linker of, respectively, *b*-PIBSI-DETA and *b*-PIBSI-TETA reacted with EC, and that about one of the three secondary amines of *b*-PIBSI-TEPA and one of the four secondary

amines of *b*-PIBSI-PEHA did not react with EC strongly suggests that steric hindrance as well as H-bonding with succinimide carbonyls must contribute to lowering the extent of EC modification. This conclusion agrees with all experimental evidence obtained thus far such as the difficulty in using ^{1}H NMR and FTIR to determine the extent of modification in the M*b*-PIBSI dispersants due to the existence of strong H-bonds, and the fluorescence quenching experiments that clearly demonstrate that not all secondary amines have reacted with EC. The higher reactivity of the secondary amines of M*b*-PIBSI-PEHA is attributed to their better accessibility to, and thus better reactivity with EC.

Table 3.4. Number of unreacted secondary amines and level of modification for M*b*-TEPA and M*b*-PEHA in THF determined by fluorescence quenching measurements.

Dispersant	# of unreacted secondary amines	Level of Modification
M*b*-PIBSI-TEPA	1.21 ± 0.04	60 ± 1%
M*b*-PIBSI-PEHA	1.13 ± 0.03	70 ± 1%

Adsorption of b-PIBSI Dispersants onto Carbon Black Particles. After having characterized the extent of EC modification applied to the *b*-PIBSI dispersants, the adsorption of the oil-soluble dispersants *b*-PIBSI-DETA, *b*-PIBSI-TEPA, *b*-PIBSI-PEHA, M*b*-PIBSI-TEPA, and M*b*-PIBSI-PEHA onto carbon black particles (CBPs) used as models for the ultrafine particles (UFPs) generated in engine oil was investigated in dodecane. Since the construction of adsorption isotherms always requires the knowledge of the quantity of unbound ligand, earlier reports used the absorption of a pH-indicator to determine the concentration of secondary amines, and thus dispersant molecules in the solution.[18,19] But since pH-indicators are usually water-soluble weak acids or bases that cannot dissolve in hexane, the procedure required a

change of solvent from hexane where the adsorption measurements were conducted to THF where the unbound dispersant concentration was determined from the absorption response of the pH-indicator. By contrast, fluorescence of the succinimide groups of the dispersants offers a means to determine the concentration of unbound dispersant in the same solvent where the adsorption measurements were carried out, down to extremely low dispersant concentrations by taking advantage of the extraordinary sensitivity of fluorescence.

A number of precautions needed to be taken when conducting these fluorescence experiments. First, while absorption is an absolute measurement, fluorescence only provides quantitative information with respect to a reference. Consequently, all the fluorescence measurements on dispersant solutions were benchmarked against the fluorescence signal of a standard which was a 2.8×10^{-5} M 1-pyrenemethanol solution in methanol that was degased, sealed, and kept in the dark for the duration of these experiments. Second, a small fraction of the succinimide chromophore was found to photobleach upon irradiation in the spectrofluorometer. While photobleaching could not be detected after acquisition of a single fluorescence spectrum, repeated irradiation for successive acquisitions of fluorescence spectra led to a noticeable decrease in fluorescence intensity. Consequently, each dispersant solution was discarded after the acquisition of its fluorescence spectrum.

Following this procedure, calibration curves were generated by plotting the fluorescence intensity of the solution normalized to that of the standard against the concentration of PIBSI dispersant. The calibration curves are shown in Figure S3.5. The slope of these lines could be used as a massic fluorescence coefficient (MFC) to retrieve the concentration of an unknown *b*-PIBSI dispersant. Table 3.5 lists the values of the MFCs obtained for the *b*-PIBSI dispersants. As the secondary amine content of the spacer increased, the MFC decreased as expected since

secondary amines were found to quench the succinimide fluorescence.[20] EC modification increased the MFC of the modified dispersants M*b*-PIBSI-TEPA and M*b*-PIBSI-PEHA to a level close to that of *b*–PIBSI-DETA. This result is reasonable since those two modified dispersants were found to retain one unreacted secondary amine (Table 3.5) making their secondary amine content similar to that of *b*-PIBSI-DETA.

Table 3.5. Summary of the massic fluorescence coefficients (MFC) calculated from steady-state measurements in dodecane. (λ_{ex} = 360 nm)

Polymer	MFC (L. g^{-1})	Polymer	MFC ($L.g^{-1}$)
b-PIBSI-DETA	16.6 ± 0.5		
b-PIBSI-TEPA	14.1 ± 0.2	M*b*-PIBSI-TEPA	17.1 ± 0.0
b-PIBSI-PEHA	8.6 ± 0.1	M*b*-PIBSI-PEHA	15.5 ± 0.7

The MFCs could be used to determine the concentration of unbound dispersants in the adsorption experiments which were conducted as follows. A 3 g/L dispersant solution was prepared in dodecane and masses of 0.01 to 0.4 g of CBPs were added to the solutions. The solutions were agitated at room temperature for 24 hrs, long enough for the solutions to reach equilibrium.[18] The solids were then filtered through 0.2 μm Millipore Teflon filters and each sample was weighed to determine the solution volume from the known density of dodecane (0.78 $g.mL^{-1}$). The fluorescence emission of the *b*-PIBSI and M*b*-PIBSI dispersant solutions were measured at 420 nm and it was converted to the concentration of unbound dispersant C_{eq} using the corresponding MFC value. The amount of adsorbed dispersant at equilibrium per unit surface of CBPs (Γ) expressed in $\mu mol/m^2$ was calculated using Equation 3.6,

$$\Gamma = \frac{(C_0 - C_{eq}) \times V}{m \times A} \tag{3.6}$$

where C_0 and C_{eq} represent the initial dispersant concentration and the equilibrium concentration of unbound dispersant after adsorption, respectively, V is the volume of the solution, m is the mass of CBPs, and A (= 764 m^2/g) is the surface area of the CBPs.[18]

Two concentration regimes could be identified for the adsorption isotherms of the *b*–PIBSI dispersants onto the CBPs as shown in Figure 3.5. At low C_{eq}, binding of dispersant molecules occurs at single sites on the CBPs surface. As those sites become occupied, additional surfactant molecules adsorb on top of already adsorbed dispersant molecules leading to multilayer coverage of the CBPs that is associated with the precipitous increase in Γ observed for larger C_{eq} values (C_{eq} > 400 $mmol/m^3$) in Figure 3.5. Consequently, the binding equilibrium constant of the *b*-PIBSI dispersants onto single sites at the surface of CBPs could be determined from the analysis of the Γ values in the concentration regime corresponding to low C_{eq} values.[19,25]

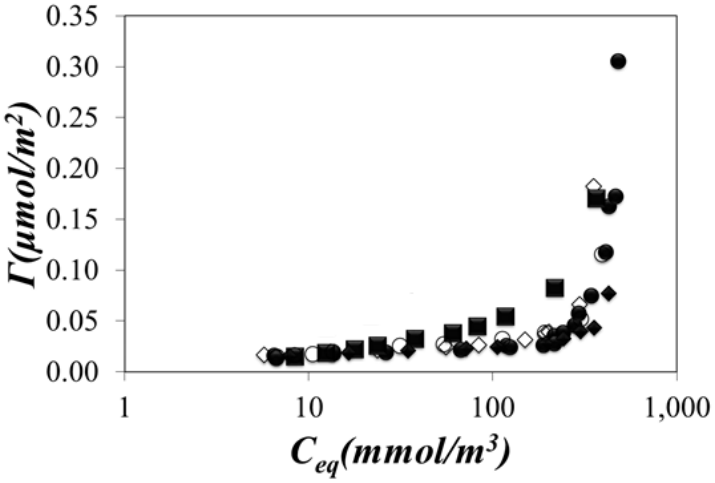

Figure 3.5. Adsorption isotherms of (●) *b*-PIBSI-PEHA, (○) M*b*-PIBSI-PEHA, (♦) *b*-PIBSI-TEPA, (◊) M*b*-PIBSI-TEPA, and (■) *b*-PIBSI-DETA dispersants in dodecane.

The binding isotherms Γ of *b*-PIBSI-DETA, *b*-PIBSI-TEPA, and *b*-PIBSI-PEHA are shown in Figure 3.5 where Γ was plotted as a function of C_{eq} to study the contribution of the different polyamine spacers on adsorption. For all three dispersants, the adsorption isotherm or the amount of dispersant adsorbed onto the CBPs increased as more dispersant was added to the solutions. For a given concentration of free dispersant in dodecane, *b*-PIBSI-DETA had the largest amount of dispersant adsorbed onto the CBPs, followed by *b*-PIBSI-TEPA and *b*-PIBSI-PEHA.

Comparison of the adsorption isotherms of the different PIBSI dispersants was conducted with the Langmuir model, which only handles the binding of the dispersants at low coverage of CBPs. To this end, Equation 3.7 was applied. In Equation 3.7, Γ_{max} is the maximum amount of dispersant adsorbed per unit area and K is the binding constant of the adsorption process.

$$\Gamma = \frac{\Gamma_{max} K C_{eq}}{1 + K C_{eq}} \tag{3.7}$$

Γ_{max} and K were retrieved by rearranging Equation 3.7 into Equation 3.8. The simple Langmuir model could not fit the whole concentration range shown in Figure 3.5 for *b*-PIBSI-DETA, *b*-PIBSI-TEPA and *b*-PIBSI-PEHA since multiple binding regimes were observed from the low to high end of the C_{eq} range. Therefore, Equation 3.8 was only used to fit the linear region of Figure 3.6A corresponding to the larger $1/C_{eq}$ values as shown in Figure 3.6B.

$$\frac{1}{\Gamma} = \frac{1}{\Gamma_{max} K C_{eq}} + \frac{1}{\Gamma_{max}} \tag{3.8}$$

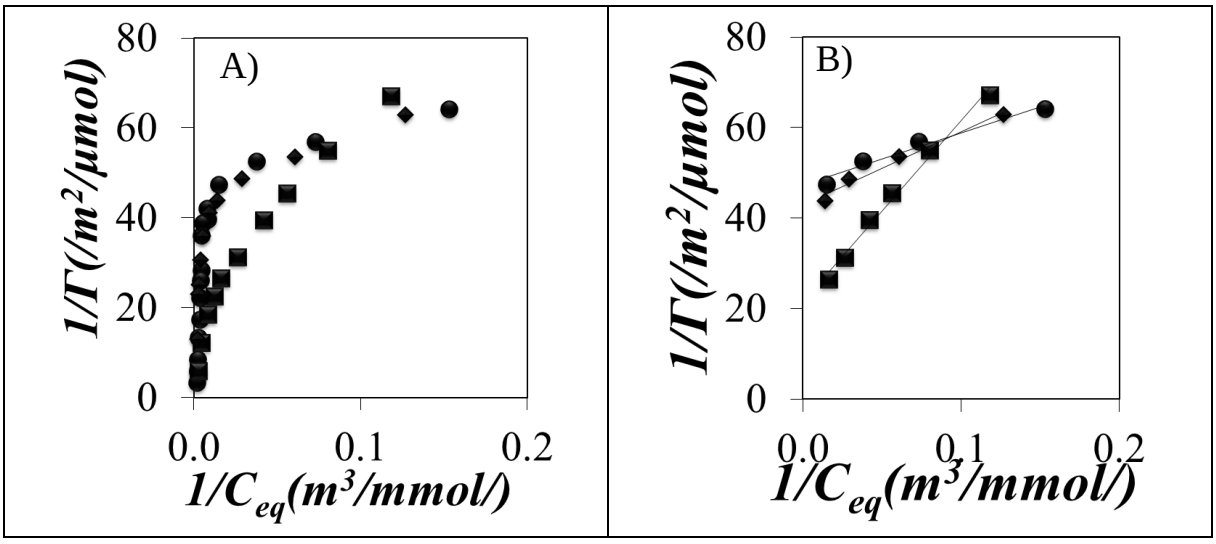

Figure 3.6. Plot of $1/\Gamma$-vs-$1/C_{eq}$ for A) entire concentration range and B) fitted concentration range for (●) *b*-PIBSI-PEHA, (♦) *b*-PIBSI-TEPA, and (■) *b*-PIBSI-DETA dispersants in dodecane.

The Γ_{max} and K values retrieved by fitting the data shown in Figure 3.6B with Equation 3.8 are listed in Table 3.6. The results indicate that the binding constant K increased strongly with the number of secondary amines in the polar core of *b*-PIBSI dispersants. The amount of dispersant needed to saturate the adsorption sites Γ_{max} decreased with increasing number of amines. Based on the K values, these trends indicate that the binding of the dispersants is more efficient when the dispersants contain a higher number of secondary amines.

Table 3.6. Γ_{max} and K values retrieved by fitting the data shown in Figures 3.6 and 3.7 with Equation 3.7.

Dispersant	Solvent	$\Gamma_{max} \times 10^{10}$ (mol/m^2)	K (m^3/mol)
b-PIBSI-DETA	dodecane	464 ± 29	54 ± 1
b-PIBSI-TEPA	dodecane	233 ± 6	268 ± 1
b-PIBSI-PEHA	dodecane	211 ± 6	412 ± 1
M*b*-PIBSI-TEPA	dodecane	260 ± 1	239 ± 1
M*b*-PIBSI-PEHA	dodecane	307 ± 8	130 ± 1

The binding isotherms of *b*-PIBSI-TEPA and *b*-PIBSI-PEHA were also compared to those given in Figure 3.7 for M*b*-PIBSI-TEPA and M*b*-PIBSI-PEHA, respectively. The results in Table 3.6 indicate that the binding constant K decreased for *b*-PIBSI-TEPA and *b*-PIBSI-PEHA after modification. Urethane groups were found to decrease the drive of M*b*-PIBSI dispersants to adsorb on the surface of CBPs. Since M*b*-PIBSI-PEHA had a higher fraction of modified secondary amines, the decrease was more pronounced for M*b*-PIBSI-PEHA than for M*b*-PIBSI-TEPA. The amount of dispersant needed to saturate the adsorption sites Γ_{max} increased after modification. In effect, EC modification of *b*-PIBSI-TEPA and *b*-PIBSI-PEHA generated dispersants whose adsorption onto CBPs was more akin to that of *b*-PIBSI-DETA with smaller and larger K and Γ_{max} values compared to the values obtained with the non-modified dispersant analogues. Overall, these trends indicate that the binding of the dispersants onto CBPs is more efficient before modification as expected, since the purpose of the modification is to decrease the basicity of the solution and not increase the ability of the dispersants to adsorb onto carbonaceous particulate matter.

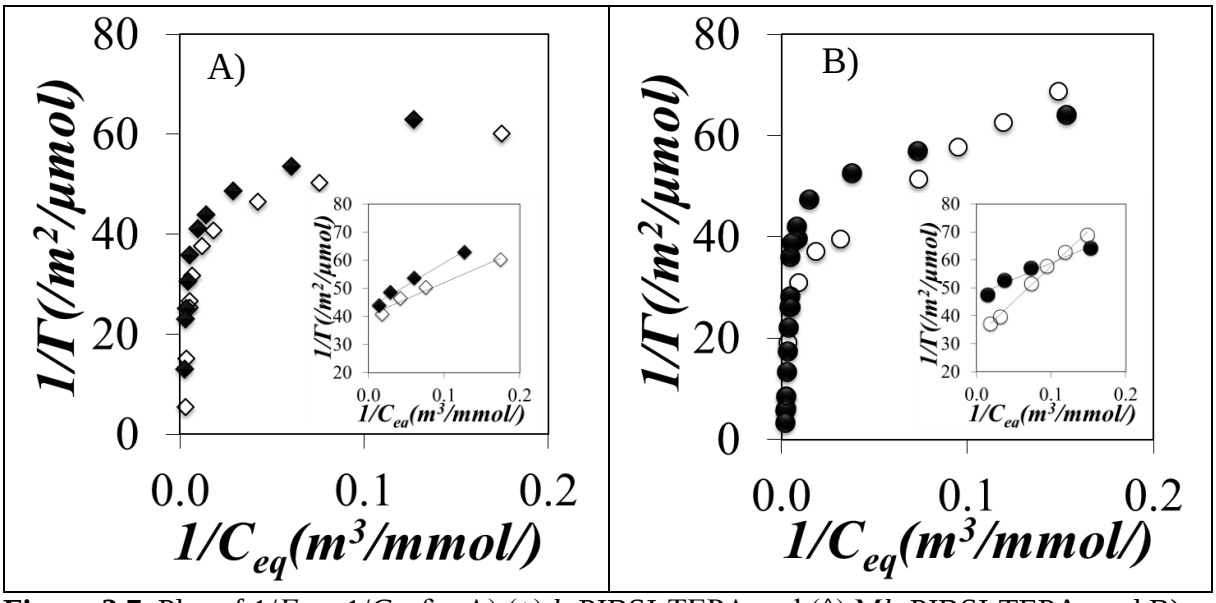

Figure 3.7. Plot of $1/\Gamma$-vs-$1/C_{eq}$ for A) (♦) *b*-PIBSI-TEPA and (◊) M*b*-PIBSI-TEPA, and B) (▲) *b*-PIBSI-PEHA and (Δ) M*b*-PIBSI-PEHA dispersants in dodecane.

3.5 Conclusions

Four *b*-PIBSI dispersants were prepared and the secondary amines in their polyamine core were modified by reaction with ethylene carbonate (EC). Successful modification of the dispersants was assessed by visual inspection of the ^{1}H NMR and FTIR spectra, but quantitative analysis of these spectra to extract the extent of secondary amine modification was complicated by inherent distortions of the spectra due to H-bonding between unreacted secondary amines and succinimide carbonyls. The existence of unreacted secondary amines in the polyamine core of the M*b*-PIBSI dispersants was unambiguously demonstrated by fluorescence measurements. As demonstrated in an earlier report,[20] secondary amines quench the fluorescence of succinimide groups very efficiently. However, quenching of succinimide moieties by urethane groups is much less efficient. Consequently, complete modification of secondary amines with EC was expected to result in a substantial increase in succinimide fluorescence for the M*b*-

PIBSI dispersants. This increase in fluorescence intensity would have been 216 and 271 % for M*b*-PIBSI-TEPA and M*b*-PIBSI-PEHA, respectively. Instead, a rather low 42 and 71 % increase in fluorescence intensity was observed for M*b*-PIBSI-TEPA and M*b*-PIBSI-PEHA, respectively. This result led to two conclusions. First, a substantial fraction α of secondary amines did not react with EC during the modification reaction. Second, fluorescence quenching experiments with the succinimide moieties should enable the determination of the level of modification of the *b*-PIBSI dispersants.

With this in mind, the fluorescence signal retrieved from the partially modified M*b*-PIBSI dispersants was analyzed to account for the reduction in fluorescence quenching experienced by the succinimide pendants when secondary amines were replaced by urethane groups. This analysis took advantage of the similarity in chemical structure between small organic molecules (DEA and HEDBC) and the secondary amines and urethane species found in the polyamine linker. The Stern-Volmer (K_{SV}) constants obtained for the quenching of *N*-methyl succinimide by DEA and HEDBC were used to estimate the K_{SV} constant for the quenching of succinimide groups in M*b*-PIBSI dispersants by urethane functions. In turn, this information was used to determine that 60 and 70% of the secondary amines of *b*-PIBSI-TEPA and *b*-PIBSI-PEHA, respectively, had reacted with EC. This result was in good agreement with an estimate of the level of secondary amine modification obtained by ^{1}H NMR assuming association of the M*b*-PIBSI dispersants in solution. The partial reaction of the secondary amines was attributed to steric hindrance due to the presence of the bulky succinimide and urethane groups as well as H-bonding between secondary amine protons and succinimide carbonyls.

After having quantified the extent of modification in the M*b*-PIBSI dispersants, their ability to adsorb onto the surface of carbon black particles (CBPs), used as mimics of the carbonaceous ultrafine particles (UFPs) found in engine oils, was compared to that of their unmodified analogs. The binding constants retrieved for the M*b*-PIBSI dispersants were smaller than those of the unmodified dispersants suggesting that the modification had reduced their ability to act as colloidal stabilizers in oil. Together, these results illustrate that fluorescence quenching experiments can be employed to quantify the level of EC modification in *b*-PIBSI dispersants and how this modification affects the ability of dispersants to stabilize the UFPs generated in engine oils.

Chapter 4

Quantifying the Level of Intermacromolecular Interactions in Ethylene-Propylene Copolymers by Using Pyrene Excimer Formation

4.1 Overview

A unique methodology based on fluorescence measurements is introduced to quantitatively measure the actual level of interpolymeric association between ethylene-propylene (EP) copolymers used as viscosity index improvers (VIIs) in engine oils. To this end, two EP copolymers, one amorphous (EP(AM)) and the other semicrystalline (EP(SM)), were maleated and then fluorescently labeled with 1-pyrenemethylamine and 2-(2-naphthyl)ethylamine to yield Py-EP and Np-EP, respectively. Successful maleation and fluorescence labeling were confirmed by Fourier transform infrared (FTIR) spectroscopy. The level of crystallinity of the EP copolymers were inferred from FTIR, carbon nuclear magnetic resonance (^{13}C NMR), and differential scanning calorimetry (DSC) experiments. The solution behaviour of the EP copolymers was characterized by conducting intrinsic viscosity measurements as a function of temperature, to define the temperature range where fluorescence studies should be conducted. Fluorescence resonance energy transfer (FRET) experiments were used to demonstrate the existence of interpolymeric associations, but a quantitative measure of the actual level of association, such as the molar fraction of interpolymeric interaction (f_{inter}) between EP copolymers, could not be determined by FRET. However, taking advantage of the fact that the fluorescence intensity ratio I_E/I_M of excimer-to-monomer is directly proportional to the local pyrene concentration $[Py]_{loc}$ of a pyrene-labeled polymer, a quantitative measure of the actual level of intermolecular association was obtained by measuring the I_E/I_M ratio. The results showed that f_{inter} of pyrene-labeled EP(SM) increased upon decreasing the temperature and increasing the polymer concentration, as would have been expected from such a polymer. This result suggests that pyrene excimer formation provides a reliable method to quantitatively

determine f_{inter} for EP copolymers used as VIIs, an information which is otherwise difficult to extract from standard FRET experiments.

4.2 Introduction

Engine oils provide the necessary lubrication between the moving parts of engines, and as a result, are vital to all internal combustion powered vehicles. Viscosity index improvers (VIIs), dispersants, detergents, antioxidants, and antiwear components are chemicals that are deliberately added to engine oils to enhance oil performance during the operation of engines.[1] In particular, VIIs are added to the oil to reduce the inherent decrease in oil viscosity that occurs with increasing temperature. Without VIIs, the oil would be too thin at high temperature to properly coat the engine parts, thus undermining its lubricating purpose, and too viscous to flow at low temperature, resulting in the lack of lubrication and possible ceasure of the engine parts. VIIs are designed to counteract the reduction in oil viscosity observed at high engine temperatures, without excessively increasing the viscosity of the oil at lower temperatures.[2-4] Thus, VIIs play a key role in substantially enhancing the oil efficiency and durability while providing maximum engine protection.[5,6]

Synthetic polymers such as polymethacrylates, ethylene-propylene copolymers (EP), and hydrogenated styrene-diene copolymers have been used as VIIs by taking advantage of the unique polymer coil expansion undergone by these polymers with increasing solution temperature.[4,7-9] Among these polymers, EP copolymers were first introduced as a lubricant additive by Exxon in the late 1960s.[10] The ethylene-to-propylene ratio in EP copolymers defines the quality of such a polymer as a VII.[7] High ethylene contents of 50-70 mol% provide optimum oil thickening and oxidative stability.[11] However, at low temperature, such high ethylene contents lead to polymer crystallization and thus insolubility, and strong interactions with wax,

an ubiquitous component of base oils.[11] Despite these drawbacks, semicrystalline EP copolymers are being used as VIIs due to their ability to undergo coil expansion with increasing temperature. As a matter of fact, an oligoethylene sequence within a semicrystalline EP copolymer will crystallize at low temperature and form dense crystalline microdomains, resulting in polymer coils having small hydrodynamic volumes (V_h). Increasing the solution temperature melts the crystalline microdomains, which results in a higher V_h for the polymer coils. Since the viscosity of the solution depends on the volume fraction of the solution that is occupied by the polymer coils, expansion of the polymer coil leads to a viscosity increase. Therefore, the decrease in engine oil viscosity that follows an increase in temperature is mitigated by the expansion of the polymer coils associated with the melting of the crystalline microdomains. By comparison, the change in V_h with temperature is less sudden and more progressive for amorphous EP copolymers so that the viscosity of their solution is less affected by temperature. The effect of the ethylene content of an EP copolymer on the temperature dependency of V_h has been well documented.[3,4]

So far, the variation of V_h with temperature has been discussed in terms of an intramolecular phenomenon happening with semicrystalline EP copolymers. However the formation of microcrystals in solution indicates that polymer-polymer interactions are favored over polymer-solvent interactions. In other words, the polymer becomes less soluble, a condition which normally leads to uncontrolled interpolymeric aggregation and eventually precipitation of the polymer. In the case of an engine oil, precipitation of a VII from the oil would have catastrophic consequences on the lubrication performance of the oil. These observations lead to the conclusion that the characterization of the extent of polymeric associations in solution, and the study of the chemicals known to affect them, is of paramount

interest to the oil-additive industry. One of the tools most commonly applied to probe intermolecular associations is fluorescence resonance energy transfer (FRET), which explains its intensive use to study polymeric systems.[2,12-14] Since an excited donor (*D*) can only transfer its energy to a ground-state acceptor (*A*) if the distance separating *D* from *A* ($d_{D\text{-}A}$) is less than twice the Förster radius (R_o), which is itself less than 10 nm for any given *D*-*A* pair, evidence of FRET between a *D*– and an *A*–labeled macromolecule provides strong evidence for intermacromolecular interactions. The strength of these interactions can be inferred qualitatively from the FRET efficiency (E_{FRET}) with E_{FRET} taking values between zero and unity depending on how $d_{D\text{-}A}$ averaged over all *D*-*A* pairs compares to R_o. Interestingly, a quantitative measure of the actual level of association, such as the molar fraction (f_{inter}) of macromolecules involved in intermolecular associations, is rarely provided when FRET is used, probably because of the complex relationship that exists between efficiency of energy transfer (E_{FRET}) and the distribution of $d_{D\text{-}A}$ values when *D* and *A* are subject to Brownian motions in solution, as well as the unavoidable contamination of the acceptor fluorescence signal by direct excitation of the acceptor.

By comparison, we provide herein evidence that f_{inter} can be determined in a simple and straightforward manner from the fluorescence intensity ratio I_E/I_M of excimer-to-monomer obtained from the fluorescence spectrum of pyrene-labeled macromolecules. These experiments take advantage of the ability of an excited pyrene to form an excimer *on contact* upon encounter with a ground-state pyrene.[15] Since the fluorescence intensity ratio I_E/I_M is directly proportional to the local pyrene concentration $[Py]_{loc}$, an increase in I_E/I_M reflects an increase in $[Py]_{loc}$ that would follow from intermolecular associations.[16-20] Comparison of the I_E/I_M ratio obtained at low and high pyrene concentrations when pyrene excimer formation

occurs, respectively, intra- and intermolecularly yields f_{inter} which can be used to probe the level of interpolymeric interactions. This study describes how these concepts can be applied to determine f_{inter} for two EP copolymers.

4.3 Experimental

***Chemicals*.** Acetone (HPLC grade), dodecane (anhydrous, 99%), toluene (HPLC, 99.9%), biphenyl (99%), maleic anhydride (98%), succinic anhydride (99%), *N*-methyl succinimide (*N*-MSI, 99%), 2-(2-naphthyl)ethylamine hydrochloride ($NpC_2H_4NH_2$ HCL, 97%), 1−pyrenemethylamine hydrochloride ($PyCH_2NH_2$ HCL, 95%), dimethyl sulfoxide-d_6 (DMSO-d_6, 99.9 %), dichloromethane (DCM, 99.8%), 1,1,2,2-tetrachloroethane-d_2 (TCE-d_2), sodium acetate (anhydrous), and *tert*-butyl peroxide (98%) were purchased from Sigma-Aldrich and were employed without further purification. Acetic acid (99.7 %, reagent) was purchased from Fischer Scientific. Two ethylene-propylene copolymers were supplied by Afton. One was semicrystalline and the other was amorphous. They were referred to as EP(SM) and EP(AM), respectively.

***Fourier Transform Infrared* (*FTIR*).** All FTIR spectra were obtained with a Bruker Tensor 27 FTIR spectrophotometer. Polymer solutions prepared with toluene were deposited drop wisely onto a sodium chloride (NaCl) FTIR plate. The solvent was evaporated under a stream of nitrogen leaving behind a thin polymer film. All the samples had an absorbance of less than unity to optimize the signal-to-noise ratio.

***Gel Permeation Chromatography* (*GPC*).** Weight- and number-average molecular weights and polydispersity indices (PDI) were determined with a Polymer Char high-temperature gel permeation chromatograph (GPC) instrument at 145 °C using a flow rate of 1 mL/min of 1,2,4-trichlorobenzene (TCB).[21] The GPC instrument was equipped with the three following

detectors placed in series, namely a differential refractive index, 15^{o} angle light scattering, and differential viscosity detectors. The GPC instrument was also calibrated with polystyrene standards having a narrow molecular weight distribution.

***UV-Visible Spectrophotometer* (*UV-Vis*).** Absorbances were measured on a Cary 100 UV-Vis spectrophotometer with quartz cells having a 0.1-10 mm path length. Absorbances were measured in the 200–600 nm wavelength range.

***Steady-State Fluorescence*.** A Photon Technology International (PTI) LS-100 steady-state fluorometer equipped with an Ushio UXL-75Xe xenon arc lamp and a PTI 814 photomultiplier detection system was used to acquire the fluorescence spectra. To avoid the inner filter effect when acquiring the fluorescence spectra, a triangular cell was used for front-face geometry measurements at polymer concentrations of 10 g.L^{-1}. For concentrations of 0.01 and 0.1 g.L^{-1}, a square cell was used to acquire the fluorescence spectra with the right-angle geometry. All solutions were degassed for 30-40 minutes under a gentle flow of N_2 to remove oxygen. Depending on whether the fluorescence experiments were targeting a naphthalene or pyrene chromophore, the solutions were excited at a wavelength of 290 or 344 nm, and the emission spectra were acquired from 300 to 550 nm or 350 to 600 nm, respectively. The fluorescence measurements were also carried out at temperatures ranging from –30 (± 0.2) °C to +25 (± 0.2) °C using a cryostat from Oxford Instruments (Optistat DN) placed in the steady-state fluorometer. Before each measurement, the solutions were heated to room temperature to erase all pre-association history before bringing the solution to the desired temperature. After the set temperature of the cryostat had been reached, the solution was left in the cryostat for 10 min before any fluorescence spectrum was acquired.

***Time-Resolved Fluorescence*.** An IBH time-resolved fluorometer with a 290 and 340 nm nano-LED light source was used to acquire the fluorescence decays of naphthalene and pyrene, respectively. Light scattering and background corrections were applied to fit the fluorescence decays. The monomer and excimer fluorescence decay curves of the pyrene-labeled EP copolymers were fitted globally with the fluorescence blob model (FBM) according to, respectively, Equations S1 and S2, which are given as Supporting Information (SI). The decay fits were considered good if the χ^2 value was smaller than 1.30 and the residuals and the autocorrelation of the residuals were randomly distributed around zero.

Differential Scanning Calorimeter (DSC). DSC measurements were performed on a TA Q2000 calorimeter calibrated with indium (T_m = 156 ^oC). Samples containing approximately 6 mg of material were weighed and sealed in crimped Tzero aluminum pans prior to analysis. An empty aluminum pan was used as the reference and the chamber was purged with nitrogen at a purge rate of 50 mL/min during analysis. Each sample underwent three temperature cycles: heating from –30 to +200 ^oC, cooling from +200 to –30 ^oC and heating from –30 to +200 ^oC. The temperature scanning rate for all cycles was 10 ^oC/min and the samples were allowed to equilibrate isothermally for 5 min between each cycle.

Carbon Nuclear Magnetic Resonance (^{13}C NMR). A Bruker 500 MHz high resolution NMR spectrometer was used to acquire the ^{13}C NMR spectra of the EP copolymers in TCE-d_2 at 120 ^oC.[21] A mass of 0.14 g of each sample was dissolved in TCE-d_2 and the solution was placed in an NMR tube. The solution was homogenized by heating the NMR tube in a heating block at 120 ^oC for a minimum of 4 hrs. The ^{13}C NMR spectra of EP(SM) and EP(AM) are shown in Figure S4.1. ^{13}C NMR was used to calculate the molar ethylene content of the EP copolymers using a well-documented procedure.[22]

***Proton Nuclear Magnetic Resonance* (^{1}*H NMR*).** A Bruker 300 MHz high resolution NMR spectrometer was used to acquire the ^{1}H NMR spectra of the model compounds in DMSO-d_6. A sample concentration of about 10 mg/mL was used to obtain ^{1}H NMR spectra of the polymer samples with a reasonable signal-to-noise (S/N) ratio.

Labeling of the EP Copolymers. The polymers were first maleated to yield EP-MA[23] and then fluorescently labeled with $PyCH_2NH_2$ and $NpC_2H_4NH_2$ to yield Py-EP-MA and Np-EP-MA, respectively,[24] according to the protocols shown in Scheme 4.1. The synthesis of Py-EP-MA is described in more details hereafter. The EP copolymer (2 g) and biphenyl (60 g) were added into a two-neck round-bottom flask equipped with a condenser. The flask was heated to 160 ^oC for 12 hrs to ensure good dissolution of the polymers. After complete dissolution, *tert*-butyl peroxide (202 mg, 1.4 mmol) radical initiator was added along with maleic anhydride (MA) (61 mg, 0.8 mmol). The flask was heated to 180-190 ^oC and left to react under nitrogen for only 4 hrs since longer reaction times led to crosslinking. After the reaction was completed, the hot biphenyl solution was poured into acetone to precipitate the polymer. The polymer was re-dissolved in toluene and precipitated in acetone four times to ensure that no unreacted MA remained in the sample. The drying step was omitted for maleated samples as earlier attempts showed that the maleated samples crosslinked in the vacuum oven.

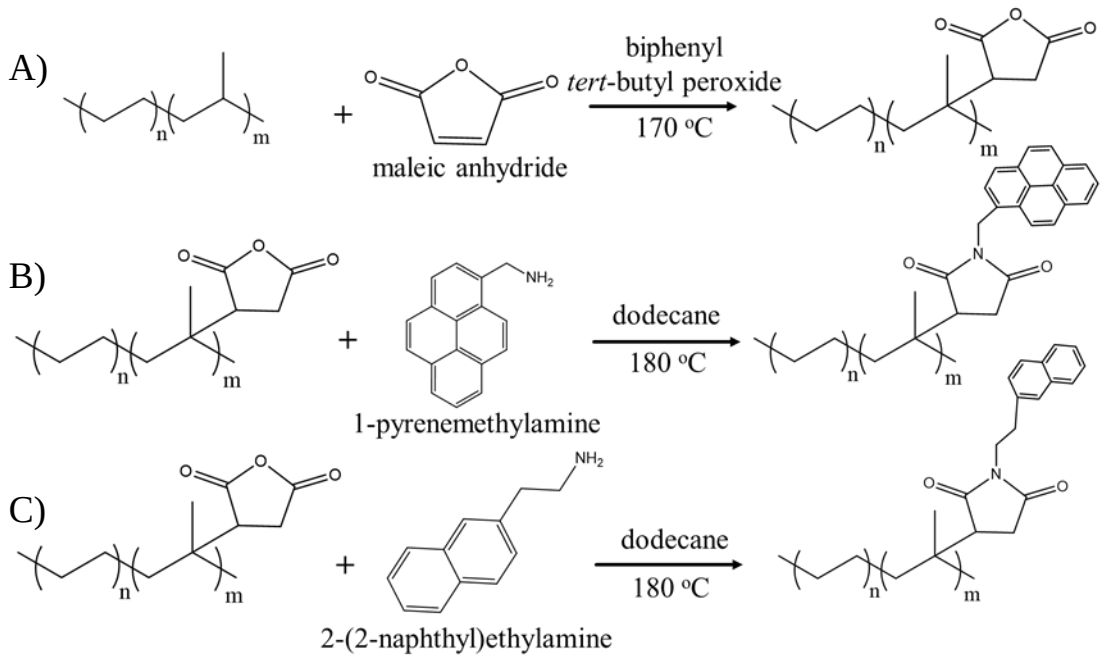

Scheme 4.1. Reaction scheme for A) the maleation of the EP copolymer and the labeling of the maleated EP copolymers with B) pyrene and C) naphthalene.

Since the succinic anhydride of EP-MA is moisture sensitive and can react with water to yield less reactive succinic acid, dehydration of the succinic acid was carried out. To this end, purified EP-MA (1 g) and dodecane (60 mL) were placed in a two-neck round-bottom flask equipped with a dean-stark apparatus to remove the water generated during the dehydration conducted at 150-160 °C for 10 hrs under nitrogen atmosphere. Successful dehydration was confirmed by FTIR spectroscopy (Figure 4.1B). After 10 hrs, $PyCH_2NH_2$ (185 mg, 0.8 mmol) prepared from $PyCH_2NH_2$ HCl according to a published procedure[24] was added to the reaction vessel and the temperature was kept at 180 °C for another 12 hrs. After the reaction was complete, the reaction mixture was poured into acetone to precipitate out the pyrene-labeled polymer. The precipitate was redissolved in toluene to be precipitated in acetone five more times to remove any unreacted $PyCH_2NH_2$. The final product was dissolved in

toluene and kept in solution to avoid crosslinking of the sample in the dry state. Full conversion of the succinic anhydride (SAH) groups into succinimides after labeling with $PyCH_2NH_2$ was also confirmed by FTIR spectroscopy (Figure 4.1C). A similar procedure was also used to label EP-MA with $NpC_2H_4NH_2$ (Scheme 4.1C and Figure 4.1D).

Synthesis of 1-Pyrenemethyl Succinimide (Py-MSI) and 2-(2-Naphthyl)ethyl Succinimide (Np–ESI). 1-Pyrenemethylamine hydrochloride ($PyCH_2NH_2 \cdot HCl$) (0.302 g, 1.11 mmol) was dissolved in water (280 mL) and transferred to a separatory funnel. After addition of three NaOH pellets to the solution, $PyCH_2NH_2$ was extracted using hexanes (~100 mL) and deionized water.[24] Finally, the extracted $PyCH_2NH_2$ was dried in a vacuum oven at 60 ^oC for 2-3 hrs.

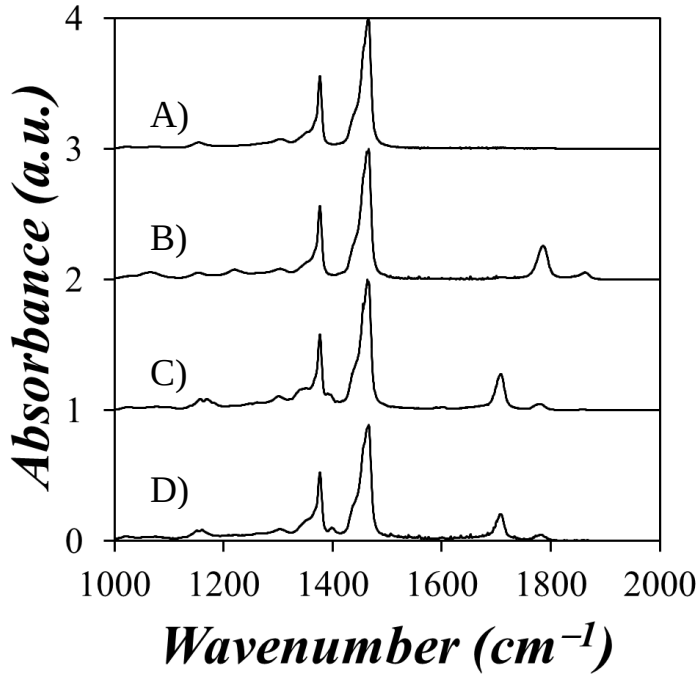

Figure 4.1. FTIR spectra of A) EP(SM), B) EP(SM)-MA, C) Py(116)-EP(SM), and D) Np(116)-EP(SM).

Succinic anhydride (214 mg, 2.14 mmol) was dissolved in a solution of acetic acid (13 mL) and sodium acetate (629 mg, 7.68 mmol). Afterward, $PyCH_2NH_2$ (146 mg, 0.61mmol) was added to the mixture and placed in a round-bottom flask equipped with a water condenser. The solution was heated to 170-180 °C for 12 hrs. The product was then dissolved in toluene (30 mL) and washed with Na_2CO_3 aqueous solution (1 M) 5-6 times followed by 3 water washes. Finally the organic layer was slowly evaporated under a gentle flow of nitrogen. The product was dried in a vacuum oven at 80-90 °C overnight. Py-MSI was further purified by column chromatography using a 70:30 mixture by volume of DCM:hexanes. A similar method was also used to synthesize the Np-ESI. The ^{1}H NMR spectra of Np-ESI and Py-MSI are shown in Figure S4.2.

4.4 Results and Disscussion

Considering the importance of characterizing the interpolymer interactions that take place between VIIs in an apolar solution, this study aimed to determine the extent to which fluorescence techniques can be applied to characterize the intermolecular associations taking place between fluorescently labeled EP copolymers in toluene as a function of temperature. How this was accomplished is described hereafter.

Chemical Characterization of EP copolymers. The FTIR spectra of EP(SM), EP(SM)-MA, Py(116)–EP(SM), and Np(116)-EP(SM) were acquired and are shown in Figure 4.1. The absorption bands at 1462 cm^{-1} and 1379 cm^{-1} in the FTIR spectra of the EP copolymers are due to the methylene and methyl groups of the EP backbone, respectively. Since the FTIR spectrum of a partially hydrated EP-MA sample has two absorptions at 1710 $cm^{-1}$and 1785 cm^{-1} due to the carbonyl groups of succinic acid and SAH, respectively, FTIR was applied to ensure complete dehydration of EP-MA. After dehydration, the absorption at 1710 cm^{-1} disappeared,

demonstrating that all succinic acids were converted back to their SAH form. The Py(116)–EP(SM) and Np(116)-EP(SM) samples showed a new absorption peak at 1710 cm^{-1} due to the carbonyl groups of the succinimide ring, while the peak at 1785 cm^{-1} disappeared due to the reaction of succinic anhydride with the amine group of the fluorescent derivatives (Scheme 4.1). No absorption was detected between 1600 and 1700 cm^{-1} confirming the absence of amide and the formation of the succinimide.

Normalization of the FTIR spectra at 1462 cm^{-1} provided a simple means to determine the Abs(1379 cm^{-1})/Abs(1462 cm^{-1}) ratio which, in turn, yielded a measure of the propylene content of the EP copolymers. These ratios are listed in Table 4.1. Comparison of the Abs(1379 cm^{-1})/Abs(1462 cm^{-1}) ratios in Table 4.1 obtained for the maleated and fluorescently labeled EP copolymers showed that the ratio did not change after the polymer had undergone the different chemical reactions. This observation led to the conclusion that the chemical composition of the EP copolymers was not affected by maleation and the subsequent naphthalene and pyrene labeling. In Table 4.1, the number in the parenthese after *Py* or *Np* for the pyrene- and naphthalene labeled polymers refers to their dye content expressed in $\mu mol.g^{-1}$.

The ^{13}C NMR spectra of EP(SM) and EP(AM) were also acquired and are shown in Figure S4.1. The ethylene content of the EP copolymers as calculated according to a published procedure.[22] This analysis yielded ethylene contents of 78 and 60 mol% for EP(SM) and EP(AM), respectively. The ethylene content of EP(SM) was found to be larger than that of EP(AM), as expected, since a larger ethylene content results in a stronger semicrystalline character for an EP copolymer.

Table 4.1. Summary of the FTIR and GPC results for the EP copolymers.

Batch	Polymer Type	$\frac{Abs(1379cm^{-1})}{Abs(1462cm^{-1})}$	$\frac{Abs(1790cm^{-1})}{Abs(1462cm^{-1})}$	$\frac{Abs(1710cm^{-1})}{Abs(1462cm^{-1})}$	M_n (g/mol)	M_w (g/mol)	PDI (M_W/M_n)
1	**EP(AM)**	0.80	-	-	59,000	125,000	2.11
	EP(AM)-MA	0.79	0.22	-	-	-	-
	Py(108)-EP(AM)	0.80	-	0.20	25,000	61,000	2.42
2	**EP(AM)**	0.80	-	-	59,000	125,000	2.11
	EP(AM)-MA	0.82	0.26	-	-	-	-
	Np(108)-EP(AM)	0.84	-	0.18	-	-	-
3	**EP(SM)**	0.55	-	-	55,000	145,000	2.63
	EP(SM)-MA	0.55	0.23	-	-	-	-
	Py(116)-EP(SM)	0.56	-	0.28	33,000	92,000	2.77
3	**EP(SM)**	0.55	-	-	55,000	145,000	2.63
	EP(SM)-MA	0.55	0.21	-	-	-	-
	Py(96)-EP(SM)	0.56	-	0.28	-	-	-
4	**EP(SM)**	0.55	-	-	55,000	145,000	2.63
	EP(SM)-MA	0.57	0.26	-	-	-	-
	Np(116)-EP(SM)	0.59	-	0.23	-	-	-
5	**EP(SM)**	0.55	-	-	55,000	145,000	2.63
	EP(SM)-MA	0.54	0.11	-	-	-	-
	Py(65)-EP(SM)	0.58	-	0.11	-	-	-

E arlier reports have shown how the SAH content of maleated EP copolymers (EP-MA) can be determined by FTIR after establishing a calibration curve using mixtures of known quantities of the naked EP copolymer and methyl succinic anhydride.[25] Unfortunately this method did not apply to EP(SM) and EP(AM) since aromatic solvents like toluene appeared to be the only solvents capable of solubilizing these EP copolymers at room temperature and methyl succinic anhydride was not soluble in toluene, therefore preventing the preparation of

homogenous mixtures in toluene of EP copolymers and methyl succinic anhydride. Consequently, 1-pyrenylmethyl succinimide (Py–MSI) and 2-(2-naphthyl)ethyl succinimide (Np-ESI) were synthesized as model compounds to estimate the SAH content of the EP-MA samples. This estimate of the SAH content assumed that the labeling reaction of the maleated EP copolymer went to completion, a reasonable assumption based on the FTIR spectra shown in Figure 1. The molar extinction coefficient of the model compounds was then measured in toluene and THF based on their absorption spectra (Figures 4.2 and S4.3). A summary of the extinction coefficients of Py-MSI and Np-ESI at different wavelengths is given in Table 4.2.

Table 4.2. Summary of the extinction coefficients for Py-MSI and Np-ESI in toluene and THF.

Model Compound		ε at 277 nm ($M^{-1}.cm^{-1}$)	ε at 290 nm ($M^{-1}.cm^{-1}$)	ε at 305 nm ($M^{-1}.cm^{-1}$)	ε at 344 nm ($M^{-1}.cm^{-1}$)	τ_m (ns)
Py-MSI	Toluene	*	*	5,100±50	44,800±300	243
	THF	45,500±500	4,000±500	6,100±300	40,600±500	-
Np-ESI	Toluene	*	*	366±5	0	68
	THF	4,800±10	2,600±10	339±5	0	-

* The absorption wall of toluene located between 280-290 nm prevents the determination of the molar absorbance coefficients at wavelengths lower than 290 nm.

The molar absorbance coefficients ε_{py} and ε_{Np} were found to equal 44,800 (±340) $M^{-1}.cm^{-1}$ at 344 nm and 366 (±5) $M^{-1}.cm^{-1}$ at 305 nm for Py-MSI and Np-ESI in toluene, respectively. Since ε_{Np} at 305 nm was about two orders of magnitude lower than ε_{py} at 344 nm, a 100 fold higher polymer concentration was required to measure the naphthalene content of the Np-EP samples (Figure 4.2).

High polymer concentrations however caused light scattering, and scattered light interferred with the absorbance peak at 305 nm. Furthermore, the naked EP copolymers

themselves showed residual absorbance in the wavelength range where naphthalene absorbed which interferred further with the weak naphthalene absorbance at 305 nm (Figure 4.2B). This did not cause a problem for the pyrene-labeled EP copolymers since the much larger ε_{py} value at 344 nm enabled the use of much smaller polymer concentrations (Figure 4.2A). Consequently, the determination of the naphthalene content of the polymers was not attempted and it was assumed to be similar to that of the corresponding Py-EP samples since they were prepared in a similar manner. Consequently, the naphthalene content of Np(116)-EP(SM) and Np(108)-EP(AM) was assumed to the same as the one determined for Py(116)-EP(SM) and Py(108)-EP(AM), respectively. Comparison of the absorbance at 344 nm for the Py-EP samples and the model compound Py-MSI enabled the determination of the pyrene content λ_{py} of the samples. The λ_{py} values listed in Table 4.3 for Py(116)-EP(SM) and Py(108)-EP(AM) are similar thus indicating that on a mass basis, both contained a similar number of pyrene labels. More detailed analysis of the absorption spectra and the fluorescence decays acquired with Py(116)-EP(SM) and Py(108)-EP(AM) provided further information about the distribution of the fluorescent labels along the chain.

One advantage of using a pyrene derivative is that its absorption spectrum reflects the existence of pyrene-pyrene interactions. This is achieved by monitoring the peak-to-valley ratio (P_A) of the $S_2^0 \leftarrow S_0^0$ transition band at 344 nm in the absorption spectrum. The ratio of the absorbance peak at 344 nm to that of the adjacent trough at 335 nm in Figure 4.2 was used to obtain the P_A value. A P_A value of 3.0 or greater suggests that no pyrene-pyrene interactions are present (Scheme 4.2) whereas a lower P_A value indicates that pyrene aggregates exist in the ground state. P_A values of 3.0 and 2.6 were obtained for Py(116)-EP(SM) and Py(108)-EP(AM), respectively, thus indicating a higher level of aggregation for Py(108)-EP(AM) (Table 4.3).

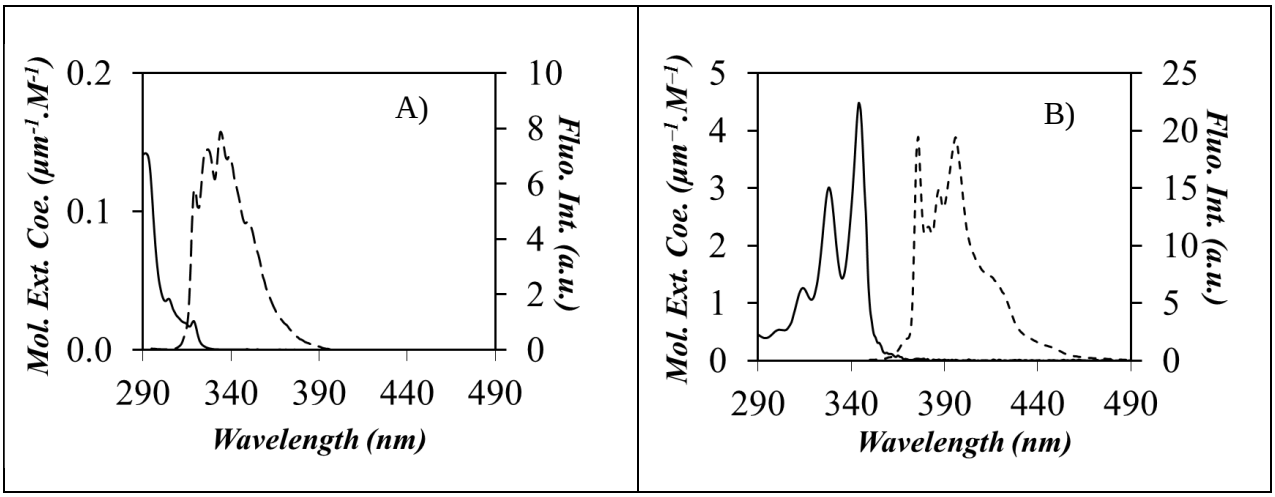

Figure 4.2. Molar extinction coefficient calculated from UV-Vis absorption (─) and fluorescence spectra (- - -) of A) 2-(2-naphthyl)ethyl succinimide normalized at 305 nm and B) 1-pyrenemethyl succinimide normalized at 344 in toluene. Note that the absorbance at wavelengths lower than 290 nm is unreliable due to the absorption wall of toluene and were not shown. ($C_{Np\text{-}ESI}$ = 1.78 mmol.L^{-1}, $C_{Py\text{-}MSI}$ = 13 μmol.L^{-1})

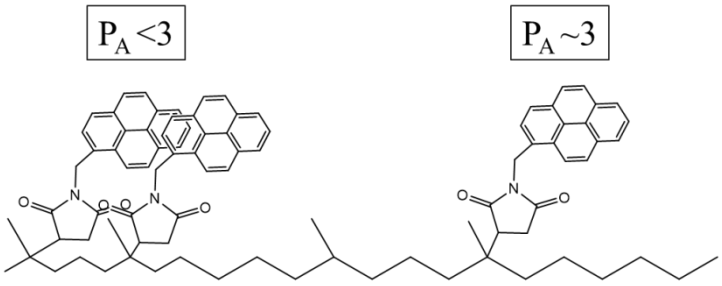

Scheme 4.2. Illustration of the effect of pyrene aggregation on the P_A value.

This conclusion was further supported by characterizing the distribution of the pyrene labels along the chain according to whether they were isolated and incapable of forming an excimer, they were not isolated and could form an excimer by diffusion, or they were aggregated. The molar fractions of the different pyrene species were calculated by applying the

fluorescence blob model (FBM) analysis to the fluorescence decays.[26] The pyrene monomer and excimer fluorescence decays were fitted according to the FBM according to Equations S4.1 and S4.2, given in the Supporting Information. All the parameters retrieved from the FBM analysis of the fluorescence decays are listed in Tables S4.1 and S4.2 as SI. A sample decay analysis is shown in Figure S4.5. Fitting the fluorescence decays with Equations S4.1 and S4.2 yielded the molar fractions f_{diff}, f_{free}, f_{k2}, and f_{agg} of those pyrenes that are forming excimer by diffusion, isolated, forming excimer via rapid rearrangement with a rate constant k_2, and aggregated, respectively. The molar fractions f_{diff}, f_{free}, f_{k2}, and f_{agg} are listed in Table 4.3.

Table 4.3. P_A values amd molar fractions of the different pyrene species obtained from the FBM analysis of the pyrene monomer and excimer fluorescence decays acquired with the Py-EP samples.

Sample Description	λ_{py} (µmol/g of polymer)	f_{diff}	f_{free}	f_{agg}	f_{k2}	P_A
Py(108)-EP(AM)	108	0.37	0.11	0.26	0.27	2.60
Py(116)-EP(SM)	116	0.61	0.10	0.10	0.19	3.00

According to the molar fractions, around 10 mol% of isolated pyrene did not form excimer (f_{free}~0.10) for both samples. The molar fraction f_{agg} of 0.26 for Py(108)-EP(AM) was larger than that of 0.11 found for Py(116)-EP(SM), in good agreement with the P_A value obtained by UV-Vis spectroscopy, with a larger f_{agg} value resulting in a smaller P_A value. This analysis also indicates that pyrene excimer is formed principally from the encounter between an excited pyrene and ground state pyrene since f_{diff}+f_{k2} equals 64% and 80% for Py(108)-EP(AM) and Py(116)-EP(SM), respectively.

Microstructure of the EP Copolymers. Viscosity measurements were carried out between −10 °C and +20 °C for solutions of EP(SM) and EP(AM) in toluene to determine how the intrinsic viscosity [η] of the polymers varied as a function of temperature. [η] remained constant with temperature for EP(AM) as expected due to the inability of EP(AM) to form microcrystal in solution and thus undergo drastic conformational changes in solution. For EP(SM), [η] decreased sharply with decreasing temperature for temperatures lower than 0 °C (Figure 4.3A). This decrease in [η] for EP(SM) is most likely due to a change in the hydrodynamic volume of the polymer coil (V_h) resulting from the formation of crystalline microdomains between long ethylene stretches inside the polymer coil at temperatures lower than 0 °C.[2-4]

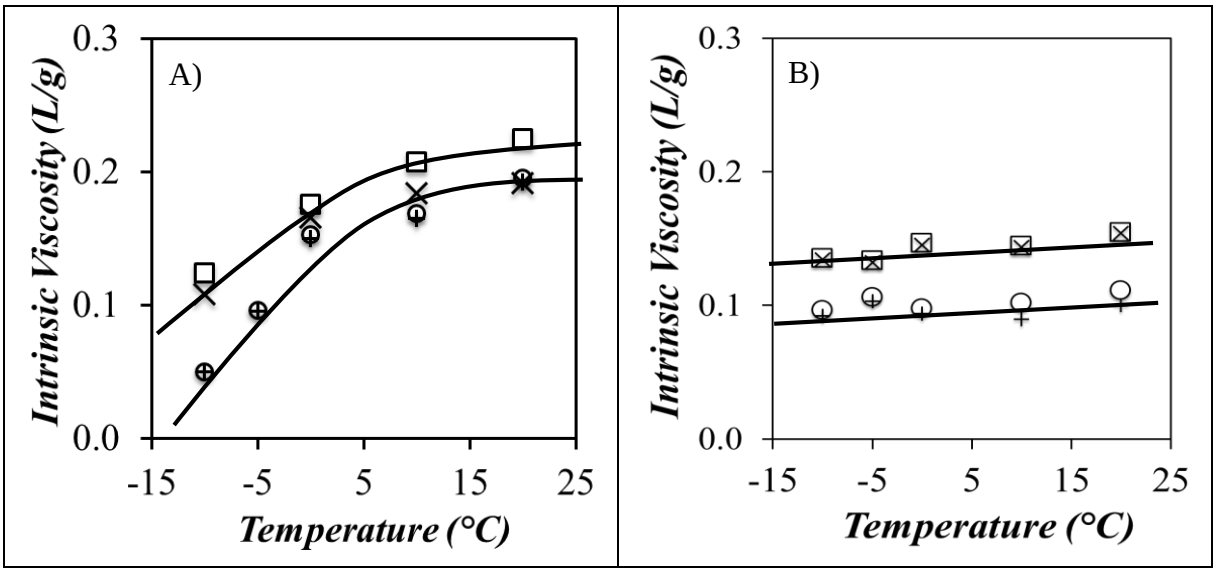

Figure 4.3. Intrinsic viscosity of A) (□) Py(116)-EP(SM) and (○) EP(SM) obtained using relative viscosity measurements, and of (×) Py(116)-EP(SM) and (+) EP(SM) obtained by using specific viscosity measurements, and of B) (□) Py(108)-EP(AM) and (○) EP(AM) obtained by using relative viscosity measurements, and of (×) Py(108)-EP(AM) and (+) EP(AM) obtained by using specific viscosity measurements in toluene at various temperatures.

Gel permeation chromatography (GPC) experiments were also conducted on the Py(116)–EP(SM) and Py(108)-EP(AM) samples where the reactive succinic anhydride groups had been capped with 1-pyrenemethylamine. The parameters describing the molecular weight distribution (MWD) of the samples obtained by GPC analysis are listed in Table 4.1. They show that the number- and weight-average molecular weights decreased and the polydispersity index (PDI) increased after maleation and pyrene labeling. Consequently, [η] was expected to vary from sample to sample due to these alterations in MWD. These changes were more pronounced in the case of Py(108)-EP(AM) suggesting that since the amorphous EP copolymer had more propylene groups, chain cleavage was more likely to happen during maleation.[27,28] But another explanation could be a change in polymer polarity after pyrene-labeling which might affect the hydrodynamic volume of the coils as the Py-EP copolymers permeate through the GPC column. Despite the variation in MWDs induced by the maleation of the EP copolymers, the trends shown in Figure 4.3 demonstrate that pyrene labeling did not change the overall [η] behavior of the EP copolymers, [η] showing a breakpoint at a similar temperature for EP(SM) and little change with temperature for EP(AM).

Finally, differential scanning calorimetry (DSC) experiments were carried out for EP(SM) and EP(AM) samples in the solid state. As shown Figure S4.5, a thermal transition due to melting was observed at 26 ^{o}C for the semicrystalline sample while no thermal transition was observed for the amorphous sample.

Fluorescence Resonance Energy Transfer (FRET). FRET experiments are typically used to help differentiate whether interactions between macromolecules such as the EP copolymers investigated in this study occur inter- or intramolecularly. To this end, the EP-MA samples were labeled with $NpC_2H_4NH_2$ and $PyCH_2NH_2$ which can act as energy donor and acceptor,

respectively. The emission spectra of the solutions prepared with Py-EP only, Np-EP only, and mixtures of the Py-EP and Np-EP samples at low (0.1 $g.L^{-1}$) and high (10 $g.L^{-1}$) concentration of EP copolymer were acquired to investigate the nature of the interactions taking place between the different polymers. The experiments were conducted in toluene and at temperatures between –25 and +25 °C, a temperature range that covers the temperatures at which a break point is observed for [η] in Figure 4.3A. Although naphthalene exhibits an absorption peak maximum around 277 nm, an excitation wavelength of 290 nm was selected in order to minimize the emission of both toluene and the EP copolymers. The fluorescence intensity of the naphthalene monomer, I_{Np}, was calculated by taking the integral of the naphthalene emission intensity between 332 and 338 nm while that of the pyrene monomer, I_{Py}, was obtained from the integral of the pyrene emission intensity between 372 and 378 nm (Figure 4.2). The I_{Py}/I_{Np} ratio provides a qualitative description of the extent of FRET efficiency, a higher I_{Py}/I_{Np} ratio indicating more efficient FRET and thus stronger intermolecular association.

The fluorescence spectra of the Np(108)-EP(AM) and Py(108)-EP(AM) mixtures acquired at different temperatures are shown in Figure 4.4. The pyrene emission intensity was found to increase with decreasing temperature whereas the naphthalene emission intensity remained relatively constant. The I_{Py}/I_{Np} ratio for Np(108)-EP(AM) and Py(108)-EP(AM) obtained for the 0.1 $g.L^{-1}$ and 10 $g.L^{-1}$ polymer mixtures was plotted as a function of temperature in Figure 4.5.

For the 0.1 $g.L^{-1}$ of naphthalene- and pyrene-labeled EP(AM) mixture, I_{Py}/I_{Np} showed a continuous decrease with increasing temperature. A higher I_{Py}/I_{Np} ratio was obtained for the 10 $g.L^{-1}$ EP(AM) mixture due to the shorter average distance between the fluorophores and the existence of direct energy transfer at higher polymer concentration. At this higher polymer

concentration, the I_{Py}/I_{Np} ratio decreased also continuously with increasing temperature. The plots of I_{Py}/I_{Np}-vs-T obtained with both the 0.1 and 10 g.L^{-1} EP(SM) mixtures differed markedly from those obtained with the EP(AM) mixtures by showing a pronounced break point in the mid-temperature range of Figure 4.5. Since an increase in I_{Py}/I_{Np} reflects an increase in intermolecular interactions, the sharp increase in I_{Py}/I_{Np} with decreasing temperature observed at −10 and −5 ^{o}C for, respectively, the 0.1 and 10 g.L^{-1} EP(SM) solutions indicates a dramatic enhancement in intermolecular association, a consequence of the formation of crystalline microdomains as expected from the intrinsic viscosity measurements. It is worth pointing out that the polymer concentrations used for the intrinsic viscosity measurements ranged between 0.5 and 3.5 g.L^{-1} and are thus intermediate between the two EP(SM) concentrations used for the FRET experiments. It is thus quite satisfying that the onset temperature between −10 and −5 ^{o}C for intermolecular associations observed by FRET matches relatively well that found for the drop in intrinsic viscosity observed in Figure 4.3 for EP(SM). The 0.1 g.L^{-1} solution used in the FRET experiment being more dilute, a lower temperature of –10 ^{o}C was required to worsen the solvent quality toward EP(SM) sufficiently to induce EP(SM) to associate intermolecularly.

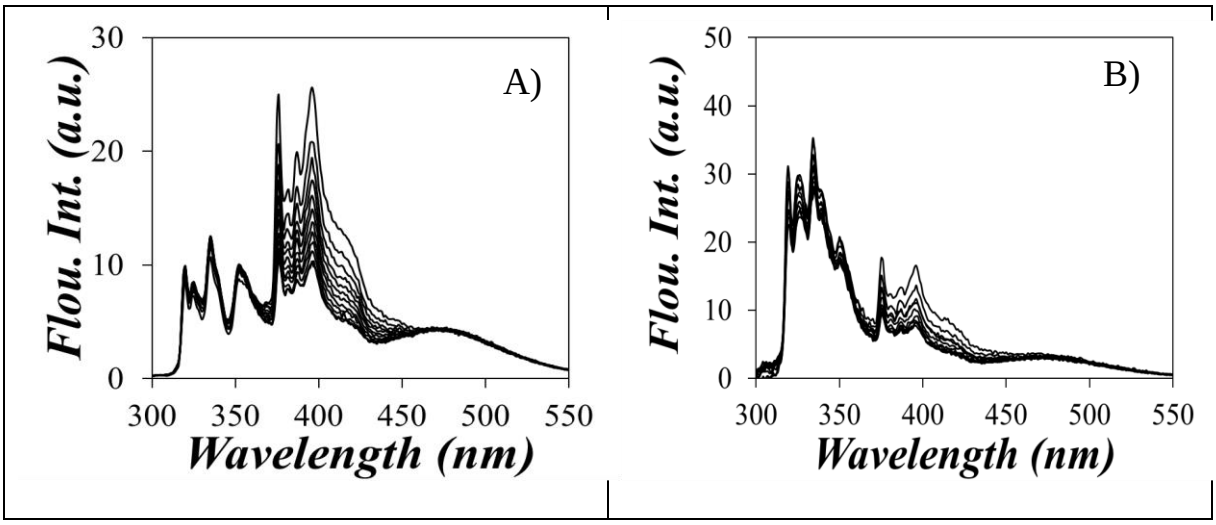

Figure 4.4. Fluorescence spectra of EP copolymers obtained from of a 9:1 mass ratio mixture of Np(108)-EP(AM):Py(108)-EP(AM) as a function of temperature for an overall polymer concentration of A) 10 $g.L^{-1}$ and B) 0.1 $g.L^{-1}$. From top to bottom, the temperature increases from –25 °C to +25 °C. (solvent: toluene; λ_{ex} = 290 nm)

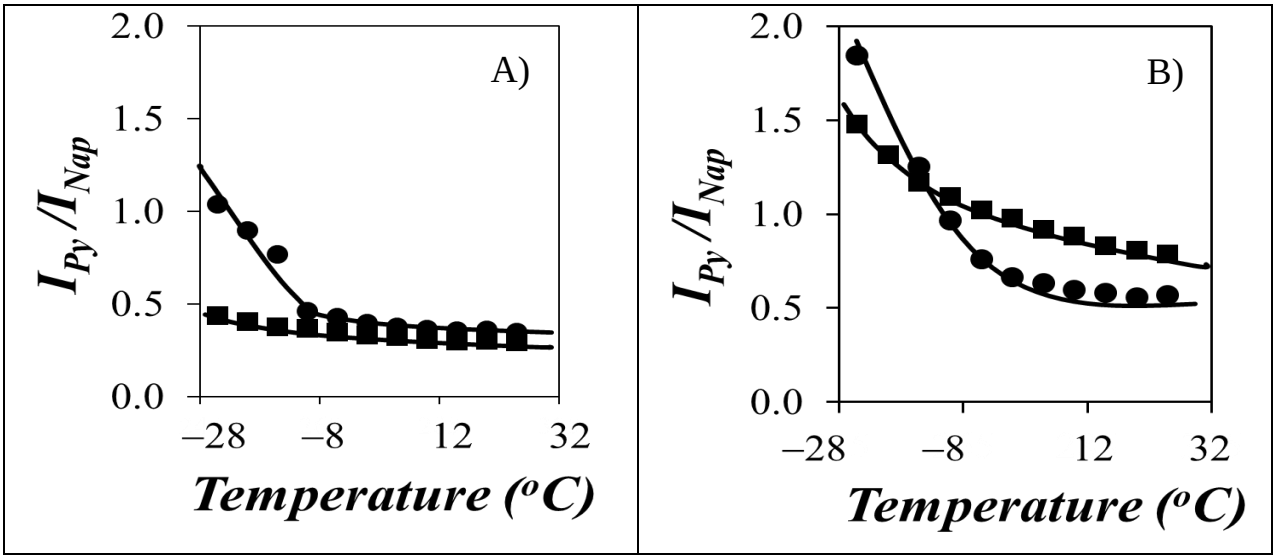

Figure 4.5. I_{Py}/I_{Np} ratio for mixtures of a 9:1 mass ratio of (■) Np(108)-EP(AM):Py(108)-EP(AM) and (●) Np(116)-EP(SM):Py(116)-EP(SM) as a function of temperature. A) 0.1 $g.L^{-1}$ and B) 10 $g.L^{-1}$.

The existence of FRET at low temperature for both polymers can be demonstrated for the low concentration mixtures where direct energy transfer can be neglected. This is achieved by comparing the sum of the individual fluorescence spectra acquired with a 0.09 $g.L^{-1}$ solution of the Np-EP sample and with a 0.01 $g.L^{-1}$ solution of the Py-EP sample with the fluorescence spectrum of the mixture containing 0.09 $g.L^{-1}$ Np-EP and 0.01 $g.L^{-1}$ Py-EP. On the one hand, a perfect overlap between the sum of the spectra acquired with the individual Np-EP and Py-EP samples and the spectrum acquired with the mixture of Np-EP and Py-EP ensures that no FRET is taking place and that no intermolecular association occurs. On the other hand, an enhancement in the pyrene fluorescence for the spectrum acquired with the mixture would be a clear indication that intermolecular association is taking place. The result of these comparisons can be seen in Figure 4.6. At low concentration, Figure 4.6 demonstrates that for both polymers, intermolecular associations can be ruled out at high temperature but not at low temperature, even for EP(AM). However, it is noticeable that the enhancement in pyrene fluorescence is much stronger for EP(SM) than for EP(AM) as a consequence of the crystalline microdomains generated in solution by the latter polymer.

The existence of intermolecular interactions for the high polymer concentration mixture is further supported by the appearance of a pronounced fluorescence emission at 353 nm in the fluorescence spectra shown in Figure 4.4A.[29,30] This peak is only detected in the concentrated Np-EP and Py-EP mixtures and is absent from the individual fluorescence spectra of Np-EP and Py-EP. Diluting a 5 $g.L^{-1}$ solution of a 9:1 Np-EP:Py-EP mixture results in a progressive decrease of the peak at 353 nm, as shown in Figure S4.7. Together, these experiments where naphthalene is excited selectively at 290 nm where pyrene has little absorbance suggest that an excited naphthalene can form an exciplex with a ground state pyrene upon diffusive encounters

and that this exciplex emits at 353 nm. Dilution of the 9:1 Np-EP:Py-EP mixtures prevent naphthalene-pyrene encounters and no exciplex is formed. A similar behavior was also observed for a mixture of Py-MSI (1 mmol/L) and Np-ESI (9 mmol/L) as shown in Figure S4.8. Most importantly, the evidence of exciplex formation between an excited naphthalene and a ground state pyrene further support the existence of intermolecular interactions at high polymer concentration.

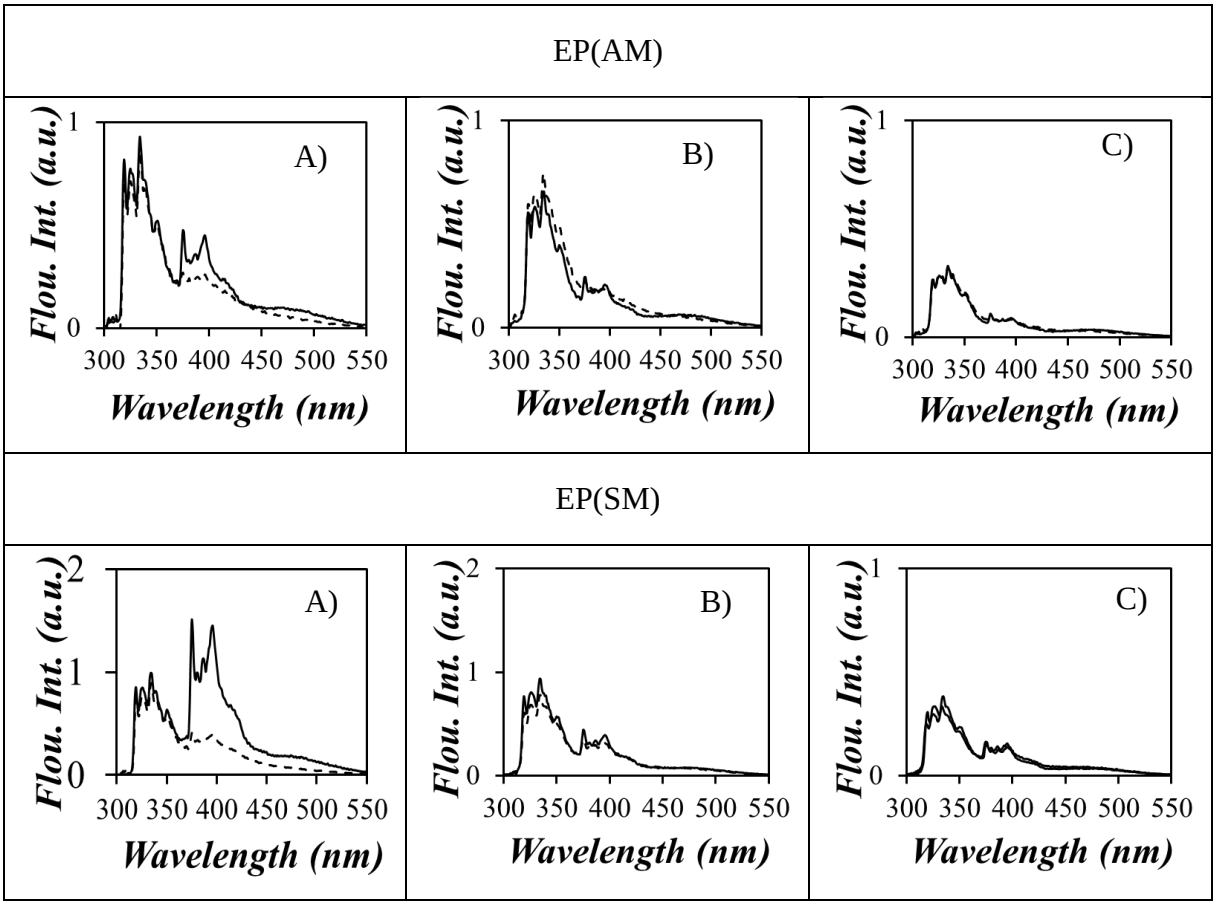

Figure 4.6. Fluorescence spectra of EP copolymers obtained from a 9:1 mixture (─) of (top) Np(108)-EP(AM) and Py(108)-EP(AM) and (bottom) Np(116)-EP(SM) and Py(116)-EP(SM) and from the addition of the individual spectra acquired with separate solutions of the labeled polymers (- - -) in toluene. Temperatures A) –20 °C, B) 0 °C, and C) 25 °C.

Pyrene Excimer Formation. While FRET experiments demonstrate the existence of interpolymeric association, a quantitative measure of the actual level of intermolecular association between fluorescently labeled macromolecules is usually quite challenging to obtain by FRET. By comparison, the molar fraction of pyrene labels forming pyrene excimer intermolecularly (f_{inter}) can be determined in a straightforward manner as illustrated hereafter.

In the fluorescence spectrum of pyrene-labeled macromolecules (PLMs), the excited pyrene monomer emission is characterized by several sharp peaks between 360 nm and 425 nm, whereas the pyrene excimer features a broad and structureless emission centered at 480 nm.[15] The fluorescence intensity of the pyrene excimer (I_E) and monomer (I_M) can be calculated by integrating the fluorescence spectrum over the wavelength ranges between 372 and 379 nm and between 500 and 530 nm, respectively. The fluorescence intensity ratio I_E/I_M is widely accepted to be directly proportional to the local pyrene concentration $[Py]_{loc}$ as described by Equation 4.1.[31]

$$I_E/I_M = K(T) \times [Py]_{loc} \quad (4.1)$$

In Equation 4.1, the multiplication factor $K(T)$ is a function of the quantum yields of the pyrene monomer and excimer, the bimolecular rate constant of excimer formation, the acquisition geometry and the instrument response of the fluorometer. As such, $K(T)$ is expected to vary with temperature according to the activation energy of the different photophysical parameters associated with the process of pyrene excimer formation. According to this relationship, an increase in I_E/I_M observed at a same temperature reflects an increase in $[Py]_{loc}$ which would result from intermolecular interactions. In turn, intermolecular interactions can be the result of an increase in the concentration of the PLM or a change in the solvent quality

toward the macromolecule. If experimental conditions can be determined where a PLM of interest undergoes both intra- and intermolecular interactions, its fluorescence spectrum will yield the ratio $I_E/I_M\begin{pmatrix} intra\ \& \\ inter \end{pmatrix}$ whereas if the PLM undergoes solely intramolecular interactions, the fluorescence spectrum will yield the ratio I_E/I_M(intra). In turn, the ratios $I_E/I_M\begin{pmatrix} intra\ \& \\ inter \end{pmatrix}$ and I_E/I_M(intra) are equal to $K(T)\times[Py]_{loc}\begin{pmatrix} intra\ \& \\ inter \end{pmatrix}$ and $K(T)\times[Py]_{loc}$(intra), respectively, so that the molar fraction of pyrene labels forming excimer intermolecularly (f_{inter}) can be determined from Equation 4.2.

$$f_{inter}=\frac{[Py]_{loc}\left(\begin{smallmatrix}\text{inter\&}\\ \text{intra}\end{smallmatrix}\right)-[Py]_{loc}(\text{intra})}{[Py]_{loc}\left(\begin{smallmatrix}\text{inter\&}\\ \text{intra}\end{smallmatrix}\right)}=\frac{I_E/I_M\left(\begin{smallmatrix}\text{inter\&}\\ \text{intra}\end{smallmatrix}\right)-I_E/I_M(\text{intra})}{I_E/I_M\left(\begin{smallmatrix}\text{inter\&}\\ \text{intra}\end{smallmatrix}\right)} \qquad (4.2)$$

In Equation 4.2, f_{inter} is also equal to the molar fraction of macromolecules that interact intermolecularly. We note with interest that the constant $K(T)$ introduced in Equation 4.1 cancels out in the expression of f_{inter}, a welcomed simplification as the determination of the activation energies of all the photophysical parameters related to the process of excimer formation with randomly labeled polymers would be a challenging task.

Experimentally, the ratio $I_E/I_M\begin{pmatrix} intra\ \& \\ inter \end{pmatrix}$ can be obtained in a straightforward manner, simply by acquiring the fluorescence spectrum of a PLM under conditions where it undergoes intermolecular interactions. In the case of the EP(SM) sample where intrinsic viscosity measurements established that the hydrodynamic volume decreased substantially with decreasing temperature thus reflecting a decrease in the solvent quality toward EP(SM), an

increase in polymer concentration and a decrease in temperature both contribute to induce intermolecular interactions. For such a sample, I_E/I_M(intra) is more challenging to determine as EP(SM) has an inherent tendency to associate intermolecularly even at low polymer concentration as the FRET experiments have established. To ensure that intramolecular excimer formation would only be observed for the determination of I_E/I_M(intra), the fluorescence spectrum of dilute (0.01 $g.L^{-1}$) solutions of the PLMs was acquired in the presence of 10 $g.L^{-1}$ of the unlabeled macromolecule. Under such conditions, the large excess of unlabeled macromolecule ensures that the formation of intermolecular polymeric aggregates would only incorporate one PLM per aggregate thus ensuring that the fluorescence spectrum of such a solution would report solely on pyrene excimer formed intramolecularly from PLMs isolated in large aggregates of unlabeled macromolecules.

Since engine oils are polymer solutions containing a few wt% of VII, the fluorescence spectra of 10 $g.L^{-1}$ Py(116)-EP(SM) and Py(108)-EP(AM) solutions in toluene were acquired as a function of temperature andare shown in Figure 4.7. In the case of Py(108)-EP(AM), the fluorescence intensity of the excimer (I_E) at 480 nm remained more or less constant with temperature, but the fluorescence intensity of the pyrene monomer (I_M) at 375 nm increased continuously with decreasing temperature, a consequence of the increase in solvent viscosity associated with a decrease in temperature, which reduces pyrene excimer formation by diffusion and increases the monomer quantum yield. The behavior of Py(116)-EP(SM) was similar to that of Py(108)-EP(AM) at temperatures lower and higher than −10 ^oC whereby I_E decreased a little and I_M increased more substantially and continuously with decreasing temperature. Compared to these gradual variations in fluorescence signal with decreasing

temperature, I_E showed a step-increase at −10 °C for Py(116)-EP(SM) however, a consequence of an increase in intermolecular associations taking place for that sample around −10 °C.

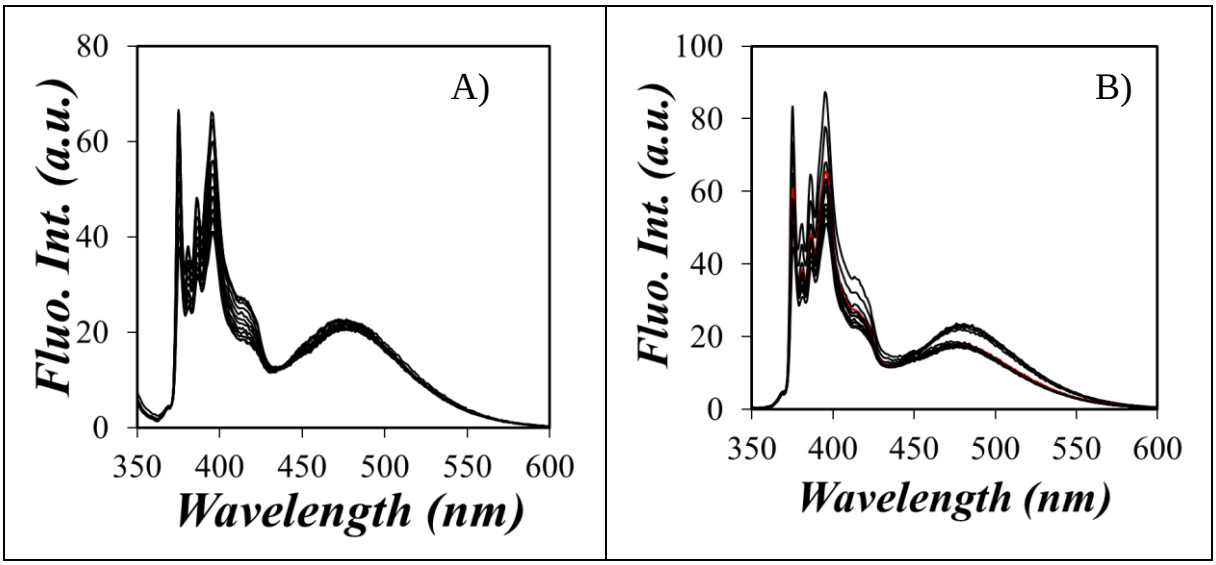

Figure 4.7. Fluorescence spectra of A) Py(108)-EP(AM) (10 g.L^{-1}) and B) Py(116)-EP(SM) (10 g.L^{-1}). From top to bottom: temperature increases from −35 °C to +25 °C. Solvent is toluene and λ_{ex} = 344 nm.

Beside the experiments conducted in Figure 4.7, the fluorescence spectra of toluene solutions containing 0.01 g.L^{-1} Py-EP were also acquired as a function of temperature for the EP(SM) and EP(AM) samples as well as the fluorescence spectra of a solution in toluene containing 10 g.L^{-1} of unlabeled EP copolymer and 0.01 g.L^{-1} Py-EP to obtain the ratio I_E/I_M(intra). The I_E/I_M ratios of all the fluorescence spectra were calculated and they were plotted in Figure 4.8 as a function of temperature. For all Py(108)-EP(AM) solutions, the I_E/I_M ratio increased continuously with increasing temperature in Figure 4.8B and D. This is the expected behavior for pyrene-labeled macromolecules at temperatures lower than 35 °C.[32] In this temperature regime, the dissociation rate constant of the pyrene excimer is negligible and

I_E/I_M is proportional to the product of the bimolecular rate constant for excimer formation by diffusion (k_{diff}) and $[Py]_{loc}$. Since EP(AM) is soluble in toluene at all temperatures, $[Py]_{loc}$ does not change much with temperature and the increase in I_E/I_M with increasing temperature reflects the increase in k_{diff} due to the decrease in the solvent viscosity associated with an increase in temperature.

Interestingly EP(SM) yields a very different plot of I_E/I_M as a function of temperature in Figure 4.8A and C. For both the 10 $g.L^{-1}$ Py(116)-EP(SM) and 0.01 $g.L^{-1}$ Py(96)-EP(SM) solutions without an excess of unlabeled EP(SM), an increase in solution temperature induces first an increase in I_E/I_M, followed by a decrease in I_E/I_M at intermediate temperatures, before the expected increase in I_E/I_M resumes at higher temperatures. The anomalous behavior observed for Py(116)-EP(SM) and Py(96)-EP(SM) at intermediate temperatures reflects a change in excimer formation which could have two origins. The first origin would be the result of the volume expansion of the polymer coil happening as the compact crystalline microdomains of EP(SM) melt, thus decreasing $[Py]_{loc}$. The second cause would be the dissociation of Py-EP(SM) aggregates happening at intermediate temperatures which would also result in a decrease in $[Py]_{loc}$. The FRET experiments discussed earlier confirmed that intermolecular association takes place for EP(SM) at low temperatures, but a reduction in the overall dimension of the polymer coil happening in the low temperature regime cannot be ruled out. In any case, both effects contribute to the decrease in $[Py]_{loc}$ that is probed through the decrease in the I_E/I_M ratio with increasing temperature observed at intermediate temperatures. We also note with interest that the break point seen in the I_E/I_M profile shown in Figure 4.8A and C matches that observed with another pyrene-labeled semicrystalline EP copolymer, implying that this behavior seems to be representative of such polymers.[2]

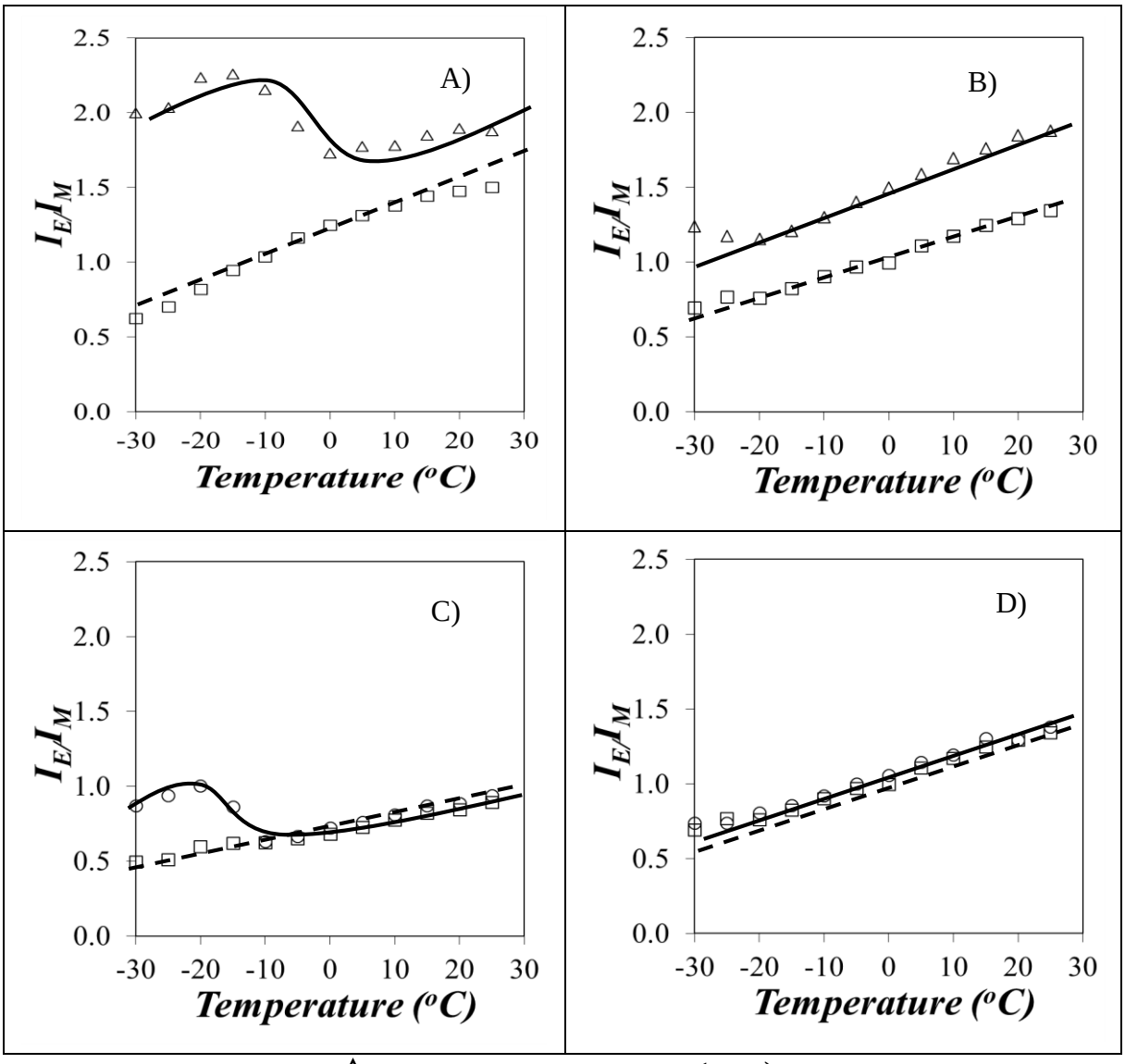

Figure 4.8. I_E/I_M -vs-*T*. A) (△) Py(116)-EP(SM) (10 g.L^{-1}), (□) mixture of Py(116)-EP(SM) (0.01 g.L^{-1}) and EP(SM) (10 g.L^{-1}). B) (△) Py(108)-EP(AM) (10 g.L^{-1}), (□) mixture of Py(108)-EP(AM) (0.01 g.L^{-1}) and EP(AM) (10 g.L^{-1}). C) (○) Py(96)-EP(SM) (0.01 g.L^{-1}), (□) mixture of Py(96)-EP(SM) (0.01 g.L^{-1}) and EP(SM) (10 g.L^{-1}). D) (○) Py(108)-EP(AM) (0.01 g.L^{-1}), (□) mixture of Py(108)-EP(AM) (0.01 g.L^{-1}) and EP(AM) (10 g.L^{-1}).

In the presence of 10 g.L^{-1} excess EP copolymer, all 0.01 g.L^{-1} Py-EP solutions showed a continuous increase in I_E/I_M with increasing temperature. This behaviour is expected for a pyrene-labeled macromolecule where excimer formation occurs intramolecularly and with a rate constant that increases with increasing temperature. This behaviour confirms that the presence of 10 g.L^{-1} excess unlabeled EP prevents intermolecular interactions so that these trends yield I_E/I_M(intra) in Equation 4.2.

Equation 4.2 was applied to the trends shown in Figure 4.8 to yield f_{inter} that was plotted as a function of temperature in Figure 4.9. Compared to the complex trends obtained with the I_E/I_M-vs-T profiles in Figure 4.8, the f_{inter}-vs-T plots shown in Figure 4.9 are much simpler to interpret. For all EP(AM) solutions, f_{inter} remained constant with temperature as expected from a polymer for which temperature does not induce intermolecular associations. At a low 0.01 g.L^{-1} Py(108)-EP(AM) concentration, little-to-no intermolecular interactions should be observed for this non-associative polymer as is indeed the case in Figure 4.9B that yields an f_{inter} value of 0.03 ± 0.03 over the entire temperature range. Increasing the Py(108)-EP(AM) concentration to 10 g.L^{-1} in Figure 4.9B increases the probability of pyrene-pyrene encounters in the solution and diffusive intermolecular excimer formation results in the higher f_{inter} value of 0.31 ± 0.02. The transition induced by the formation of crystalline microdomains for the Py(116)-EP(SM) solutions appears now quite clearly in Figure 4.9A where the two regimes at temperature below and above the transition can be easily assigned. For the 10 g.L^{-1} Py(116)-EP(SM) solution, f_{inter} increases from 0.23 ± 0.03 at high temperature to 0.62 ± 0.07 at low temperature, the inflexion point of the transition being at T = –5 ± 3 ^{o}C. For the more dilute Py(96)-EP(SM) solution of 0.01 g.L^{-1}, no intermolecular interactions are taking place at high

temperatures where f_{inter} equals 0.04 ± 0.02. After passing through an inflexion point at T = −15 ± 3 °C, f_{inter} increases to 0.43 ± 0.03 at low temperature. The shift in the transition temperature from −5 to −15 °C when the concentration is reduced from 10 to 0.01 g.L^{-1} reflects the difficulty for two polymer coils to encounter each other at such a low concentration. At a Py(96)-EP(SM) concentration of 0.01 g.L^{-1}, the quality of the solvent needs to be made considerably worse for intermolecular associations to take place. This explains why these interactions are observed at a lower temperature for this polymer concentration. The f_{inter} values obtained in the different temperature regimes have been listed in Table 4.4.

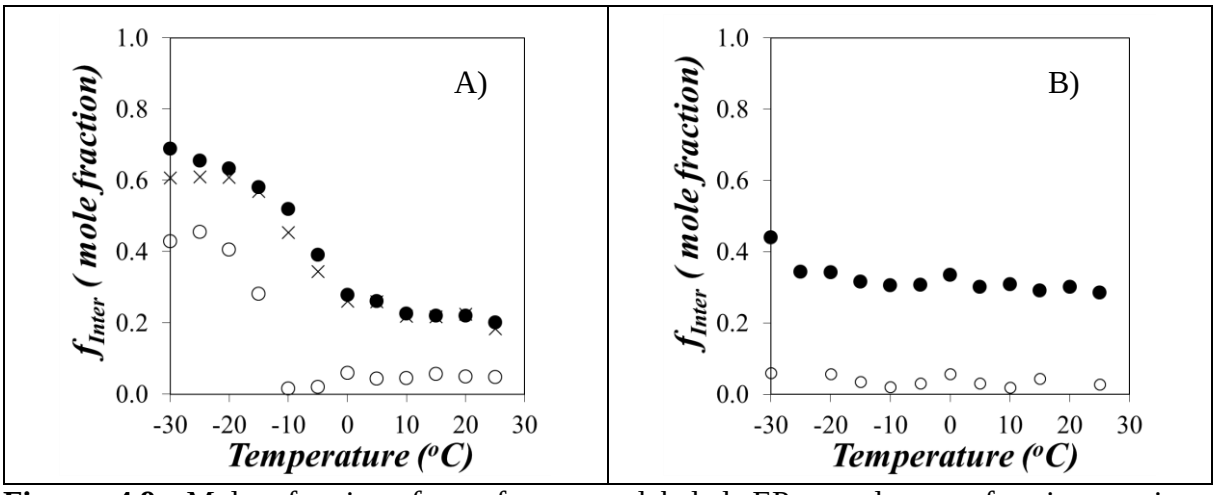

Figure 4.9. Molar fraction f_{inter} of pyrene labeled EP copolymers forming excimer intermolecularly for A) (●) Py(116)-EP(SM) and (×) Py(65)-EP(SM) at a concentration of 10 g.L^{-1}, and (○) Py(96)-EP(SM) at a concentration of 0.01 g.L^{-1} and B) Py(108)-EP(AM) at a concentration of (●) 10 g.L^{-1} and (○) 0.01 g.L^{-1}.

To investigate the robustness of the procedure, a Py(65)-EP(SM) sample was also synthesized with a lower pyrene content λ_{Py} of 65 µmol.g^{-1}. f_{inter} was determined as a function

of temperature as shown in Figure 4.9A. Interestingly, despite the difference in pyrene content for the two Py-EP(SM) samples, the procedure used to obtain f_{inter} appears to yield a same trend regardless of pyrene content. This result demonstrates the validity of the procedure which appears to report on the solution behaviour of the EP copolymers and is not influenced by differences in pyrene labeling.

Table 4.4. Summary of the molar fraction (f_{inter}) obtained for the different Py-EP samples.

	λ_{py}	Concentration ($g.L^{-1}$)	Temp (^oC) –30 to –10	Temp (^oC) –5 to 25
Py-EP(SM)	116	10	0.62 ± 0.07	0.23 ± 0.03
	65	10	0.57 ± 0.07	0.24 ± 0.03
Py-EP(AM)	108	10	0.31 ± 0.02	
Py-EP(SM)	96	0.01	0.43 ± 0.03	0.04 ± 0.02
Py-EP(AM)	108	0.01	0.03 ± 0.03	

Naphthalene Excimer Formation. Naphthalene was used as the energy donor in the FRET experiments conducted to assess whether EP(SM) and EP(AM) associate intermolecularly in solution. To this end, the fluorescence of Np-EP(SM) and Np-EP(AM) was characterized as a function of temperature. The fluorescence spectra of the Np-EP samples where acquired for dilute (0.09 $g.L^{-1}$) and concentrated (9.0 $g.L^{-1}$) solutions in toluene and plotted in Figure 4.10. Between 310 and 370 nm, the fluorescence spectrum exhibits well-defined peaks characteristic of the fluorescence of the naphthalene monomer. A broad structureless emission centered at 400 nm is observed that is due to the naphthalene excimer. The monomer and excimer fluorescence intensities were integrated from 332 to 338 nm and 420 to 450 nm to yield I_M and

I_E, respectively. The I_E/I_M ratios obtained from the spectra shown in Figure 4.10 were determined and plotted as a function of temperature in Figure 4.11.

Most trends in Figure 4.11 showed a decreasing I_E/I_M ratio with increasing temperature for naphthalene, a quite different behavior compared to what was previously observed for pyrene (see Figure 4.8). The conflicting trends observed for pyrene and naphthalene can be reconciled by considering a Steven-Ban (SB) plot where the ratio I_E/I_M is plotted as a function of temperature. A SB plot exhibits a bell-shaped curve.[33] At low temperature where the excimer dissociation is negligible, I_E/I_M increases with increasing temperature as chromophore encounters are favored and excimer formation is increased. At high temperature, excimer dissociation becomes the dominant process and the excimer dissociates more quickly than it is being formed. As a result, I_E/I_M decreases with increasing temperature. The main question to resolve when probing excimer formation as a function of temperature is to determine which side of the bell-shaped SB plot is being probed. Pyrene with its four fused benzene rings has a negligible k_{-1} at temperature below 35 ^oC[32] and I_E/I_M increases with increasing temperature. In the case of naphthalene with its two fused benzene rings excimer has a much weaker binding energy and has a larger k_{-1} value at room temperature. As the temperature is decreased, k_{-1} decreases and I_E/I_M increases for naphthalene which rationalized the different trends obtained for pyrene (Figure 4.8) and naphthalene (Figure 4.11).

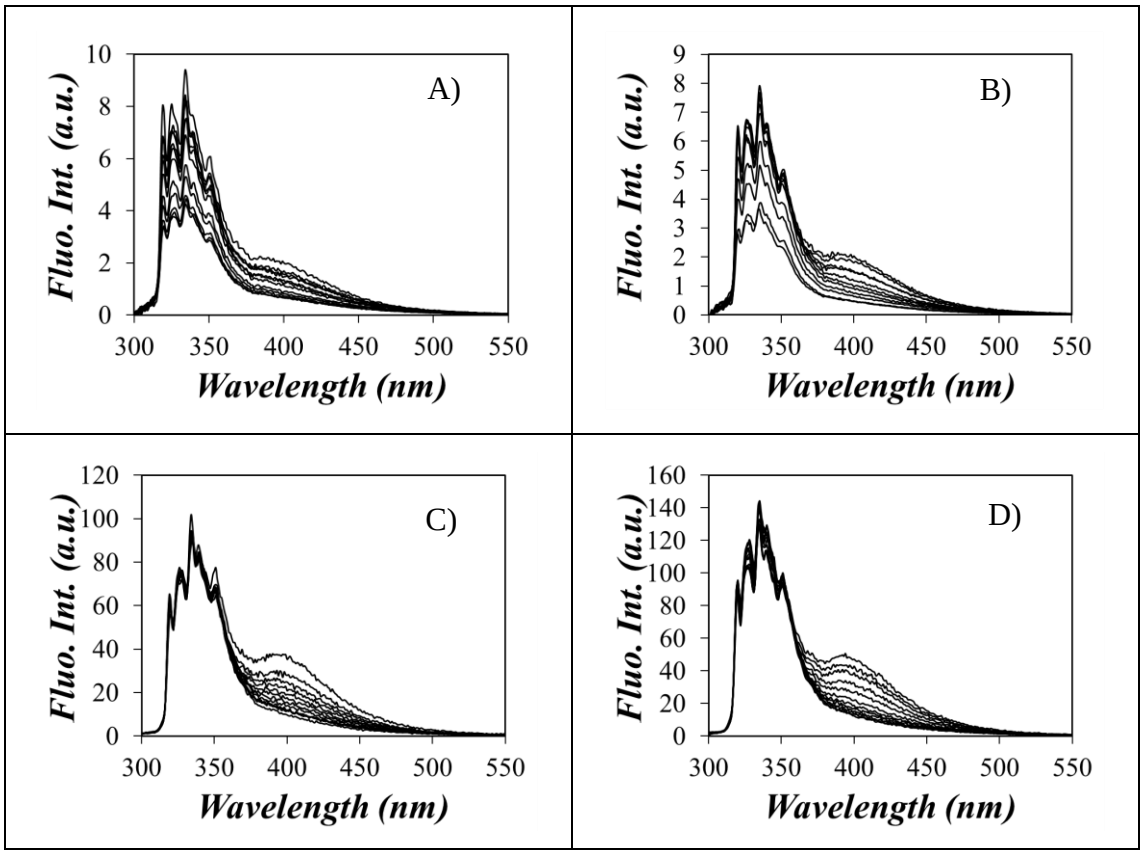

Figure 4.10. Fluorescence spectra for A) Np(108)-EP(AM) (0.09 g.L^{-1}), B) Np(116)-EP(SM) (0.09 g.L^{-1}), C) Np(108)-EP(AM) (9 g.L^{-1}), and D) Np(116)-EP(SM) (9 g.L^{-1}) as a function of temperature from –30 ^{o}C to 25 ^{o}C. (solvent: toluene; λ_{ex} = 290 nm)

Furthermore, the trends shown in Figure 4.11 lead to a number of interesting observations. First, the trends of I_E/I_M-vs-T were similar regardless of the nature of the polymer showing very little difference between Np-EP(SM) and Np-EP(AM). This observation suggests that the fluorescence signal emitted by the Np-EPs is insensitive to the changes in solubility experienced by the polymers at low temperature despite the fact that these changes should be substantial according to the intrinsic viscosity measurements. This result was somewhat unexpected because the I_E/I_M ratio is supposed to be proportional to the local naphthalene concentration $[Np]_{loc}$ which should increase when the volume of the Np-EP(SM) coil decreases

at low temperatures. Second, the I_E/I_M ratios remained more or less constant with temperature for the 0.09 $g.L^{-1}$ Np-EP solutions but the I_E/I_M ratios of the concentrated solutions took larger values at low temperature before decreasing at high temperature to the I_E/I_M ratios obtained with the low Np-EP concentration. Again, this result was unexpected as an increase in $[Np]_{loc}$ should result in a larger I_E/I_M ratio as observed at low temperature, but surprisingly not at high temperature.

We believe that these effects are due to the fact that the naphthalene monomer does not form excimer efficiently, particularly so at room temperature where the excimer dissociation rate constant is large, and its short lifetime does not allow an excited naphthalene to probe a sufficiently large sub-volume of the polymer coil. The monomer lifetime of Np-ESI is more than three times smaller than Py-MSI in toluene (Table 4.2). Consequently, excimer formation occurs over shorter distances at high temperature, certainly within naphthalene clusters along the chain which all form excimer in the same manner regardless of the overall polymer concentration. At low temperature, the longer lifetime of naphthalene allows the excited naphthalene to probe a larger volume, excimer formation is facilitated by the smaller excimer dissociation rate constant, and it becomes sensitive to the increase in $[Np]_{loc}$ induced by increasing the concentration from 0.09 $g.L^{-1}$ to 9.0 $g.L^{-1}$. However, the distance travelled by a relatively short-lived excited naphthalene tethered to the much larger EP chain remains much shorter than the length scale reflecting the contraction undergone by EP(SM) at low temperature which results in no obvious difference in the I_E/I_M ratios of Np-EP(SM) and Np-EP(AM) in the low-temperature range. Contrary to naphthalene excimer formation that takes place over short distances, FRET between a naphthalene donor and pyrene acceptor and pyrene excimer formation are two photophysical phenomena that occur over several nanometers and these two

techniques report on the volume contraction experienced by EP(SM) upon decreasing the solution temperature as observed experimentally earlier.[2]

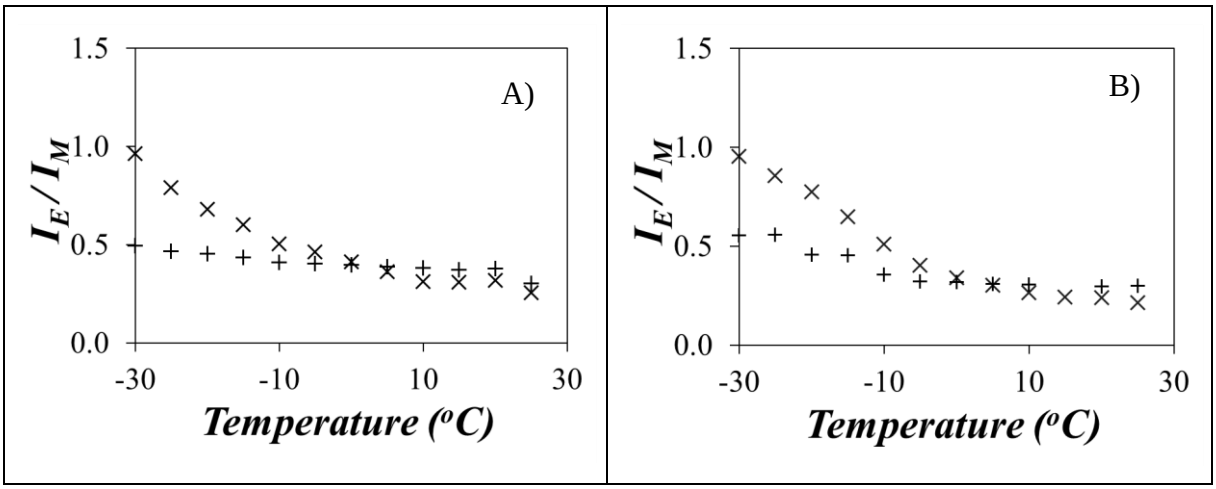

Figure 4.11. I_E/I_M -vs-T for (×) Np-EP (9 g.L^{-1}) and (+) Np-EP (0.09 g.L^{-1}). A) Np(108)-EP(AM) and B) Np(116)-EP(SM).

4.5 Conclusions

Two different EP copolymers were maleated and subsequently labeled with 1-pyrenemethylamine or 2-(2-naphtyl)ethylamine. FTIR and DSC measurements performed in the solid state confirmed that EP(SM) was semicrystalline while EP(AM) was amorphous. The FTIR measurements also confirmed that the chemical composition of the copolymers in terms of ethylene and propylene content was not affected by the maleation and labeling reaction, although GPC experiments showed that some chain scission took place after these reactions. Nevertheless, intrinsic viscosity experiments indicated that the solution behaviour of the fluorescently labeled EP copolymers was similar to that of the unmodified polymers.

To probe the interactions taking place between polymer chains at the molecular level, fluorescence experiments based on FRET and excimer formation were conducted on the

pyrene- and naphthalene-labeled EP copolymers. The FRET experiments showed that low temperatures induced intermolecular interactions in toluene for both EP copolymers, but that these interactions were much stronger for the EP(SM) sample. While informative, the FRET experiments did not yield a parameter that would qualify the strength of these intermolecular interactions.

Fluorescence experiments based on pyrene excimer formation were implemented to achieve this goal. The pyrene-labeled EP(AM) and EP(SM) samples yielded very different profiles of I_E/I_M-vs-T. While I_E/I_M increased continuously with increasing temperature for Py(108)-EP(AM) as would be expected for any pyrene-labeled macromolecule in solution, a much more complex profile was found for Py(116)-EP(SM) with a marked transition in the same temperature range where a breakpoint had been observed for the profile of the intrinsic viscosity versus temperature in Figure 4.3. Comparison of the I_E/I_M profiles obtained with 10 $g.L^{-1}$ toluene solution of pyrene-labeled EP copolymer with a toluene solution containing 0.01 $g.L^{-1}$ of pyrene-labeled EP and 10 $g.L^{-1}$ of unlabeled polymer yielded f_{inter}, the molar fraction of pyrene labels that formed excimer intermolecularly. Although the derivation of f_{inter} was based on the determination of the I_E/I_M ratio that depended on the activation energy of numerous photophysical processes, this complicated temperature-dependency was fortuitously eliminated in the calculation of f_{inter}. Plots of f_{inter} as a function of temperature showed that f_{inter} did not depend much on temperature for a 10 $g.L^{-1}$ EP(AM) solution in toluene remaining constant at 0.31 ± 0.02. For the 10 $g.L^{-1}$ EP(SM) solution, two clear regimes were identified depending on whether the solution temperature was below or above -5 ^oC where f_{inter} took a large or small value of about 0.60 ± 0.07 or 0.23 ± 0.03, respectively. The increase in f_{inter} at low temperature observed for EP(SM) was attributed to the intermolecular formation of microcrystals. Finally

the trend obtained with Py(116)-EP(SM) was duplicated with Py(65)-EP(SM), an EP(SM) copolymer prepared with a lower pyrene content to demonstrate that the results obtained with f_{inter} were describing the behaviour of the polymer itself and were insensitive to the pyrene content of the polymer.

The successful interpretation of the I_E/I_M trends obtained with pyrene-labeled polymers to determine f_{inter} led us to investigate whether this procedure could be applied to other excimer forming chromophores such as naphthalene. To this end, the I_E/I_M ratio of solutions of the naphthalene-labeled EP copolymers was monitored as a function of temperature and polymer concentration. Surprisingly, the trend obtained with the I_E/I_M ratio of the 10 $g.L^{-1}$ naphthalene labeled EP copolymers were similar regardless of their ethylene content. The similarity in the trends obtained with the I_E/I_M ratio for the two naphthalene-labeled EP copolymers were attributed to the much lower efficiency of naphthalene at forming an excimer, particularly at room temperature where its dissociation constant is large, and its shorter lifetime compared to pyrene. Both effects resulted in naphthalene excimer formation taking place between nearby naphthalenes through a process that depends much more weakly on the local chromophore concentration.

In summary, this study has demonstrated that FRET and pyrene excimer formation that occur over distances of several nanometers respond to changes in the local polymer concentration induced by a worsening of the solvent quality toward the polymer. But whereas FRET provides qualitative evidence that intermolecular interactions are taking place, analysis of the fluorescence spectra acquired with the pyrene-labeled EP copolymers yielded f_{inter}, a parameter that describes quantitatively the strength of intermolecular associations. Considering how strongly the rheological properties of polymer solutions are affected by intermolecular

associations, the ability to describe the strength of these intermolecular associations via a single parameter should prove extremely valuable to the numerous scientists aiming to rationalize the complex rheological behaviour of solutions of associating polymers.

Chapter 5

Using Pyrene Excimer Fluorescence to Study the Microcrystallization of Ethylene-Propylene Copolymers in Solution

5.1 Overview

Fluorescence experiments were carried out on six different ethylene-propylene (EP) copolymers to study their intermolecular association in solution. These six EP copolymers were maleated to yield EP-MA and then fluorescently labeled with 1-pyrenemethylamine to yield Py-EP. Successful labeling was confirmed by Fourier transform infrared (FTIR) and UV-Vis absorption spectroscopy. Differential scanning calorimetry (DSC), Carbon Nuclear Magnetic Resonance (^{13}C NMR), and FTIR measurements confirmed that four of the EP copolymers were semicrystalline and two were amorphous. The intrinsic viscosity of the EP copolymers was also measured as a function of temperature. The semicrystalline samples showed a decrease in intrinsic viscosity around −5 °C suggesting a decrease of the hydrodynamic volume of the polymer coils, as would be expected if these polymers formed microcrystalline domains at lower temperatures in solution. The associative behaviour of the EP copolymers were characterized by pyrene excimer formation, which was used to quantitatively measure the molar fraction of intermolecular interaction (f_{inter}) between different EP copolymer chains. Plots of f_{inter} as a function of temperature provided a description of the associative behaviour of a given EP copolymer in solution. The results of this study indicate that with decreasing temperature, f_{inter} increased in a stepwise manner for the semicrystalline samples with a high ethylene content, increased continuously for the semicrystalline sample having a lower ethylene content, and remained constant for the amorphous samples. The close agreement observed between the expected behaviour of these EP copolymers and their chemical composition confirms the robustness of this method and suggests that pyrene excimer fluorescence provides a reliable tool to quantitatively determine the level of intermolecular associations for different types of EP copolymers used as viscosity index improvers (VIIs).

5.2 Introduction

Viscosity index improvers (VIIs) are polymers that are purposely added to engine oils. As their name suggests, these polymers boost the viscosity index (VI) of the engine oil. The VI was introduced in 1929 as a measure of the change in viscosity of an oil with temperature, with the lowest VI corresponding to the largest change in viscosity with temperature.[1] Since an engine oil is expected to retain a constant viscosity from the moment the cold engine is started to the time the engine operates with some of its parts reaching up to 200 ^{o}C, there has been a sustained effort since the 1940s' to increase the VI of engine oils.[1] A higher VI ensures that a proper lubrication is attained at the high temperature where the engine operates and that an easy oil flow is achieved at the low temperature where the engine is started.[2-4] Higher VIs are attained through the addition of VIIs to the oil.

A number of synthetic polymers are being used as VIIs. They include acrylate copolymers, polyolefins such as ethylene-propylene (EP) copolymers, and hydrogenated styrene-diene copolymers.[4-7] In the case of semicrystalline EP copolymers having a high ethylene content, long ethylene sequences crystallize at low temperature to form dense crystalline microdomains resulting in polymer coils having small hydrodynamic volumes (V_h). Therefore their presence has a small influence on the overall viscosity of the oil which depends on the fraction of the solution volume that is occupied by the polymer. Upon increasing the temperature, these semicrystalline microdomains melt which results in a higher V_h reflecting the expansion of the polymer coils, a larger fraction of the solution volume being occupied by the polymer, and thus an increase in viscosity.[2] Therefore addition of a VII to an oil counteracts the inherent decrease in the viscosity of the base oil with increasing temperature and ensures

that the engine oil viscosity does not change significantly as a function of temperature during the operation of the engine.

The quality of EP copolymers as VIIs depends on their ethylene content. The ethylene contents of EP copolymers used as VIIs are normally in the 50–70 mol% range.[8] A higher ethylene content results in a higher thickening efficiency, but also in lower solubility at low temperature that induces the formation of polymer aggregates which thicken the oil and lowers its VI. Additionally, copolymers with high ethylene contents interact with wax at low temperatures. On the other hand, higher propylene contents result in EP copolymers having a lower oxidative stability. Consequently, the selection of an optimal chemical composition for an EP copolymer must be based on several factors that include its effect on the oil VI and the solubility and stability of the VII in the oil. Nowadays EP copolymers can be prepared with randomly distributed monomers to improve the oil flow at low-temperature and minimize undesirable wax interactions.[8] The excellent thickening ability of EP copolymers has led to their extensive use in the oils of both diesel and gasoline engines.

There are scattered reports in the literature that have discussed the behaviour of EP copolymers in solution.[3,4,9-11] Intermolecular interactions between EP copolymers in solution have been investigated by viscosity, light scattering, differential scanning calorimetry (DSC), and pyrene excimer formation.[2,3,12-14] In 1990, Rubin and Sen used viscosity measurements to study the behaviour of EP copolymers in toluene.[3] They observed a sharp decrease in the intrinsic viscosity of semicrystalline EP copolymers upon decreasing the solution temperature below 20 °C which they attributed to the formation of microcrystalline domains below the crystallization temperature (T_c) of the copolymers. In 2007, Zhang et al. used fluorescence resonance energy transfer (FRET) and pyrene excimer formation to study the

microcrystallization of EP copolymers in toluene, where the polymers had an ethylene-rich semicrystalline core flanked by two amorphous overhangs.[2] These experiments demonstrated that the crystallization of this semicrystalline EP copolymer in toluene occurred mostly intramolecularly. However, the majority of EP copolymers used as VIIs are prepared with ethylene and propylene randomly distributed along the chain and such a chemical composition leads to their intermolecular association. In this context, it becomes important to quantify the level of intermolecular interactions of these EP copolymers with random distributions of ethylene and propylene monomers. A quantitative measure of the intermolecular interactions of EP copolymers in solution such as the molar fraction (f_{inter}) of intermolecular associations can only be determined from the excimer fluorescence generated by pyrene labels that were covalently attached onto an EP backbone.[15] The fraction f_{inter} can be calculated directly from the fluorescence intensity of the excimer (I_E) over that of the monomer (I_M) obtained from the fluorescence spectrum of any type of pyrene-labeled macromolecules including pyrene labeled EP copolymers (Py-EP). The ability to measure the fraction f_{inter} provides a novel and powerful analytical tool that allows one to probe and compare the behaviour of different macromolecules in solution. So far, the procedure applied to determine f_{inter} has been used to monitor the level of intermolecular association taking place in solution as a function of temperature for one amorphous and one semicrystalline EP copolymer.[15] The fraction f_{inter} reported faithfully on the expected behavior of these two polyolefins, indicating a substantial increase at the temperature (T_c) where the semicrystalline EP copolymer underwent microcrystal formation while remaining constant for the amorphous EP copolymer over the entire temperature range.

These interesting results led us to further investigate the sensitivity of the procedure and its robustness. To this end, six EP copolymers were investigated, two amorphous samples with

an ethylene content of 60 mol% (EP(60)), three semicrystalline samples with an ethylene content of 78 mol% (EP(78)), and one semicrystalline sample with an intermediate ethylene content of 70 mol% (EP(70)). Application of the procedure yielded f_{inter}-vs-T profiles whose shape reflected faithfully the level of crystallinity of the polyolefins, showing a sharp transition at T_c for all semicrystalline EP(78) samples, a constant profile for the two amorphous EP(60) samples, and an intermediate behaviour for the EP(70) sample. These experiments establish on firm ground the suggestion made earlier[15] that Py-EP copolymers can be used to determine quantitatively their level of intermolecular interactions using the parameter f_{inter}. A description of the experiments carried out to reach this conclusion is presented hereafter.

5.3 Experimental

***Chemicals*.** Acetone (HPLC grade), dodecane (anhydrous, 99%), toluene (HPLC, 99.9%), biphenyl (99%), maleic anhydride (98%), 1,1,2,2-tetrachloroethane-d_2 (TCE-d_2), 1-pyrenemethylamine hydrochloride ($PyCH_2NH_2$ HCL, 95%), and *tert*-butyl peroxide (98%) were purchased from Sigma-Aldrich and were employed without further purification. Six EP copolymers with different ethylene contents were supplied by Afton. Four of the EP copolymers were semicrystalline and two were amorphous.

***Carbon Nuclear Magnetic Resonance* (^{13}C *NMR*).** The ^{13}C NMR spectra of the EP copolymers were acquired on a high resolution Bruker 500 MHz spectrometer at 120 ^oC. Before each measurement, the EP copolymers were first dissolved in TCE-d_2 and kept at 120 ^oC for 4 hrs in a heating block to homogenize the solutions.[16] The molar ethylene and propylene contents of the EP copolymers were calculated by using a reported procedure based on their ^{13}C NMR spectra.[17] The ^{13}C NMR spectra of Py(108)-EP(60-1) and Py(116)-EP(78-1) are presented in

Figure S5.1. The ^{13}C NMR spectra for the four other EP copolymers are patent protected and are not presented here.

Differential Scanning Calorimeter (DSC). The melting point (T_m) and enthalpy (ΔH) of the EP copolymers were determined using DSC with TA Q2000 calorimeter with temperature scanning rate of 10 °C/min. The samples were prepared following a procedure described previously.[15] Each sample was first heated from –30 to +200 °C followed by cooling from +200 to –30 °C, and finally heating from –30 to +200 °C.

***Fourier Transform Infrared* (*FTIR*).** The FTIR spectra of all polymer solutions in toluene were obtained with a Bruker Tensor 27 FTIR spectrophotometer. To obtain a thin film on a NaCl FTIR plate, a few drops of polymer solutions were deposited onto the cell and the toluene was then evaporated under a stream of nitrogen. The absorbance of all polymer films was kept smaller than unity to optimize the signal-to-noise ratio.

***Steady-State Fluorescence*.** Steady-state fluorescence emission spectra of EP copolymers were acquired with a Photon Technology International (PTI) LS-100 equipped with an Ushio UXL-75Xe xenon arc lamp. The pyrene-labeled EP solutions were excited at a wavelength of 344 nm and their emission spectra were acquired between 350 to 600 nm. The fluorescence measurements were carried out at various temperatures using a cryostat from Oxford Instruments (Optistat DN) placed in the steady-state fluorometer. Before bringing the solutions to the desired temperature, the solutions were heated to +25 (± 0.2) °C to erase all pre-association history. Furthermore, the solutions were left in the cryostat for 10 min after reaching the desired temperature. Additionally, all the solutions were degassed for 30-40 minutes under a gentle flow of N_2 to remove oxygen before any fluorescence spectrum was acquired.[15]

UV-Visible Spectrophotometer. A Cary 100 UV-Vis spectrophotometer was used to acquire the absorption spectra between 200–600 nm. These experiments were carried out in quartz cells with a 0.1-10 mm path length.

Labeling of the EP Copolymers. The EP copolymers were first reacted with maleic anhydride[18] and then labeled with 1-pyrenemethylamine ($PyCH_2NH_2$)[19] according to a published procedure[15] based on the reactions shown in Scheme 5.1.

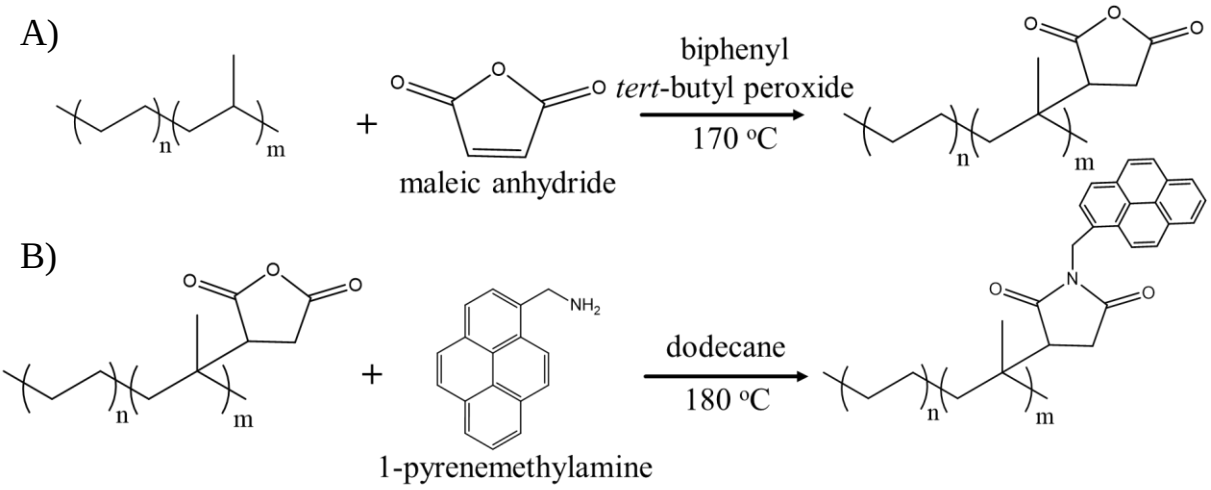

Scheme 5.1. Reaction scheme for A) the maleation of an EP copolymer and B) the labeling of the maleated EP copolymer with pyrene.

5.4 Results and Discussion

As already alluded to in the introduction, the characterization of the level of intermolecular interactions in solution is of paramount importance to industries that rely on the specific properties of multicomponent mixtures such as the oil formulations used by the oil additive industry. Since intermolecular associations induced by other additives can lead to uncontrolled viscosity changes that could be detrimental to the performance of an engine oil, the

determination of f_{inter} via pyrene excimer fluorescence described in an earlier report provides a crucial means to probe the level of intermolecular interactions.[15] The procedure developed to determine f_{inter} was established by comparing the f_{inter}-vs-T profiles of solutions of one semicrystalline and one amorphous EP copolymer that showed characteristic features reflecting the different chemical compositions of these two polyolefins. This earlier study is now expanded to investigate the reproducibility and reliability of the proposed procedure by acquiring the f_{inter}-vs-T profiles for solutions of six different EP copolymers, two amorphous samples with an ethylene content of 60 mol% (EP(60-1) and EP(61-2)), one semicrystalline sample with an ethylene content of 70 mol% (EP(70)), and three semicrystalline samples with an ethylene content of 78 mol% (EP(78-1), EP(78-2), and EP(78-3)). The determination of the chemical composition of these samples, their level of crystallinity, solution behavior, and f_{inter}-vs-T profiles is described hereafter.

Chemical Composition of the Py-EP Samples. The ethylene content of the EP samples was determined by using a procedure developed by Randall based on ^{13}C NMR. To this end, ^{13}C NMR spectra of all EP copolymers were acquired and two representative examples are shown in Figure S5.1. Using Randall's procedure, the ethylene content was determined and provided in Table 5.1. In this report, the polyolefin samples are described based on their ethylene content in mol% where EP(78) indicates an EP copolymer with a 78 mol% ethylene content.

The EP copolymers were then maleated to yield EP-MA and fluorescently labeled with 1−pyrenemethylamine according to Scheme 5.1. To this end, FTIR spectroscopy was applied to assess the success of the different reactions. The FTIR spectrum of EP(78) in Figure S5.2 shows two absorption bands at 1462 cm^{-1} and 1379 cm^{-1} which are due to the methylene and methyl units along the EP backbone, respectively. Since the FTIR spectrum of a completely

hydrated EP-MA sample has a strong absorption band at 1785 cm^{-1} due to the succinic anhydride carbonyls and no absorption at 1705 cm^{-1} where the succinic acid carbonyl absorb, FTIR was applied to ensure complete dehydration of EP-MA by monitoring the absence of absorption at 1705 cm^{-1}. After pyrene-labeling, a new absorption band appeared at 1710 cm^{-1} characteristic of the succinimide carbonyls while the band at 1785 cm^{-1} disappeared (trace C in Figure S5.2) following the reaction of succinic anhydride with 1-pyrenemethylamine.

Table 5.1. Chemical composition of Py-EP sample.

Polymer Type	λ_{py} ($\mu mol.g^{-1}$) (UV-Vis absorption)	$\frac{Abs(1379cm^{-1})}{Abs(1462cm^{-1})}$	$\frac{Abs(1785cm^{-1})}{Abs(1462cm^{-1})}$	$\frac{Abs(1710cm^{-1})}{Abs(1462cm^{-1})}$	Ethylene Content Mole% (^{13}C NMR)
EP(60-1)	-	0.80	-	-	60
EP(60-1)-MA	-	0.79	0.22	-	-
Py(108)-EP(60-1)	108	0.80	-	0.20	-
EP(61-2)	-	0.79	-	-	61
EP(61-2)-MA	-	0.78	0.23	-	-
Py(103)-EP(61-2)	103	0.78	-	0.17	-
EP(70-1)	-	0.72	-	-	70
EP(70-1)-MA	-	0.71	0.21	-	-
Py(82)-EP(70-1)	82	0.71	-	0.22	-
EP(78-1)	-	0.55	-	-	78
EP(78-1)-MA	-	0.55	0.23	-	-
Py(116)-EP(78-1)	116	0.56	-	0.28	-
EP(78-2)	-	0.55	-	-	78
EP(78-2)-MA	-	0.54	0.23	-	-
Py(81)-EP(78-2)	81	0.54	-	0.29	-
EP(78-3)	-	0.66	-	-	78
EP(78-3)-MA	-	0.60	0.21	-	-
Py(123)-EP(78-3)	123	0.61	-	0.22	-

All FTIR spectra were normalized at 1462 cm^{-1} and the absorbance ratios *Abs*(1379 cm^{-1})/*Abs*(1462 cm^{-1}), *Abs*(178 cm^{-1})/*Abs*(1462 cm^{-1}), and *Abs*(1710 cm^{-1})/*Abs*(1462 cm^{-1}) were determined. They are listed in Table 5.1. The *Abs*(1379 cm^{-1})/*Abs*(1462 cm^{-1}) provided a measure of the ethylene content of the EP copolymers which agreed with the ^{13}C NMR results, with a larger *Abs*(1379 cm^{-1})/*Abs*(1462 cm^{-1}) ratio indicating a smaller ethylene content. EP copolymers having a similar ethylene content as determined by ^{13}C NMR also yielded similar *Abs*(1379 cm^{-1})/*Abs*(1462 cm^{-1}) ratios. Finally, the *Abs*(1379 cm^{-1})/*Abs*(1462 cm^{-1}) ratio of the EP copolymers did not change after conducting the maleation and pyrene-labeling reaction confirming that the chemical composition of the copolymers in terms of ethylene and propylene contents was not affected by these reactions.

The pyrene content (λ_{Py}) of the Py-EP samples was determined by UV-Vis absorption by comparison of the pyrene absorbance at 344 nm in toluene with that of 1-pyrenemethyl-succinimide used as a model compound as was done in an earlier publication.[15] The λ_{Py} values are listed in Table 5.1 and they were used to describe the Py-EP samples. For example, the sample Py(116)-EP(78-1) had a pyrene content of 116 μmol/g and was the first sample with an ethylene content of 78 mol% to be studied.

Microstructure of EP Copolymers. Differential scanning calorimetry (DSC) experiments were conducted on the EP copolymer samples in the solid state. As shown in Figure S5.3, a thermal transition due to melting was observed for the semicrystalline samples while no thermal transition was observed for the amorphous samples. The T_m and enthalpy (ΔH) values retrieved from the DSC experiments conducted with the EP copolymers are listed in Table 5.2. The ΔH and T_m results for EP(781-1), EP(78-2), and EP(78-3) clearly indicate that these samples are

similar in terms of crystallinity and melting profile. In turn this conclusion agrees with their similar chemical composition found by FTIR and ^{13}C NMR spectroscopy (see Table 5.1). EP(70-1) had a substantially lower ΔH value in comparison with the EP(78) copolymer series as a consequence of its lower ethylene content and thus lower crystallinity.

***Solution Behaviour of EP Copolymers*.** Viscosity measurements were carried out between −10 °C and +20 °C for all EP copolymers in toluene to determine how their intrinsic viscosity [η] varied as a function of temperature. The resulting trends are shown in Figure 5.1. For all the semicrystalline samples (Figure 5.1C-F), [η] increased sharply with increasing temperature up to 0 °C and remained relatively constant afterward. The break point in the [η] profile is most likely due to a change in the hydrodynamic volume of the polymer coil (V_h) resulting from the melting of crystalline microdomains between long ethylene stretches inside the polymer coil at temperatures higher than 0 °C.[4] For the amorphous Py(103)-EP(61-2) and Py(108)-EP(60-1) samples, [η] remained relatively constant with increasing temperature in Figures 5.1A and B as expected based on the inability of the amorphous samples to form crystalline microdomains in solution and thus undergo drastic changes in hydrodynamic volume.

Table 5.2. Melting temperature (T_m) and enthalpy (ΔH) of EP copolymers obtained from DSC measurements.

Polymer Type	Polymer Name	T_m (°C)	ΔH (J.g^{-1})
Semicrystalline	EP(70-1)	33	5
	EP(78-1)	31	31
	EP(78-2)	31	32
	EP(78-3)	32	25

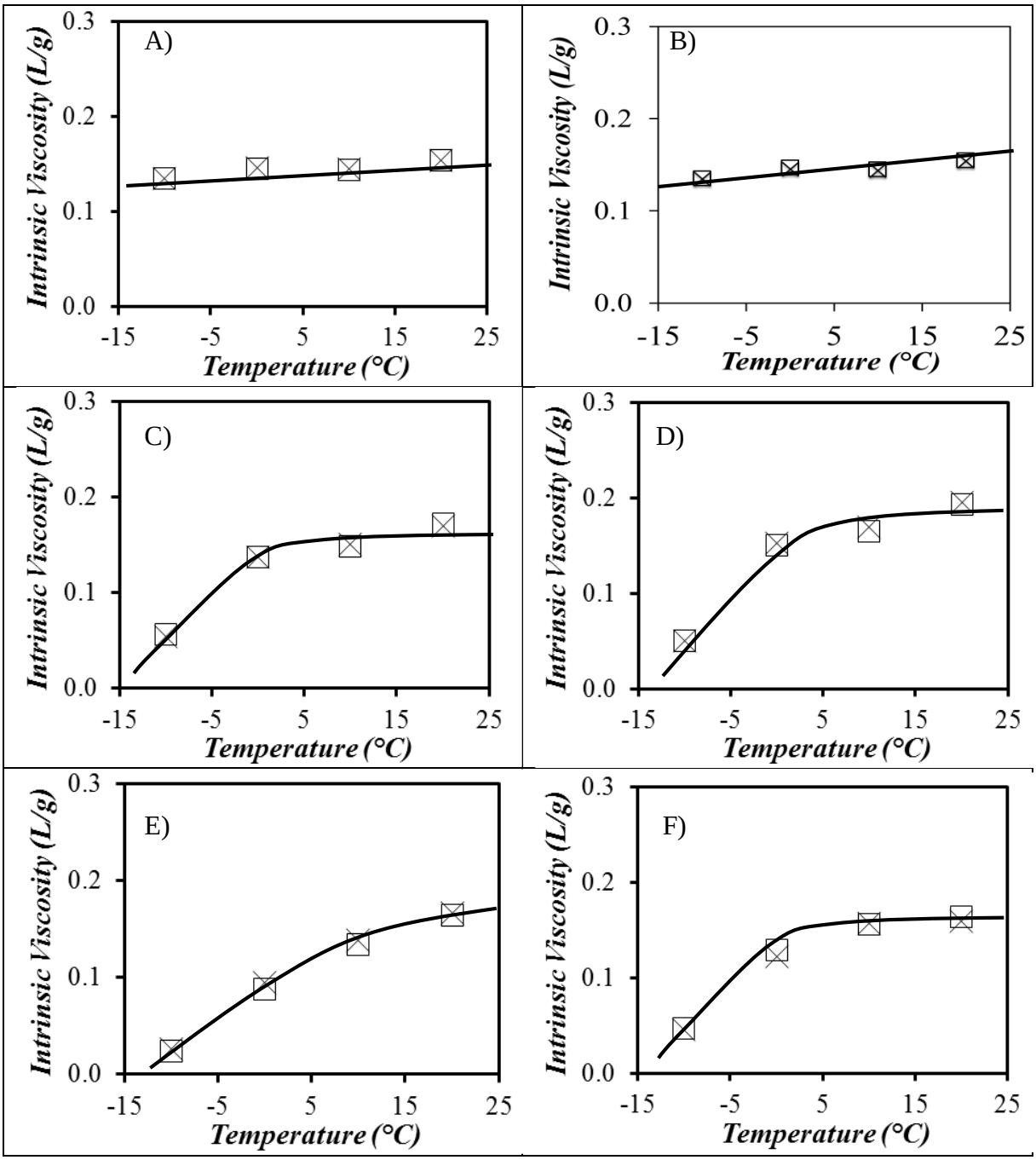

Figure 5.1. Intrinsic viscosity obtained by using (×) relative and (□) specific viscosity measurements in toluene at various temperatures, for A) Py(108)-EP(60-1), B) Py(103)–EP(61-2), C) Py(82)-EP(70-1), D) Py(116)-EP(78-1), E) Py(81)-EP(78-2), and F) Py(123)-EP(78-3).

Pyrene Excimer Formation. According to an earlier report, the level of intermolecular interactions between EP copolymers can be measured by applying a procedure based on pyrene excimer fluorescence.[15] These experiments yield the molar fraction (f_{inter}) of pyrene labels covalently attached onto the EP backbone that form excimer intermolecularly in solution. This method was applied to compare the level of intermolecular interactions between the EP copolymers whose chemical composition has been described earlier (see Table 5.1 and 5.2). The process of excimer formation between pyrene labels covalently attached onto a macromolecule, or PLM for pyrene labeled macromolecule, is described in Scheme 5.2.

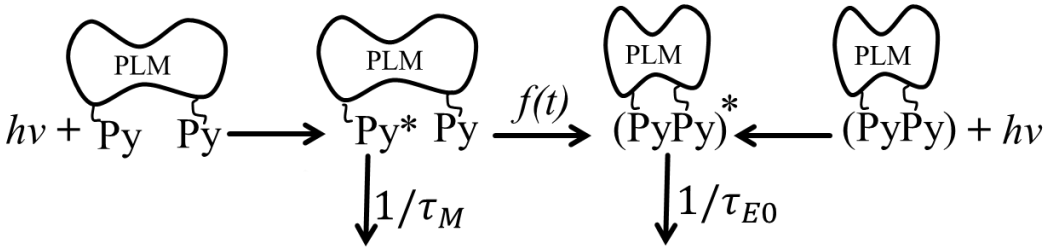

Scheme 5.2. Kinetic scheme for excimer formation in a PLM.

Irradiation of a PLM with UV light results in the emission of the pyrene monomer which is characterized by several sharp peaks between 360 nm and 425 nm and that of the pyrene excimer which is broad, structureless, and centered at 480 nm.[20] The fluorescence intensity of the pyrene excimer (I_E) and monomer (I_M) for the Py-EP samples can be calculated by integrating the fluorescence spectrum over the wavelength ranges between 372 and 379 nm and between 500 and 530 nm, respectively. As described in Equation 5.1, the fluorescence intensity ratio I_E/I_M is directly proportional to the local pyrene concentration $[Py]_{loc}$ experienced by an excited pyrene monomer covalently attached to a PLM.[21]

$$I_E/I_M = K(T) \times [Py]_{loc} \quad (5.1)$$

In Equation 5.1, $K(T)$ is a temperature-dependent multiplication factor whose origin has been described in more details earlier.[15] It depends on the fluorescence quantum yield of the pyrene monomer and excimer, the rate constants of formation and dissociation of the excimer, all quantities that depend on the solution temperature. However under isothermal conditions, an increase in I_E/I_M reflects an increase in $[Py]_{loc}$ as a result of intermolecular interactions between PLMs. When a PLM undergoes solely intramolecular interactions, the fluorescence spectrum yields the ratio I_E/I_M(intra) whereas if the PLM undergoes both intra- and intermolecular interactions, its fluorescence spectrum yields the ratio $I_E / I_M\begin{pmatrix}\text{intra }\&\\ \text{inter}\end{pmatrix}$. The molar fraction of pyrene labels forming excimer intermolecularly (f_{inter}) can be determined by Equation 5.2.

$$f_{\text{inter}} = \frac{[Py]_{loc}\left(\begin{smallmatrix}\text{inter}\&\\ \text{intra}\end{smallmatrix}\right) - [Py]_{loc}(\text{intra})}{[Py]_{loc}\left(\begin{smallmatrix}\text{inter}\&\\ \text{intra}\end{smallmatrix}\right)} = \frac{I_E / I_M\left(\begin{smallmatrix}\text{inter}\&\\ \text{intra}\end{smallmatrix}\right) - I_E / I_M(\text{intra})}{I_E / I_M\left(\begin{smallmatrix}\text{inter}\&\\ \text{intra}\end{smallmatrix}\right)} \quad (5.2)$$

In this study, the ratio $I_E / I_M\begin{pmatrix}\text{intra }\&\\ \text{inter}\end{pmatrix}$ was obtained simply by acquiring the fluorescence spectrum of a 10 g.L^{-1} Py-EP samples in toluene. Calculating the ratio I_E/I_M(intra) was more challenging for the semicrystalline samples since they have an inherent tendency to associate intermolecularly even at low polymer concentration as shown previously.[15] Therefore, I_E/I_M(intra) was calculated from a dilute (0.01 g.L^{-1}) solution of Py-EP in the presence of 10

g.L^{-1} of the unlabeled macromolecule to ensure that only intramolecular excimer formation would be observed.

The fluorescence spectra of solutions containing 10 g.L^{-1} of a Py-EP sample in toluene were acquired as a function of temperature to obtain the ratio $I_E / I_M\left(\begin{matrix}\text{intra \&}\\ \text{inter}\end{matrix}\right)$. The I_E/I_M ratios of all the fluorescence spectra were calculated and they were plotted in Figure 5.2 as a function of temperature. The I_E/I_M ratio of the Py(108)-EP(60-1) and Py(103)-EP(61-2) solutions increased continuously with increasing temperature in Figure 5.2A and B, respectively. Since $[Py]_{loc}$ is not expected to change much with temperature for the amorphous EP copolymers as determined by the $[\eta]$ measurements shown in Figures 5.1A and B, the increase in I_E/I_M with increasing temperature only reflects the increase in the diffusion rate constant (k_{diff}).[22] The increase in k_{diff} is due to the decrease in toluene viscosity associated with an increase in temperature. The $I_E / I_M\left(\begin{matrix}\text{intra \&}\\ \text{inter}\end{matrix}\right)$ ratio obtained for Py(82)-EP(70-1) in Figure 5.2C showed a minimal increase with increasing temperature, a behavior which is similar to that of the Py-EP amorphous samples observed in Figure 5.2A-B.

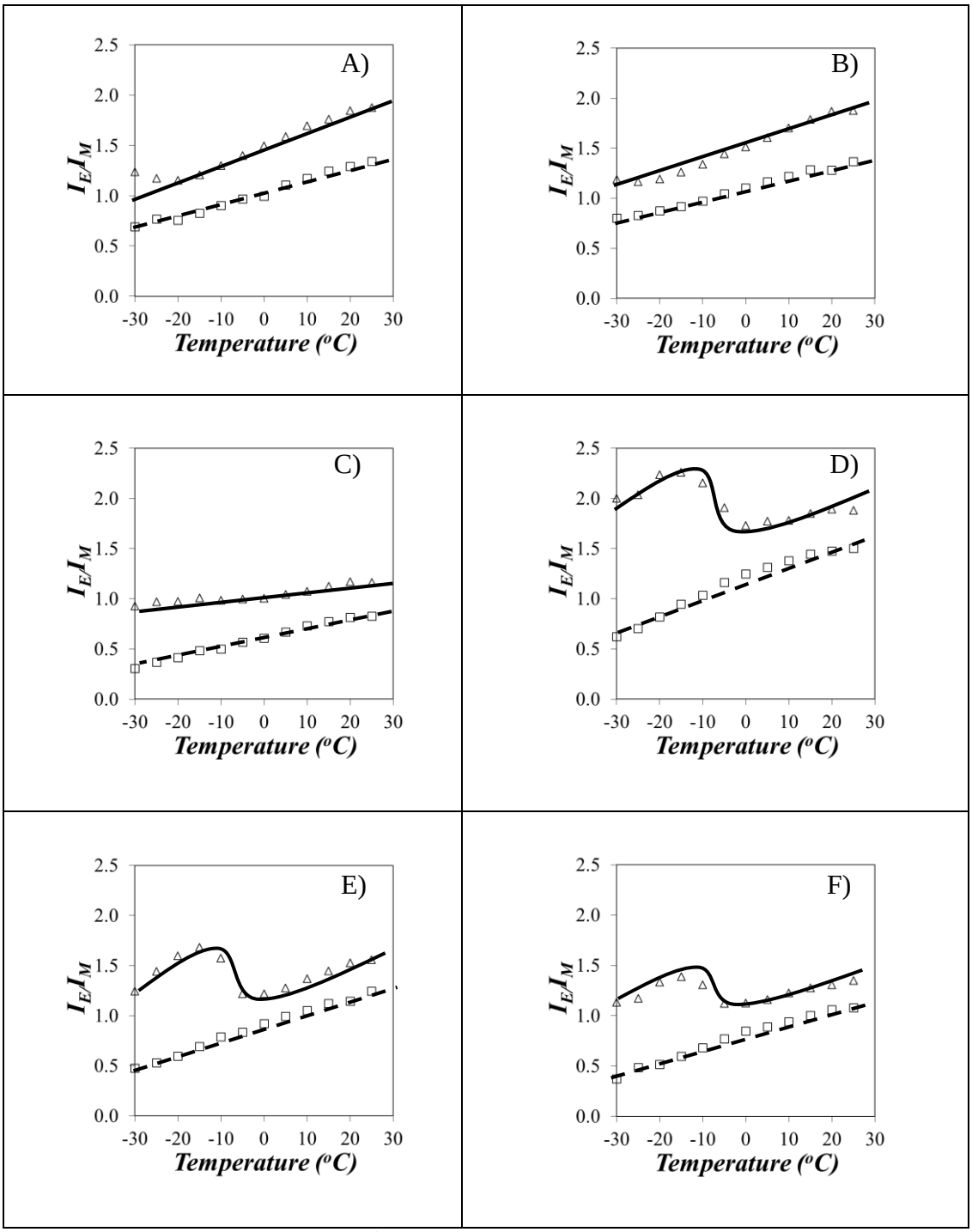

Figure 5.2. Plots of I_E/I_M -vs-T for (△) Py-EP (10 g.L^{-1}) and the mixtures of (□) Py-EP (0.01 g.L^{-1}) and EP (10 g.L^{-1}). A) Py(108)-EP(60-1), B) Py(103)–EP(61-2), C) Py(82)-EP(70-1), D) Py(116)-EP(78-1), E) Py(81)-EP(78-2), and F) Py(123)-EP(78-3).

The $I_E / I_M\begin{pmatrix}\text{intra \&}\\ \text{inter}\end{pmatrix}$ vs-T plots for Py(116)-EP(78-1), Py(81)-EP(78-2), and Py(123)-EP(78-3) samples showed a very different trend in Figure 5.2D-F. For all the samples, I_E/I_M first increased, then decreased at intermediate temperatures, before increasing again as the solution temperature was increased from –30 tpo 25 ^oC. The change in the I_E/I_M profiles for the Py-EP semicrystalline samples at intermediate temperatures has been attributed to a decrease in excimer formation due to a decrease in $[Py]_{loc}$.[2,15] The decrease in $[Py]_{loc}$ can be due to the expansion of the polymer coil happening as the compact crystalline microdomains melt and also, the dissociation of polymer aggregates occurring at intermediate temperatures, both effects resulting in a decrease in $[Py]_{loc.}$

The fluorescence spectra of toluene solutions containing a 10 $g.L^{-1}$ excess of unlabeled EP copolymer and 0.01 $g.L^{-1}$ Py-EP were also acquired for all six EP copolymers to obtain the ratio I_E/I_M(intra). The I_E/I_M ratios of all the fluorescence spectra were calculated and they were plotted in Figure 5.2 as a function of temperature. For all six Py-EP solutions, the ratio I_E/I_M(intra) increased continuously with increasing temperature. This behavior was expected since the Py-EP macromolecules were well separated with the excess of unlabeled EP copolymer present in the solution. Therefore, $[Py]_{loc}$ remained constant with temperature so that the I_E/I_M ratio responded solely to the decrease in solvent viscosity taking place with increasing temperature.

Equation 5.2 was applied to the trends shown in Figure 5.2 to yield f_{inter} which was plotted as a function of temperature in Figure 5.3. The f_{inter}-versus-T plots presented much simpler trends to interpret compared to those shown in Figure 5.2. For the amorphous Py(108)-EP(60-1) and Py(103)-EP(61-2) samples, f_{inter} remained constant with temperature as expected

from a polymer whose conformation in solution is unaffected by temperature. The fraction f_{inter} took a similar value for Py(108)-EP(60-1) and Py(103)-EP(61-2) since they both had a similar ethylene content. On the other hand, the transition induced by the formation of crystalline microdomains for Py(116)-EP(78-1), Py(81)-EP(78-2), and Py(123)-EP(78-3) samples appeared now quite clearly in Figure 5.3D-F where two regimes at temperatures below and above the transition could be easily assigned. For all semicrystalline solutions, f_{inter} increased from 0.23 ± 0.02 at high temperature to 0.60 ± 0.07 at low temperature, the inflexion point of the transition being at T = –5 ± 3 ºC. The fact that similar f_{inter} values were obtained for EP copolymers having similar crystallinity levels confirm that the proposed procedure yields reproducible f_{inter} values with different types of polyolefins.

Table 5.3. Molar fraction (f_{inter}) of intermolecular associations between EP copolymer in a 10 g.L^{-1} copolymer solution in toluene.

Polymer Type	Polymer Name	Temp (ºC) –30 to –10	Temp (ºC) –5 to 25
Amorphous	Py(108)-EP(60-1)	0.31±0.02	
	Py(103)-EP(61-2)	0.27±0.01	
Semicrystalline	Py(82)-EP(70-1)	*	*
	Py(116)-EP(78-1)	0.62±0.07	0.23±0.03
	Py(81)-EP(78-2)	0.62±0.02	0.23±0.02
	Py(123)-EP(78-3)	0.56±0.06	0.22±0.02

* This sample did not yield a constant f_{inter} value between –30 and –10 ºC and –5 and 25 ºC.

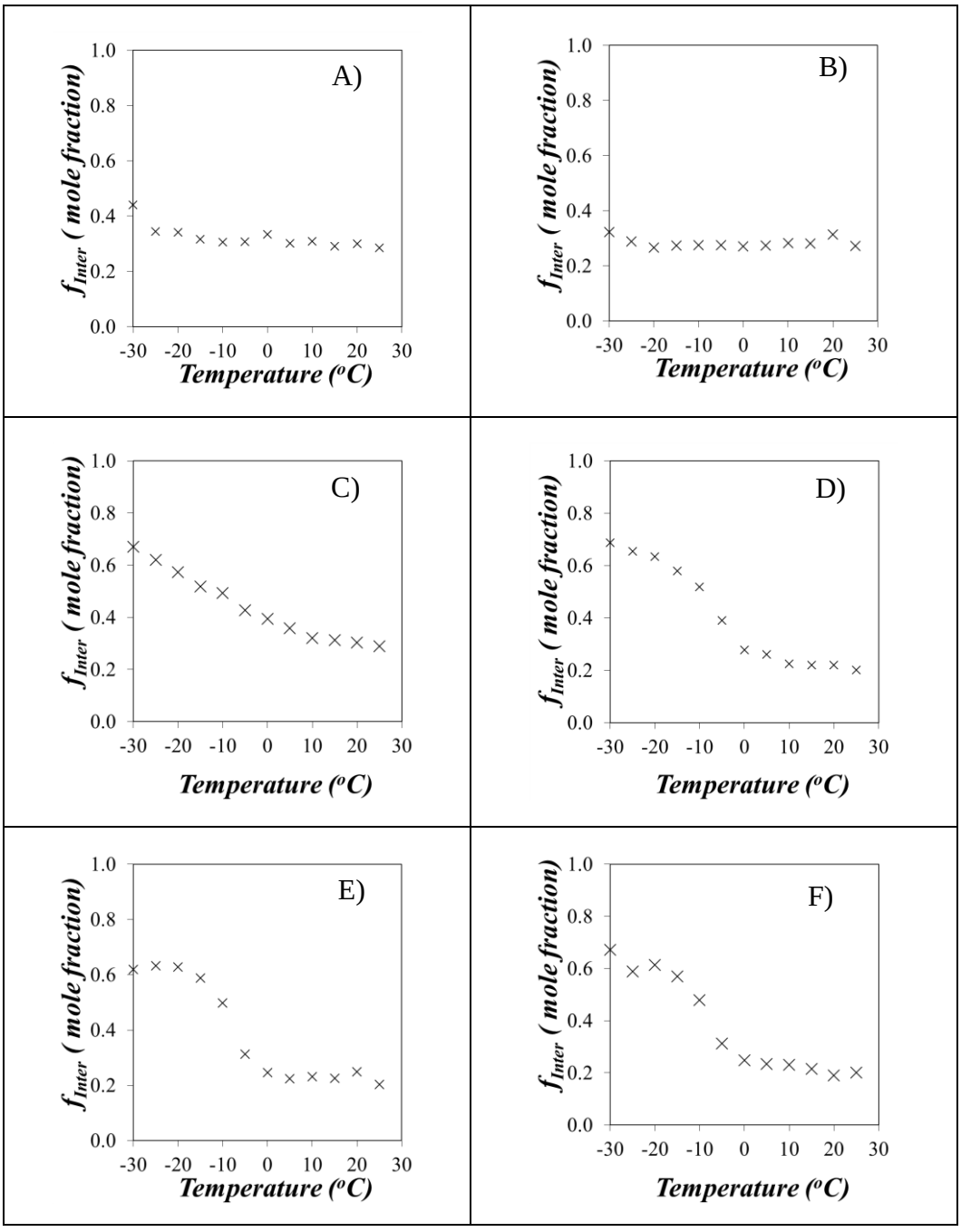

Figure 5.3. Molar fraction f_{inter} of pyrene labeled EP copolymers forming excimer intermolecularly for A) Py(108)-EP(60-1), B) Py(103)–EP(61-2), C) Py(82)-EP(70-1), D) Py(116)-EP(78-1), E) Py(81)-EP(78-2), and F) Py(123)-EP(78-3) at a concentration of 10 g.L^{-1}.

In the case of Py(82)-EP(70-1), f_{inter} decreased with increasing temperature over the entire temperature range and no clear break point was observed. The Py(82)-EP(70-1) solution showed an intermediate behaviour between the semicrystalline and amorphous samples as expected from the ethylene content of Py(82)-EP(70-1) which was determined by ^{13}C NMR and FTIR measurements to be intermediate between those of the semicrystalline and amorphous samples. The f_{inter} values obtained in the different temperature regimes have been listed in Table 5.3 for the different polyolefins.

The results listed in Table 5.3 reflect accurately and quantitatively the expected solution behaviour of the EP copolymers under study. It appears that the procedure used to determine f_{inter} by pyrene excimer fluorescence provides a powerful analytical means to probe the associations of polyolefins in solution.

5.5 Conclusions

Six different EP copolymers were maleated and then labeled with 1-pyrenemethylamine. DSC, FTIR, and ^{13}C NMR measurements were performed in the solid state and in solution. They confirmed that four of the EP copolymers were semicrystalline and two were amorphous, although EP(70) with an intermediate ethylene content was less crystalline than the EP(78) samples. Intrinsic viscosity measurements were also carried out in toluene as a function of temperature. They showed that $[\eta]$ did not change much with temperature for the amorphous samples. For the semicrystalline samples, $[\eta]$ remained relatively constant between –5 and 30 °C while showing a marked decrease with decreasing temperature when the temperature was below –5 °C. This behaviour reflected the progressive shrinkage of the polymer hydrodynamic volume with decreasing temperature.

To probe the intermolecular associations between EP copolymers, fluorescence experiments based on pyrene excimer formation were conducted on the Py-EP copolymers. The Py-EP samples yielded very different trends of I_E/I_M-vs-T based on their crystallinity. While I_E/I_M remained relatively constant for Py(82)–EP(70-1) and increased continuously for Py(108)–EP(60−1) and Py(103)-EP(61-2) with increasing temperature, a much more complex profile was found for the Py(116)-EP(78-1), Py(81)-EP(78-2), and Py(123)-EP(78-3) samples. As concluded earlier,[15] this behaviour was due to the formation of microcrystals in solution.

The combination of the results obtained for the chemical composition of the EP copolymers by FTIR and ^{13}C NMR, their level of crystallinity by DSC, their solution behaviour from intrinsic viscosity measurements, and the level of intermolecular association by fluorescence provides a solid understanding of the effect that the ethylene content of EP copolymers has on their ability to self-assemble in solution at low temperature due to microcrystallization. In this context, this study has demonstrated that experiments based on pyrene excimer formation provide a powerful tool to characterize the intermolecular associations between polyolefins in solution.

Chapter 6

Using Pyrene Excimer Fluorescence to Probe the Interactions Between Viscosity Index Improvers and Waxes Present in Automotive Oil

6.1 Overview

A new methodology based on pyrene excimer formation was applied to quantitatively measure the actual level of intermolecular association between ethylene-propylene (EP) copolymers in toluene in the presence of wax typically present in engine oils. EP copolymers are commonly used as viscosity index improvers (VIIs) in engine oils. Unfortunately engine oils contain waxes, an undesirable by-product that thickens the oil and associates with VIIs at low temperature. In this study, four EP copolymers were maleated to yield EP–MA and then fluorescently labeled with 1-pyrenemethylamine to yield Py-EP. Successful maleation and fluorescence labeling were confirmed by Fourier transform infrared (FTIR) and UV-Vis absorption spectroscopy. The solution behaviour of the EP copolymers in the presence of wax was characterized by pyrene excimer formation, which was used to quantitatively measure the molar fraction of intermolecular interactions (f_{inter}) between EP copolymers in the absence or presence of wax. The fraction f_{inter} was determined through the analysis of the fluorescence spectra of the Py-EP solutions acquired as a function of temperature. Upon excitation, the Py-EP solutions generated excimer upon encounter between an excited and a ground state pyrene. The ratio of the excimer fluorescence intensity (I_E) over that of the monomer (I_M) yielded the I_E/I_M ratio which was employed to determine f_{inter}. Plots of f_{inter} as a function of temperature provided a description of the solution behaviour of a given VII with or without wax present in solution. The results of this study indicate that wax in solution binds onto EP copolymers dissolved in toluene, which increases macromolecular associations as reflected by an increase in f_{inter}. The formation of polymeric microcrystals however induces strong polymer-polymer interactions that result in the dissociation of the wax from the polymers.

6.2 Introduction

An engine oil formulation is usually a mixture of base oils and oil-additives. Oil-additives enhance the base oil lubricating properties and the base oil must maintain proper solvency of these oil additives during the operation of the engine. Dispersants, detergents, viscosity index improvers (VIIs), pour point depressants (PPDs), and antiwear and antioxidant agents are different types of oil additives typically present in an engine oil.[1] VIIs are long chain, high molecular weight polymers used to reduce the decrease in viscosity of the base oil upon increasing temperature without excessively increasing the viscosity of the oil at lower temperatures.[2–4] Consequently, VIIs are essential components in engine oil to enhance the oil efficiency and durability while providing maximum engine protection. The performance of the VII depends on the polymer solubility, its interactions with other species in the oil, and its shear and oxidation resistance.[5,6]

The best known VIIs are polymethacrylates, polyisoprene-polybutadiene-polyisoprene star polymers, ethylene-propylene copolymers (EP), and hydrogenated styrene-diene copolymers.[4,7-10] As they are the focus of this study, EP copolymers are described in more details hereafter. EP copolymers were first introduced as VIIs in the late 1960s.[11] The ethylene-to-propylene molar ratio defines the quality of a given EP copolymer as a VII.[7,11] The presence of long ethylene sequences in EP copolymers induces polymer crystallinity that changes the hydrodynamic volume of the polymer coil in a way that yields desirable lubrication properties for an engine oil as a function of temperature. But higher ethylene contents can also interact strongly with wax present in the engine oil at very low temperatures.[12] Even though most of the wax is removed during dewaxing, a small amount of wax is required in the oil to obtain a desired viscosity. These waxes are composed of asphaltenes and long chain hydrocarbons which vary

in molecular weight and composition.[13,14] Consequently the study of the effect that the presence of wax has on the interactions taking place between EP copolymers is of high interest to the oil-additive industry.

Intermolecular association between macromolecules is typically investigated by fluorescence resonance energy transfer (FRET)[2,15-17] and pyrene excimer formation.[2] But a quantitative measure of the molar fraction (f_{inter}) of macromolecules involved in intermolecular association is only provided when pyrene excimer fluorescence is used.[18] As was shown in a previous study,[18] f_{inter} can be determined in a simple and straightforward manner from the ratio I_E/I_M of the fluorescence intensity of the excimer over that of the monomer obtained from the fluorescence spectrum of pyrene-labeled macromolecules. Since the fluorescence intensity ratio I_E/I_M is directly proportional to the local pyrene concentration $[Py]_{loc}$ experienced by an excited pyrene surrounded by ground state pyrenes covalently attached onto a macromolecule,[19-23] an increase in I_E/I_M due to intermolecular interactions reflects an increase in $[Py]_{loc}$ which can be taken advantage of to measure f_{inter}. The ability to measure the fraction f_{inter} provides a novel and powerful analytical tool that allows one to probe macromolecular interactions in solution under different conditions. In the present study, the effects induced on f_{inter} by temperature and the presence of wax are being investigated in solution for a series of EP copolymers exhibiting a range of crystallinity.

6.3 Experimental

***Chemicals*.** Acetone (HPLC grade), dodecane (anhydrous, 99%), toluene (HPLC, 99.9%), biphenyl (99%), 1,1,2,2-tetrachloroethane-d_2 (TCE-d_2), methyl ethyl ketone (MEK, 99.5%), maleic anhydride (98%), 1-pyrenemethylamine hydrochloride ($PyCH_2NH_2$ HCL, 95%), and *tert*-butyl peroxide (98%) were purchased from Sigma-Aldrich and were employed without

further purification. Four EP copolymers, two amorphous polymers with an ethylene content of 60 mol% and two semicrystalline polymers with an ethylene content of 78 mol%, and an engine oil wax were supplied by Afton.

Carbon Nuclear Magnetic Resonance (*^{13}*C NMR*). ^{13}C NMR was used to calculate the molar ethylene content of the EP copolymers.[24] To acquire the ^{13}C NMR spectra of the EP copolymers at 120 ^{o}C, a Bruker 500 MHz high resolution NMR spectrometer was used.[25] EP copolymers (0.14 g) were dissolved in TCE-d_2. Before acquiring each NMR spectrum, the solution in the NMR tube was homogenized by placing it in a heating block at 120 ^{o}C for a minimum of 4 hrs.

***Fourier Transform Infrared* (*FTIR*).** A Bruker Tensor 27 FTIR spectrophotometer was used to obtain all FTIR spectra. To produce a thin polymer film on a NaCl FTIR plates, a few drops of polymer solution in toluene were deposited onto the cell and the solvent was then evaporated under a stream of nitrogen. All samples had an absorbance of less than unity to optimize the signal-to-noise ratio.

***Oil Dewaxing*.** Engine oil lubricants are formulated from a range of base oils and additives. The base oil is mostly produced by the refining of crude oil. The American Petroleum Institute (API) has categorized base oils into five categories as shown in Table 6.1. Oils from Group I – III are derived from petroleum crude oil and are ranked according to their sulfur and saturated alkane content and their viscosity index (VI). Group IV oils are synthesized from α–olefins and are thus sulfur-free and fully saturated while Group V oils represent all other types of oil that do not belong to the Group I – IV oils. A group II base oil was used in this study. The base oil was mixed with methyl ethyl ketone (MEK, 5.0 wt%) at room temperature until an homogenous solution was obtained. The solution was placed in a –20 ^{o}C freezer for 24 hrs to allow

precipitation of the wax. The wax was separated by suction filtration with a filter paper and application of vacuum. The final product was dried in a vacuum oven at 70 ^{o}C for 2 hrs.

Table 6.1. American Petroleum Institute (API) base oil categories.[26]

Group	Sulfur (wt%)	Saturates (wt%)	Viscosity Index (VI)
I	>0.03	<90	80-120
II	>0.03	>90	80-120
III	>0.03	>90	>120
IV	Polyalphaolefins Synthetic Lubricants		
V	All base oils not included above		

***Steady-State Fluorescence*.** Acquisition of the fluorescence spectra of the pyrene-labeled EP copolymers (Py-EPs) was conducted on a Photon Technology International (PTI) LS-100 steady-state fluorometer equipped with an Ushio UXL-75Xe xenon arc lamp and a PTI 814 photomultiplier detection system. A 1 cm × 1 cm quartz cell was used to acquire the fluorescence spectra with the right-angle geometry for a Py-EP concentration of 0.01 g.L^{-1}. A triangular quartz cell was used for front-face geometry measurements to avoid the inner filter effect when acquiring the fluorescence spectra at Py-EP concentrations of 10 g.L^{-1}. Fluorescence spectra of solutions of Py-EPs in toluene were acquired by exciting the solution at 344 nm and acquiring the emission spectra from 350 to 600 nm. The fluorescence spectra of the wax were acquired between 300 and 600 nm using different excitation wavelengths. The fluorescence measurements were acquired with a cryostat from Oxford Instruments (Optistat DN) fitted inside the steady-state fluorometer. Before each measurement, the solutions were

placed in the cryostat where they were degassed for 30-40 minutes under a gentle flow of N_2 to remove undesired oxygen that quenches pyrene fluorescence. Measurements were carried out at temperatures ranging from –30 (± 0.2) to +25 (± 0.2) °C and before each set of experiments, the solutions were heated to room temperature to erase all pre-association history before bringing the solution to the desired temperature. The solutions were left in the cryostat for 10 min after the set temperature of the cryostat had been reached before any fluorescence spectrum was acquired.

UV-Visible Spectrophotometer. Absorption spectra were acquired between 200-600 nm on a Cary 100 UV-Vis spectrophotometer. Quartz cells having a 0.1-10 mm path length were employed for these measurements.

Labeling of the EP Copolymers. The polymers were first maleated to yield EP-MA[27] and then fluorescently labeled with 1-pyerenemethylamine ($PyCH_2NH_2$)[28] according to a procedure described earlier[18,21] and shown in Scheme 6.1.

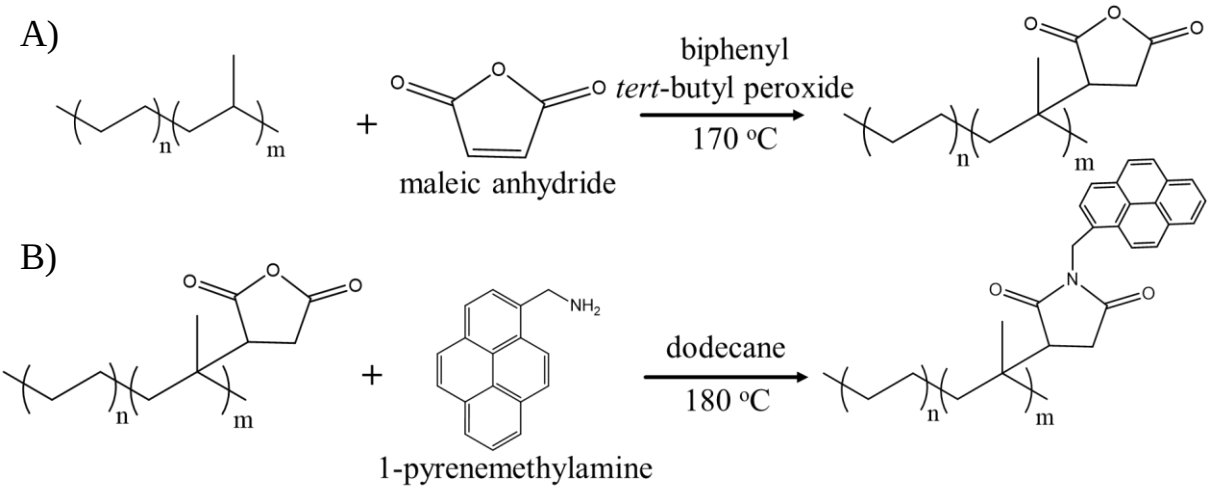

Scheme 6.1. Reaction scheme for A) the maleation of the EP copolymer and B) the labeling of the maleated EP copolymers with pyrene.

6.4 Results and Discussion

An earlier study has established that the parameter f_{inter} accurately describes the level of interactions between Py-EP copolymers in toluene.[18] In particular, a plot of f_{inter} as a function of temperature provides valuable information on the effect of temperature on the interactions between EP copolymers. Such f_{inter}-vs-T plots were constructed in the present study to assess the effect that the presence of wax has on the interactions between EP copolymers having different crystallinities. The crystallinity of the different EP copolymers was characterized earlier,[18] as well as their maleation and pyrene labeling.

Table **6.2** summarizes the main chemical properties of these polymers.

Table 6.2. Pyrene content (λ_{py}) and ethylene content of EP copolymers obtained from UV-Vis and ^{13}C NMR measurements, respectively.

Polymer Name	Polymer Type	λ_{py} ($\mu mol.g^{-1}$)	Ethylene Content (mol %)
Py(108)-EP(60-1)	Amorphous	108	60
Py(103)-EP(61-2)		103	61
Py(116)-EP(78-1)	Semicrystalline	116	78
Py(123)-EP(78-3)		123	78

The nomenclature used to describe the chemical composition of the Py-EP samples is described by using the sample Py(108)-EP(60-1) as example. The number in brackets after Py indicates the pyrene content of the polymer expressed in μmol of pyrene per gram of polymer whereas the number in brackets after EP refers to the ethylene content of the polyolefin

expressed in mol%. The number "1" following the ethylene content indicates that this sample with a 60 mol% ethylene content was the first to be investigated. The EP samples listed in

Table **6.2** with an ethylene content of 60 and 78 mol% where amorphous and semicrystalline respectively.[18]

Pyrene Excimer Formation in the Presence of Wax. Previous experiments based on FRET and pyrene excimer fluorescence demonstrated that the existence of intermolecular associations between EP copolymers could be demonstrated qualitatively and quantitatively by the former and latter techniques, respectively.[18] In particular, pyrene excimer fluorescence experiments were shown to yield the molar fraction of pyrene labels forming pyrene excimer intermolecularly (f_{inter}) in solution.[18] This procedure is now employed to determine the effect that the presence of wax has on the level of EP interactions in the solution as a function of temperature. The process of excimer formation between pyrene labels covalently attached onto a macromolecule, or PLM for pyrene-labeled macromolecule, is described inScheme 6.2.

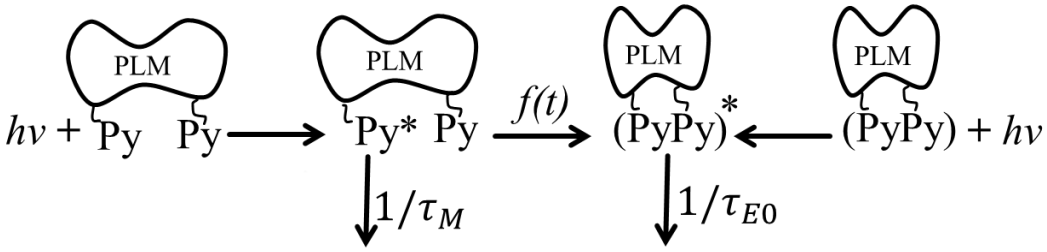

Scheme 6.2. Kinetics of pyrene excimer formation for a PLM.

In Scheme 6.2, irradiation of a PLM with UV light leads to the excitation of some pyrene monomers and pyrene aggregates. Excitation of a pyrene aggregate results in instantaneous excimer formation with excimers that emit with a natural lifetime τ_{E0}. Excitation of a pyrene monomer can lead to monomer fluorescence that occurs with a lifetime τ_M or excimer formation if diffusive encounters take place between the excited pyrene and a nearby ground state pyrene. The excited pyrene monomer emission is characterized by four sharp fluorescence bands between 360 nm and 425 nm, whereas the pyrene excimer features a broad and structureless emission centered at 480 nm. These spectral features are presented in Figure 6.1 that shows the typical fluorescence spectrum of a Py-EP sample in toluene in the absence and presence of wax. The fluorescence intensity of the pyrene excimer I_E and monomer I_M can be calculated by integrating the fluorescence spectrum over a well-defined range of wavelengths. Traditionally, this laboratory has used a wavelength range between 372 and 379 nm corresponding to the first peak (I) in the fluorescence spectrum to calculate I_M for Py-EP samples in toluene. The choice of the fluorescence peak furthest to the left to calculate I_M was made to minimize a possible overlap between the monomer and excimer emissions. In the present case however this procedure appeared to be flawed as the presence of wax led to an apparent decrease in the intensity of the fluorescence peak at 376 nm. The origin of this effect was attributed to light scattering generated by wax aggregates that resulted in a sunstantial reabsorption of the first fluorescence peak. As shown in Figure 6.1A and B, the peak at 376 nm was supressed after adding wax to the 10 $g.L^{-1}$ Py(81)-EP(78-3) solution. Inspection of the fluorescence spectra indicated that the fourth peak (IV) was much less affected by the presence of wax. Therefore, the wavelengths between 394 and 399 nm corresponding to the fourth peak (IV) in the spectrum were selected instead to calculate I_M to minimize the interference induced by light scattering on

the fluorescence spectrum at the lower wavelengths. The wavelengths range between 500 and 530 nm was chosen for I_E to minimize any overlap that might exist between the fluorescence of the monomer and excimer.

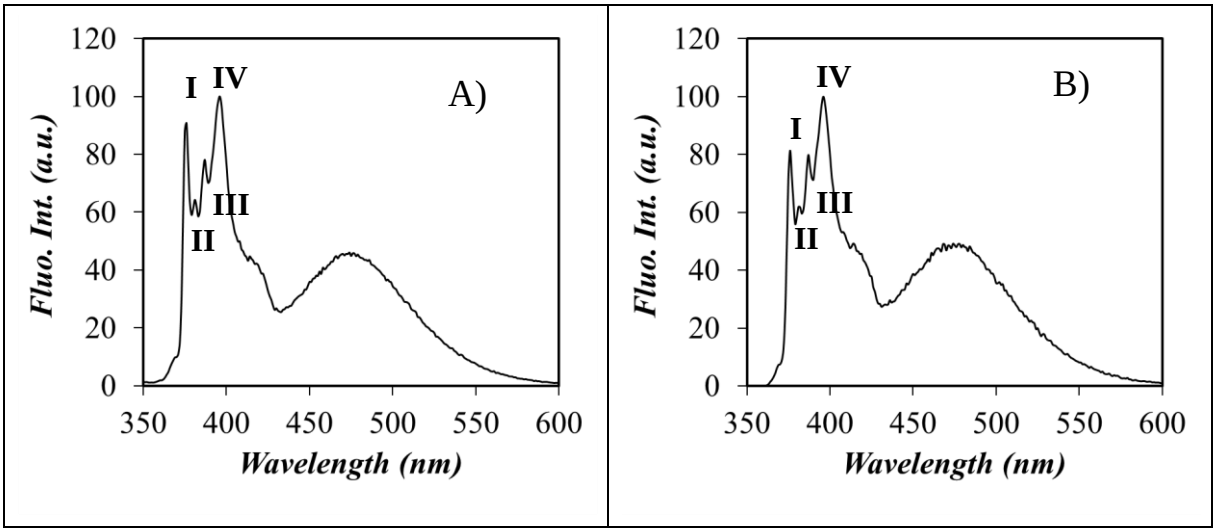

Figure 6.1. Steady-state fluorescence spectra of a Py-EP sample A) without wax and B) with wax in toluene. ([Poly] = 10 g.L^{-1}, λ_{ex} = 344 nm)

Having determined the I_E/I_M ratio for the Py-EP samples, Equation 6.1 could be applied to relate the I_E/I_M ratio to the local pyrene concentration $[Py]_{loc}$ experienced by an excited pyrene monomer attached onto the Py-EP samples.[29] In Equation 6.1, $K(T)$ is a multiplication factor which is a function of the quantum yields of the pyrene monomer and excimer and the rate constants for excimer formation and dissociation. As a result, $K(T)$ is expected to vary with temperature as already discussed in an earlier report.[18] At a same temperature however, an increase in I_E/I_M reflects an increase in $[Py]_{loc}$ which results from increased intermolecular interactions. In turn, a rise in intermolecular interactions can be due to an increase in the concentration of the PLMs, a change in the solvent quality toward the macromolecule, or the

presence of an external species that would enhance intermolecular associations such as wax could do to the Py-EP chains in solution. When a PLM undergoes both intra- and intermolecular interactions, its fluorescence spectrum yields the ratio $I_E / I_M\left(\begin{matrix}\text{intra }\&\\ \text{inter}\end{matrix}\right)$ whereas if the PLM undergoes solely intramolecular interactions, the fluorescence spectrum yields the ratio I_E/I_M(intra). In turn, the ratios $I_E / I_M\left(\begin{matrix}\text{intra }\&\\ \text{inter}\end{matrix}\right)$ and I_E/I_M(intra) are equal to $K(T)\times[Py]_{loc}\left(\begin{matrix}intra\,\&\\ inter\end{matrix}\right)$ and $K(T)\times[Py]_{loc}$(intra), respectively. The molar fraction of PLMs forming excimer intermolecularly (f_{inter}) can then be determined from Equation 6.2. Consequently, the purpose of this study was to determine the temperature profile of f_{inter} for the Py-EP copolymers listed in Table 6.2 where the EP backbone exhibits different levels of crystallinity, in the absence and presence of wax. Comparison of the trends obtained for plots of f_{inter}-vs-T without and with wax should provide valuable information on the effect that wax has on the aggregation of Py-EP samples in solution.

$$I_E/I_M=K(T)\times[Py]_{loc} \tag{6.1}$$

$$f_{inter}=\frac{[Py]_{loc}\left(\begin{matrix}inter\,\&\\ intra\end{matrix}\right)-[Py]_{loc}(intra)}{[Py]_{loc}\left(\begin{matrix}inter\,\&\\ intra\end{matrix}\right)}=\frac{I_E/I_M\left(\begin{matrix}inter\,\&\\ intra\end{matrix}\right)-I_E/I_M(intra)}{I_E/I_M\left(\begin{matrix}inter\,\&\\ intra\end{matrix}\right)} \tag{6.2}$$

To this end, the ratio $I_E / I_M\left(\begin{matrix}\text{intra }\&\\ \text{inter}\end{matrix}\right)$ was obtained by acquiring the fluorescence spectra of the Py-EP samples in the presence of wax. To calculate I_E/I_M(intra), the fluorescence spectrum of a dilute (0.01 g.L^{-1}) solution of Py-EP needed to be acquired in the presence of 10

g.L^{-1} of the unlabeled macromolecule to ensure that only intramolecular excimer formation would be observed. Calculating I_E/I_M(intra) in the presence of wax was challenging due to the strong emission of the 10 g.L^{-1} wax solution that interfered with the emission of a 0.01 g.L^{-1} Py-EP solution as shown in Figure 6.2.

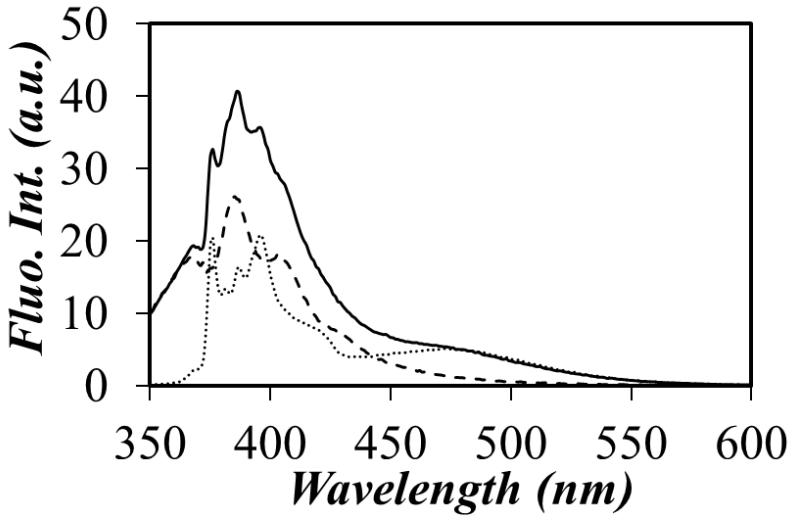

Figure 6.2. Fluorescence spectra of (—) the mixture of 0.01 g.L^{-1} Py(108)-EP(60-1), 10 g.L^{-1} EP(60-1), and 10 g.L^{-1} wax, (····) the mixture of 0.01 g.L^{-1} Py(108)-EP(60-1) and 10 g.L^{-1} EP(60-1), and (- - -) the 10 g.L^{-1} wax solution.(Solvent: toluene, λ_{ex}=344 nm)

The fluorescence spectra of the 10 g.L^{-1} wax solution were acquired at several excitation wavelengths between 280-400 nm. They are presented in Figure 6.3A. The fluorescence spectra of the wax showed several emission bands. The emission shifted to higher wavelengths as the excitation wavelength was increased (Figure 6.3A). This behaviour indicates that different emitting species are present in the wax sample since changing the excitation wavelength enabled the photoselection of these different chromophores. Therefore, subtracting the fluorescence spectrum of the 10 g.L^{-1} wax solution in toluene from the fluorescence spectrum

of the mixture containing 10 g.L^{-1} wax, 10 g.L^{-1} EP and 0.01 g.L^{-1} Py-EP was necessary to obtain the actual spectrum of Py-EP which was used to calculate I_E/I_M(intra). The fluorescence spectra of the 10 g.L^{-1} wax solution were acquired as a function of temperature as shown in Figure 6.3B. To account for differences in fluorometer configuration between the different days that the fluorescence experiments were carried out, the fluorescence spectra of the 10 g.L^{-1} wax solution and the 10 g.L^{-1} wax, 10 g.L^{-1} EP and 0.01 g.L^{-1} Py-EP mixture were normalized at 360 nm where pyrene does not emit and the wax spectrum was subtracted from the latter spectrum to yield the fluorescence spectrum of the 0.01 g.L^{-1} Py-EP and 10 g.L^{-1} EP mixture as shown by the dotted line in Figure 6.2.

Since engine oils contain a few wt% of VII and wax, the fluorescence spectra of toluene solutions containing 10 g.L^{-1} Py-EP and 10 g.L^{-1} wax were acquired as a function of temperature to obtain the ratio $I_E / I_M\begin{pmatrix}\text{intra \&}\\ \text{inter}\end{pmatrix}$. The I_E/I_M ratios of all the fluorescence spectra were calculated and they were plotted in Figure 6.4 as a function of temperature. The I_E/I_M ratio of the Py(108)-EP(60-1) and Py(103)-EP(61-2) solutions were found to increase continuously with increasing temperature in Figure 6.4A and B, respectively. This is the expected behavior for amorphous samples because the dissociation rate constant (k_{-1}) of the pyrene excimer is negligible in this temperature regime,[29] and $[Py]_{loc}$ does not change much with temperature for these amorphous samples. Under these conditions, the increase in I_E/I_M with increasing temperature only reflects the increase in the rate constant (k_{diff}) for diffusion-controlled pyrene excimer formation associated with the decrease in solvent viscosity due to the increase in temperature.

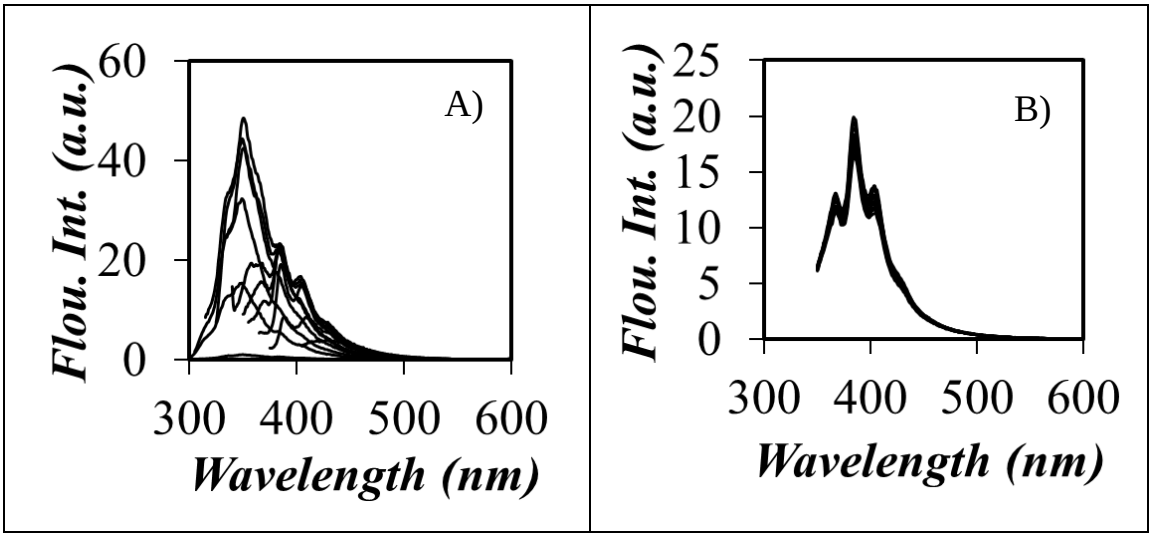

Figure 6.3. Steady-state fluorescence spectra of wax (10 $g.L^{-1}$) in toluene. A) Excitation at different wavelength (λ_{ex}=280-400 nm). B) As a function of temperature. From top to bottom, temperature increases from –30 ^{o}C to +25 ^{o}C. (λ_{ex} = 344 nm)

For the two EP(78) semicrystalline samples shown in Figure 6.4C and D, the plots of I_E/I_M in the presence of wax as a function of temperature resulted in a very different behavior from that of the amorphous samples. An increase in solution temperature induced first an increase in I_E/I_M, followed by a decrease in I_E/I_M at intermediate temperatures, before the increase in I_E/I_M resumed upon increasing the solution temperature further. The anomalous behavior observed for the Py-EP semicrystalline samples at intermediate temperatures has been attributed to a decrease in excimer formation due to a decrease in $[Py]_{loc}$ resulting from the melting of microcrystals generated by long polyethylene sequences in the copolymer.[2,18]

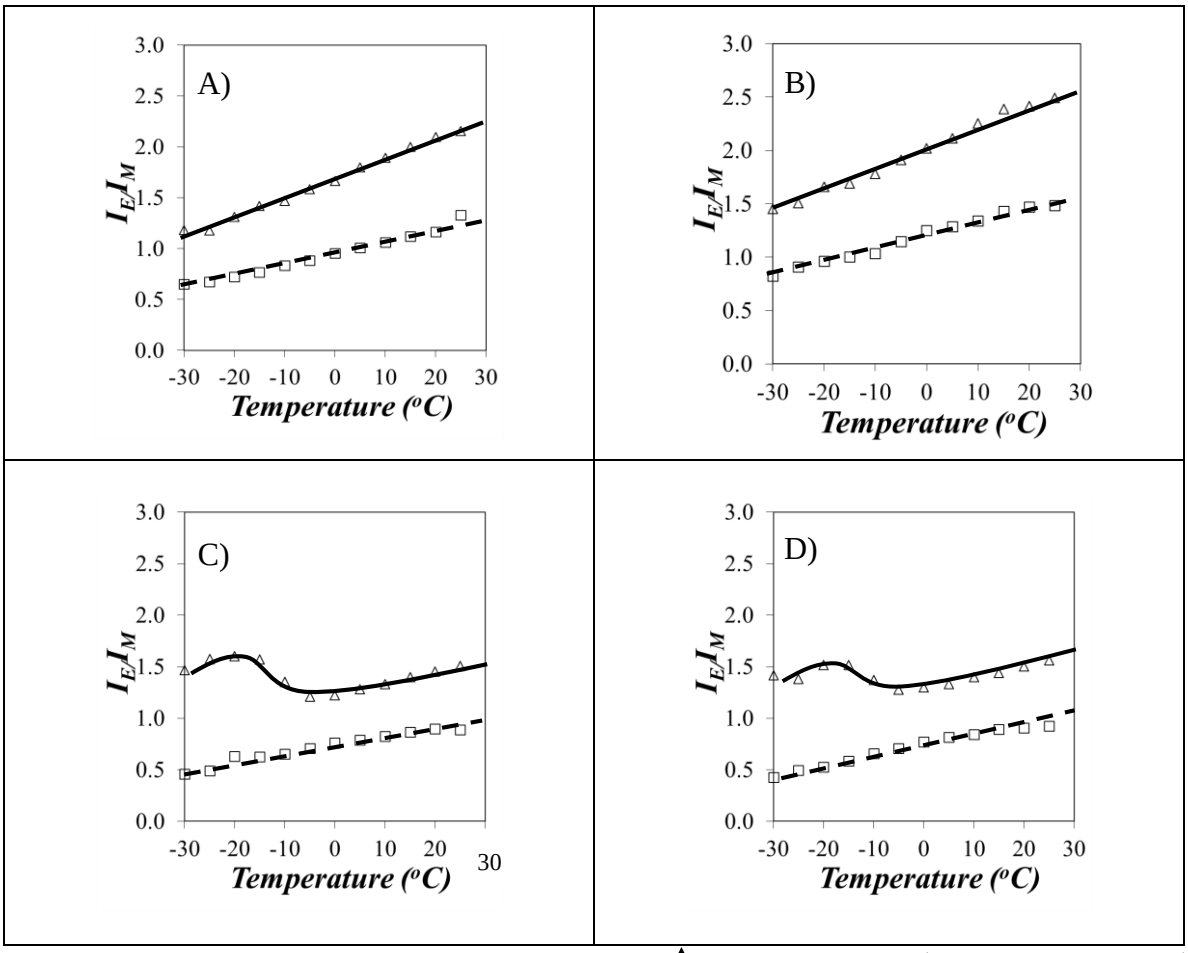

Figure 6.4. Plots of I_E/I_M -vs-T for the mixtures of (△) Py-EP (10 g.L^{-1}) and wax (10 g.L^{-1}) and (□) Py-EP (0.01 g.L^{-1}), EP (10 g.L^{-1}), and wax (10 g.L^{-1}). A) Py(108)-EP(60-1), B) Py(103)–EP(61-2), C) Py(116)-EP(78-1), and D) Py(123)–EP(78-3).

Beside the experiments conducted on the mixture containing 10 g.L^{-1} Py-EP and 10 g.L^{-1} wax, the fluorescence spectra of toluene solutions containing a 10 g.L^{-1} excess of unlabeled EP copolymer, 0.01 g.L^{-1} Py-EP, and 10 g.L^{-1} wax were also acquired as a function of temperature for all the EP copolymers to obtain the ratio I_E/I_M(intra). The I_E/I_M ratios of all the fluorescence spectra were calculated and they were plotted in Figure 6.4 as a function of temperature. For all four Py-EP solutions, the ratio I_E/I_M(intra) increased continuously with increasing temperature

in Figure 6.4. This behavior was expected, since the Py-EP macromolecules were well separated thanks to the excess of unlabeled EP copolymer present in the solution ensuring that $[Py]_{loc}$ remained constant with temperature and that the I_E/I_M ratio responded solely to the decrease in viscosity taking place with increasing temperature. As was already pointed out, a decrease in viscosity leads to an increase in diffusive encounters, which is reflected by an increase in excimer formation, and thus in the I_E/I_M ratio. It is important to point out at this stage that pyrene excimer formation is a phenomenon that involves a few tens of monomers in a PLM so that polymer entanglements are not relevant at the low polymer concentrations studied.[30–32]

Equation 6.2 was applied to the trends shown in Figure 6.4 to yield the f_{inter} values which were plotted as a function of temperature in Figure 6.5. The f_{inter} values obtained in Chapter 4 in the absence of wax were also shown in Figure 6.5 for comparison. For all Py-EP amorphous solutions, f_{inter} increased after adding wax to the solution. This behavior indicates that the presence of wax in the oil induces aggregation of amorphous Py-EP copolymers. The aggregation then resulted in an increase in the probability of having pyrene-pyrene encounters in the solution and thus a higher f_{inter} value. In the case of the two Py(108)-EP(60-1) and Py(103)-EP(61-2) samples, f_{inter} increased from 0.28 ± 0.02 to 0.43 ± 0.01 and from 0.22 ± 0.02 to 0.40 ± 0.01 upon addition of wax, respectively.

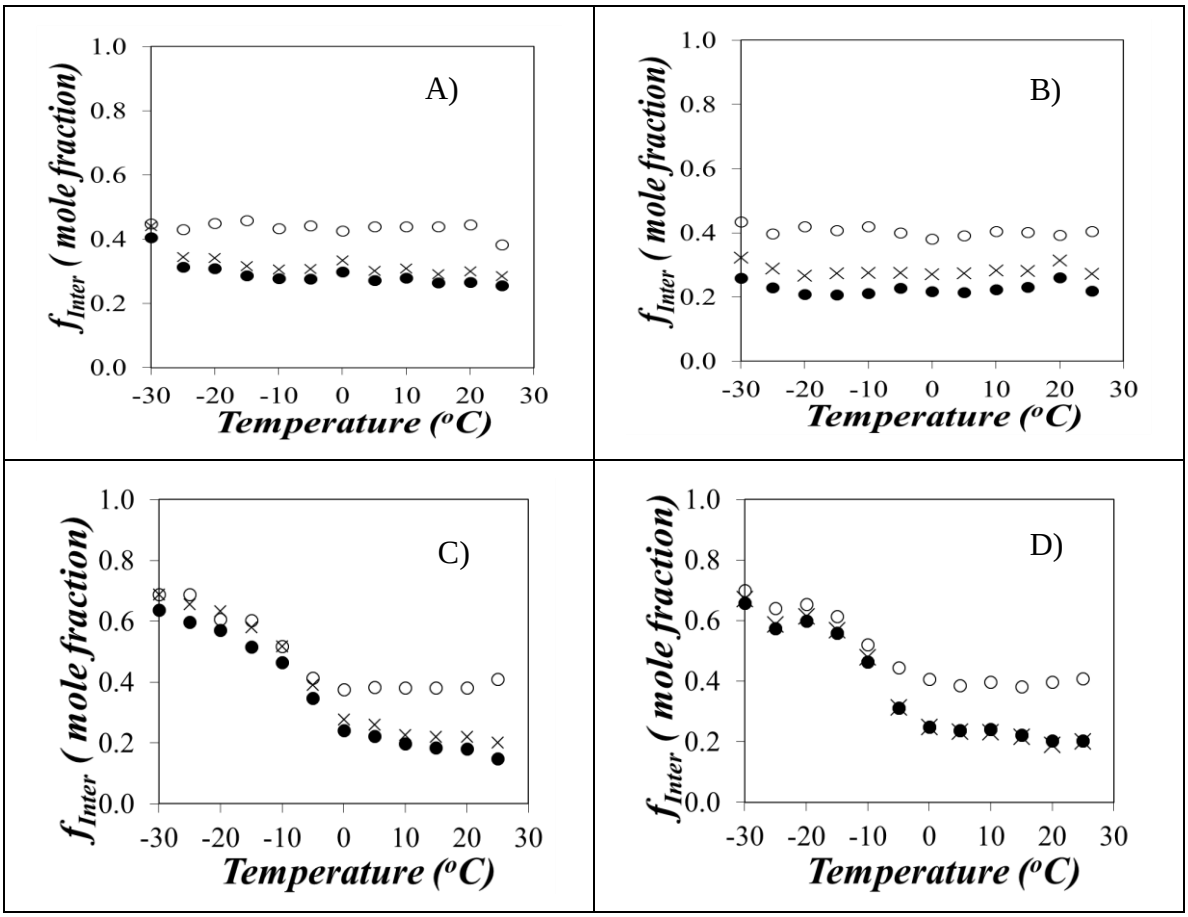

Figure 6.5. Molar fraction f_{inter} of pyrene-labeled EP copolymers forming excimer intermolecularly calculated from the ratio I_E(500-530 nm)/I_M(394-399 nm) (●) without wax and (○) with 10 g.L^{-1} wax. (×) Molar fraction f_{inter} calculated from the ratio I_E(500-530 nm)/I_M(372-379 nm) without wax. For A) Py(108)-EP(60-1), B) Py(103)–EP(61-2), C) Py(116)-EP(78-1), and D) Py(123)-EP(78-3) at a concentration of 10 g.L^{-1}.

For the solutions of all semicrystalline Py-EPs, the transition induced by the formation of crystalline microdomains was still observed in the presence of wax. Moreover, f_{inter} increased after addition of wax at temperatures larger than the crystallization temperature (T_C) where the polymers were soluble. At temperatures lower than T_C however, the formation of microcrystals

in the Py-EP semicrystalline samples maximized polymer-polymer contacts and the wax molecules were expelled from the microcrystals. Since f_{inter} reflected $[Py]_{loc}$ after the wax had been expelled from the microcrystals, it was little affected by the presence of wax at temperatures lower than T_C. The f_{inter} values obtained in the different temperature regimes for all EP samples have been listed in Table 6.3.

To investigate the validity of the f_{inter} values calculated from the ratio of I_E(500-530 nm) over I_M(394-399 nm), f_{inter} was also calculated by taking the ratio of I_E(500-530 nm) over I_M(372-379 nm) for polymer solutions that were determined in Chapter 4 without wax. These alternative f_{inter} values were plotted as a function of temperature in Figure 6.5. Despite the difference in the wavelength range to calculate I_M, similar f_{inter}-vs-T profiles were obtained. This result demonstrates that the new integration range used to calculate I_M did not affect much the trends for f_{inter}. The importance of these results are now briefly discussed.

Due to their importance in numerous applications that involve oil flow, the interactions of waxes and polymers have been the object of intensive research as illustrated by a number of recent reviews.[33-35] Wax crystallization in the oil as stacked lamellar crystals leads to gelation of the oil that can no longer flow at a temperature referred to as the pour point (PP). Copolymers of ethylene and vinyl acetate, polyethylene-*b*-poly(ethylene-*co*-propylene) diblock copolymers (PE-PEP), or poly(maleic anhydride amide-*co*-α–olefin) have been used as pour point depressants (PPDs). Their co-crystallization with waxes changes the size and shape of the wax crystals in a process that lowers the PP of the oil. In comparison with the vast pool of studies documenting the interactions between wax and PPDs, much less seems to be known about the interactions between waxes and VIIs such as the EP copolymers studied herein. In particular, interactions between waxes and EP copolymers having a high ethylene content were found to

be reduced at low temperatures as illustrated in Figures 6.5C and D contrary to reported expectations.[12] The suggestion that waxes do not co-crystallize with long polyethylene stretches of the EP(78) copolymers at low temperature is supported by studies of the interactions of waxes with PE-PEP. The diblock copolymers were found to self-assemble into platelets composed of the PE blocks stabilized by the amorphous PEP blocks.[36] Addition of wax to the solution did not result in co-crystallization of wax and the PE blocks. Rather, the wax crystallized at the surface of the PE platelet.[37] The EP(78) samples seemed to behave similarly with their long polyethylene stretches forming microcrystals in a process that releases into the bulk the wax responsible for increasing intermolecular interactions at high temperatures. As a result, the presence of wax did not increase intermolecular interactions of the EP(78) copolymers at low temperatures as indicated by the similar f_{inter} value obtained with or without wax in Figures 6.5C and D. The amorphous EP(60) copolymers consistently interacted with wax over the entire temperature range, maintaining a constant f_{inter} value in the presence of wax that was larger than the f_{inter} value obtained without wax.

Wax is believed to interact with long ethylene sequences in EP(60) and since the polymer remains fully soluble in toluene over the entire temperature range, these long ethylene sequences do not form microcrystals and interact effectively with wax in a process that induces intermolecular association. Interestingly, the semicrystalline EP copolymers were also found to interact strongly with wax at temperatures above T_C where they were fully soluble in toluene. In effect, amorphous and semicrystalline EP copolymers above T_C behaved similarly in solution, interacting strongly with wax in a process that resulted in increased intermolecular interactions.

Table 6.3. Molar fraction (f_{inter}) representing the intermolecular interactions between EP copolymer for 10 g.L^{-1} copolymer and 10 g.L^{-1} wax solutions in toluene.

	Temp (°C) –30 to –10	Temp (°C) –5 to 25	Temp (°C) –30 to –10	Temp (°C) –5 to 25
	Without Wax		With Wax	
Py(108)-EP(60-1)	0.28±0.02		0.43±0.01	
Py(103)-EP(61-2)	0.22±0.02		0.40±0.01	
Py(116)-EP(78-1)	0.56±0.07	0.20±0.03	0.57±0.07	0.39±0.01
Py(123)-EP(78-3)	0.55±0.06	0.23±0.02	0.63±0.07	0.39±0.01

6.5 Conclusions

Four EP copolymers were maleated and then labeled with 1-pyrenemethylamine. Two EP copolymers were semicrystalline and two were amorphous.[18] To probe the interactions taking place between polymer chains in the presence of wax, fluorescence experiments based on pyrene excimer formation were conducted on the Py-EP copolymers. The Py-EP samples yielded very similar trends for the I_E/I_M-vs-T plots in the presence or absence of wax. While I_E/I_M increased continuously with increasing temperature for Py(108)-EP(60-1) and Py(103)-EP(61-2), a much more complex profile was found for Py(116)-EP(78-1) and Py(123)–EP(78-3). As concluded earlier,[18] this behaviour was due to the formation of microcrystals in solution that took place at low temperatures.

Application of Equation 6.2 to the I_E/I_M profiles obtained with a 10 g.L^{-1} Py-EP copolymer solution and a solution containing 0.01 g.L^{-1} of Py-EP and 10 g.L^{-1} of EP copolymer in the presence of 10 g.L^{-1} of wax yielded f_{inter}, the molar fraction of pyrene labels that formed

excimer intermolecularly when wax was added to toluene. Plots of f_{inter} as a function of temperature for the two amorphous polymers, namely Py(108)-EP(60-1) and Py(103)–EP(61-2), showed that the presence of wax led to an increase in f_{inter} from 0.28 ± 0.02 to 0.43 ± 0.01 and from 0.22 ± 0.02 to 0.40 ± 0.01, respectively. For the semicrystalline Py-EP solutions, two regimes were clearly identified depending on whether the solution temperature was below or above T_C. The increase in f_{inter} upon addition of 10 g.L^{-1} wax was more pronounced at temperatures higher than T_C where the semicrystalline EP copolymers did not form microcrystals. At lower temperatures, much smaller changes in f_{inter} were observed. The presence of 10 g.L^{-1} waxin the EP solutions seemed to increase intermolecular associations between EP copolymers under solution conditions where no microcrystals could form ($T > T_C$). This observation suggests that the formation of polymer microcrystals at temperatures below T_C led to the release of wax from the polymers. It also supports the notion that wax interacts strongly with long ethylene sequences along the EP copolymer since wax would not be released into the bulk if it was binding to amorphous propylene-rich sequences that are unaffected by microcrystal formation. As a result, the semicrystalline polymers at low temperatures showed little-to-no difference in behaviour with or without wax present in the solution.

In summary, this study illustrates how the parameter f_{inter} can be used to probe the association between PLMs in solution. In the present application, it was employed to probe the effect that wax present in engine oils has on the aggregation of VIIs. While this information is highly relevant to scientists aiming to control the viscosity of engine oils, the use of f_{inter} is general and is applicable to probe the solution behaviour of any associating polymers.

Chapter 7

Summary and Future Work

7.1 Summary of Thesis

Since the early 1900's, polymeric oil additives have been used in engine oils to improve overall engine durability and performance and decrease pollution emission.[1] These polymeric oil additives include dispersants, pour point depressants (PPDs), and viscosity index improvers (VIIs). The goals of this thesis were several but could be divided into two main categories. The first was to investigate the effect that post-modification of secondary amines in the polyamine linker of *b*-PIBSI dispersants had on their properties in solution, particularly on their ability to adsorb onto carbon-rich particles found in engine oils. Reaction of the secondary amines of *b*-PIBSI dispersants with ethylene carbonate (EC) yielded the modified M*b*-PIBSI dispersants. But to gauge the effect that the post modification of the *b*-PIBSI dispersants had on their properties, the extent of modification needed to be carefully characterized which required accurate determination of their chemical composition. This turned out to be incredibly challenging with ^{1}H NMR and FTIR failing to provide reliable information about the chemical composition of the dispersants due to their inherent aggregation in solution or in the bulk. These complications led to the establishment of an alternate and novel characterization method of PIBSI dispersants that was based on the quenching of the fluorescence of the succinide groups of the dispersants by the secondary amines of their polyamine linker. These fluorescence experiments provided a reliable means to assess the level of EC modification of PIBSI dispersants.

The second goal of this thesis was to uncover an analytical means that would quantitatively characterize the level of intermolecular interactions taking place between EP copolymers typically used as VIIs. This was accomplished by labeling the EP copolymers with the fluorophore pyrene to yield Py-EP samples and comparing the pyrene excimer fluorescence

of concentrated Py-EP solutions where intermolecular interactions took place and dilute Py-EP solutions with an excess of EP copolymers where only intrapolymeric interactions occured. These pyrene excimer fluorescence experiments yielded f_{inter}, the molar fraction of intermolecular interactions, which could be monitored as a function of solution temperature, and ethylene content of the EP copolymers, or in the presence of wax. How these studies were completed is described in more details hereafter.

The first study of this thesis investigated the chemical composition of several polyisobutylene succinimide (PIBSI) dispersants prepared with different molar ratios of polyisobutylene succinic anhydride (PIBSA) and polyamine.[2] Beside octylamine, diethylenetriamine (DETA), triethylenetetramine (TETA), tetraethylenepentamine (TEPA), pentaethylenehexamine (PEHA), and hexamethylenediamine (HMDA) were used as polyamines in this study. Initially, a combination of Fourier transform infrared (FTIR) and proton nuclear magnetic resonance (^{1}H NMR) was employed to determine the chemical composition of PIBSA and PIBSI dispersants. The chemical composition of PIBSA and PIBSI dispersants was reported in terms of the ratios N_{SA}/N_{IB} or N_{SI}/N_{IB} representing the number of succinic anhydride (N_{SA}) or succinimide moieties (N_{SI}) per isobutylene monomers (N_{IB}) for PIBSA or the PIBSI dispersants, respectively. An N_{SA}/N_{IB} ratio of 1:52±4 was found for PIBSA by a variety of techniques that included ^{1}H NMR and FTIR, while ^{1}H NMR and FTIR yielded an N_{SI}/N_{IB} ratio of 1:32±2 for all the *b*-PIBSI dispersants. This represented a substantial discrepancy between the chemical compositions of PIBSA and the PIBSI dispersants, despite the fact that the PIBSI dispersants were derived from PIBSA in the first place, and thus should have equal N_{SA}/N_{IB} and N_{SI}/N_{IB} ratios. UV-visible spectrophotometry (UV-Vis) was also applied to determine the chemical composition of PIBSA and to further investigate the reason

for the observed discrepancy in chemical composition. To this end, PIBSA was reacted with 1-pyrenemethylamine ($PyNH_2$) to yield *m*-PIBSI-$PyNH_2$. The molar absorbance coefficient of 1-pyrenemethylsuccinimide in THF was used to determine the pyrene, and thus succinimide, content of *m*-PIBSI-$PyNH_2$ and consequently calculate the N_{SI}/N_{IB} ratio for *m*-PIBSI-$PyNH_2$. An N_{SI}/N_{IB} ratio of 1:55±1 was determined for *m*-PIBSI-$PyNH_2$, in good agreement with the N_{SA}/N_{IB} ratio of 1:52±4 found for PIBSA. UV-Vis absorption measurements also confirmed that H-bonding between the secondary amines in the polar core and the succinimide carbonyls of the PIBSI dispersants affected the FTIR and ^{1}H NMR results which in turn was responsible for the erroneous chemical compositions retrieved for the PIBSI dispersants.

The substantial discrepancy between the chemical composition of PIBSA and the PIBSI dispersants led us to apply a combination of gel permeation chromatography (GPC) and FTIR to characterize the chemical composition of these macromolecules. GPC was applied to probe the doubling in size expected from the reaction of two PIBSA molecules with a polyamine to form a *b*-PIBSI dispersant. FTIR was applied to monitor the chemical composition of the reaction products. For this set of measurements, PIBSA was reacted with different amounts of HMDA because full reaction of HMDA with PIBSA eliminates the possibility that secondary amines might adsorb onto the GPC column. The GPC and FTIR results showed that the reaction mixture containing 0.17 mmol of polyamine per gram of PIBSA resulted in a *b*-PIBSI dispersant that would contain a minimum amount of unreacted PIBSA and a maximum amount of *b*-PIBSI dispersant. As it turned out, a 0.17 mmol/g ratio corresponded to a N_{SA}/N_{IB} ratio of 1:52 for PIBSA, again in very good agreement with the expected chemical composition of PIBSA of 1:52±4.

While these experiments all confirmed that the PIBSA sample contained one succinic anhydride unit per 52 isobutylene monomers, it still did not provide much information about the chemical composition of the PIBSI dispersants. Such an information was inferred by conducting steady-state and time-resolved fluorescence quenching experiments on the fluorescent succinimide moiety of the *b*-PIBSI dispersants. To this end, a series of *b*-PIBSI dispersants was prepared where the dispersants contained a known number of secondary amines. The results showed that the fluorescence intensity (I) and average lifetime (τ) of the *b*-PIBSI dispersants decreased with increasing number of secondary amines in the polyamine linker. Stern-Volmer plots were obtained by representing the ratios I_0/I and τ_0/τ as a function of the number of secondary amines. Both plots showed a linear behavior suggesting that succinimide fluorescence quenching measurements could be used to measure the secondary amine content of a given *b*-PIBSI dispersant.

The second study of this thesis took advantage of this insight to characterize the chemical composition of modified *b*-PIBSI (M*b*-PIBSI) dispersant. The M*b*-PIBSI dispersants were generated by modification of *b*-PIBSI dispersants with ethylene carbonate (EC). *b*-PIBSI dispersants generally have better dispersancy properties compared to M*b*-PIBSI. However the secondary amines in the polar core of the PIBSI dispersants are not compatible with the fluorocarbon elastomers that are used for engine seals. Therefore post modification of the secondary amines of PIBSI dispersants is often conducted with reactants such as EC.

While the fluorescence of succinimide groups in the *b*-PIBSI dispersants is efficiently quenched by secondary and tertiary amines, it is much less affected by the urethane groups that are generated by the reaction of secondary amines with EC. Indeed the fluorescence intensity of *b*-PIBSI succinimides was enhanced after modification with EC. However, a full recovery

of the fluorescence signal was not observed in any of the M*b*-PIBSI dispersants most probably due to incomplete reaction of the secondary amines in the polyamine linker.

The level of fluorescence intensity recovered by the M*b*-PIBSI dispersants after modification was compared to that of *N*-methyl succinimide (*N*-MSI) quenched by either diethylamine (DEA) or 2-hydroxyethyl *N*,*N*-dibutyl carbamate (HEDBC) in order to calculate the level of modification. Results showed that 60 ± 1 and 70 ± 1 % of the secondary amines in M*b*-PIBSI-TEPA and M*b*-PIBSI-PEHA had reacted, respectively. Taking the erroneous N_{SI}/N_{IB} ratio of 1:32±2 obtained by ^{1}H NMR for the *b*-PIBSI dispersants at face value and using it as a reference against which the 2-hydroxyethylcarbamate content of the M*b*-PIBSI dispersants was compared, similar levels of modification were found for M*b*-PIBSI-TEPA and M*b*-PIBSI-PEHA as obtained by fluorescence measurements. Furthermore, no modification was observed for the *b*-PIBSI-DETA and *b*-PIBSI-TETA dispersants strongly suggesting that steric hindrance combined with H-bonding of the secondary amine protons with the succinimide carbonyls prevent the EC modification.

The succinimide fluorescence was employed to build the adsorption isotherm of *b*-PIBSI and M*b*-PIBSI dispersants onto CBPs. The adsorption isotherms of the *b*-PIBSI dispersants showed an increase in binding constant with increasing number of secondary amines in the polar core of *b*-PIBSI dispersants. The binding isotherms of *b*-PIBSI-TEPA and *b*-PIBSI-PEHA were also compared to those of their modified analogues and the results indicated that the binding constant decreased for *b*-PIBSI-TEPA and *b*-PIBSI-PEHA after modification as expected.

In the fourth study, the intermolecular interactions between EP copolymers were investigated by fluorescence in toluene, an apolar solvent.[3,4] To this end, the EP copolymers

were maleated first and then labeled with 1-pyrenemethylamine or 2-(2-naphtyl)ethylamine to yield Py-EP and Np-EP, respectively. The chromophores pyrene and naphthalene were used since they are sensitive to the local concentration of chromophores present inside the polymer coil. FTIR was used to confirm the full conversion of the succinic anhydride (SAH) groups into succinimides after labeling with 1-pyrenemethylamine or 2-(2-naphtyl)ethylamine. Two EP copolymers were used in this study. Based on FTIR, differential scanning calorimetry (DSC), and viscosity measurements, one of the EP copolymers was found to be semicrystalline (EP(78-1)) while the other was amorphous (EP(60-1)).

Fluorescence resonance energy transfer (FRET) and fluorescence excimer formation were used to determine the level of intermolecular interactions between these two EP copolymers qualitatively and quantitatively, respectively. FRET is the most common method to probe intermolecular interactions but it is not well-suited to describe quantitatively the level of macromolecular interactions in solution. Therefore, fluorescence excimer formation was used instead to calculate the molar fraction (f_{inter}) of macromolecules involved in intermolecular associations. f_{inter} was calculated from the ratio I_E/I_M of excimer-to-monomer fluorescence intensity. The I_E/I_M ratio obtained from the fluorescence spectrum of pyrene-labeled macromolecules is directly proportional to the local pyrene concentration $[Py]_{loc}$ and consequently reflects intra- and intermolecular associations (Equation 7.1).[5]

$$I_E/I_M = K(T)\times[Py]_{loc} \tag{7.1}$$

The existence of intermolecular interactions between EP copolymers was established by conducting FRET experiments on 1:9 mixtures of Py-EP:Np-EP at overall polymer

concentrations of 0.01 and 10 g.L^{-1}. Plots of the fluorescence intensity ratios I_{Py}/I_{Np} of pyrene-to-naphthalene versus temperature were obtained for both the amorphous and semicrystalline samples. The FRET experiments showed higher intermolecular interactions at lower temperatures for both EP copolymers, but that these interactions were more pronounced for the semicrystalline sample.

Fluorescence experiments based on pyrene excimer formation were measured for both the amorphous and semicrystalline samples at concentrations of 0.01 and 10 g.L^{-1} in toluene. Very different profiles of the I_E/I_M-vs-T plots were obtained for the amorphous and semicrystalline samples. As the solution temperature was increased from −25 to +25 ^{o}C, a 10 g.L^{-1} solution of Py(116)-EP(78-1) in toluene showed first an increase in I_E/I_M, followed by a decrease in I_E/I_M at intermediate temperatures, before resuming the original increase in I_E/I_M. The decrease in I_E/I_M behavior observed for the semicrystalline Py(116)-EP(78-1) sample around −5 ^{o}C reflected a change in the process of excimer formation. In turn, this decrease in excimer formation could be attributed to fisrt, the volume expansion of the polymer coil that results from the melting of the compact crystalline microdomains, thus decreasing $[Py]_{loc}$ and/or second, the dissociation of the Py(116)-EP(78–1) aggregates happening around −5 ^{o}C which would also result in a decrease in $[Py]_{loc}$.

A much simpler I_E/I_M-vs-T profile was obtained for the semicrystalline and amorphous samples at a concentration of 0.01 g.L^{-1} in the presence of a large excess of naked EP copolymer and for the amorphous sample at a concentration of 10 g.L^{-1}. In all these cases, I_E/I_M increased continuously with increasing temperature and no distinct temperature regime could

be identified. Finally, f_{inter} was calculated by applying Equation 7.2 to the trends obtained from the I_E/I_M ratios.

$$f_{\text{inter}} = \frac{[Py]_{loc}\left(\begin{smallmatrix}\text{inter\&}\\ \text{intra}\end{smallmatrix}\right) - [Py]_{loc}(\text{intra})}{[Py]_{loc}\left(\begin{smallmatrix}\text{inter\&}\\ \text{intra}\end{smallmatrix}\right)} = \frac{I_E / I_M\left(\begin{smallmatrix}\text{inter\&}\\ \text{intra}\end{smallmatrix}\right) - I_E / I_M(\text{intra})}{I_E / I_M\left(\begin{smallmatrix}\text{inter\&}\\ \text{intra}\end{smallmatrix}\right)} \qquad (7.2)$$

Plots of f_{inter} as a function of temperature for the 10 g.L^{-1} amorphous polymer solution in toluene showed that f_{inter} remained constant at 0.31 ± 0.02 and did not depend much on temperature. The 10 g.L^{-1} semicrystalline solution in toluene showed two clear regimes depending on whether the solution temperature was below or above −5 °C. f_{inter} took values that were large and small depending on whether the solution temperature was below or above −5 °C. At temperature below −5 °C, microcrystal formation led to an increase in intermolecular interactions. At temperatures above −5 °C, microcrystals were absent from the solution and fewer intermolecular interactions took place.

In the fourth study, fluorescence experiments were carried out on four more EP copolymers, in addition to the two EP copolymers studied in Chapter 4 in order to check the robustness of the procedure established in Chapter 4. Based on FTIR, DSC, ^{13}C NMR, and viscosity experiments, four of the EP copolymers were found to be semicrystalline and the two others amorphous. EP(60-1) and EP(61-2) on the one hand and EP(78-1), EP(78-2), and EP(78-3) on the other hand had the lowest and highest ethylene contents of 60 and 78 mol%, respectively. EP(70) was semicrystalline but had an intermediate ethylene content of 70 mol%. After preliminary characterisation, these six EP copolymers were maleated and then labeled with 1-pyrenemethylamine to yield Py-EP. Maleation and pyrene labeling was confirmed first

by the appearance and then disappearance of the peak at 1785 cm^{-1} in their FTIR spectra, respectively.

The intermolecular interaction between the Py-EP copolymers were characterized by pyrene excimer formation. Pyrene excimer formation was then used to determine f_{inter} quantitatively for the different Py-EP copolymers by applying Equation 7.2. Plots of I_E/I_M and f_{inter}-vs-T showed very different behaviors whose origin could be traced back to the crystallinity of the EP copolymers. The I_E/I_M ratio increased continuously for Py(108)-EP(60-1) and Py(103)-EP(61-2) with increasing temperature and remained relatively constant for Py(82)-EP(70-1). The three polymers with a higher ethylene content showed different profiles due to the formation of microcrystals which was also observed earlier in Chapter 4.[3,4] By comparison, the f_{inter}-vs-T profiles were much simpler to interpret. f_{inter} remained constant with temperature for the Py(108)-EP(60-1) and Py(103)-EP(61-2) samples, as expected for amorphous samples. For all semicrystalline samples with a 78 mol% ethylene content, two clear regimes were observed below and above $T = -5 \pm 3$ °C. Finally, Py(82)-EP(70-1) showed an intermediate behaviour between the most crystalline and amorphous samples as expected from its intermediate ethylene content of 70 mol%. The results of these experiments confirmed that the procedure based on the use of the I_E/I_M ratio to calculate f_{inter} is robust and provides a clear description of the level of intermolecular interactions that exist between EP copolymers in solution.

The procedure developed in Chapters 4 and 5 to generate the f_{inter}-vs-T profiles for the EP copolymers was applied in Chapter 6 to study the effect that wax found in engine oil has on the aggregation of VIIs in solution. The study focused on the two amorphous Py(108)-EP(60-1) and Py(103)-EP(61-2) samples and the two semicrystalline Py(116)-EP(78-1) and Py(123)-

EP(78-3) samples. Following the determination of the I_E/I_M-vs-T for all four Py-EP samples, the corresponding f_{inter}-vs-T profiles were generated. After addition of wax, f_{inter} remained constant over the entire temperature range but it increased from 0.28 ± 0.02 to 0.43 ± 0.01 and from 0.22 ± 0.02 to 0.40 ± 0.01 for the Py(108)-EP(60-1) and Py(103)-EP(61-2) samples, respectively. This result demonstrated that wax increases interactions between the amorphous Py-EP copolymers in toluene. For Py(116)-EP(78-1) and Py(123)-EP(78-3), two distinct temperature regimes were observed depending on whether the solution temperature was below or above T_C. At temperatures above T_C, f_{inter} showed a much larger increase upon the addition of 10 g.L^{-1} wax than at temperatures below T_C. Microcrystal formation at temperatures below T_C led to an increase in polymer-polymer interactions and a reduction in polymer-wax interactions. Consequently wax was certainly expelled into the bulk reducing its ability to promote intermolecular interactions so that its presence had little effect on f_{inter} at temperatures below T_C.

As mentioned several times in the thesis, engine oils are multicomponent formulations whose performance depends critically on the compatibility of these different components and their ability to function optimally in the presence of each other. In view of these requirements, the industry is clearly lacking the ability to probe how the presence of one component affects the behaviour of another. The studies conducted in this thesis have tried to address this need, particularly through the development of a procedure that allows one to monitor the extent of intermolecular interactions taking place in solution between VIIs as a function of the crystallinity of the EP copolymer or the presence of wax found in any engine oil. This thesis has demonstrated that f_{inter} can be used effectively to probe intermolecular associations in

multicomponent systems and provides a robust analytical tool to probe the level of interactions taking place between the different components found in oil formulations.

7.2 Future Work

Dispersants, VIIs, and pour point depressants (PPDs) are three additives commonly found in engine oils. In Chapters 2 and 3, PIBSA was reacted with a series of polyamines to generate *mono*-PIBSI (*m*-PIBSI) and *bis*-PIBSI (*b*-PIBSI) dispersants which were further reacted with ethylene carbonate (EC) to form modified *b*-PIBSI dispersant. Due to steric hindrance as well as H-bonding, none of the secondary amines in the linker of, respectively, *b*-PIBSI-DETA and *b*-PIBSI-TETA could react with EC, and that about one out of the three secondary amines of *b*-PIBSI-TEPA and one out of the four secondary amines of *b*-PIBSI-PEHA did not react with EC. To reduce the steric hindrance caused by the succinimide groups in the *b*-PIBSI dispersant, longer polyamine linkers such as 1,2-*bis*(3-aminopropylamino)ethane or *bis*(3-aminopropyl)amine could be used. The level of modification of these new M*b*-PIBSI dispersants could be determined by applying the fluorescence measurements which were introduced in Chapter 3.[2]

In Chapters 4 and 5, the molar fraction of intermolecular interaction (f_{inter}) between VIIs such as EP copolymers was determined by a new method based on pyrene eximer formation. However, f_{inter} has not yet been determined between dispersants and PPDs. Thus, the determination of f_{inter} between dispersants and PPDs both separately and in the presence of other oil additives remains to be done. In the case of PPDs and dispersants, f_{inter} can be determined by labeling the polymers with a chromophores such as pyrene and apply the same method described in Chapter 4. In Chapters 4 and 5, f_{inter} measurements were conducted at temperatures between –30 and 25 ^{o}C. The results showed distinct behavior between the amorphous and

semicrystalline samples in toluene. However, it would be interesting to measure f_{inter} at higher temperatures, specifically at temperatures where the engine operates.[6]

In the final chapter, f_{inter} was also measured between pyrene-labeled EP copolymers in toluene in the presence of wax that had been extracted from engine oil. In these experiments, an increase in intermolecular associations between semicrystalline EP copolymers could only be observed at higher temperatures. It would be informative to measure f_{inter} between both semicrystalline and amorphous samples in an actual engine oil.

Appendices

Chapter 2

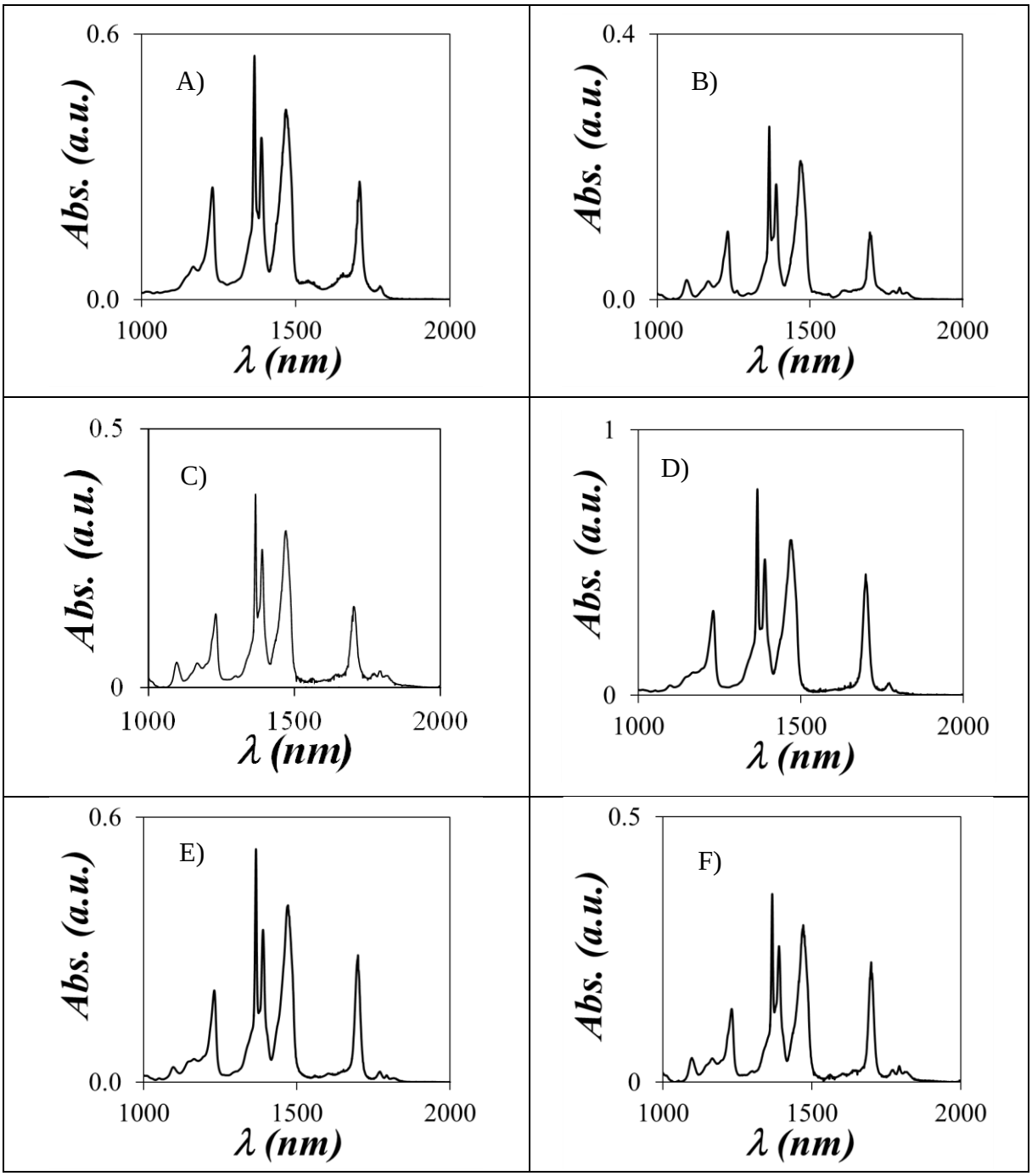

Figure S2.1. FTIR spectra of A) *m*-PIBSI-octylamine, B) *b*-PIBSI-HMDA, C) *b*-PIBSI-DETA, D) *b*-PIBSI-TETA, E) *b*-PIBSI-TEPA, and F) *b*-PIBSI-PEHA.

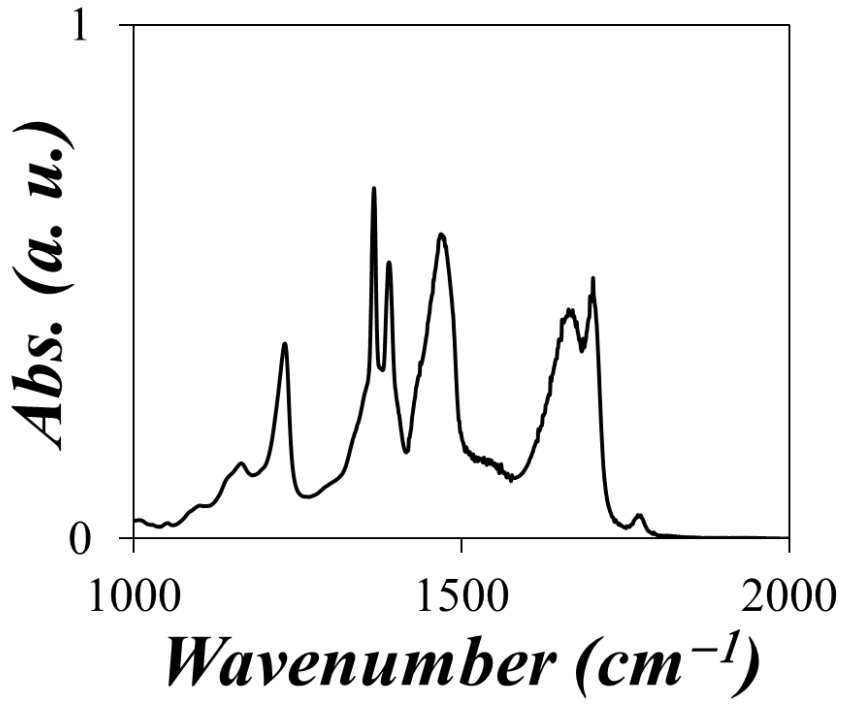

Figure S2.2. FTIR spectrum of a mixture of *m*-PIBSI-TEPA with absorbance at 1705 cm^{-1}, and opened ring *m*-PIBSA-TEPA with absorbance at 1640 cm^{-1}.

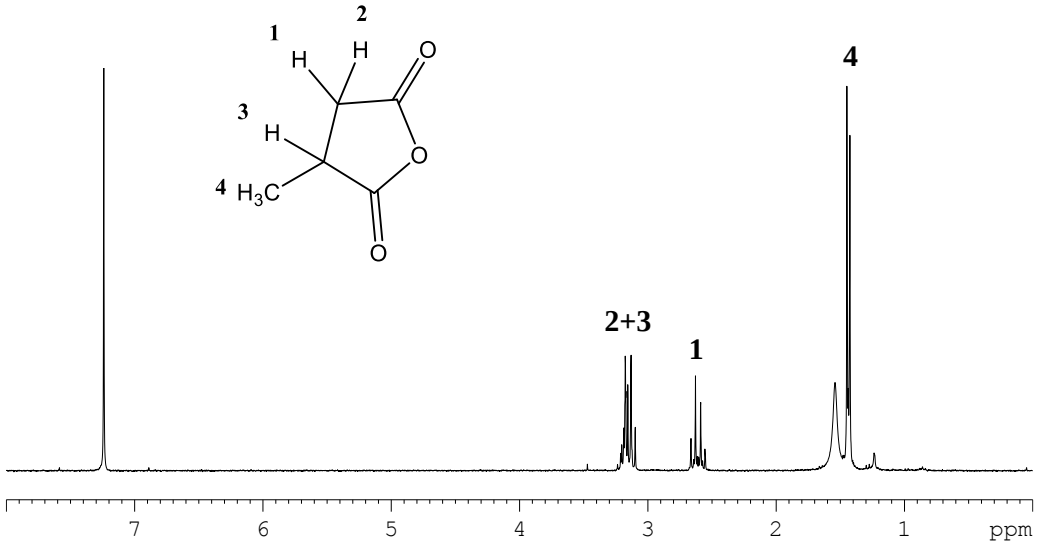

Figure S2.3. ^{1}H NMR spectrum of MSA in $CDCl_3$.

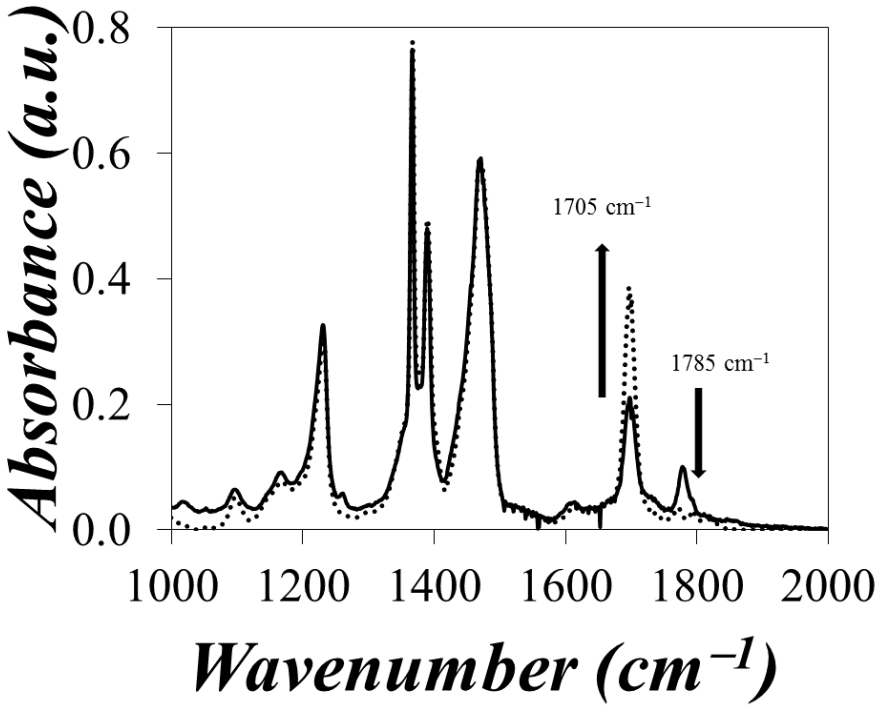

Figure S2.4. FTIR spectra of *b*-PIBSI-HMDA for [HMDA]/[PIBSA] ratios equal to 0.1 and 0.4 mmol/g.

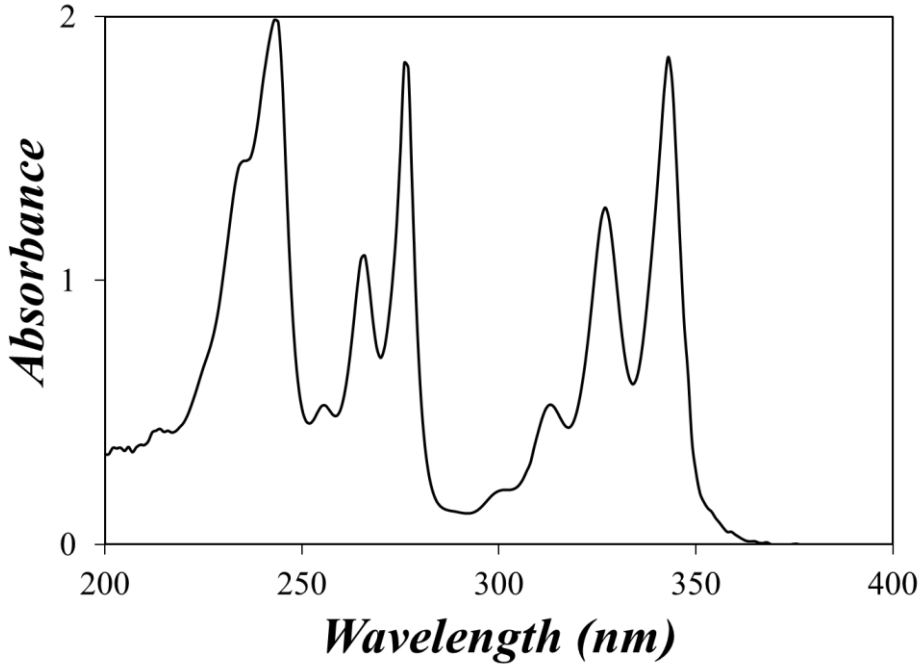

Figure S2.5. UV-Vis absorption spectrum of 10 mg/ml m-PIBSI- $PyNH_2$ in THF.

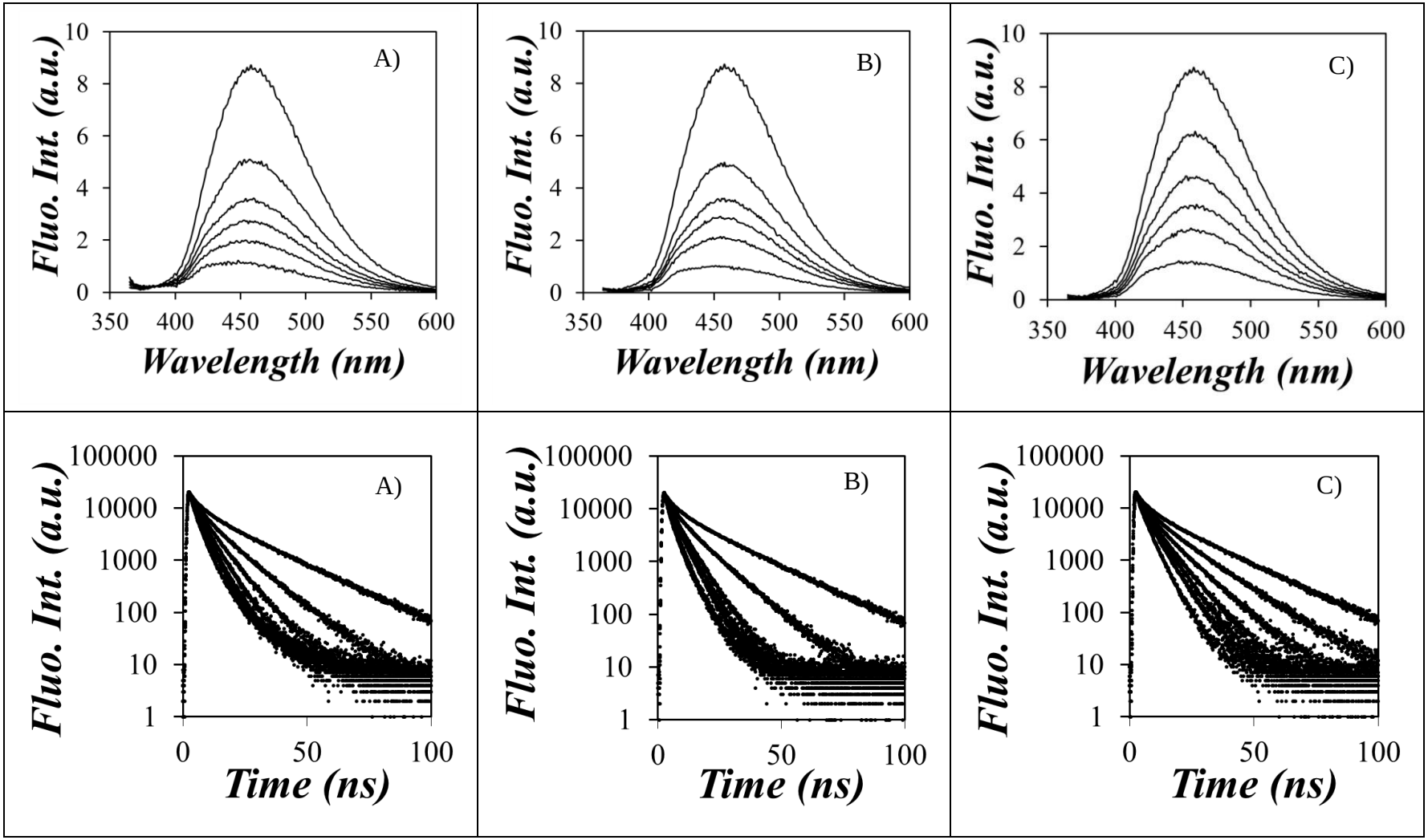

Figure S2.6. Steady-state fluorescence spectra (top) and fluorescence decay (bottom) of *N*-MSI with A) BUA, B) DEA, and C) TEA in THF. From top to bottom: The BUA, DEA, and TEA concentration is varied from 0 M to 0.22 M. ($C_{N\text{-MSI}}$ = 0.45 mol/L, λ_{ex} = 360 nm, and λ_{em} = 428 nm).

Table S2.1. Pre-exponential factors and decay times retrieved from the tri or four-exponential analysis of the fluorescence decays acquired with the PIBSI samples. (λ_{ex} = 360 nm, λ_{em} = 428 nm, and C_{PIBSI} = 8 g/L)

Polymer	solvent	a_1	a_2	a_3	a_4	τ_1(ns)	τ_2(ns)	τ_3(ns)	τ_4(ns)	χ^2
PIBSA	dodecanone	0.17	0.35	0.48	0.00	11.09	4.23	0.82	0.00	1.11
b-PIBSI-HMDA	dodecanone	0.06	0.22	0.38	0.34	20.22	8.46	0.99	3.06	0.92
b-PIBSI-DETA	dodecanone	0.05	0.18	0.42	0.35	17.95	7.53	0.58	2.26	1.11
b-PIBSI-TETA	dodecanone	0.04	0.15	0.36	0.45	16.92	7.26	2.36	0.73	1.02
b-PIBSI-TEPA	dodecanone	0.03	0.32	0.14	0.52	15.43	2.21	6.29	0.57	1.07
b-PIBSI-PEHA	dodecanone	0.02	0.15	0.36	0.46	14.95	5.77	1.92	0.57	1.00
PIBSA	dodecane	0.07	0.46	0.48	0.00	9.67	0.89	3.50	0.00	1.10
b-PIBSI-HMDA	dodecane	0.37	0.05	0.20	0.38	0.91	25.83	9.80	3.31	1.02
b-PIBSI-DETA	dodecane	0.37	0.05	0.17	0.41	1.91	18.53	6.60	0.38	1.02
b-PIBSI-TETA	dodecane	0.37	0.04	0.17	0.42	1.97	16.81	6.17	0.46	1.01
b-PIBSI-TEPA	dodecane	0.33	0.02	0.17	0.48	2.22	15.02	6.11	0.59	1.10
b-PIBSI-PEHA	dodecane	0.36	0.02	0.16	0.47	1.77	12.66	5.09	0.42	1.14
PIBSA	THF	0.18	0.41	0.41	0.00	10.90	1.00	4.34	0.00	1.04
b-PIBSI-HMDA	THF	0.06	0.34	0.37	0.24	19.40	0.83	2.82	7.93	1.11
b-PIBSI-DETA	THF	0.08	0.15	0.31	0.46	15.58	6.66	2.47	0.74	1.10
b-PIBSI-TETA	THF	0.37	0.03	0.11	0.49	2.26	15.94	6.62	0.66	1.03
b-PIBSI-TEPA	THF	0.03	0.17	0.35	0.46	14.30	5.77	2.11	0.68	1.13
b-PIBSI-PEHA	THF	0.02	0.12	0.37	0.49	14.43	5.33	2.03	0.60	1.14

Table S2.2. Pre-exponential factors and decay times retrieved from the three-exponential analysis of the fluorescence decays acquired with the *N*-MSI in presence of BUA in THF. (λ_{ex} = 360 nm, λ_{em} = 428 νμ, and $C_{N\text{-MSI}}$ = 0.45 mol/L)

Name	[BUA](mol/L)	a_1	a_2	a_3	τ_1(ns)	τ_2(ns)	τ_3(ns)	χ^2
N-MSI	0.00	0.38	0.34	0.27	19.85	6.00	1.64	1.12
N-MSI+BUA	0.03	0.40	0.22	0.38	4.32	0.90	11.14	1.06
N-MSI+BUA	0.06	0.07	0.60	0.34	11.11	6.13	1.90	1.11
N-MSI+BUA	0.09	0.02	0.66	0.33	13.50	5.17	1.60	1.16
N-MSI+BUA	0.12	0.01	0.32	0.67	15.16	1.30	4.43	1.05
N-MSI+BUA	0.14	0.03	0.65	0.31	9.85	3.77	0.88	1.28
N-MSI+BUA	0.22	0.05	0.58	0.36	8.03	3.10	0.91	1.16

Table S2.3. Pre-exponential factors and decay times retrieved from the three-exponential analysis of the fluorescence decays acquired with the *N*-MSI in presence of DEA in THF. (λ_{ex} = 360 nm, λ_{em} = 428 νμ, and $C_{N\text{-MSI}}$ = 0.45 mol/L)

Name	[DEA](mol/L)	a_1	a_2	a_3	τ_1(ns)	τ_2(ns)	τ_3(ns)	χ^2
N-MSI	0.00	0.38	0.34	0.27	19.85	6.00	1.64	1.12
N-MSI+DEA	0.03	0.36	0.0.26	0.38	10.94	1.29	4.52	1.17
N-MSI+DEA	0.06	0.27	0.36	0.37	0.90	7.71	3.72	1.00
N-MSI+DEA	0.08	0.34	0.37	0.29	6.44	3.60	0.78	1.23
N-MSI+DEA	0.11	0.14	0.55	.31	6.72	4.16	1.06	1.17
N-MSI+DEA	0.13	0.03	0.61	0.37	8.78	4.14	0.87	1.13
N-MSI+DEA	0.19	0.07	0.35	0.58	6.48	0.79	3.07	1.09

Table S2.4. Pre-exponential factors and decay times retrieved from the three-exponential analysis of the fluorescence decays acquired with the *N*-MSI in presence of TEA in THF. (λ_{ex} = 360 nm, λ_{em} = 428 νμ, and $C_{N\text{-MSI}}$ = 0.45 mol/L)

Name	[TEA](mol/L)	a_1	a_2	a_3	τ_1(ns)	τ_2(ns)	τ_3(ns)	χ^2
N-MSI	0.00	0.38	0.34	0.27	19.85	6.00	1.64	1.12
N-MSI+TEA	0.02	0.35	0.38	0.27	13.54	4.35	0.79	1.03
N-MSI+TEA	0.04	0.36	0.39	0.25	10.20	4.32	1.28	1.00
N-MSI+TEA	0.06	0.35	0.30	0.35	7.98	0.96	3.86	1.05
N-MSI+TEA	0.07	0.31	0.37	0.34	7.07	3.76	0.85	1.00
N-MSI+TEA	0.09	0.21	0.45	0.34	6.78	4.18	1.10	1.08
N-MSI+TEA	0.13	0.59	0.05	0.36	3.68	7.47	0.91	1.21
N-MSI+TEA	0.18	0.45	0.07	0.49	0.65	6.20	3.11	1.13

Chapter 3

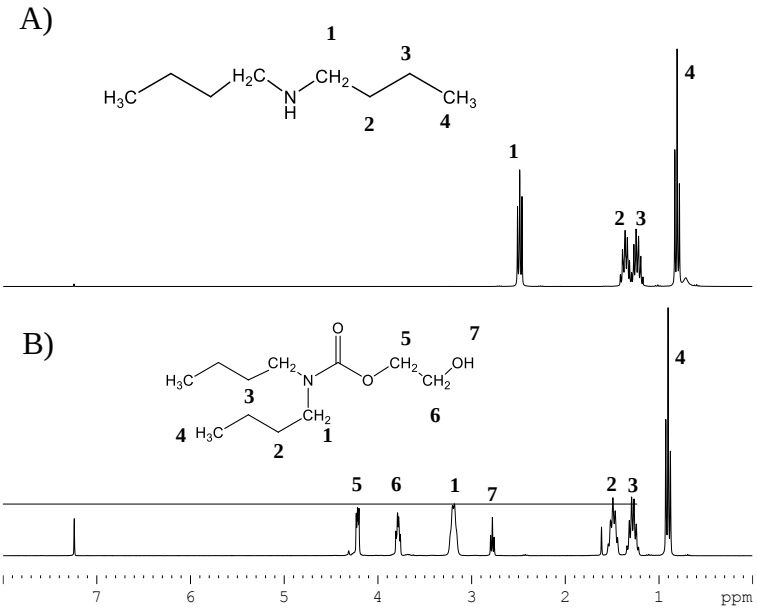

Figure S3.1. Comparison of the ^{1}H NMR spectra of A) DBA and B) HEDBC. (300 MHz, $CDCl_3$)

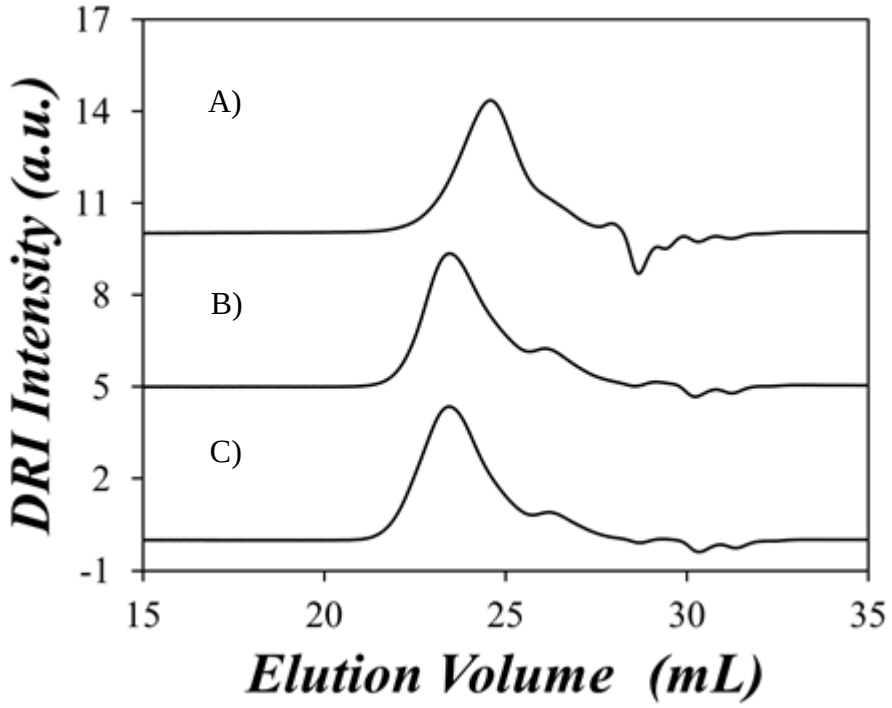

Figure S3.2. GPC traces of A) PIBSA, B) *b*-PIBSI-PEHA, and C) M*b*-PIBSI-PEHA.

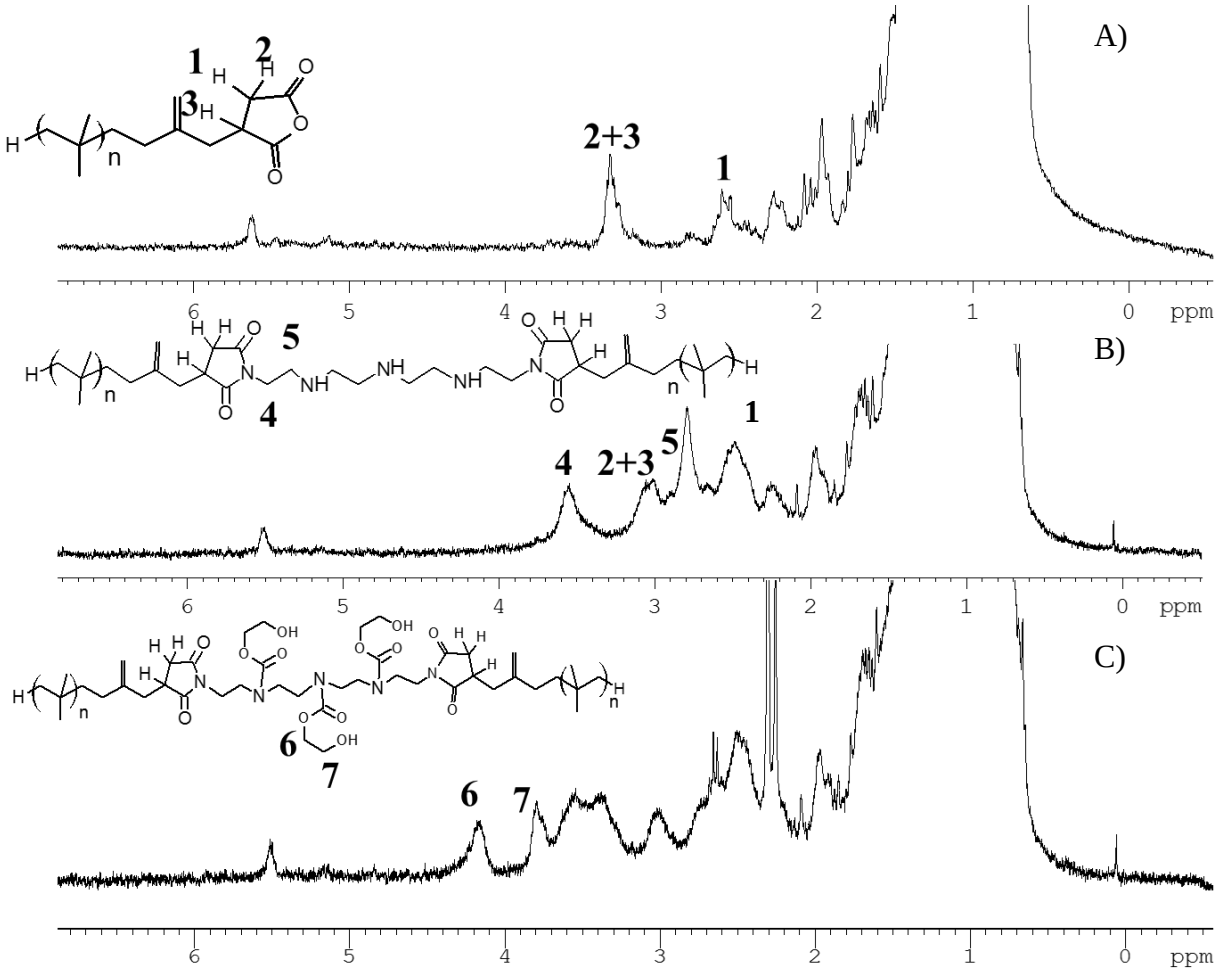

Figure S3.3. ^{1}H NMR spectrum of A) PIBSA, B) *b*-PIBSI-TEPA, and C) M*b*-PIBSI-TEPA. (300 MHz, $CDCl_3$)

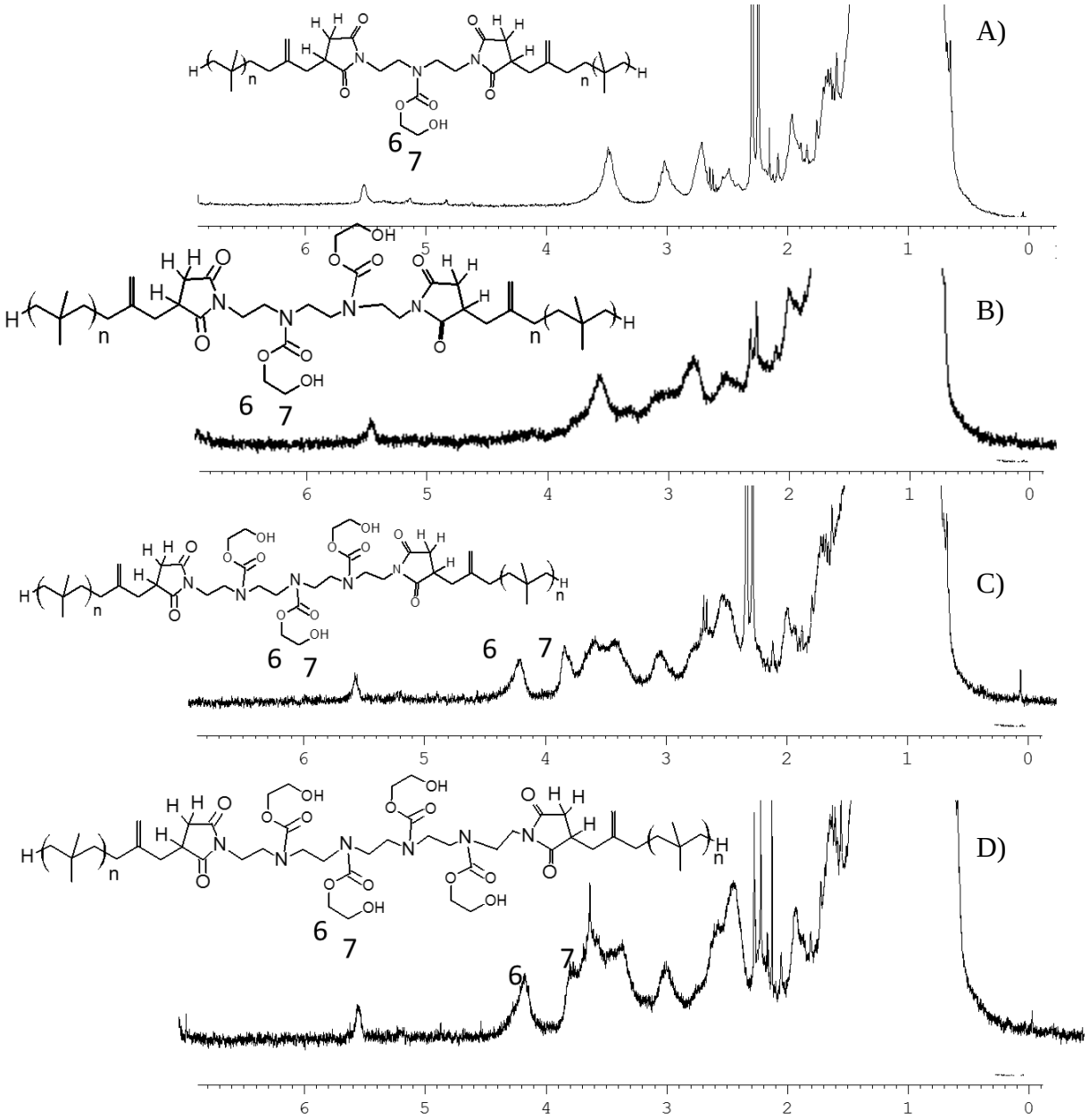

Figure S3.4. ^{1}H NMR spectrum of A) M*b*-PIBSI-DETA, B) M*b*-PIBSI-TETA, C) M*b*-PIBSI-TEPA, and D) M*b*-PIBSI-PEHA. (300 MHz, $CDCl_3$)

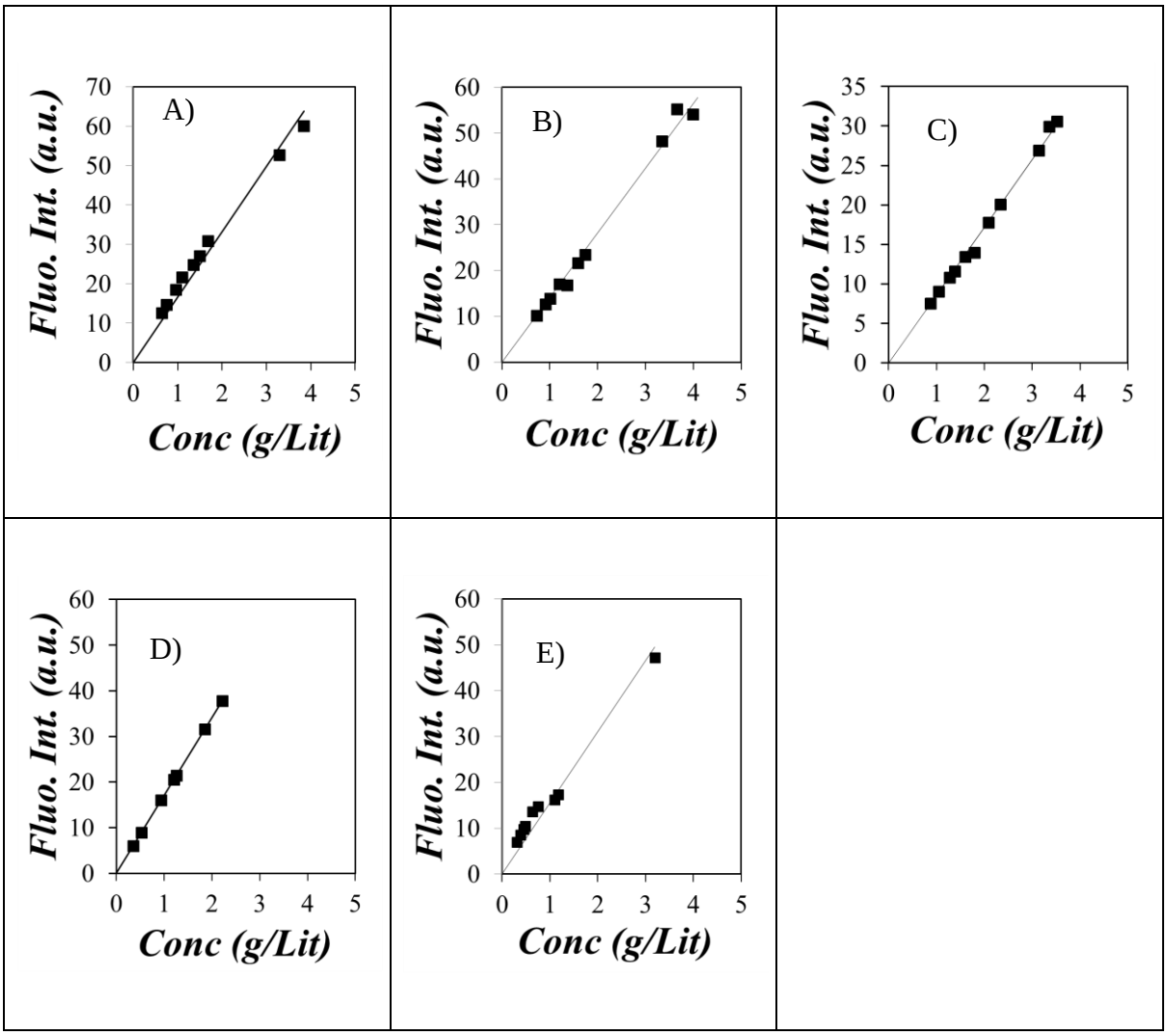

Figure S3.5. Steady-state calibration curve of A) *b*–PIBSI–DETA, B) *b*–PIBSI–TEPA, C) *b*–PIBSI–PEHA, D) M*b*–PIBSI–TEPA, and E) M*b*–PIBSI–PEHA in dodecane. (λ_{ex} = 360 nm)

Table S3.1. Pre-exponential factors and decay times retrieved from the tri or four-exponential analysis of the fluorescence decays acquired with the PIBSI samples. (λ_{ex} = 360 nm, λ_{em} = 428 nm, and C_{PIBSI} = 8 g/L)

Polymer	solvent	a_1	a_2	a_3	a_4	τ_1(ns)	τ_2(ns)	τ_3(ns)	τ_4(ns)	χ^2
PIBSA	dodecanone	0.17	0.35	0.48	0.00	11.09	4.23	0.82	0.00	1.11
b-PIBSI-HMDA	dodecanone	0.06	0.22	0.38	0.34	20.22	8.46	0.99	3.06	0.92
M*b*-PIBSI-TEPA	dodecanone	0.03	0.32	0.14	0.52	15.43	2.21	6.29	0.57	1.07
M*b*-PIBSI-PEHA	dodecanone	0.04	0.144	0.33	0.50	15.64	6.07	2.27	0.72	1.06
PIBSA	dodecane	0.07	0.46	0.48	0.00	9.67	0.89	3.50	0.00	1.10
b-PIBSI-HMDA	dodecane	0.37	0.05	0.20	0.38	0.91	25.83	9.80	3.31	1.02
M*b*-PIBSI-TEPA	dodecane	0.45	0.04	0.16	0.35	0.41	13.83	5.21	1.77	0.99
M*b*-PIBSI-PEHA	dodecane	0.43	0.03	0.14	0.40	0.61	17.73	6.80	2.25	1.19
PIBSA	THF	0.18	0.41	0.41	0.00	10.90	1.00	4.34	0.00	1.04
b-PIBSI-HMDA	THF	0.06	0.34	0.37	0.24	19.40	0.83	2.82	7.93	1.11
M*b*-PIBSI-TEPA	THF	0.04	0.15	0.32	0.49	13.15	5.20	2.15	0.71	0.97
M*b*-PIBSI-PEHA	THF	0.03	0.14	0.40	0.43	15.07	5.57	1.97	0.61	1.11

Table S3.2. Pre-exponential factors and decay times retrieved from the four-exponential analysis of the fluorescence decays acquired with the *N*-MSI in presence of HEDBC in THF. (λ_{ex} = 360 nm, λ_{em} = 428 nm, and $C_{N\text{-MSI}}$ = 0.45 mol/L)

Name	a_1	a_2	a_3	a_4	τ_1(ns)	τ_2(ns)	τ_3(ns)	τ_4(ns)	χ^2
N-MSI	0.21	0.25	0.17	0.36	3.37	14.54	19.58	0.31	1.03
N-MSI+HEDBC	0.22	0.16	0.40	0.22	3.15	9.92	17.85	0.72	1.04
N-MSI+HEDBC	0.19	0.16	0.35	0.29	3.34	9.27	17.75	0.81	1.04
N-MSI+HEDBC	0.33	0.18	0.26	0.23	0.65	8.76	18.12	2.54	0.99
N-MSI+HEDBC	0.04	0.18	0.20	0.22	0.57	8.77	18.48	2.36	1.12
N-MSI+HEDBC	0.26	0.18	0.14	0.43	2.07	8.81	19.97	0.47	0.94

Chapter 4

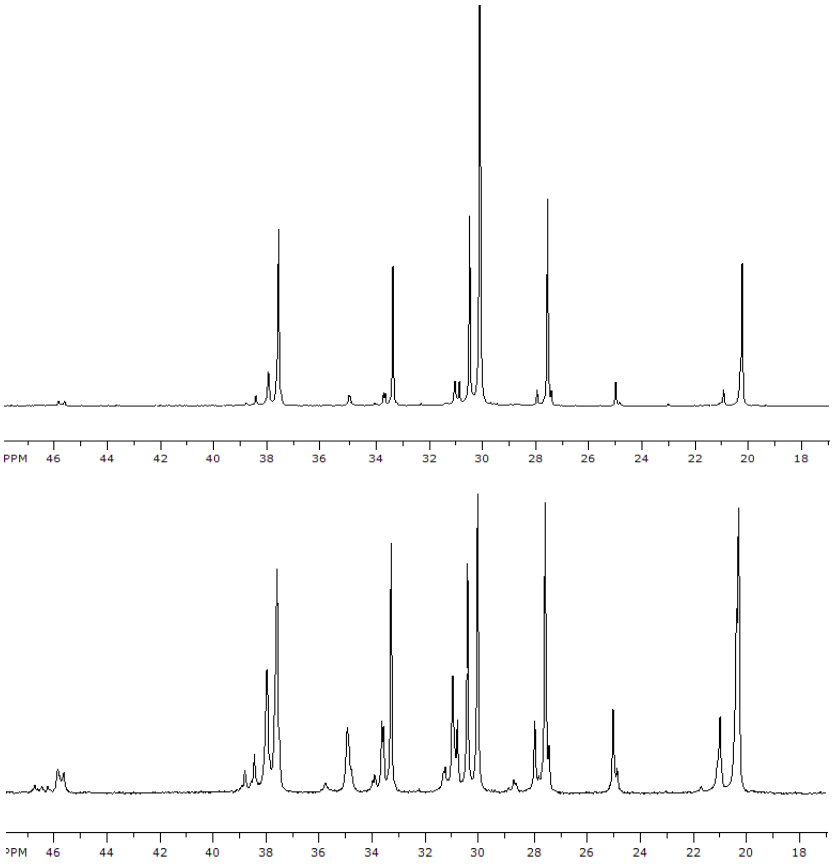

Figure S4.1. ^{13}C NMR spectrum of (top) EP(SM) and (bottom) EP(AM) in TCE-d_2.

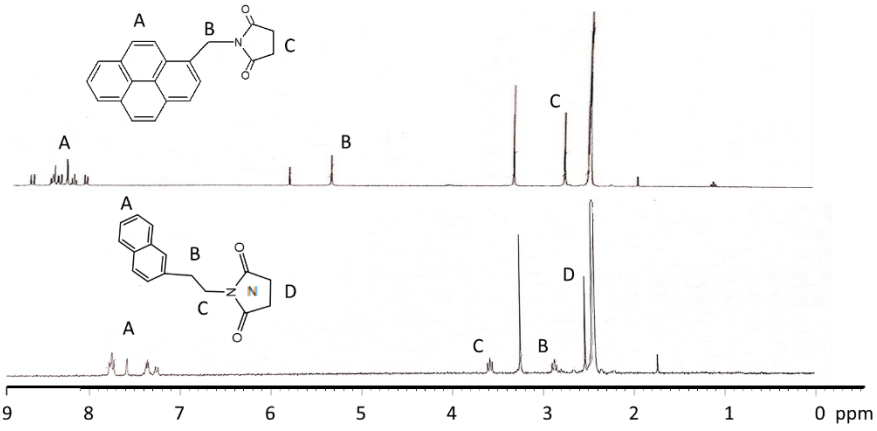

Figure S4.2. ^{1}H NMR spectrum of (top) Py-MSI and (bottom) Np-ESI in DMSO-d_6. The peaks at 2.4, 3.3, and 5.7 nm are due to DMSO-d_6, H_2O, and DCM, respectively.

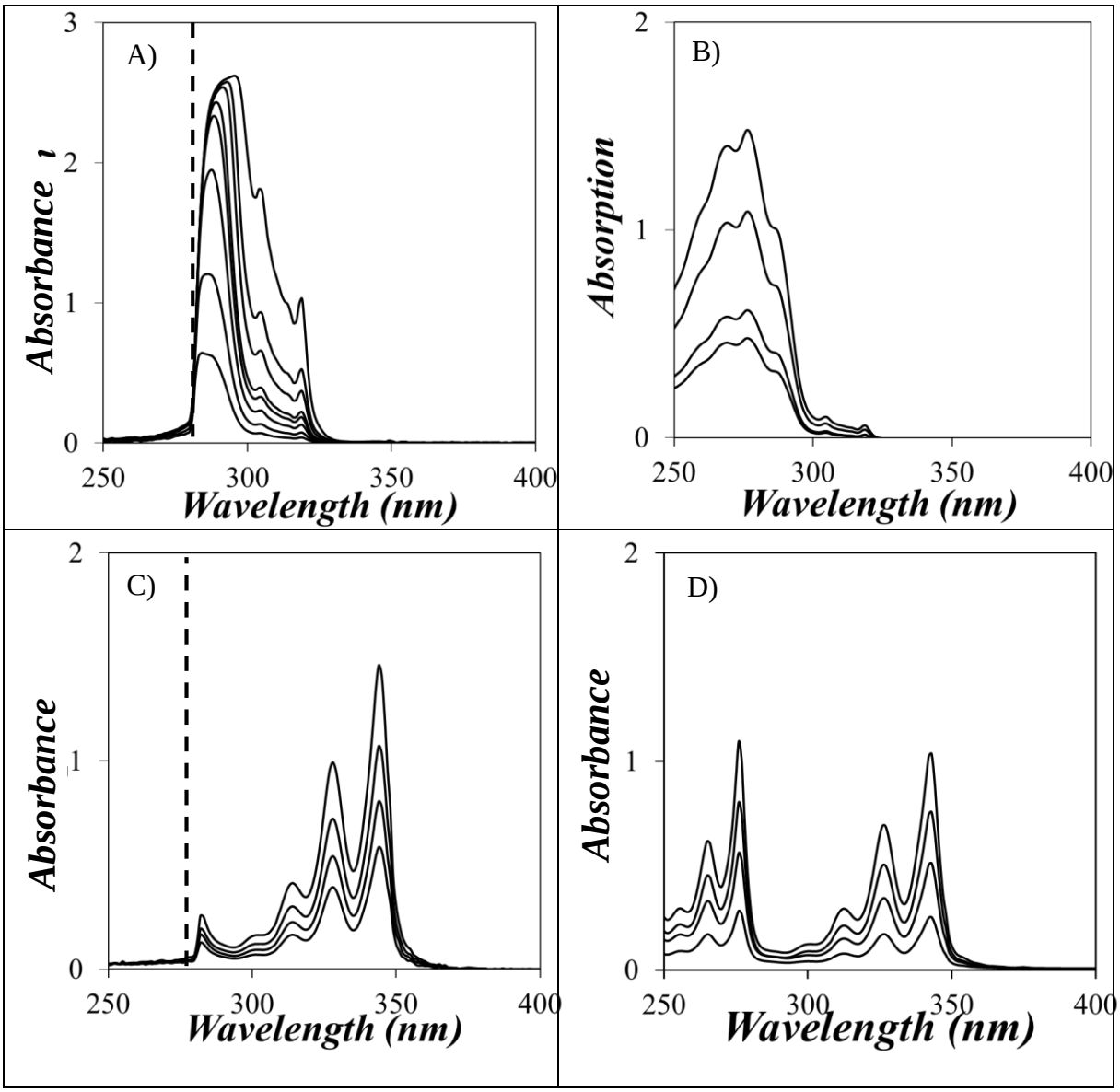

Figure S4.3. UV-Vis absorption of spectra 2-(2-naphthylethyl) succinimide in A) toluene (0.3-5.0 mmol.L^{-1}) and B) THF (0.1-7 mmol.L^{-1}), and 1-pyrenemethyl succinimide in C) toluene (10-30 × 10^{-6} mol.L^{-1}) and D) THF (10-20 × 10^{-6} mol.L^{-1}). The dashed line in panels A) and C) indicates the absorption wall of toluene.

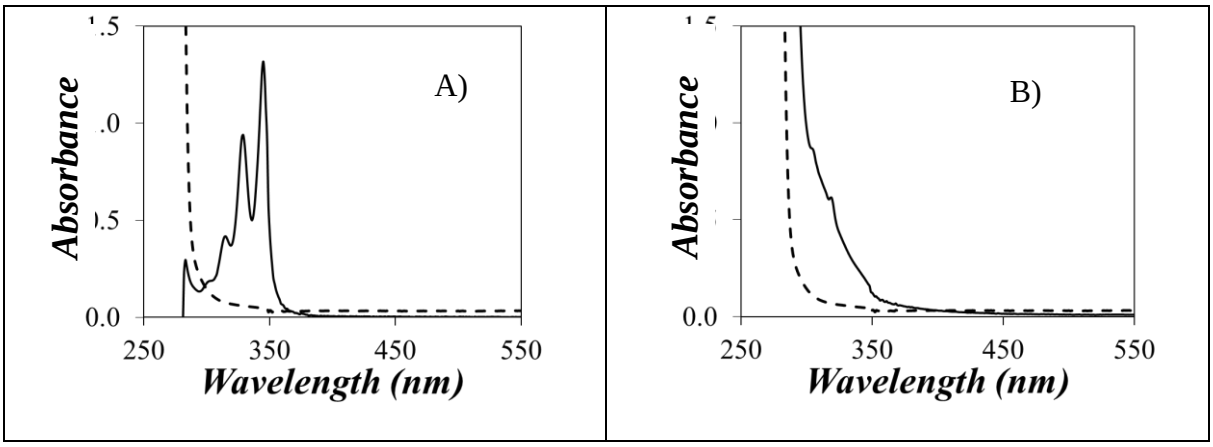

Figure S4.4. UV-Vis absorption spectra of A) Py(108)-EP(AM) (—) and B) Np-EP(AM) (—) in toluene (– – –).

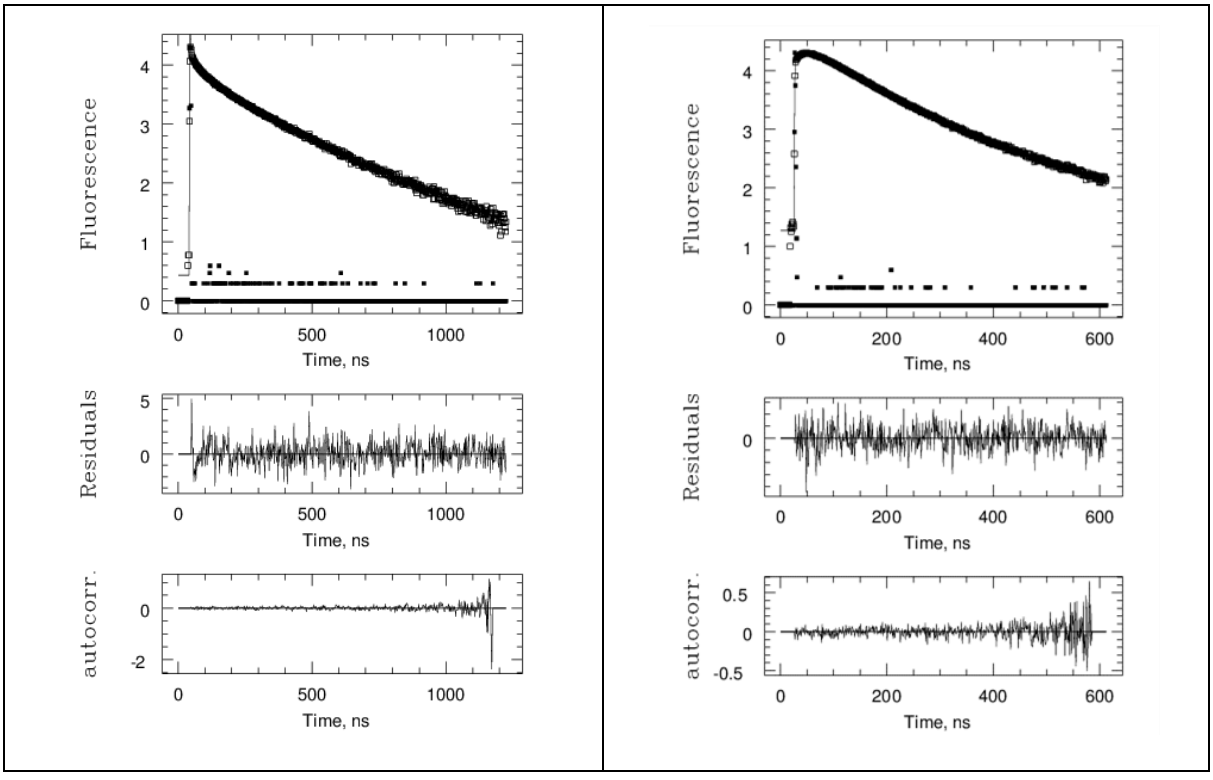

Figure S4.5. Monomer (left; λ_{ex} = 344 nm, λ_{em} = 375 nm; TPC = 2.04 ns/ch) and excimer (right; λ_{ex} = 344 nm, λ_{em} = 510 nm; TPC = 1.02 ns/ch) fluorescence decays of Py(108)-EP(AM) in toluene fitted according to the fluorescence blob model (FBM), χ^2 = 1.15.

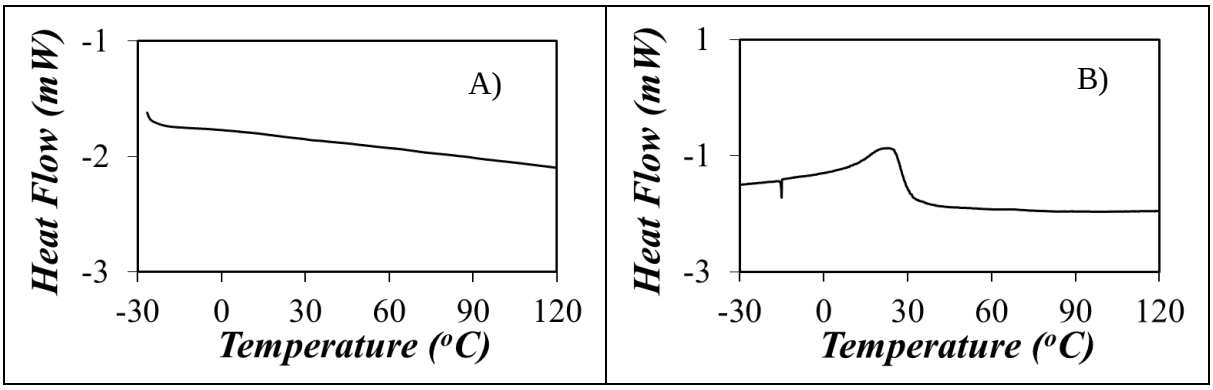

Figure S4.6. DSC traces of A) EP(AM) and B) EP(SM) in the solid state.

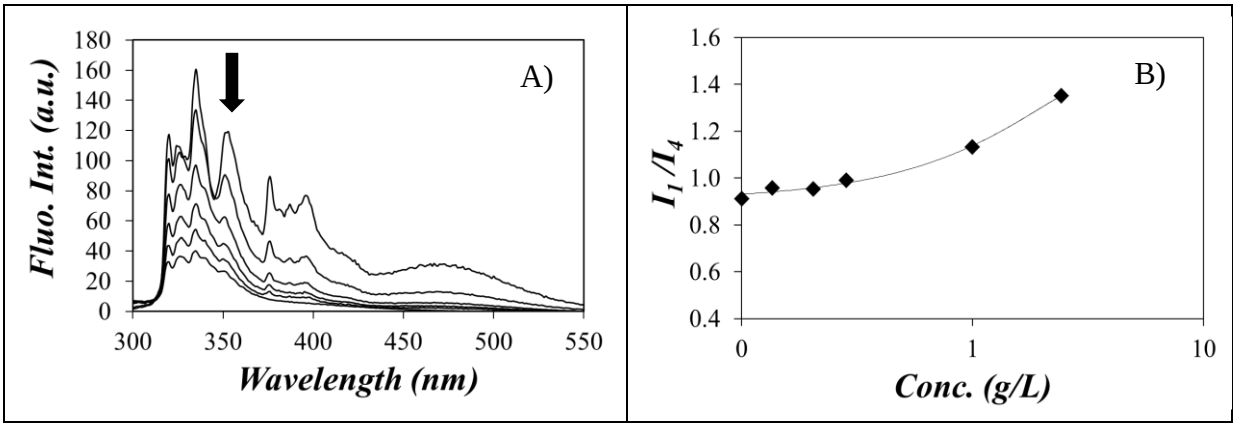

Figure S4.7. A) Fluorescence spectra of EP copolymers obtained from diluting a 5 $g.L^{-1}$ solution of a 9:1 mixture of Np(108)-EP(AM) and Py(108)-EP(AM) in toluene. [Poly]= 5.0, 2.5, 1.0, 0.3, 0.2, and 0.1 $g.L^{-1}$. B) Plot of I_1/I_4 as a function of polymer concentration. (I_1 at 319 nm and I_4 at 353 nm). (T = 25 °C; λ_{ex} = 290 nm). Arrow indicates the putative exciplex emission at 353 nm.

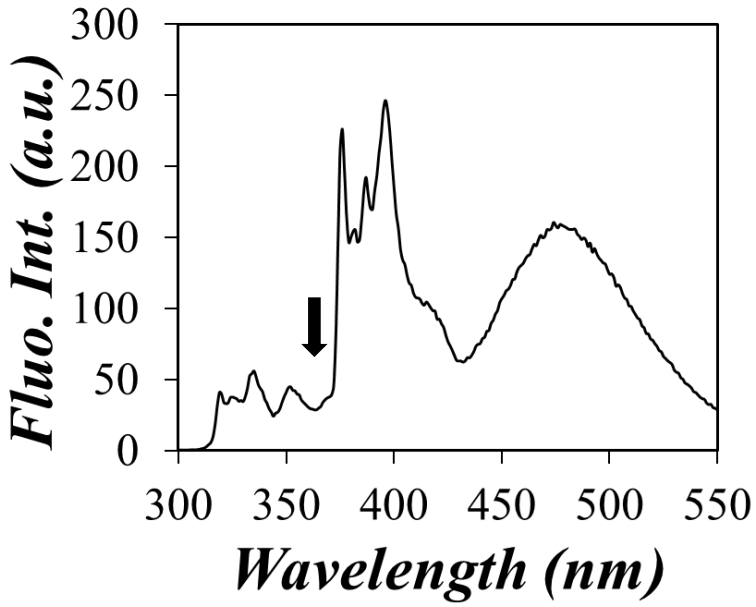

Figure S4.8. Fluorescence spectra obtained from a mixture of Py-MSI (1 mmol/L) and Np-ESI (9 mmol/L). Arrow indicates the putative exciplex emission at 353 nm.

Table S4.1. Parameters retrieved from the global FBM analysis of the monomer decays of Py-EP-MA samples in toluene with Equation S4.1. τ_M was fixed to 243 ns in the analysis.

	k_e[blob] (10^6 s^{-1})	k_2 (10^7 s^{-1})	k_{blob} (10^6 s^{-1})	f_{Mdiff}	f_{Mk2}	f_{Mfree}	$<n>$	χ^2
Py(116)-EP(SM)	2.12	8.80	6.57	0.68	0.21	0.11	1.22	1.01
Py(108)-EP(AM)	4.20	6.29	7.33	0.49	0.36	0.14	1.23	1.15

Table S4.2. Parameters retrieved from the global FBM analysis of the excimer decays of Py-EP-MA samples in toluene with Equation S4.2. τ_M was fixed to 243 ns in the analysis.

	τ_{EEL} (ns)	τ_{EE0} (ns)	f_{Ediff}	f_{Ek2}	f_{EEL}	f_{EE0}	χ^2
Py(116)-EP(SM)	125	43.45	0.68	0.21	0.10	0.01	1.01
Py(108)-EP(AM)	163.03	57.10	0.41	0.30	0.04	0.25	1.15

The fluorescence decays of the pyrene monomer and excimer were fitted globally according to Equations S4.1 and S4.2.

$$[Py^*]_{(t)} = [Py^*_{diff}]_{(t)} + [Py^*_{k2}]_{(t)} + [Py^*_{free}]_{(t)} = [Py^*_{diff}]_o \exp\left(-\left(A_2 + \frac{1}{\tau_M}\right)t - A_3\left(1-\exp(-A_4 t)\right)\right)$$

$$+\left([Py^*_{k2}]_o + [Py^*_{diff}]_o e^{-A_3}\sum_{i=0}^{\infty}\frac{A_3^i}{i!}\frac{A_2+iA_4}{A_2+iA_4-k_2}\right)\exp\left(-\left(k_2+\frac{1}{\tau_M}\right)t\right)$$

$$-[Py^*_{diff}]_o e^{-A_3}\sum_{i=0}^{\infty}\frac{A_3^i}{i!}\frac{A_2+iA_4}{A_2+iA_4-k_2}\exp\left(-\left(A_2+iA_4+\frac{1}{\tau_M}\right)t\right)$$

$$+[Py^*_{free}]_o \exp\left(-\frac{t}{\tau_M}\right)\Bigg] \qquad \text{(S4.1)}$$

$$[E^*]_{(t)} = [E0^*]_{(t)} + [EL^*]_{(t)} = k_2\Bigg(\left([Py^*_{k2}]_o + [Py^*_{diff}]_o e^{-A_3}\sum_{i=0}^{\infty}\frac{A_3^i}{i!}\frac{A_2+iA_4}{A_2+iA_4-k_2}\right)$$

$$\times\frac{\exp\left(-\frac{t}{\tau_{E0}}\right)-\exp\left(-\left(k_2+\frac{1}{\tau_M}\right)t\right)}{k_2+\frac{1}{\tau_M}-\frac{1}{\tau_{E0}}}$$

$$+[Py^*_{diff}]_o e^{-A_3}\sum_{i=0}^{\infty}\frac{A_3^i}{i!}\frac{A_2+iA_4}{A_2+iA_4-k_2}\frac{\exp\left(-\left(A_2+iA_4+\frac{1}{\tau_M}\right)t\right)-\exp\left(-\frac{t}{\tau_{E0}}\right)}{A_2+iA_4+\frac{1}{\tau_M}-\frac{1}{\tau_{E0}}}\Bigg)$$

$$+ [E0^*]_o \times \exp\left(-\frac{t}{\tau_{E0}}\right) + [EL^*]_o \times \exp\left(-\frac{t}{\tau_{EL}}\right) \quad \text{(S4.2)}$$

The expression of the parameters A_2, A_3, and A_4 used in Equations S4.1 and S4.2 are given in Equation S4.3 as a function of <*n*>, the average number of pyrenes per *blob*, k_{blob}, the rate constant describing the slow diffusive motions undergone by the polymer to bring two monomers located inside a same *blob* and bearing a pyrene label in close proximity from each other, and $k_e \times [blob]$ that describes the rate at which ground state pyrene species exchange among *blobs.*

$$A_2 = < n > \frac{k_{blob} k_e [blob]}{k_{blob} + k_e [blob]} \qquad A_3 = < n > \left(\frac{k_{blob}}{k_{blob} + k_e [blob]}\right)^2 \qquad A_4 = k_{blob} + k_e [blob]$$

(S4.3)

The fluorescence decays of the pyrene monomer and excimer were fitted globally according to Equations S4.1 and S4.2 and the parameters used in these equations were optimized with the Marquardt-Levenberg algorithm. The fit yielded the parameters <*n*>, k_{blob}, and $k_e[blob]$. The monomer decay analysis yielded the molar fractions f_{Mdiff}, f_{Mk2}, and f_{Mfree} representing the pyrene species Py^*_{diff}, Py^*_{k2}, and Py^*_{free} contributing to the monomer decays, respectively. In a similar manner, the excimer decay analysis with Equation S4.2 yielded the fractions f_{Ediff}, f_{Ek2}, f_{EE0}, and f_{EEL} which represent the molar fractions of the pyrene species Py^*_{diff}, Py^*_{k2}, $E0^*$, and EL^* contributing to the excimer decays, respectively. The fractions f_{Mdiff}, f_{Mk2},

f_{Mfree}, f_{Ediff}, f_{Ek2}, f_{EE0}, and f_{EEL} were then be combined to determine the overall molar fractions of each pyrene species present in solution f_{diff}, f_{k2}, f_{free}, f_{E0}, and f_{EL}. This type of analysis has been described in numerous instances.[1-4]

Chapter 5

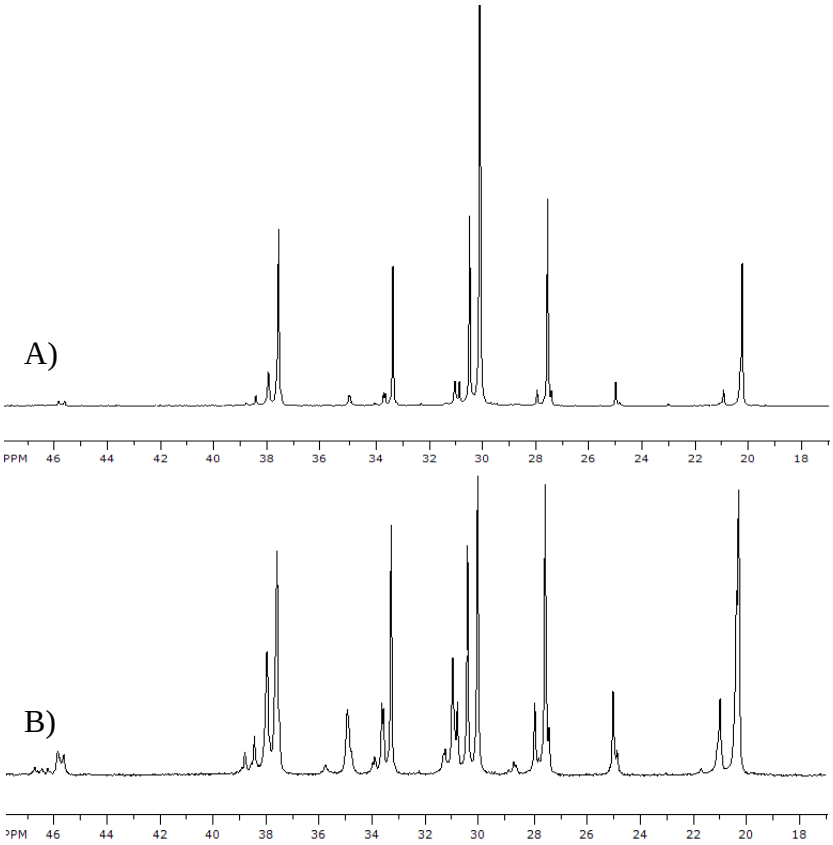

Figure S5.1. ^{13}C NMR spectrum of A) Py(116)-EP(78-1) and B) Py(108)-EP(60-1) in TCE–d_2.

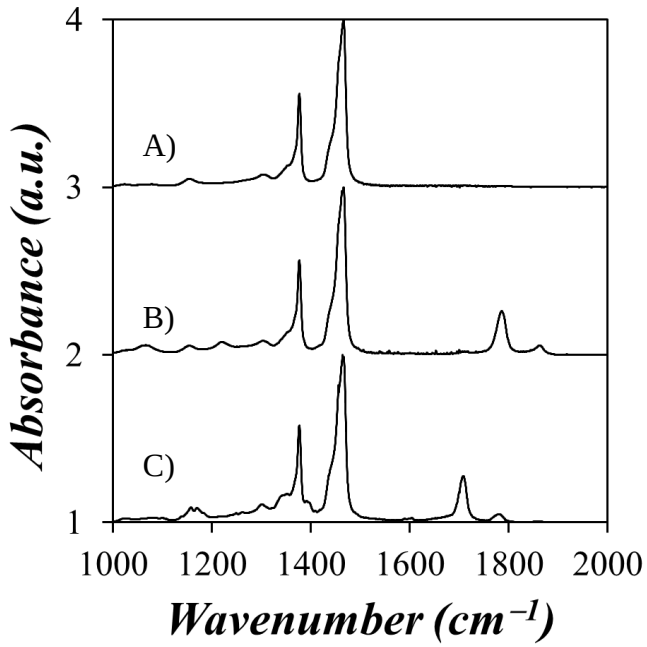

Figure S5.2. FTIR spectra of A) EP(78-1), B) EP(78-1)-MA, and C) Py(116)-EP(78-1).

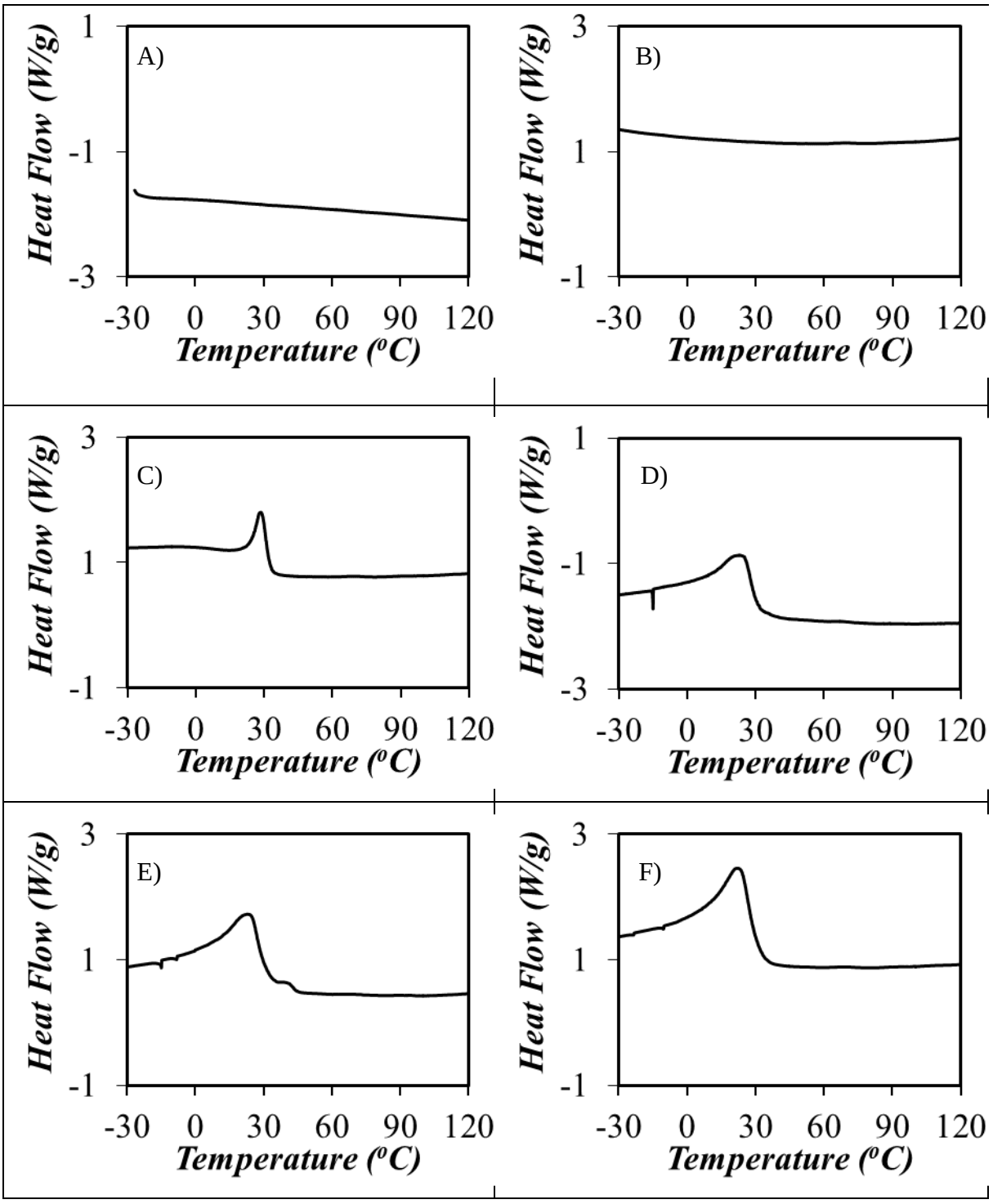

Figure S5.3. DSC traces of A) Py(108)-EP(60-1), B) Py(103)–EP(61-2), C) Py(82)-EP(70-1), D) Py(116)-EP(78-1), E) Py(81)-EP(78-2), and F) Py(123)-EP(78-3).in the solid state.

Letters of Copyright Permission

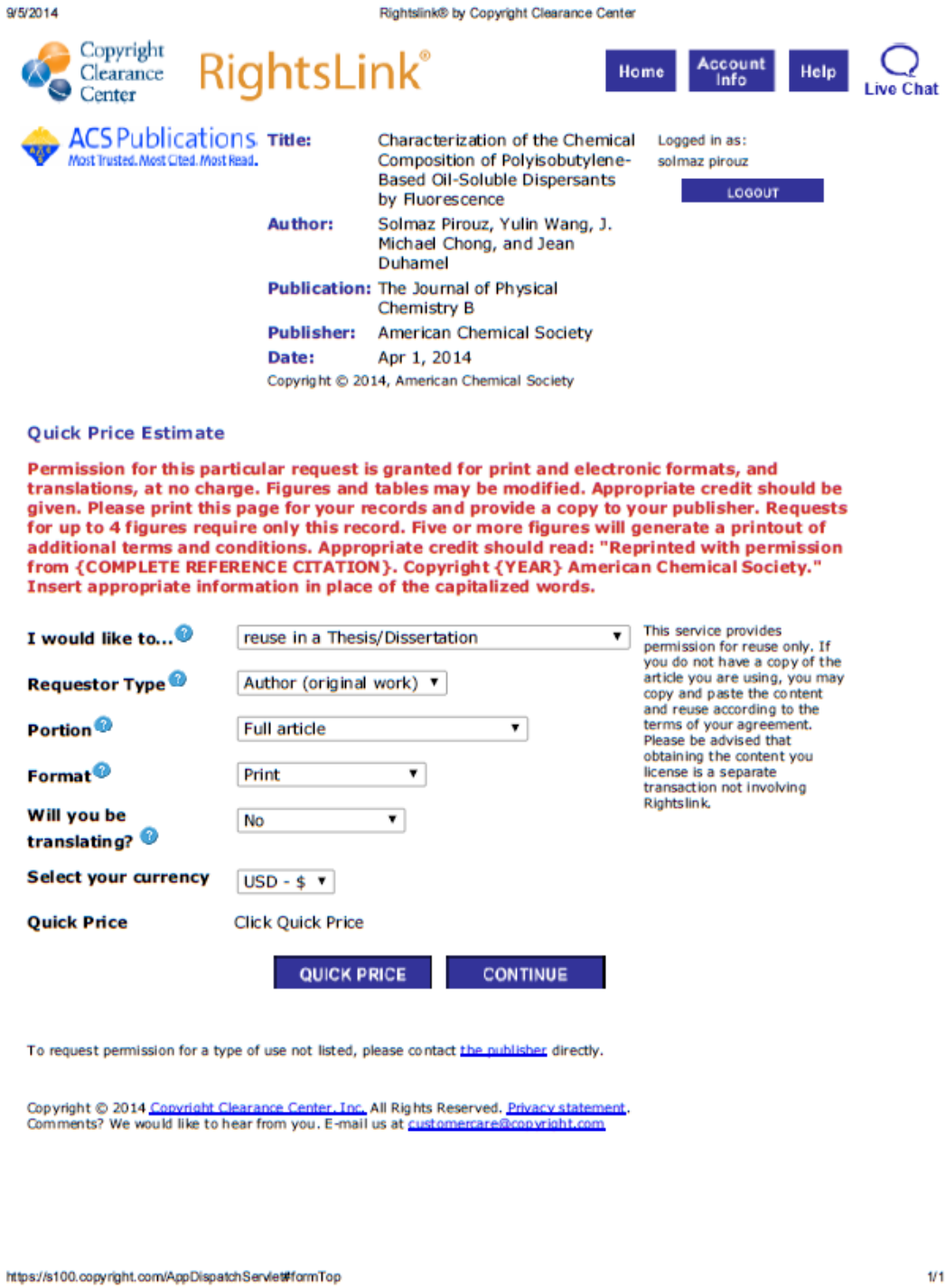

9/5/2014 Rightslink® by Copyright Clearance Center

Copyright Clearance Center RightsLink® Home Account Info Help Live Chat

ACS Publications Most Trusted. Most Cited. Most Read.

Title: Characterization of the Chemical Composition of Polyisobutylene-Based Oil-Soluble Dispersants by Fluorescence

Author: Solmaz Pirouz, Yulin Wang, J. Michael Chong, and Jean Duhamel

Publication: The Journal of Physical Chemistry B

Publisher: American Chemical Society

Date: Apr 1, 2014

Copyright © 2014, American Chemical Society

Logged in as: solmaz pirouz

LOGOUT

Quick Price Estimate

Permission for this particular request is granted for print and electronic formats, and translations, at no charge. Figures and tables may be modified. Appropriate credit should be given. Please print this page for your records and provide a copy to your publisher. Requests for up to 4 figures require only this record. Five or more figures will generate a printout of additional terms and conditions. Appropriate credit should read: "Reprinted with permission from {COMPLETE REFERENCE CITATION}. Copyright {YEAR} American Chemical Society." Insert appropriate information in place of the capitalized words.

I would like to... reuse in a Thesis/Dissertation

Requestor Type Author (original work)

Portion Full article

Format Print

Will you be translating? No

Select your currency USD - $

Quick Price Click Quick Price

QUICK PRICE CONTINUE

This service provides permission for reuse only. If you do not have a copy of the article you are using, you may copy and paste the content and reuse according to the terms of your agreement. Please be advised that obtaining the content you license is a separate transaction not involving Rightslink.

To request permission for a type of use not listed, please contact the publisher directly.

https://s100.copyright.com/AppDispatchServlet#formTop 1/1

Title: Characterization of the Chemical Composition of Polyisobutylene-Based Oil-Soluble Dispersants by Fluorescence

Author: Solmaz Pirouz, Yulin Wang, J. Michael Chong, and Jean Duhamel

Publication: The Journal of Physical Chemistry B

Publisher: American Chemical Society

Date: Apr 1, 2014

PERMISSION/LICENSE IS GRANTED FOR YOUR ORDER AT NO CHARGE

This type of permission/license, instead of the standard Terms & Conditions, is sent to you because no fee is being charged for your order. Please note the following:

- Permission is granted for your request in both print and electronic formats, and translations.
- If figures and/or tables were requested, they may be adapted or used in part.
- Please print this page for your records and send a copy of it to your publisher/graduate school.
- Appropriate credit for the requested material should be given as follows: "Reprinted (adapted) with permission from (COMPLETE REFERENCE CITATION). Copyright (YEAR) American Chemical Society." Insert appropriate information in place of the capitalized words.
- One-time permission is granted only for the use specified in your request. No additional uses are granted (such as derivative works or other editions). For any other uses, please submit a new request.

BACK | CLOSE WINDOW

References

Chapter 1

(1) Pawlak, Z. In *Tribochemistry of lubricating oils;* Elsevier: Poland, 2003; Vol. 45.

(2) Nassar, A. M.; Ahmed, N. S.; Kamal, R. S.; Abdel Azim, A. A.; El-Nagdy, E. Preparation and Evaluation of Acrylate Polymers as Viscosity Index Improvers for Lube Oil. *Petrol. Sci. Tech.* **2005**, *23*, 537-546.

(3) Barbadsz, E. A.; Lamb, G. D. Eds. In *Chapter 19: Additives for Crankcase Lubricant Applications*; Rudnik, L. R. Lubricant Additives: Chemistry and Application*;* CRC Press, Boca Raton: Florida, 2003; pp 458-490.

(4) Mortier, R. M.; Malcolm, F. F.; Orszulik, S. T. In *Chemistry and Technology of Lubricants;* Springer: London, 2009.

(5) Jao, T. -C.; Passut, C. A. In *Part D: Formulation, Surfactant Science Series;* Showell, M. S., Ed.; Handbook of Detergents; CRC Press, Boca Raton: Florida, 2006.

(6) Jao, T. -C.; Passut, C. A. In *Part A: Properties;* Broze, G., Ed.; Handbook of Detergents*;* CRC Press, New York, 1999.

(7) Heilman, W. J.; Wilburn, B. E. Olefin Polymer Pour Point Depressants. USP 5188724, 1993.

(8) Horne, W. V. Polymethacrylates as Viscosity Index Improvers and Pour Point Depressants. *Ind. Eng. Chem.* **1949**, *41*, 952-959.

(9) Naga, H. H.; Azim, W. M.; Ahmed, M. M. Polymeric Additives for Pour Point Depression of Residual Fuel Oils. *J. Chem. Tech. Bio.* **1985**, *35*, 241-247.

(10) Hafiz, A.; Khidr, T. Hexa-Triethanolamine Oleate Esters as Pour Point Depressant for Waxy Crude Oils. *J. Petr. Sci. Eng.* **2007**, *56*, 296-302.

(11) Fang, L.; Zhang, X.; Ma, J.; Zhang, B. Investigation into a Pour Point Depressant for Shengli Crude Oil. *Ind. Eng. Chem. Res.* **2012**, *51*, 11605-11612.

(12) Horowitz, H. Predicting Effects of Temperature and Shear Rate on Viscosity of Viscosity Index–Improved Lubricants. *Ind. Eng. Chem.* **1958**, *50*, 1089-1094.

(13) El Mehbad, N. Efficiency of Amphoteric Surfactants as Flow Improvers and Pour Point Depressants. *J. Power Ener. Eng.* **2013**, *1*, 90-94.

(14) Cravey, R. L.; Mead, S. L. Pour Point Depressant Additives for Oil Compositions. USP 7942941, 2011.

(15) Clague, A. D. H.; Donnet, J. B.; Wang, T. K.; Peng, J. C. M. A Comparison of Diesel Engine Soot with Carbon Black. *Carbon* **1999**, 37, 1553-1565.

(16) Gwinn, M. R.; Vallyathan, V. Nanoparticles: Health Effects - Pros and Cons. *Environ. Health Perspect.* **2006**, *114*, 1818-1825.

(17) Farnlund, J.; Holman, C.; Kageson, P. Emissions of Ultrafine Particles from Different Types of Light Duty Vehicles. *Eur. Env. News Info. Service* **2001**, *10*, 1-22.

(18) Le Suer, W. M.; Norman, G. R. Reaction Product of High Molecular Weight Succinic Acids and Succinic Anhydrides with an Ethylene Polyamine. USP 3172892, 1967.

(19) Odian, G. Principles of Polymerization*;* Wiley: New York, 2004.

(20) Wollenberg, R. H.; Rafael, S.; Plavac, F. Modified Succinimides. USP 4612132, 1986.

(21) Tomlinson, A.; Danks, T. N.; Heyes, D. M.; Taylor, S. E.; Moreton, D. J. Interfacial Characterization of Succinimide Surfactants. *Langmuir* **1997**, *13*, 5881-5893.

(22) Forbes, E. S.; Neustadter, E. L. The Mechanism of Action of Polyisobutenyl Succinimide Lubricating Oil Additives. *Tribology* **1972**, *5*, 72-77.

(23) Harrison, J. J.; Novara, C. Polymeric Dispersants Having Alternating Polyalkylene and Succinic Groups. USP 5112507, 1992.

(24) Wollenberg, R. H.; Rafael, S.; Plavac, F. Modified Succinimide. USP 4802893, 1989.

(25) Smeeth, M.; Spikes, H.; Gunsel, S. Boundary Film Formation by Viscosity Index Improvers. *Tribol. Trans.* **1996**, *39*, 726-734.

(26) Tanveer, S.; Prasad, R. Enhancement of Viscosity Index of Mineral Base Oils. *Indian J. Chem. Technol.* **2006**, *13*, 398.

(27) Wouters, M. E. L.; Litvinov, V. M.; Binsbergen, F. L.; Goossens, J. G. P.; Van Duin, M.; Dikland, H. G. Morphology of Ethylene-Propylene Copolymer Based Ionomers as Studied by Solid State NMR and Small Angle X- Ray Scattering in Relation to some Mechanical Properties. *Macromolecules* **2003**, *36*, 1147-1156.

(28) Spiess, H. W. Nuclear Magnetic Resonance Spectroscopy in Macromolecular Science. *Macromol. Chem. Phys.* **2003**, *204*, 340-346.

(29) Mitsui, K.; Hara, M.; Ikai, A. Mechanical Unfolding of A2- Macroglobulin Molecules with Atomic Force Microscope. *FEBS Lett.* **1996**, *385*, 29-33.

(30) Duhamel, J. Polymer Chain Dynamics in Solution Probed with a Fluorescence Blob Model. *Acc. Chem. Res.* **2006**, *39*, 953-960.

(31) Zhang, M.; Duhamel, J. Study of the Microcrystallization of Ethylene-Propylene Random Copolymers in Solution by Fluorescence. *Macromolecules* **2007**, *40*, 661-669.

(32) Lakowicz, J. R. In *Principles of Fluorescence Spectroscopy;* Plenum Press: Baltimore, Maryland, 1986.

(33) Ono, K.; Ueda, K.; Sasaki, T.; Murase, S.; Yamamoto, M. Fluorescence Depolarization Study of Local Motions in Polymers at the Θ Temperature. *Macromolecules* **1996**, *29*, 1584-1588.

(34) Wilemski, G.; Fixman, M. Diffusion-Controlled Intrachain Reactions of Polymers. I Theory. *J. Chem. Phys.* **1974**, *60*, 866-877.

(35) Wilemski, G.; Fixman, M. Diffusion-Controlled Intrachain Reactions of Polymers. II Results for a Pair of Terminal Reactive Groups. *J. Chem. Phys.* **1974**, *60*, 878-890.

(36) Mathew, A. K.; Siu, H.; Duhamel, J. A Blob Model to Study Chain Folding by Fluorescence. *Macromolecules* **1999**, *32*, 7100-7108.

(37) Berlman, I. B. *Handbook of Fluorescence Spectra of Aromatic Molecules*; Academic Press Inc: University of Michigan 1965.

(38) Birks, J. B. *Photophysics of Aromatic Molecules*; Wiley: New York, 1970.

(39) Duhamel, J. New Insights in the Study of Pyrene Excimer Fluorescence to Characterize Macromolecules and their Supramolecular Assemblies in Solution. *Langmuir* **2012**, *28*, 6527-6538.

(40) Nakajima, A. Fluorescence Spectra of Pyrene in Chlorinated Aromatic Solvents. *J. Lumin.* **1976**, *11*, 429-432.

(41) Farhangi, S.; Weiss, H.; Duhamel; J. Effect of Side-Chain Length on the Polymer Chain Dynamics of Poly(alkyl methacrylate)s in Solution. *Macromolecules* **2013**, *24*, 9738-9747.

(42) Duggal, A.; Jiang, S.; Duhamel, J.; Pirouz, S. Quantifying the Level of Intermacromolecular Interactions by Using Pyrene Excimer Formation. USP(pending), 2014.

(43) Winnik, M. A.; Li, X.-B.; Guillet, J. E. Cyclization Dynamics of Polymers. 13. Effects of Added Polymer on the Conformation and Dynamics of Polystyrene Containing Evenly Spaced Pyrene Groups. Macromolecules **1984**, 17, 699-702.

(44) Jao, T. -C.; Mishra, M. K.; Rubin, I. D. Studies on Ethylene-Propylene Copolymer in Hydrocarbon Solvents by Fluorescence Probe Method. *Macromol. Reports* **1992**, *29*, 283-292.

(45) Ingratta, M.; Duhamel, J. Effect of Viscosity on Long Range Polymer Chain Dynamics in Solution Studied with a Fluorescence Blob Model. *Macromolecules* **2009**, *42*, 1244-1251.

(46) Kalyanasundaram, K.; Thomas, J. K. Environmental Effects on Vibronic Band Intensities in Pyrene Monomer Fluorescence and their Application in Studies of Micellar Systems. *J. Am. Chem. Soc.* **1977**, *99*, 2039-2044.

(47) Birks, J. B.; Dyson, D. J.; Munro, I. H. Excimer Fluorescence. II. Lifetime Studies of Pyrene Solutions. *Proc. Royal Soc. Series A, Math. Phys. Sci.* **1963**, *275*, 575-588.

(48) Duhamel, J. Internal Dynamics of Dendritic Molecules Probed by Pyrene Excimer Formation. *Polymers* **2012**, *4*, 211-239.

(49) Winnik, M.A.; Redpath, T.; Richards, D.H. The Dynamics of End-to-End Cyclization in Polystyrene Probed by Pyrene Excimer Formation. *Macromolecules* **1980**, *13*, 328–335.

(50) Siu, H.; Duhamel, J. Comparison of the Association Level of a Hydrophobically Modified Associative Polymer Obtained from an Analysis Based on Two Different Models. J. Phys. Chem. B **2005**, 109, 1770−1780.

(51) Winnik, M. A. End-to-End Cyclization of Polymer Chains. *Acc. Chem. Res.* **1985**, *18*, 73-79.

(52) Ingratta, M.; Hollinger, J.; Duhamel, J. A Case for Using Randomly Labeled Polymers to Study Long-Range Polymer Chain Dynamics by Fluorescence. *Am. Chem. Soc.* **2008,** *130*, 9420-9428.

(53) Yip, J.; Duhamel, J.; Qiu, X. P.; Winnik, F. M. Long-Range Polymer Chain Dynamics of Pyrene-Labeled Poly(*N*-Isopropylacrylamide)s Studied by Fluorescence. *Macromolecules* **2011**, *44*, 5363-5372.

(54) Yip, J.; Duhamel, J.; Bahun, G. J.; Adronov, A. A Study of the Dynamics of the Branch Ends of a Series of Pyrene-Labeled Dendrimers Based on Pyrene Excimer Formation. *J. Phys. Chem. B* **2010**, *114*, 10254-10265.

(55) Fowler, M. A.; Duhamel, J.; Bahun, G. J.; Adronov, A.; Zaragoza-Galán, G.; Rivera, E. Studying Pyrene-Labeled Macromolecules with the Model Free Analysis. *J. Phys. Chem. B* **2012**, *116*, 14689-14699.

(56) Nemeth, S.; Jao, T. -C.; Fendler, J. H. Concentration- and Solvent-Dependent Excimer Formation of 1-Pyrenylmethanamine, Covalently Attached to Maleic Anhydride-Grafted Ethylene-Propylene Copolymers. *Macromolecules* **1994**, *27*, 5449-5456.

(57) Winnik, F. M. Photophysics of Preassociated Pyrenes in Aqueous Polymer Solutions and in Other Organized Media. *Chem. Rev.* **1993**, *93*, 587-614.

(58) Jao, T. -C.; Mishra, K. M.; Rubin, I. D.; Duhamel, J.; Winnik, M. A. Characterization of the Ground-State Pyrene Complex in Ethylene-Propylene Copolymer Solutions. *J. Polym. Sci. Part B Polym. Phys*, **1995**, *33*, 1173-1181.

(59) Duhamel, J. Global Analysis of Fluorescence Decays to Probe the Internal Dynamics of Fluorescently Labeled Macromolecules. *Langmuir* **2014**, *30*, 2307-2324.

(60) Duhamel, J.; Yekta, A.; Winnik, M. A.; Jao, T.-C.; Mishra, M. K.; Rubin, I. D. A Blob Model to Study Polymer Chain Dynamics in Solution. *J. Phys. Chem.* **1993**, *97*, 13708-13712.

(61) Nemeth, S.; Jao, T. -C.; Fendler, J. H. Distribution of Functional Groups Grafted Onto an Ethylene-Propylene Copolymer. *J. Polym. Sci.: Part B Polym. Phys.* **1996**, *34*, 1723-1732.

(62) Vangani, V.; Duhamel, J. Study of a Polymeric Network by Dynamic Fluorescence Quenching Using a Blob Model. *Macromolecules* **1999**, *32*, 2845-2854.

(63) Mathew, A. K.; Duhamel, J.; Gao, J. Maleic Anhydride Modified Oligo (Isobutylene): Effect of Hydrogen Bonding on its Associative Strength in Hexane Characterized by Fluorescence Spectroscopy. *Macromolecules* **2001**, *34*, 1454-1469.

(64) Zhang, M.; Duhamel, J.; Van Duin, M.; Meessen, P. Characterization by Fluorescence of the Distribution of Maleic Anhydride Grafted Onto Ethylene-Propylene Copolymers. *Macromolecules* **2004**, *37*, 1877-1890.

(65) Zhang, M.; Duhamel, J. Study of Maleated Ethylene-Propylene Copolymers by Fluorescence: Evidence for Succinimide Induced Polar Associations in an Apolar Solvent. *Eur. Polym. J.* **2008**, *44*, 3005-3014.

(66) Zhang, M.; Duhamel, J. Effect of Solvent Quality toward the Association of Succinimide Pendants of a Modified Ethylene-Propylene Copolymer in Mixtures of Toluene and Hexane. *Macromolecules* **2005**, *38*, 4438-4446.

(67) Stevens, B.; Ban, M. I. Spectrophotometric Determination of Enthalpies and Entropies of Photoassociation for Dissolved Aromatic Hydrocarbons. *Trans. Far. Soc*. **1964**, *60*, 1515–1523.

(68) Cuniberti, C.; Perico, A. Intramolecular Excimer Formation in Polymers: Pyrene Labeled Polyvinylacetate. *Eur. Polym. J.* **1980**, *16*, 887-893.

(69) Pirouz, S.; Wang, Y.; Chong, J. M.; Duhamel, J. Characterization of the Chemical Composition of Polyisobutylene-Based Oil-Soluble Dispersants by Fluorescence. *J Phys. Chem. B* **2014**, *118*, 3899-3911.

Chapter 2

(1) Rudnik, L. R. In *Chemistry and Application;* Barbadsz, E. A., Lamb, G. D., Eds.; Lubricant Additives; CRC Press, Boca Raton: Florida, 2003; pp 458-490.

(2) Mortier, R. M.; Malcolm, F. F.; Orszulik, S. T. In *Chemistry and Technology of Lubricants;* Springer: London, 2009.

(3) Jao, T. C.; Passut, C. A. In *Part D: Formulation, Surfactant Science Series;* Showell, M. S., Ed.; Handbook of Detergents; CRC Press, Boca Raton: Florida, 2006; pp 437-471.

(4) Wollenberg, R. H.; Rafael, S.; Plavac, F. Modified Succinimides. USP 4612132, 1986.

(5) Gwinn, M. R.; Vallyathan, V. Nanoparticles: Health Effects - Pros and Cons. *Environ. Health Perspect.* **2006**, *114*, 1818-1825.

(6) Farnlund, J.; Holman, C.; Kageson, P. Emissions of Ultrafine Particles from Different Types of Light Duty Vehicles. *Eur. Env. News Info. Service* **2001**, *10*, 1-22.

(7) Wood, J. Canadian Environmental Indicators-Air Quality. *Studies in Environmental Policies. Fraser Inst.* 2012, pp 1-69.

(8) Reisch, M. S. Tough Diesel Rule Fuels Opportunity. *Chem. Eng. News* **2005**, *5*, 20-22.

(9) Aldajah, S.; Ajayi, O. O.; Fenske, G. R.; Goldblatt. I. L. Effect of Exhaust Gas Recirculation (EGR) Contamination of Diesel Engine Oil on Wear. *Wear* **2007**, *263*, 93-98.

(10) Tomlinson, A.; Scherer, B.; Karakosta, E.; Oakey, M.; Danks, T. N.; Heyes, D. M.; Taylor, S. E. Adsorption Properties of Succinimide Dispersants on Carbonaceous Substrates. *Carbon* **2000**, *38*, 13-28.

(11) Tomlinson, A.; Danks, T. N.; Heyes, D. M.; Taylor, S. E.; Moreton, D. J. Interfacial Characterization of Succinimide Surfactants. *Langmuir* **1997**, *13*, 5881-5893.

(12) Forbes, E. S.; Neustadter, E. L. The Mechanism of Action of Polyisobutenyl Succinimide Lubricating Oil Additives. *Tribology* **1972**, *5*, 72-77.

(13) Atta, A. M.; El-Ghazawy, R. A. M.; Farag, R. K.; Abdel-Azim, A.-A. A. Crosslinked Reactive Macromonomers Based on Polyisobutylene and Octadecyl Acrylate Copolymers as Crude Oil Sorbers. *React. Funct. Polym.* **2006**, *66*, 931-943.

(14) Lee, P. T. C.; Chiu, C.-W.; Lee, T.-M.; Chang, T.-Y.; Wu, M.-T.; Cheng, W.-Y.; Kuo, S.-W.; Lin, J.-J. First Fabrication of Electrowetting Display by Using Pigment-in-Oil Driving Pixels. *ACS Appl. Mat. Interfraces* **2013**, *5*, 5914-5920.

(15) Hsu, C.-P.; Chang, L.-Y. ; Chiu, C.-W. ; Lee, P. T. C. ; Lin, J.-J. Facile Fabrication of Robust Superhydrophobic Epoxy Film with Polyamine Dispersed Carbon Nanotubes. *ACS Appl. Mat. Interfaces* **2013**, *5*, 538-545.

(15) Le Suer, W. M.; Norman, G. R. Reaction Product of High Molecular Weight Succinic Acids and Succinic Anhydrides with an Ethylene Polyamine. USP 3172892, 1967.

(17) Stuart, A. F.; Orinda, R. G.; Anderson, N.; Drummond, A. Y. Alkenyl Succinimides of Tetraethylene Pentamine. USP 3202678, 1965.

(18) Myers, D. In *Surfactant Science and Technology;* John Wiley & Sons: Hoboken, New Jeresey, 2006.

(19) Le Suer, W. M.; Norman, G. R. Fire Resistant Hydraulic Fluid. USP 3272747, 1966.

(20) Mark, E. J.; Ermama, B.; Eirich, F. R. In *Science and Technology of Rubber;* Elsevier: Akron, Ohio, 2005.

(21) Tessier, M.; Marechal, E. Synthesis of A-Phenyl-Ω-Anhydride Oligoisobutylene and A,Ω-Dianhydride Oligoisobutylene. *Eur. Polym. J.* **1990**, *26*, 499-508.

(22) Shen, Y.; Duhamel, J. Micellization and Adsorption of a Series of Succinimide Dispersants. *Langmuir* **2008**, *24*, 10665-10673.

(23) Dubois-Clochard, M. C.; Durand, J. P.; Delfort, B.; Gateau, P.; Barré, L.; Blanchard, I.; Chevalier, Y.; Gallo, R. Adsorption of Polyisobutenylsuccinimide Derivatives at a Solid-Hydrocarbon Interface. *Langmuir* **2001**, *17*, 5901-5910.

(24) Tessier, M.; Maréchal, E. Synthesis of Mono and Difunctional Oligoisobutylenes-III. Modification of a-Chlorooligoisobutylene by Reaction with Maleic Anhydride. *Eur. Polym. J.* **1984**, *20*, 269-280.

(25) Wollenberg, R. H.; Rafael, S.; Plavac, F. Modified Succinimide. USP 4802893, 1989.

(26) Harrison, J. J.; Ruhe, W. R. Fuel Compositions Having Polyalkylene Succinimides and Preparation Thereof. USP 5853434, 1998.

(27) Walch, E.; Gaymans, R. J. Telechelic Polyisobutylene with Unsaturated End Groups and with Anhydride End Groups. *Polymer* **1994**, *35*, 1774-1778.

(28) Mathew, A. K.; Duhamel, J.; Gao, J. Maleic Anhydride Modified Oligo(Isobutylene): Effect of Hydrogen Bonding on its Associative Strength in Hexane Characterized by Fluorescence Spectroscopy. *Macromolecules* **2001**, *34*, 1454-1469.

(29) Sippel, T. O. Microfluorometric Analysis of Protein Thiol Groups with a Coumarinylphenylmaleimide. *J. Histochem. Cytochem.* **1981**, *29*, 1377-1381.

(30) Phelan, J. C.; Sung, C. S. P. Fluorescence Characteristics of Cure Products in Bis(Maleimide)/Diallylbisphenol A Resin. *Macromolecules* **1997**, *30*, 6837-6844.

(31) Kanaoka, Y.; Machida, M.; Ban, Y.; Takamitsu, S. Fluorescence and Structure of Proteins as Measured by Incorporation of Fluorophore. II. Synthesis of Maleimide Derivatives as Fluorescence-Labeled Protein-Sulfhydryl Reagents. *Chem. Pharm. Bull.* **1967**, *15*, 1738-1743.

(32) Pucci, A.; Rausa, R.; Ciardelli, F. Aggregation-Induced Luminescence of Polyisobutene Succinic Anhydrides and Imides. *Macromol. Chem. Phys.* **2008**, *209*, 900-906.

(33) Winnik, M. A.; Bystryak, S. M.; Liu, Z.; Siddiqui, J. Synthesis and Characterization of Pyrene-Labeled Poly(Ethylenimine). *Macromolecules* **1998**, *31*, 6855-6864.

(34) Lakowicz, J. R. In *Principles of Fluorescence Spectroscopy;* Plenum Press: Baltimore, Maryland, 1986.

(35) Winnik, F. M. Photophysics of Pre-associated Pyrenes in Aqueous Polymer Solutions and in Other Organized Media. *Chem. Rev.* **1993**, *93*, 587 – 614.

Chapter 3

(1) Mortier, R. M.; Malcolm, F. F.; Orszulik, S. T. In *Chemistry and Technology of Lubricants;* Springer: London, 2009.

(2) Jao, T. C.; Passut, C. A. In *Part D: Formulation, Surfactant Science Series;* Showell, M. S., Ed.; Handbook of Detergents; CRC Press, Boca Raton: Florida, 2006.

(3) Barbadsz, E. A.; Lamb, G. D. Eds. In *Chapter 19: Additives for Crankcase Lubricant Applications*; Rudnik, L. R. Lubricant Additives: Chemistry and Application*;* CRC Press, Boca Raton: Florida, 2003; pp 458-490.

(4) Gwinn, M. R.; Vallyathan, V. Nanoparticles: Health Effects-Pros and Cons. *Environ. Health Perspect.* **2006**, *114*, 1818-1825.

(5) Tomlinson, A.; Danks, T. N.; Heyes, D. M.; Taylor, S. E.; Moreton, D. J. Interfacial Characterization of Succinimide Surfactants. *Langmuir* **1997**, *13*, 5881-5893.

(6) Forbes, E. S.; Neustadter, E. L. The Mechanism of Action of Polyisobutenyl Succinimide Lubricating Oil Additives. *Tribology* **1972**, *5*, 72-77.

(7) Le Suer, W. M.; Norman, G. R. Fire Resistant Hydraulic Fluid. USP 3272747, 1966.

(8) Le Suer, W. M.; Norman, G. R. Reaction Product of High Molecular Weight Succinic Acids and Succinic Anhydrides with an Ethylene Polyamine. USP 3172892, 1967.

(9) Stuart, A. F.; Orinda, R. G.; Anderson, N.; Drummond, A. Y. Alkenyl Succinimides of Tetraethylene Pentamine. USP 3202678, 1965.

(10) Myers, D. In *Surfactant Science and Technology;* John Wiley & Sons: Hoboken, New Jeresey, 2006.

(11) Harrison, J. J.; Novara, C. Polymeric Dispersants Having Alternating Polyalkylene and Succinic Groups. USP 5112507, 1992.

(12) Nalesnik, T. E.; Cusano, C. M. Dibaisic Acid Lubricating Oil Dispersant and Viton Seal Additives. USP 4663064, 1987.

(13) Wollenberg, R. H.; Rafael, S.; Plavac, F. Modified Succinimide. USP 4802893, 1989.

(14) Wollenberg, R. H.; Rafael, S.; Plavac, F. Modified Succinimides. USP 4612132, 1986

(15) Odian, G. Principles of Polymerization*;* Wiley: New York, 2004.

(16) Mark, E. J.; Ermama, B.; Eirich, F. R. In *Science and Technology of Rubber;* Elsevier: The University of Akron, Akron, Ohio, 2005.

(17) Tessier, M.; Maréchal, E. Synthesis of Mono and Difunctional Oligoisobutylenes-III. Modification of a-Chlorooligoisobutylene by Reaction with Maleic Anhydride. *Eur. Poly. J.* **1984**, *20*, 269-280.

(18) Shen, Y.; Duhamel, J. Micellization and Adsorption of a Series of Succinimide Dispersants. *Langmuir* **2008**, *24*, 10665-10673.

(19) Dubois-Clochard, M. C.; Durand, J. P.; Delfort, B.; Gateau, P.; Barré, L.; Blanchard, I.; Chevalier, Y.; Gallo, R. Adsorption of Polyisobutenyl Succinimide Derivatives at a Solid-Hydrocarbon Interface. *Langmuir* **2001**, *17*, 5901-5910.

(20) Pirouz, S.; Wang, Y.; Chong, J. M.; Duhamel, J. Characterization of the Chemical Composition of Polyisobutylene-Based Oil-Soluble Dispersants by Fluorescence. *J. Phys. Chem. B* **2014**, *118*, 3899-3911.

(21) Chevalier, Y.; Dubois-Clochard, M. C.; Durand, J. P. Adsorption of Poly(Isobutenylsuccinimide) Dispersants at a Solid-Hydrocarbon Interface. *Prog. Colloid Polym. Sci.* **2001**, *18*, 110-114.

(22) Won, Y.; Meeker, S. P.; Trappe, V.; Weitz, D. A. Effect of Temperature on Carbon-Black Agglomeration in Hydrocarbon Liquid with Adsorbed Dispersant. *Langmuir* **2005**, 21, 924-932.

(23) Phelan, J. C.; Sung, C. S. P. Fluorescence Characteristics of Cure Products in Bis(Maleimide)/Diallylbisphenol A Resin. *Macromolecules* **1997**, *30*, 6837-6844.

(24) Kanaoka, Y.; Machida, M.; Ban, Y.; Takamitsu, S. Fluorescence and Structure of Proteins as Measured by Incorporation of Fluorophore. II. Synthesis of Maleimide Derivatives as Fluorescence-Labeled Protein-Sulfhydryl Reagents. *Chem. Pharm. Bull.* **1967**, *15*, 1738-1743.

(25) Pucci, A.; Rausa, R.; Ciardelli, F. Aggregation-Induced Luminescence of Polyisobutene Succinic Anhydrides and Imides. *Macromol. Chem. Phys.* **2008**, *209*, 900-906.

(26) Winnik, M. A.; Bystryak, S. M.; Liu, Z.; Siddiqui, J. Synthesis and Characterization of Pyrene-Labeled Poly(Ethylenimine). *Macromolecules* **1998**, *31*, 6855-6864.

(27) Tomlinson, A.; Scherer, B.; Karakosta, E.; Oakey, M.; Danks, T. N.; Heyes, D. M.; Taylor, S. E. Adsorption Properties of Succinimide Dispersants on Carbonaceous Substrates. *Carbon* **2000**, *38*, 13-28.

Chapter 4

(1) Pawlak, Z. In *Tribochemistry of lubricating oils;* Elsevier: Poland, 2003; Vol. 45.

(2) Zhang, M.; Duhamel, J. Study of the Microcrystallization of Ethylene-Propylene Random Copolymers in Solution by Fluorescence. *Macromolecules* **2007**, *40*, 661-669.

(3) Rubin, I. D.; Sen, A. Solution Viscosities of Ethylene-Propylene Copolymers in Oils. *J. Appl. Polym. Sci.* **1990**, *40*, 523-530.

(4) Sen, A.; Rubin, I. D. Molecular Structures and Solution Viscosities of Ethylene-Propylene Copolymers. *Macromolecules* **1990**, *23*, 2519-2524.

(5) LaRiviere, D.; Asfour, A. A.; Hage, A.; Gao, J. Viscometric Properties of Viscosity Index Improvers in Lubricant Base Oil over a Wide Temperature Range. Part I: Group II Base Oil. *Lubr. Sci.* **2000**, *12*, 133-143.

(6) Tanveer, S.; Prasad, R. Enhancement of Viscosity Index of Mineral Base Oils. *Indian J. Chem. Technol.* **2006**, *13*, 398-403.

(7) Mihaljuš S. V.; Podobnik, M.; Bambić, J. Engine Oil Viscosity Index Improver Behaviour at Extended Shear Stability. *Fuels Lubr.* **2008**, *47*, 118-128.

(8) Kucks, M. J.; Ou-Yang, H. D.; Rubin, I. D. Ethylene-Propylene Copolymer Aggregation in Selective Hydrocarbon Solvents. *Macromolecules* **1993**, *26*, 3846-3850.

(9) Port, W. S.; O'Brien, J. W.; Hansen, J. E.; Swern, D. Viscosity Index Improvers for Lubricating Oils. Polyvinyl Esters of Long-Chain Fatty Acids. *Ind. & Eng. Chem.* **1951**, *43*, 2105-2107.

(10) Rudnik, L. R. In *Chemistry and Application;* Barbadsz, E. A.; Lamb, G. D. Eds.; Lubricant Additives; CRC Press, Boca Raton: Florida, 2003; pp 458-490.

(11) Mortier, R. M.; Malcolm, F. F.; Orszulik, S. T. In *Chemistry and Technology of Lubricants;* Springer: London, 2009.

(12) Anghel, D. F.; Alderson, V.; Winnik, F. M.; Mizusaki, M.; Morishima, Y. Fluorescent Dyes as Model 'Hydrophobic Modifiers' of Polyelectrolytes: A Study of Poly(Acrylic Acid)s Labeled with Pyrenyl and Naphthyl Groups. *Polymer* **1998**, *39*, 3035-3044.

(13) Yamamoto, H.; Mizusaki, M.; Yoda, K.; Morishima, Y. Fluorescence Studies of Hydrophobic Association of Random Copolymers of Sodium 2-(Acrylamido)-2-Methylpropanesulfonate and N-Dodecylmethacrylamide in Water. *Macromolecules* **1998**, *31*, 3588-3594.

(14) Winnik, F. M.; Regismond, S. T. A. Fluorescence Methods in the Study of the Interactions of Surfactants with Polymers. *Colloid Surf. A. Physicochem. Eng. Aspects* **1996**, *118*, 1-39.

(15) Birks, J. B.; Dyson, D. J.; Munro, I. H. Excimer Fluorescence. II. Lifetime Studies of Pyrene Solutions. *Proc. Royal Soc. Series A, Math. Phys. Sci.* **1963**, *275*, 575-588.

(16) Vangani, V.; Drage, J.; Mehta, J.; Mathew, A. K.; Duhamel, J. Maleated Ethylene-Propylene Random Copolymers: Determination of the Microstructure and Association Level by Fluorescence Spectroscopy. *J. Phys. Chem. B* **2001**, *105*, 4827-4839.

(17) Zhang, M.; Duhamel, J. Effect of Solvent Quality Toward the Association of Succinimide Pendants of a Modified Ethylene-Propylene Copolymer in Mixtures of Toluene and Hexane. *Macromolecules* **2005**, *38*, 4438-4446.

(18) Zhang, M.; Duhamel, J. Study of Maleated Ethylene-Propylene Copolymers by Fluorescence: Evidence for Succinimide Induced Polar Associations in an Apolar Solvent. *Eur. Polym. J.* **2008**, *44*, 3005-3014.

(19) Kim, S. D.; Torkelson, J. M. Nanoscale Confinement and Temperature Effects on Associative Polymers in Thin Films: Fluorescence Study of a Telechelic, Pyrene-Labeled Poly(Dimethylsiloxane). *Macromolecules* **2002**, *35*, 5943-5952.

(20) Ingratta, M.; Duhamel, J. Correlating Pyrene Excimer Formation with Polymer Chain Dynamics in Solution. Possibilities and Limitations. *Macromolecules* **2007**, *40*, 6647-6657.

(21) Alshaiban, A.; Soares, J. B. P. Effect of Hydrogen and External Donor on Propylene Polymerization Kinetics with a 4th Generation Ziegler-Natta Catalyst. *Macro. React. Eng.* **2012**, *6*, 265-274.

(22) Randall, J. C. A Review of High Resolution Liquid 13Carbon Nuclear Magnetic Resonance Characterizations of Ethylene-Based Polymers. *J. Macro. Sci. Rev. Macr. Chem. Phys.* **1989**, *C29*, 201-317.

(23) Heinen, W.; Rosenmöller, C. H.; Wenzel, C. B.; De Groot, H. J. M..; Lugtenburg, J. ^{13}C NMR Study of the Grafting of Maleic Anhydride onto Polyethene, Polypropene, and Ethene−Propene Copolymers. *Macromolecules* **1996**, *29*, 1151-1157.

(24) Nemeth, S.; Jao, T.-C.; Fendler, J. H. Excimer Formation in 1-Pyrenyl-methane-amine *Photochem. Photobiol. A: Chem*. **1994**, *78*, 22-235.

(25) Wollenberg, R. H.; Rafael, S.; Plavac, F. Modified Succinimide. USP 4802893, 1989.

(26) Mathew, A. K.; Siu, H.; Duhamel, J. A Blob Model to Study Chain Folding by Fluorescence. *Macromolecules* **1999**, *32*, 7100-7108.

(27) Gaylord, N. G.; Mishra, M. K. Nondegradative Reaction of Maleic Anhydride and Molten Polypropylene in the Presence of Peroxides. *J. Polym. Sci.: Polym. Let. Ed.* **1983**, *21*, 23-30.

(28) Gaylord, N. G.; Mehta, M.; Mehta, R. Degradation and Cross-linking of Ethylene-propylene Copolymer Rubber on Reaction with Maleic Anhydride and/or Peroxides. *J. Appl. Polym. Sci.* **1987**, *33*, 2549-2558.

(29) Mizusaki, M.; Morishima, Y.; Winnik, F. M. Hydrophobically Modified Poly(Sodium 2-Acrylamido-2-Methylpropanesulfonate)s Bearing Octadecyl Groups: A Fluorescence Study of their Solution Properties in Water. *Macromolecules* **1999**, *32*, 4317-4326.

(30) Kujawa, P.; Liu, R. C.; Winnik, F. M. Do Fluorocarbon, Hydrocarbon, and Polycyclic Aromatic Groups Intermingle? A Study of the Interactions in Water between Fluorocarbon-and Hydrocarbon-Modified Poly(*N*-Isopropylacrylamides). *J. Phys. Chem. B* **2002**, *106*, 5578-5585.

(31) Nemeth, S.; Jao, T.-C.; Fendler, J. H. Concentration- and Solvent-Dependent Excimer Formation of 1-Pyrenemethylamine Covalently Attached to Maleic Anhydride-Grafted Ethylene-Propylene Copolymers. *Macromolecules* **1994**, *27*, 5449-5456.

(32) Duhamel, J. Internal Dynamics of Dendritic Molecules Probed by Pyrene Excimer Formation. *Polymers* **2012,** *4*, 211-239.

(33) Stevens, B.; Ban, M. I. Spectrophotometric Determination of Enthalpies and Entropies of Photoassociation for Dissolved Aromatic Hydrocarbons. *Trans. Far. Soc*. **1964**, *60*, 1515–1523.

Chapter 5

(1) Pawlak, Z. In *Tribochemistry of Lubricating Oils;* Elsevier: Poland, 2003; Vol. 45.

(2) Zhang, M.; Duhamel, J. Study of the Microcrystallization of Ethylene-Propylene Random Copolymers in Solution by Fluorescence. *Macromolecules* **2007**, *40*, 661-669.

(3) Rubin, I. D.; Sen, A. Solution Viscosities of Ethylene–Propylene Copolymers in Oils. *J. Appl. Polym. Sci.* **1990**, *40*, 523-530.

(4) Sen, A.; Rubin, I. D. Molecular Structures and Solution Viscosities of Ethylene-Propylene Copolymers. *Macromolecules* **1990**, *23*, 2519-2524.

(5) Mihaljuš S. V.; Podobnik, M.; Bambić, J. Engine Oil Viscosity Index Improver Behaviour at Extended Shear Stability. *Fuels Lubr.* **2008**, *47*, 118-128.

(6) Kucks, M. J.; Ou-Yang, H. D.; Rubin, I. D. Ethylene-Propylene Copolymer Aggregation in Selective Hydrocarbon Solvents. *Macromolecules* **1993**, *26*, 3846-3850.

(7) Port, W. S.; O'Brien, J. W.; Hansen, J. E.; Swern, D. Viscosity Index Improvers for Lubricating Oils. Polyvinyl Esters of Long-Chain Fatty Acids. *Ind. Eng. Chem.* **1951**, *43*, 2105-2107.

(8) Mortier, R. M.; Malcolm, F. F.; Orszulik, S. T. In *Chemistry and Technology of Lubricants;* Springer: London, 2009.

(9) Marsden, K. Literature Review of OCP Viscosity Modifiers. *Lubr. Sci.* **1989**, *1*, 265-280.

(10) Delmas, G.; Daviet, V.; Filiatrault, D. Determination of Composition of Ethylene-Propylene Copolymers by Intrinsic Viscosity. *J. Polym. Sci., Polym. Phys. Ed.* **1976**, *14*, 1629-1639.

(11) Filiatrault, D.; Delmas, G. Intrinsic Viscosities and Huggins' Constant for Ethylene-Propylene Copolymers. *Macromolecules* **1979**, *12*, 65-68.

(12) Zhang, M.; Duhamel, J.; Van Duin, M.; Meessen, P. Characterization by Fluorescence of the Distribution of Maleic Anhydride Grafted onto Ethylene-Propylene Copolymers. *Macromolecules* **2004**, *37*, 1877-1890.

(13) Zhang, M.; Duhamel, J. Effect of Solvent Quality Toward the Association of Succinimide Pendants of a Modified Ethylene-Propylene Copolymer in Mixtures of Toluene and Hexane. *Macromolecules* **2005**, *38*, 4438-4446.

(14) Jao, T. C.; Mumnmaya, K. M.; Rubin, I. D.; Duhamel, J.; Winnik, M. A. Characterization of the Ground State Pyrene Complex in Ethylene-Propylene Copolymer Solutions. *J. Polym. Sci., Polym. Phys. Ed.* **1995**, *83*, 1173-1181.

(15) a) Duggal, A.; Jiang, S.; Duhamel, J.; Pirouz, S. Quantifying the Level of Intermacromolecular Interactions by Using Pyrene Excimer Formation. USP(pending), 2014. b) Pirouz, S.; Duhamel, J.; Jiang, S.; Duggal, A. Quantifying the Level of Intermacromolecular Between EP Copolymer Interactions by Using Pyrene Excimer Formation. *Macromolecules* **2015**, 48, 4620-4630.

(16) Alshaiban, A.; Soares, J. B. P. Effect of Hydrogen and External Donor on Propylene Polymerization Kinetics with a 4th Generation Ziegler-Natta Catalyst. *Macro. React. Eng.* **2012**, *6*, 265-274.

(17) Randall, J. C. A Review of High Resolution Liquid 13Carbon Nuclear Magnetic Resonance Characterizations of Ethylene-Based Polymers. *J. Macro. Sci. Rev. Macr. Chem. Phys.* **1989**, *C29*, 201-317.

(18) Heinen, W.; Rosenmöller, C. H.; Wenzel, C. B.; De Groot, H. J. M..; Lugtenburg, J. ^{13}C NMR Study of the Grafting of Maleic Anhydride onto Polyethene, Polypropene, and Ethene−Propene Copolymers. *Macromolecules* **1996**, *29*, 1151-1157.

(19) Nemeth, S.; Jao, T.-C.; Fendler, J. H. Excimer Formation in 1-Pyrenyl-methane-amine *Photochem. Photobiol. A: Chem*. **1994**, *78*, 22-235.

(20) Birks, J. B.; Dyson, D. J.; Munro, I. H. Excimer Fluorescence. II. Lifetime Studies of Pyrene Solutions. *Proc. Royal Soc. Series A, Math. Phys. Sci.* **1963**, *275*, 575-588.

(21) Nemeth, S.; Jao, T. C.; Fendler, J. H. Concentration- and Solvent-Dependent Excimer Formation of 1-Pyrenemethylamine Covalently Attached to Maleic Anhydride-Grafted Ethylene-Propylene Copolymers. *Macromolecules* **1994**, *27*, 5449-5456.

(22) Duhamel, J. Internal Dynamics of Dendritic Molecules Probed by Pyrene Excimer Formation. *Polymers* **2012,** *4*, 211-239.

Chapter 6

(1) Pawlak, Z. In *Tribochemistry of Lubricating Oils;* Elsevier: Poland, 2003; Vol. 45.

(2) Zhang, M.; Duhamel, J. Study of the Microcrystallization of Ethylene-Propylene Random Copolymers in Solution by Fluorescence. *Macromolecules* **2007**, *40*, 661-669.

(3) Rubin, I. D.; Sen, A. Solution Viscosities of Ethylene-Propylene Copolymers in Oils. *J. Appl. Polym. Sci.* **1990**, *40*, 523-530.

(4) Sen, A.; Rubin, I. D. Molecular Structures and Solution Viscosities of Ethylene-Propylene Copolymers. *Macromolecules* **1990**, *23*, 2519-2524.

(5) LaRiviere, D.; Asfour, A. A.; Hage, A.; Gao, J. Viscometric Properties of Viscosity Index Improvers in Lubricant Base Oil over a Wide Temperature Range. Part I: Group II Base Oil. *Lubr. Sci.* **2000**, *12*, 133-143.

(6) Tanveer, S.; Prasad, R. Enhancement of Viscosity Index of Mineral Base Oils. *Indian J. Chem. Technol.* **2006**, *13*, 398-403.

(7) Mihaljuš S. V.; Podobnik, M.; Bambić, J. Engine Oil Viscosity Index Improver Behaviour at Extended Shear Stability. *Fuels Lubr.* **2008**, *47*, 118-128.

(8) Kucks, M. J.; Ou-Yang, H. D.; Rubin, I. D. Ethylene-Propylene Copolymer Aggregation in Selective Hydrocarbon Solvents. *Macromolecules* **1993**, *26*, 3846-3850.

(9) Port, W. S.; O'Brien, J. W.; Hansen, J. E.; Swern, D. Viscosity Index Improvers for Lubricating Oils. Polyvinyl Esters of Long-Chain Fatty Acids. *Ind. Eng. Chem.* **1951**, *43*, 2105-2107.

(10) Handlin, D. L.; Rhodos, R. B.; Stevens, C. A. Star Polymer Viscosity Index Improver for Lubricating Oil Compositions. UP 0700942A2, 1996.

(11) Rudnik, L. R. In *Chemistry and Application;* Barbadsz, E. A.; Lamb, G. D. Eds.; Lubricant Additives; CRC Press, Boca Raton: Florida, 2003; pp 458-490.

(12) Staumbaugh, R. L.; Kinder, B. G. Viscosity Index and Thickeners In *Chemistry and Technology of Lubricants*. Eds. Mortier, R. M.; Malcolm, F. F.; Orszulik, S. T., Springer: London, 2009, pp 158.

(13) Simon, A. M.; Herbert, F. X-ray Fluorescence Detection of Waste Engine Oil Residue in Asphalt and its Effect on Cracking in Service. *Int. J. Pav. Eng.* **2010**, *11*, 541-553.

(14) Castro, L. V.; Vazquez, F. Copolymers as Flow Improvers for Mexican Crude Oils. *Energy Fuel.* **2008**, *22*, 4006-4011.

(15) Anghel, D. F.; Alderson, V.; Winnik, F. M.; Mizusaki, M.; Morishima, Y. Fluorescent Dyes as Model 'Hydrophobic Modifiers' of Polyelectrolytes: A Study of Poly(Acrylic Acid)s Labeled with Pyrenyl and Naphthyl Groups. *Polymer* **1998**, *39*, 3035-3044.

(16) Yamamoto, H.; Mizusaki, M.; Yoda, K.; Morishima, Y. Fluorescence Studies of Hydrophobic Association of Random Copolymers of Sodium 2-(Acrylamido)-2-Methylpropanesulfonate and N-Dodecylmethacrylamide in Water. *Macromolecules* **1998**, *31*, 3588-3594.

(17) Winnik, F. M.; Regismond, S. T. A. Fluorescence Methods in the Study of the Interactions of Surfactants with Polymers. *Colloid Surf. A. Physicochem. Eng. Aspects* **1996**, *118*, 1-39.

(18) a) Duggal, A.; Sheng, J.; Duhamel, J.; Pirouz, S. Quantifying the Level of Intermacromolecular Interactions by Using Pyrene Excimer Formation. USP(pending), 2014. b) Duggal, A.; Sheng, J.; Duhamel, J.; Pirouz, S. Quantifying the Level of Intermacromolecular Between EP Copolymer Interactions by Using Pyrene Excimer Formation. Submitted for Publication, 2015.

(19) Vangani, V.; Drage, J.; Mehta, J.; Mathew, A. K.; Duhamel, J. Maleated Ethylene-Propylene Random Copolymers: Determination of the Microstructure and Association Level by Fluorescence Spectroscopy. *J. Phys. Chem. B* **2001**, *105*, 4827-4839.

(20) Zhang, M.; Duhamel, J. Effect of Solvent Quality Toward the Association of Succinimide Pendants of a Modified Ethylene-Propylene Copolymer in Mixtures of Toluene and Hexane. *Macromolecules* **2005**, *38*, 4438-4446.

(21) Zhang, M.; Duhamel, J. Study of Maleated Ethylene-Propylene Copolymers by Fluorescence: Evidence for Succinimide Induced Polar Associations in an Apolar Solvent. *Eur. Polym. J.* **2008**, *44*, 3005-3014.

(22) Kim, S. D.; Torkelson, J. M. Nanoscale Confinement and Temperature Effects on Associative Polymers in Thin Films: Fluorescence Study of a Telechelic, Pyrene-Labeled Poly(Dimethylsiloxane). *Macromolecules* **2002**, *35*, 5943-5952.

(23) Ingratta, M.; Duhamel, J. Correlating Pyrene Excimer Formation with Polymer Chain Dynamics in Solution. Possibilities and Limitations. *Macromolecules* **2007**, *40*, 6647-6657.

(24) Randall, J. C. A Review of High Resolution Liquid Carbon Nuclear Magnetic Resonance Characterizations of Ethylene-Based Polymers. *J. Macro. Sci. Rev. Macr. Chem. Phys.* **1989**, *C29*, 201-317.

(25) Alshaiban, A.; Soares, J. B. P. Effect of Hydrogen and External Donor on Propylene Polymerization Kinetics with a 4th Generation Ziegler-Natta Catalyst. *Macro. React. Eng.* **2012**, *6*, 265-274.

(26) API Base Oil Interchangeability Guidelines for Passenger Car Motor Oils and Diesel Engine Oils. *American Petroleum Institute*, API 1509, Appendix E, 2011.

(27) Heinen, W.; Rosenmöller, C. H.; Wenzel, C. B.; De Groot, H. J. M..; Lugtenburg, J. ^{13}C NMR Study of the Grafting of Maleic Anhydride onto Polyethene, Polypropene, and Ethene−Propene Copolymers. *Macromolecules* **1996**, *29*, 1151-1157.

(28) Nemeth, S.; Jao, T.-C.; Fendler, J. H. Excimer Formation in 1-Pyrenyl-Methane-Amine *Photochem. Photobiol. A: Chem*. **1994**, *78*, 22-235.

(29) Duhamel, J. Internal Dynamics of Dendritic Molecules Probed by Pyrene Excimer Formation. *Polymers* **2012,** *4*, 211-239.

(30) Irondi, K.; Zhang, M.; Duhamel, J. Study of the Semidilute Solutions of Poly(*N*,*N*-dimethylacrylamide) by Fluorescence and its Implications to the kinetics of Coil-to-Globule Transitions. *J. Phys. Chem. B*, **2006**, *110*, 2628-2637.

(31) Ingratta, M.; Mathew, M.; Duhamel,J. How Switching the Substituent of a Pyrene Derivative from a Methyl to a Butyl Affects the Fluorescence Response of Polystyrene Randomly Labeled with Pyrene. *Can. J. Chem.* **2010**, *88*, 217-227.

(32) Duhamel, J. New Insights in the Study of Pyrene Excimer Fluorescence to Characterize Macromolecules and their Supramolecular Assemblies in Solution. *Langmuir* **2012**, *28*, 6527-6538.

(33) Wei, B. Recent Advances on Mitigating Wax Problem Using Polymeric Wax Crystal Modifier. *J. Petrol. Explor. Prod. Technol. ASAP* **2015**.

(34) Radulescu, A.; Fetters, L. J.; Richter, D. Tailored Polymer Additives for Wax (Paraffin) Crystal Control. In Crude Oil Emulsions-Composition Stability and Composition. *Eds* El-Sayed Abdel-Raouf, M., InTech, Rijeka, Croatia, 2012, pp 205-230.

(35) Radulescu, A.; Fetters, L. J.; Richter, D. Polymer-Driven Wax Crystal Control Using Partially Crystalline Polymeric Materials. *Adv. Polym. Sci.* **2008**, *210*, 1-100.

(36) Richter, D.; Schneiders, D.; Monkenbush, M.; Willner, L.; Fetters, L. J.; Huang, J. S.; Lin, M.; Mortensen, K.; Farago, B. Polymer Aggregates with Crystalline Cores: The System Polyethylene-Poly(ethylenepropylene). *Macromolecules* **1997**, *30*, 1053-1068.

(37) Leube, W.; Monkenbush, M.; Schneiders, D.; Richter, D.; Adamson, D.; Fetters, L.; Dounis, P.; Lovegrove, R. Wax-Crystal Modification for Fuel Oils by Self-Aggregating Partially Crystallizable Hydrocarbon Block Copolymers. *Energy Fuels* **2000**, *14*, 419-430.

Chapter 7

(1) Mortier, R. M.; Malcolm, F. F.; Orszulik, S. T. In *Chemistry and Technology of Lubricants;* Springer: London, 2009.

(2) Pirouz, S.; Wang, Y.; Chong, J. M.; Duhamel, J. Characterization of the Chemical Composition of Polyisobutylene-Based Oil-Soluble Dispersants by Fluorescence. *J. Phys. Chem. B* **2014**, *118*, 3899-3911.

(3) Duggal, A.; Sheng, J.; Duhamel, J.; Pirouz, S. Quantifying the Level of Intermacromolecular Interactions by Using Pyrene Excimer Formation. USP(pending), 2014.

(4) Pirouz, S.; Duhamel, J; Sheng, J.; Duggal, A. Quantifying the Level of Intermacromolecular Between EP Copolymer Interactions by Using Pyrene Excimer Formation. Submitted for Publication, **2015**.

(5) Cuniberti, C.; Perico, A. Intramolecular Excimer Formation in Polymers: Pyrene Labeled Polyvinylacetate. *Eur. Polym. J.* **1980**, *16*, 887-893.

(6) Zhang, M.; Duhamel, J. Study of the Microcrystallization of Ethylene-Propylene Random Copolymers in Solution by Fluorescence. *Macromolecules* **2007**, *40*, 661-669.

Appendices

(1) Duhamel, J. Polymer Chain Dynamics in Solution Probed with a Fluorescence Blob Model. *Acc. Chem. Reaserch* **2006**, *3*9, 953-960.

(2) Siu, H.; Duhamel, J. Global Analysis of the Fluorescence Decays of a Pyrene-Labeled Polymer Using a Blob Model. *Macromolecules* **2004**, *37*, 9287-9289.

(3) Ingratta, M.; Mathew, M.; Duhamel, J. How Switching the Substituent of a Pyrene Derivative from a Methyl to a Butyl Affects the Fluorescence Response of Polystyrene Randomly Labeled with Pyrene. *Can. J. Chem.* **2010**, *88*, 217-227.

(4) Farhangi, S.; Weiss, H.; Duhamel; J. Effect of Side-Chain Length on the Polymer Chain Dynamics of Poly(Alkyl Methacrylate)s in Solution. *Macromolecules* **2013**, *24*, 9738-9747